UNIVERSITY OF SOUTHAMPTON

An experimental investigation into wing in ground effect over flat and wavy surfaces

by
Nicholas John Moore

A thesis submitted for the degree of
Doctor of Philosophy

Fluid Structure Interaction Research Group
School of Engineering Sciences
Faculty of Engineering, Science and Mathematics

December 2004

This thesis is dedicated to my beloved Angela.

Abstract

The effect that wavy and flat surfaces have on the aerodynamics of aerofoils operating In Ground Effect (IGE) has been investigated. Experiments were conducted in the Southampton University rolling road wind tunnel and the Circulating Water Channel (CWC) at QinetiQ Haslar. Two aerofoils were tested a DHMTU 12-35.3-10.2-80.12.2 and a NACA 0012. The DHMTU aerofoil was the primary section of interest to this research and the NACA 0012 was used as a control. Force measurements, flow visualisation and pressure measurements were used to assess the DHMTU aerodynamic characteristics in ground effect. The operating Reynolds Number was 830,000 and 550,000 in the wind tunnel and CWC respectively. Wings operating at these low Reynolds Numbers are applicable to a novel small Unmanned Wing In Ground Effect Vehicle (UWIGV) described in this thesis.

Analysis of data obtained in the rolling road wind tunnel showed that the overall drag of both the DHMTU and NACA 0012 aerofoils is greater in ground effect than out of ground effect. A significant reduction in the vortex drag of both aerofoils is produced as a result of flying in ground effect. Unfortunately the significant reduction in vortex drag coupled with the increase in the zero lift drag is not sufficient enough to reduce the overall drag of the trial sections in ground effect. As the altitude of both the aerofoils decreases the lift increases. This showed that the increase in aerodynamic efficiency as a result of flying IGE is due to the increase in lift.

Analysis of simulated flight over wavy surfaces in the CWC shows that as a wing flies over a wavy surface the lift varies from a maximum to a minimum. The amplitude of the lift force oscillation increases with decreasing altitude. A general result is that as the wavelength of the surface decreases the maximum lift experienced by the wing decreases and the minimum lift increases. The drag on the wing over a wavy surface in ground effect varies with altitude and as a function of wing position over the wavelength. Like lift it varies between a minimum and maximum value. The positions over the wavy surfaces where minimum and maximum drag was recorded are identical to the extremes of lift.

CONTENTS

APPENDICES

List of Figures

List of Tables

Abbreviations and Symbols

AoA	Angle of Attack
AR	Aspect Ratio
CCD	Charge Coupled Device
CFD	Computational Fluid Dynamics
CWC	Circulating Water Channel
D	Drag force
DC	Direct Current
DHMTU	Department of Hydrodynamics of the Marine Technical University
EO	Electro Optical
FCS	Flight Control System
FSU	Former Soviet Union
FMCW	Frequency Modulated Continuous Wave
GE	Ground Effect
GPS	Global Positioning System
H	height above wave centreline
h	height above flat ground or wave crest
h/b	height to wingspan ratio
h/c	height to chord ratio
IGE	In Ground Effect
IR	Infra Red
ISA	International Standard Atmosphere
L	Lift force
L/D	Lift to drag ratio
M	Pitching moment
NACA	National Advisory Committee on Aeronautics
NASA	National Air and Space Agency
OGE	Out of Ground Effect
PAR	Power Augmented Ram
PC	Personnel Computer
R	Range
RCS	Radar Cross Section
ROW	Rest of the World

SONAR	Sound Navigation And Ranging
TsAGI	Tsentrahl'nyy Aero-igidrodinameecheskiy Institoot (Central Aerodynamics Institute)
TV	Television
t/c	thickness to chord ratio
UAV	Unmanned Air Vehicle
UCAV	Unmanned Combat Vehicle
US	United States
USA	United States of America
UWIGV	Unmanned Wing In Ground effect Vehicle
V	Free stream speed
v	Volume
W	Weight
WIG	Wing In Ground effect
WIG_{Chord}	WIG wing chord

ARe	Effective aspect ratio
a_∞	Lift curve slope of wing of infinite aspect ratio
a	Lift curve slope of wing of finite aspect ratio
b	Wingspan
b_t	Length of wind tunnel side parallel to wing
c	Wingchord
C_L	Lift coefficient, $L/\frac{1}{2}\rho v^2 S$
C_{Lmax}	Maximum lift coefficient
C_{Lmin}	Minimum lift coefficient
C_{L0}	Lift coefficient at trim
C_{LOGE}	Lift coefficient out of ground effect
C_D	Drag coefficient, $D/\frac{1}{2}\rho v^2 S$
C_{Dflat}	Drag coefficient over flat surface
C_{Dmax}	Maximum drag coefficient
C_{Dmin}	Maximum drag coefficient
C_{DO}	Zero lift drag coefficient
C_{DV}	Vortex drag coefficient
C_{Dwave}	Drag coefficient over wavy surface

C_m	Pitching moment coefficient, $M/½\rho v^2 Sc$
C_{m0}	Pitching moment coefficient at zero lift
C_n	Normal force coefficient
C_p	Pressure coefficient
D_V	Vortex drag force
dy	Element width of wingspan
e	Span efficiency factor
F_H	Horizontal force
F_V	Vertical force
g	Acceleration due to gravity (9.81 ms^{-2})
$H_{\frac{1}{3}}$	Significant wave height
H_d	Endplate depth
h_t	Length of wind tunnel opposite to b_t
k	Vortex drag factor
L	Lift
L_E	Endplate Length
L_{LE}	Endplate protrusion from section leading edge
L_{TE}	Endplate protrusion from section trailing edge
m	WIG mass
n	Load factor
R_T	Turn radius
Re	Reynolds Number based on aerofoil chord
R_T	Radius of turn
r1, r2	Distance from wingtip to a specified point on the wing
S	Wing area
S'	Semi-span of elliptic load distribution
u	Relative velocity of air parallel to ground
u1	Change in velocity due to model blockade in wind tunnel
v	Relative velocity of air perpendicular to ground
W	Weight
w	Downwash velocity
w_{IGE}	Downwash velocity in ground effect

w_{OGE}	Downwash velocity out of ground effect
x	Position on wing from aerofoil leading edge
x_C	Characteristic length, taken in this thesis to be the wing chord
X_O	Location of aerodynamic centre
x_W	Rotation point of wing
y	Distance from centrespan of wing to point under consideration
z	Altitude

Greek Symbols

Γ_0	Vorticity
Φ	Vortex drag reduction factor
α	Angle of attack
α_{eff}	Effective angle of attack
ε	Downwash angle
λ	Wavelength
μ	Dynamic viscosity
ν	Coefficient of kinematic viscosity
ρ	Density
ϕ	Bank angle

Acknowledgements

I would like to thank Professor Wilson for providing me with the opportunity to embark upon this research and spend three very enjoyable years at Southampton University. His guidance and encouragement during my work were much appreciated. Special thanks go out to Alan Tiller at QinetiQ Haslar for his enthusiasm for my work and his supreme efforts in assisting me during my experiments in the CWC. They went 'far beyond the call of duty' and for that I am very grateful. Without the modifications made by Richard 'Dicky boy' Wheaton the CWC rig would never have got near the water. His aid was invaluable and unflinching over what was a very stressful period for all personnel at QinetiQ Haslar.

1 Introduction

1.1 General

This thesis is based upon an experimental investigation into the aerodynamic behaviour of a wing operating in ground effect over flat and wavy surfaces. The fundamental issues of Wing In Ground (WIG) effect are addressed, however there is an emphasis on the use of ground effect at low Reynolds Number over wavy surfaces.

Wing In Ground effect describes the improvement in aerodynamic efficiency of a wing when it is flying very close to the ground due to an increase in lift and a reduction in vortex drag. This results in the aerodynamic efficiency (ratio of Lift to Drag) increasing, the higher the L/D the more efficient the wing. The phenomenon of ground effect has been observed from the earliest days of flight. Chapter 2 discusses the historical application of ground effect in more detail.

Ground effect can be divided up into two distinct regimes [1]:

- Moderate ground effect
- Ram ground effect

Moderate ground effect is a result of the wing compressing the airflow under the wing's lower surface due to the proximity of the ground. This coupled with the improvement in spanwise lift distribution due to the reduction of downwash results in an increase in lift. Moderate ground effect is noticeable at altitudes from half the wingspan down to the ram effect region.

Ram ground effect occurs where the wing is at an altitude of h/c of 0.1 or less. The altitude of a wing when in ground effect is usually expressed in terms of the height to wing chord (h/c) ratio. This allows comparison of aerofoils operating in ground effect regardless of size. This convention is adopted and followed throughout this thesis. At an altitude of h/c 0.1 the wing is so close to the ground that the trailing edge of the wing is creating a sealed envelope. The wing-ground boundary prevents flow under the wing expanding as it would in free air. This results in additional lift due to a rise in

static pressure under the wing. This rise in the static pressure is often referred to as 'ram pressure' hence the 'ram ground effect'.

1.2 Overview of the Present Work

The experimental work presented in this thesis comprises studies of a DHMTU 12-35.3-10.2-80.12.2 aerofoil operating in a wind tunnel with a rolling road. The lift and drag forces have been measured using a conventional wind tunnel balance. Other results have been derived from surface pressure measurements on the aerofoil surface and surface flow oil patterns.

Little published experimental data exists on the effect of an aerofoil operating in ground effect over wavy surfaces. To investigate the effect of 'wavy' surfaces on the lift and drag of the DHMTU experiments were conducted in a Circulating Water Channel (CWC). This has allowed an assessment to be made of the effect of operating in ground effect over wavy surfaces.

The author proposes using ground effect flight to increase the survivability and endurance of Unmanned Air Vehicles (UAV) in a marine environment. The novelty of this approach is that no one has yet proposed or explored using UAVs that operate in ground effect. Due to the unique nature of the flight regime it is felt that such a craft deserves a new designation and from now on shall be known as an Unmanned Wing In Ground Effect Vehicle (UWIGV). Appendix G presents a more detailed discussion of this concept.

1.3 Research Aims

The aims of this research program are:

- To increase the knowledge base on aerofoil flight in ground effect over wavy surfaces and compare the aerodynamic performance with that of a flat surface
- To examine the aerodynamic performance of a ground effect aerofoil at low Reynolds Numbers
- To asses the benefits of adding endplates to the ground effect aerofoil of a UWIGV

2 Literature Survey

2.1 Scope of Literature Survey

This research is concerned with the aerodynamic performance of aerofoils at low Reynolds Number operating in ground effect over flat and wavy surfaces. Though there have been many papers published on ground effect aerodynamics over the years, very few serious overviews on ground effect physics and technology are in print. One such example is Hooker [2] who in 1982 identified the technical issues that need to be addressed to realise WIG flight. Two areas that stand out from his review as relevant to this study are the need for:

- Effects of flight over irregular surfaces
- Refined endplate design

Hooker's paper was written when Russian WIG research was classified due to military applications and the Cold War environment. With the passage of time Russian progress on WIG aerofoil research has become available in the West (section 2.6), but the information published on Russian WIG aerofoil design is not very detailed. The author has found no papers or other evidence that invalidates Hookers observations made over 20 years ago.

2.2 Historical Ground Effect Survey

Initial research in the 1920s was concerned with the effect that ground proximity has on conventional aircraft landing performance. A good illustration of the research of this era is Raymond [3] who considered a selection of contemporary aerofoil sections operating in ground effect. His experimental approach was to use an image aerofoil in an attempt to eliminate the boundary layer effects of a stationary surface, which are encountered in a conventional wind tunnel. As is well known today the Lift to Drag (L/D) of the sections tested increased when in ground effect. Interestingly enough even during the early 1920s Raymond suggests that ground effect "promises economy for low skimming flight over smooth water, *provided such flight be practical*".

In the early 1930s the Dornier DO-X seaplane purposely utilised ground effect to extend its payload and range during transatlantic crossings. Then during the 1930s various engineers in Finland, Sweden, FSU (Former Soviet Union) and the USA developed small ground effect vehicles to cross swamps, marshes, snow covered countryside and open water. From the 1960s attention was given to developing large WIG craft for commercial or military purposes. The FSU dominated the development of WIG craft until the late 1980s resulting in the testing of large WIGs such as the KM ekranoplan (Figure 2-1) which at 500 tons is the largest WIG craft built to date. Other developments included the ORLYONOK troop transport/assault craft (140 tonnes) and the missile firing LUN anti-ship craft (400 tonnes). These designs were of conventional aircraft appearance with low aspect ratio wings and large stabilising tailplanes positioned Out of Ground Effect (OGE). They were operated until the 1990s and to the best knowledge of the author are no longer flown.

The USA has generated three WIG craft concepts, Boeing in the 1960s with its LOW BOY anti-submarine warfare concept and the then Lockheed-Georgia in 1977 with a 700-ton WIG cargo concept [4]. The LOW BOY is interesting in that it employs a low slung wing possessing an aspect ratio of 12 and not employing endplates. This suggests that the craft would have possessed a respectable OGE performance capability. The Lockheed cargo WIG employed a low aspect ratio wing that housed payload.

None of these projects developed beyond the concept stage because the US concluded that WIG craft was a technology that it did not need to cultivate, though it would keep a watching brief on their development and capabilities [5]. As of 2002 Boeing is now studying a concept for a heavy lift (1400-ton payload) cargo WIG known as the PELICAN [6]. This is seen as a way of addressing the requirement to deploy armour into a conflict zone faster than conventional sea transport but with a greater payload capacity than conventional transport aircraft.

No evidence exists in any literature that small Unmanned WIG craft (UWIGV) have been proposed for operational purposes (see Appendix G). All WIG design

efforts have concentrated on manned craft to carry personnel for recreation, transport and other roles.

2.3 Lift Behaviour In Ground Effect

It is well documented that the proximity of the ground considerably increases the magnitude of lift experienced by an aerofoil. Experimental results obtained by Hayashi and Endo [7] indicate that at low Reynolds Numbers ($Re<3.2 \times 10^5$) and high Angle of Attack (AoA), flow separation phenomena of an aerofoil is stronger IGE than OGE.

As altitude is decreased the effect of the viscous interaction between the ground and wing becomes very important. Hayashi and Endo presented data that at low Reynolds Numbers, high AoA and very small ground clearances indicated that viscous effects couldn't be neglected. Hsiun and Chen [8] interestingly state that few aerodynamic studies have been conducted within this extremely low altitude flight regime. Hsiun and Chen [8] have applied the steady, incompressible Navier-Stokes equations to carry out a CFD investigation into a NACA 4412 aerofoil operating IGE.

There studies have shown that C_L increases with increasing Reynolds Number, as is also the case when operating OGE. Their paper states that in extreme ground effect (h/c 0.05) the gradient dC_L/dRe is higher than at moderate ground effect altitudes (h/c 0.25, 0.5, 0.1) and when operating OGE. Their modelling also indicated that at a h/c 0.05 lift coefficient decreases to values lower than for moderate ground effect and OGE. This is contrary to experimental data obtained by the author in this research and by other authors.

Steinbach [9] notes that Hsiun and Chen kept the ground stationary in their CFD modelling by applying the 'no-slip condition' (u=0, v=0) to the ground. This implies a boundary layer along the ground in steady flow that does not mirror reality. The authors should have used the 'slip condition' (u=1, v=0) representing a steady flow. This incorrect setting of the initial conditions accounts for Hsiun and Chen's high loss of lift whilst operating in extreme ground effect at h/c 0.05

due to the ground's boundary layer. Steinbach reinforces the point by stating that aerofoils of moderate thickness (t/c=12%) and moderate camber, such as the NACA 4412, when operating at moderate AoA produce an increase in lift with decreasing altitude.

Chun and Chang [10] have conducted an interesting adjunct study to boundary layer effects. The authors have investigated the boundary layer effects on a two dimensional NACA 4412 aerofoil IGE when operating over moving and fixed boundaries using CFD. The fixed ground represents the conditions that exist in a conventional wind tunnel. They showed that the pressure under the aerofoil increases as altitude decreases due to the slow down of the flow under the section and a resultant increase in pressure. They also showed that the suction peak on the upper surface near the leading edge increased due to the escape of flow beneath the wing as altitude decreased.

Chun and Chang results show that when the ground is stationary a thick boundary layer on the ground develops resulting in a different pressure distribution over the aerofoil. Using a moving ground surface C_L increases with decreasing altitude when the ground is stationary, the authors went down to Hsiun and Chens minimum altitude of h/c 0.05. This in stark contrast to Hsiun and Chen results discussed above where C_L decreased at this altitude with a stationary ground, due to their incorrect ground boundary conditions.

Chun and Chang make an interesting point in their introduction, which is applicable to this research. They discuss that most wind tunnels posses fixed floors that develop a boundary layer detrimental to accurately simulating WIG flight conditions. They state that there are very few facilities world-wide where rolling road wind tunnels exist. The University of Southampton possesses such facilities and these were available to gather data for this research.

2.4 Operational Environment and WIG Flight Altitude

WIG craft have been proposed for operations over ice and the sea. The prospects of WIG operations over the sea have attracted the most attention and

commercial interest. The sea presents an interesting surface to operate over due to its dynamic properties. The amplitude and the periods of the waves vary with time and rogue conditions can occur that a WIG craft may not have been designed for. Operation over the sea is probably the most challenging issue facing the operational deployment of WIG craft. Any discussion of the sea must encompass a consideration of the sea conditions to be encountered and the cruising altitude of a WIG and hence it's wing above the waves. The cruise height limitation of a WIG is stated as being typically h/c 0.1 to 0.3, any higher and the aerodynamic efficiency reduces that to flying OGE [11].

A WIG craft will be designed to operate within certain sea conditions that make the vehicle economically viable. The first step in the design process is to undertake a study of the sea conditions on the operating trade routes or mission areas.

There are not very many papers that discuss the actual operating conditions for a WIG. Handler [12] presents an illuminating discussion of the effect that the ocean's topography will have on a WIG. Handler raises the issue of 'Exceptionally High Waves' on a WIG, which could be disastrous for a WIG craft and occur more commonly than predicted. Chapter 3 provides a detailed discussion of wave conditions and a study that illustrates the interrelationship between WIG mass and seaworthiness.

The flight altitude of a WIG is set by the height that will exclude the influence of the waves on the craft when cruising and manoeuvring. Lange and Moore [13] in their concept study have designed their craft to operate at a h/c 0.1 with a clearance of 0.9 m between the wave crest of the $1/1000^{th}$ wave height and the wing underside. Though no data on the expected aerodynamic performance of the wing over the waves was discussed.

Maskalik [14] in his otherwise superb work on ekranoplan design devotes only a few paragraphs to cruising altitude over the waves. He makes general statements about determining the extremes of the sea state conditions and than

choosing the safe height above these waves, again with no reference to resulting performance.

Some Russian WIG designers have suggested operating in extreme ground effect (h/c<0.1), using large chord wings to realise a safe operating altitude. Rozhdestvensky [15] proposes that the cruising altitude should be in the range h/c 0.1-0.05 to maximise aerodynamic performance. Kirillovikh [16] states that a wing of aspect ratio between 2-3 flying at a height of h/c 0.2 is considered acceptable as an efficient transport vehicle.

No methodological or analytical treatment of WIG seaworthiness and the effect sea conditions have on performance has been found in any papers or texts on the subject of WIG craft. The author sees this as a failing in the current literature.

To the author's knowledge there are only two experimental works that have been conducted into WIG flight over a wavy surface. Grebeshev [17] of TsAGI conducted research in this field during the mid 1970s, unfortunately his paper was not available for review. More recent investigations into flight over a wavy surface are Byelinkskyy's and Zinchuk's [18] of the Ukrainian Institute of Hydrodynamics, work of the late 1990s. No experimental work outside the FSU was found on this area of research.

Byelinsky and Zinchuk initially tested aerofoils in air above a wavy surface in a towing tank. They found that the results obtained were not very accurate when compared to flying the aerofoils above the calm surface of the water tank. The authors state that this was due to the:

- High towing speeds (up to 25 ms^{-1}) of the large wing models (wing span 2 m)
- Small absolute values of the aerodynamic forces being measured
- Low natural frequency of the measuring installation

Similar problems were encountered with running an aerofoil over the surface of a towing tank in the preliminary considerations of the research (see Appendix C). Byelinsky et al overcame these problems by placing the wing underwater. This had the effect of addressing each of the three shortcomings mentioned above.

The towing speeds could also be reduced to 5-6 ms^{-1}, due to the thousand fold increase in forces as a result of operating in water instead of air, whilst maintaining high Reynolds operating numbers ($R_e \leq 2 \times 10^6$). The Russian aeronautical research organisation TsAGI have corroborated this method of investigation.

Byelinsky and Zinchuk observed that the lift and drag coefficients do not comply to a sinusoidal law as the aerofoil passes over the sinusoidal wave set in the towing tank. The maxima of C_L and C_D take place earlier than the position of the wave crest. The authors provide no discussion or analysis why this altitude dependence behaviour occurs.

At an h/c 0.7 the wavy surface was found to produce no influence on the lift coefficient of the aerofoil, no data regarding the behaviour of the drag was presented.

2.5 WIG Aerofoil Design

As the Russians have produced extensive research into all aspects of WIG design, especially dedicated ground effect aerofoils, this section discusses Russian research findings and the Rest Of the World (ROW) research separately.

Surveying available literature on IGE aerofoil design the following general guidelines have been found:

- A large leading edge radius is required to produce a leading edge suction peak to minimise the shift in centre of pressure.
- A trailing edge cusp produces an aft loaded section that provides maximum L/D ratios.
- Drooping leading edges or leading edge flaps produce no benefit in performance
- Thicker wings create more lift than thinner wings, this applies in and out of ground effect
- Low aspect ratio wings (AR<4) require endplates for maximum L/D benefit

- Increasing the thickness of an aerofoil result in a reduction of C_L at small angles of attack when IGE and an increase in parasite drag.
- Favourable WIG effect is maintained up to Mach 0.7. For a wing of aspect ratio 2 Russian research has found that L/D increases up to Mach 0.6-0.65 where upon a rapid decrease in aerodynamic efficiency occurs. Maskalik et al [14] does not describe the section used in these trials.

The under surface of an aerofoil is dominant in determining a section's lift capability IGE, the upper surface is stated as being insignificant in this respect according to Maskalik et al [19]. The lower geometry enhances the ram air effect when close to the ground. It is known that a convex under surface can create a venturi effect between itself and the ground, resulting in the section being sucked down. On the other extreme if the under surface becomes too concave the pressure under the section will diffuse resulting in a loss of lift.

2.6 Russian WIG Aerofoil Research

The Russians relied heavily upon experimental methods to investigate the aerodynamics of ground effect. These included wind tunnels with fixed and moving ground surfaces, towing tank runs and full scale tests using a series of experimental vehicles [19].

The section profile of ground effect sections can take many shapes, three common variants include flat convex, convexo-convex and S-shaped [16]. The University of St Petersburg has developed a series of dedicated ground effect sections known as the DHMTU (Department of Hydrodynamics of the Marine Technical University) family [20]. DHMTU sections are characterised by a flat undersurface and an S-shaped mean line. A DHMTU section is described by 8 numbers, which define the geometry of the upper and lower surfaces. The format being DHMTU a-b.c-d.e-f.g.h. It is known that the South Koreans are incorporating DHMTU profiles into their designs [21].

2.7 ROW WIG Aerofoil Research

It is known that NACA and Clark Y sections have been used on ROW WIG craft [20,22]. Clark Y sections have been particularly favoured because of their flat underside. Lockheed selected a modified Clark Y section for use on their heavy lift WIG [13]. There is a dearth of information on practical dedicated ground effect sections in ROW literature. Many papers that discuss the design of a WIG vehicle do not discuss the wing section in any great detail. Table 2-1 presents the results of a survey of aerofoil sections that have been considered for use in WIGs.

More recently the Koreans have been conducting research into WIG craft over sea surfaces. Im and Chang [23] present an interesting CFD analysis of the performance of a NACA 0012 and 6409 section over a simulated sea surface. It is interesting to note that they restricted their analysis to Korean coastal waters and did not consider deep ocean conditions. The normal force (C_n) on the aerofoils increase as the section climbs towards the crest and subsequently decrease once it is over the ridge. This study quotes a fluctuation of C_n and C_m by as much as 30% over the sea states modelled.

2.8 Racing Car Aerofoil Design

Modern racing cars require the generation of a downforce to hold the vehicle to the ground, thereby allowing it to negotiate corners at a faster rate and provide increased braking ability [24, 25]. On a typical open wheeled racing car, a major part of the aerodynamic downforce is developed by the system of wings present at either end of the vehicle. Of these the front wing can be considered the most important since it operates in ground effect [26].

In order to generate a downforce the wings on racing cars are inverted compared to aircraft/WIG applications [24]. Racing car wings produce high wing loadings as a result of racing car regulations and practical size restrictions. One major difference between racing car and WIG aerofoils are that a WIG wing faces a

large range of operation in terms of speed and angle of attack. A comprehensive review of the aerodynamics of inverted wings IGE is contained in ref [27].

Historically racing cars have used conventional aerofoil profiles from the aeronautics industry. Katz recommends that when searching for a single element aerofoil shape the simplest option is to consider the large variety of aerofoil shapes that are produced by NACA or NASA [24]. These are stated as being suitable when the C_L requirement is less than 0.8 and a single element aerofoil with a small degree of camber can be used on a racing car [24, 25]. Katz discusses the NACA 64_2-415 as a representative example of this type [24].

When greater values of lift are required more camber is required and to reduce the risk of flow separation multi-element aerofoils are used. At this point dedicated racing car aerofoils have been produced and aircraft/WIG design diverge.

2.9 Wingtip Design

The design of a WIG's wingtip is very important in determining the three-dimensional flow field around it and hence the aerodynamic efficiency of the wing. It is found that on conventional aircraft, tip mounted fuel tanks or missiles reduce the lift-induced drag by blocking the lateral circulation flow. A similar function is fulfilled by endplates, which are purposely designed to inhibit the spillage of air from the lower to the upper surface of an aerofoil via the wingtips. The effect of this is to make the flow more two dimensional with the result that the wing's aspect ratio is increased. This results in a reduction in vortex drag and an increase in the lift curve slope gradient. The disadvantage of endplates is that they increase the parasitic drag of the wing.

The potential drag reduction properties of fitting endplates have been known about since the early 20^{th} Century. Reid [28] discusses using endplates OGE; his experimental results suggested that endplates only showed benefit at higher lift coefficients, above $0.3C_{Lmax}$. This is due to the extra parasite drag produced.

Riley [29] suggested that the C_L at which benefits due end plates occur appeared to be a function of end plate area.

Chawla, Edwards and Franke [30] have shown experimentally that the aerodynamic efficiency of a wing IGE is increased if endplates are fitted. They tried three different sizes of endplates each of length equal to the section chord but with depths of 0.12c, 0.15c and 0.20c. The endplates were located at the wing tips. A central plate was tried but found not to make any difference to the wing's aerodynamic properties.

Endplates were found to be beneficial upto an altitude of h/c 1, though only providing an increase in C_L of 4% at 5 degrees angle of attack. As the height above the ground decreased the increase in C_L reached 15% at h/c 0.25. There was found to be no real advantage to having endplates at altitudes greater than h/c 1. An interesting result obtained was that varying the endplate height from 0.12c to 0.20c produced no significant change in C_L.

Standingford and Tuck [31] have performed some analytical work on the optimal size and position of end plates in relation to the midpoint of the wing. They found that for small angles of attack, which were not defined in the paper, the optimal location of the end plates were at the midpoint of the aerofoil. The optimal length and height of the endplates were determined to be 0.48c and 0.15c respectively. Standingford and Tuck [32] have also investigated the effect that rectangular endplates have on wing performance using CFD. They found that for maximum C_L the endplate must be located centrally chordwise, but for minimum induced drag the endplate has to be located 0.2c towards the leading edge of the section. The reason stated for this is that the large pressures near the leading edge drive the wingtip vortices more than the pressures at the trailing edges.

Kühmstedt [33] investigated four different wingtip configurations, these were endplates which extended only below the wing, only above the wing, above and below the wing and winglets. The conclusion was that endplates extending for the lower part of the aerofoil are the most efficient. No details or references were given for the elimination of the alternative arrangements.

Hoerner [34,35] sums up research into endplates upto the 1970s. The two main results are that fitting end plates exceeding the wing's chord length does not achieve much in aerodynamic performance. Conversely the effectiveness of endplates increases as their chord length increases upto the wing chord.

2.10 Conclusions

1. The dearth of published research on the experimental investigation of the aerodynamic performance of a wing in ground effect operating over wavy surfaces has been highlighted. Only two Russian papers detail the findings of experimental research of a wing flying in ground effect over wavy surfaces.

2. The importance of the operational environment for wing in ground effect craft operating over a marine environment has been discussed. There are very few published sources and even less that are detailed, that discuss this issue.

3. The Russians have developed a family of aerofoil sections that are designed to operate in ground effect. Known as the DHMTU series of aerofoils these will form the basis of the aerofoil to be used in this experimental research.

4. The literature has highlighted the importance of any experimental research into extreme ground effect ($h/c<0.1$) employing a moving ground to correctly simulate the actual boundary layer conditions encountered. It was also stated that there are very few locations around the world where these facilities exist.

5. There is no evidence in open literature that the UWIGV concept has ever been proposed or considered. The majority of WIG research and publications have been focused towards larger WIG craft.

WIG Craft	Aerofoil Section	Reference
SEABUS	Gottingen 1020	[36]
TT test bed	Hydrowing	[33]
Lockheed WIG	Modified Clark Y	[13]
CFD WIG Model	NACA 6409	[22]
Space Shuttle Launch Concept	NACA 4415	[30]
5,000 ton WIG Concept	Modified Clark Y	[2]
Korean WIG Research	NACA 0012 and NACA 6409	[23]
Japanese WIG	Munk M6R2 upper profile and CJ-5 lower profile	[37]

Table 2-1: Survey of ROW WIG Aerofoil Sections

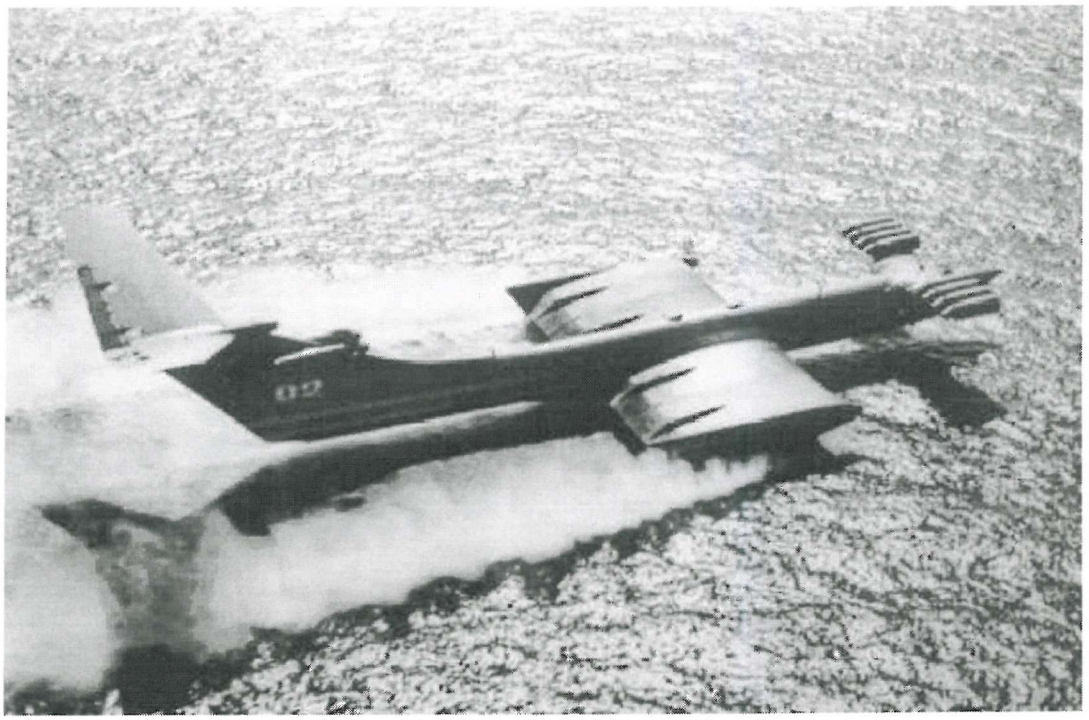

Figure 2-1: KM 'Caspian Sea Monster' ekranoplan, note the large stabilising tail positioned out of ground effect [20]

3 WIG Seaworthiness Study

3.1 Overview

An important consideration in the aerodynamic efficiency of a WIG craft is its cruising altitude. This will define the increase in lift and reduction in vortex drag and hence the overall efficiency of the craft. Over a flat surface such as ice or a calm sea, cruising in extreme ground effect (h/c 0.1) could be realised. As discussed in Chapter 2 the economic and operational niche of WIGs is in maritime applications. In this environment the wave height of the water determines the safe cruising altitude of the WIG. The determination of a WIG operating altitude over the sea is critical for safety and efficient operation.

3.2 Measures of Sea State

It is important to assess the limitations inherent in predicting the topography of the sea surface that a WIG is designed to operate over. Wave conditions cannot be exactly specified but are described in terms of probabilities of occurrence. At best the sea state is a general description of the sea surface, but it cannot be assumed that the ocean will meet this definition.

Wind action on the sea surface causes the majority of ocean waves [38]. The size of the waves depends upon the amount of energy supplied by the winds. The factors that determine this are the wind speed and the distance over which the wind blows in a constant direction, known as the fetch. The major difference between the oceans of the world is the maximum fetch over which the winds act. As an example in the North Atlantic the maximum fetch is approximately 1,000 km, if a 70 km/h wind was blowing, waves of upto 11 m in height can be produced [38]. The reader should note that this does not take into account rogue waves that could be encountered.

In reference publications wave amplitude is usually presented in terms of the mean height of the third highest waves ($H_{1/3}$), known as the 'significant wave height'. Significant wave heights can be related to a description of the sea and

denoted by a generally accepted sea state code (Table 3-1). Commercially available tables exist that detail the probability of occurrence of significant wave heights throughout the world as a function of time of year [39].

When using this data for WIG craft concept and design purposes allowance needs to be made for the possibility that higher wave amplitudes can occur. Russian [11] and US [13] WIG designers have allowed for this by considering the average height of the highest one-thousandth wave. This is obtained by applying a relative height factor to the significant wave height ($H_{1/3}$). These factors are listed in Table 3-2. This then allows the safe cruising altitude above the wave centreline 'H' to be calculated:

$$H = \frac{1.54 H_{1/3}}{2} + 0.1c \qquad \text{Equation 3-1}$$

Where c is the wing chord, the factor 1.54 converts the significant wave height into the one-thousandth wave height (Table 3-2). The additional term 0.1c allows for an additional altitude of h/c 0.1 above the centreline of the 1/1000th wave height. It should be noted that this is how Lockheed [13] have defined cruising height. In Chapter 7 the altitude of the wing is defined from the wave crest.

Table 3-3 illustrates the difference in wave height depending upon the wave height criteria selected. It highlights the importance in selection of the correct upper limit for determination of WIG cruising altitude. If a survey of a WIG operating route determined that sea state 4 was the prevailing condition, a significant variation in wave height exists depending upon the WIG designer's selection. At sea state 4 the significant wave height is 2.5 m if the 1/1000th highest wave is selected wave height has increased to 3.85 m.

3.3 WIG Seaworthiness

Small UWIGV concepts such as the example discussed in Appendix G will posses limited seaworthiness. To use this concept as an example, with a wing

chord of 0.32 m the craft would be restricted to operations in sea state 1 ($H_{1/3}$=0.1 m) at a cruising altitude of h/c 0.3. This section investigates the seaworthiness of larger WIG craft and applies to manned as well as unmanned variants.

In order to determine the seaworthiness of a WIG craft the safe operating altitude, as a function of Sea State needs to be determined. A survey of concept and contemporary aircraft configuration WIG (Table 3-4) has allowed the wing chord as a function of WIG mass to be determined (Figure 3-1). This data allows an engineering estimate of an aircraft type WIGs wing chord 'WIG_{Chord}' as a function of operating mass to be obtained.

$$WIG_{Chord} = 0.0107\,(\mathrm{m}) + 8.0788 \qquad \text{Equation 3-2}$$

Where m is the operating mass of a WIG in Mg and the wing chord WIG_{chord} is in metres. The operating mass is the loaded mass of a WIG craft including airframe, propulsion, fuel, crew (if applicable) and payload. The resulting wing chord is an approximate estimate but for low aspect ratio (AR<5) winged WIG craft is within ten percent of actual design values.

The wing chord of an aircraft configuration WIG as a function of mass can be obtained from Equation 3-2. Equation 3-1 then allows the safe cruising height of a WIG to be calculated as a function of operating mass and wing chord. The altitude of the WIG has been expressed as the height from the wave centreline in terms of h/c as illustrated in Figure 3-2.

If the criteria for efficient aerodynamic operation are defined as operating at an altitude of h/c 0.3 the mass and wing chord of the WIG for safe operation in a range of significant wave heights can be obtained. The altitude of h/c 0.3 has been selected as a compromise between favourable ground effect, controllability and safety. On Figure 3-3 four operating masses are indicated where the curves cross the h/c 0.3 altitude threshold. It can be seen that operation in significant wave heights of upto 2 m can be achieved even at a low operational mass of 10 tonnes. If the significant wave height increases to 3 m a craft in the operational

mass of 325 tonnes would be required. Examples of craft in this class are the Russian LUN and SPASTEL. Increasing the significant wave height to 4 m results in the operating mass increasing to 689 tonnes. As the significant wave height increases to 5-6 m an operating mass of 1,000 tonnes and greater is required. This is approaching the operational mass of the transoceanic Boeing PEILICAN concept.

Table 3-5 summarises the estimated minimum operating masses and wing chords for a range of significant wave heights along with some contemporary examples. It can be seen that for transoceanic WIG operations where significant wave heights can be in the order of 5-6 m wing chords of 19 m and higher are required for aircraft configuration WIGs.

To put the above into an operational context the generic WIGs presented in Table 3-5 are evaluated in a range of operational environments. The locations have been selected for examination because of their commercial or geopolitical importance. The most challenging environments are the open oceans represented by the North Atlantic, this contains some of the most severe wave conditions in the World. The English Channel and Baltic are important areas because of their commercial trading routes between areas of Europe and have been deemed worthy of inclusion. The Persian Gulf is an area of vital commercial and geopolitical interests for the Western World hence its inclusion in this study.

It was mentioned in Section 3.2 that publications are available that detail the probability of occurrence of wave heights at locations all around the world. This study has obtained statistical significant wave height data for the selected operating areas from reference [39].

The probability of each WIG operating at an altitude less than h/c 0.3 can be obtained by correlating the significant wave height that each generic WIG can safely fly over with the probability of a significant wave height occurring using the data contained within reference [39] (see Appendix F).

The following results are presented as a probability of operating at an altitude of h/c 0.3 for each WIG operating mass. Two seasons of the year have been considered representing the extremes of winter (December-February) and summer (June-August).

Figure 3-4 illustrates that a 1,000 tonne WIG would posses a high probability (>70%) of operating at an altitude of h/c 0.3 when crossing the North Atlantic. The smaller 689 tonne craft suffers a 16% reduction in the December-February period and a 6% reduction in the June-August period compared to the 1,000 tonne WIG. It can be seen that smaller 10 tonne WIG craft experiences a severe reduction in its capability to operate at an altitude of h/c 0.3 during both seasonal periods.

Figure 3-5 illustrates that a WIG displacing more than 1,000 tonnes will be able to operate at an altitude of h/c 0.3 with a probability greater than 70% over the World's major oceans. These figures reflect the highest significant wave heights to be found in each of these areas throughout the year. As the WIG operating mass increases to 1,400 tonnes the probability of cruising at h/c of 0.3 increases by 10% compared to the 1,000 tonne craft. It can be seen that the North Atlantic is the most severe ocean to operate over out of the areas investigated. This illustrates that low level transoceanic WIG operations are feasible if a solution to rogue waves can be formulated.

When these transoceanic WIGs operate in the more sheltered sea areas the results of this study indicate that these large WIGs can operate at an altitude of h/c 0.3 with a probability of 90%. The Persian Gulf is a very benign environment to operate over and the least demanding operating area considered in this survey. It can be seen from Figure 3-6 that even a small 10 tonne WIG has a 80% probability of operating at altitudes less than h/c 0.3 even during the December-February period.

The English Channel is a more demanding operating environment than the Persian Gulf. This is shown in Figure 3-7 where during the December-February period the smaller 10 tonne WIG would only be able to operate at h/c 0.3 with a

probability of 45%. To achieve an 80% probability of operating at this altitude a larger 689 tonne WIG would be required. In the Baltic the 10 tonne WIG can operate at h/c 0.3 with a probability of 60% in winter, increasing to over 80% in the summer (Figure 3-8). To increase this probability to 80% in the winter a 325 tonne WIG is sufficient.

3.4 Summary

1. US and Russian WIG designers have determined the safe operating altitude of a WIG by requiring it to clear the crest of the thousandth highest wave in the sea state spectrum. Unfortunately this requirement does not take into account the occurrence of rogue waves. These are extremely high waves of height upto 30 m that can 'suddenly' appear and could result in the destruction of a WIG craft. There are several possible causal mechanisms and research is ongoing to explain their creation. Unless rogue waves can be predicted or detected they present a serious obstacle to safe transoceanic WIG operations that need to be considered by a WIG designer.

2. An analysis indicates that transoceanic WIG operations are feasible for large craft, if rogue wave occurrence can be predicted or detected. Based upon engineering estimates it has been determined that WIGs of mass greater than 1,000 tonnes can operate at an altitude of h/c 0.3 over waves of significant height greater than 5 m. This results in WIG craft of this class possessing a probability of greater than 70% of operating IGE over the world's major oceans. To achieve this a WIG craft would require a wing chord of at least 19 m for low aspect ratio wings (AR<5). This is borne out by some of the large WIG craft generated by Russian design bureaus [14, 15].

Sea state code	Description of Sea	Significant wave height (m)
0	Calm (glass)	0
1	Calm (rippled)	0-0.1
2	Smooth (wavelets)	0.1-0.5
3	Slight	0.5-1.25
4	Moderate	1.25-2.50
5	Rough	2.50-4.00
6	Very rough	4-6
7	High	6-9
8	Very high	9-14
9	Phenomenal	>14

Table 3-1: Sea state code [38]

Wave	Relative Height Factor
Most frequent waves	0.50
Average waves	0.61
Significant wave height	1.00
Highest 1/10th wave height	1.29
Highest 1/1000th wave height	1.54

Table 3-2: Wave Height Characteristics [38]

	Wave Height (m)		
Sea State	**1/3 (SWH)**	**1/10th**	**1/1000th**
4	1.25-2.50	1.61-3.23	1.93-3.85
5	2.50-4.00	3.23-5.16	4.97-7.95
6	4-6	5.16-7.74	7.95-11.92

Table 3-3: Cruising altitude definition

Type	Operating Mass (x 10^3 kg)	Geometric Aspect Ratio	Wing Chord (m)	Wing Span (m)
Lockheed PAR-WIG	150	3.94	12.4	48.9
ORLYONOK	140	3	10.5	31.5
LUN	400	3	13.7	41
SPASTEL	390	3	15	45
MPE-100	90	4.5	6.7	30
MPE-200	210	4.5	9.3	42
MPE-300	300	4.5	10.7	48
MPE-400	450	4.5	11.8	53

Table 3-4: Aeroplane configuration WIG Metrics (Aspect Ratio<5)

Minimum Operating Mass (x 10^3 kg)	Significant Wave Height (m)	Minimum Wing Chord (m)	Example
10	2	8.2	MPE-10
325	3	11.6	LUN, SPASTEL
689	4	15.5	None
1,000	5	18.8	None
1,400	6	23.1	Boeing PELICAN

Table 3-5: WIG Seaworthiness as a function of Minimum Operating Mass

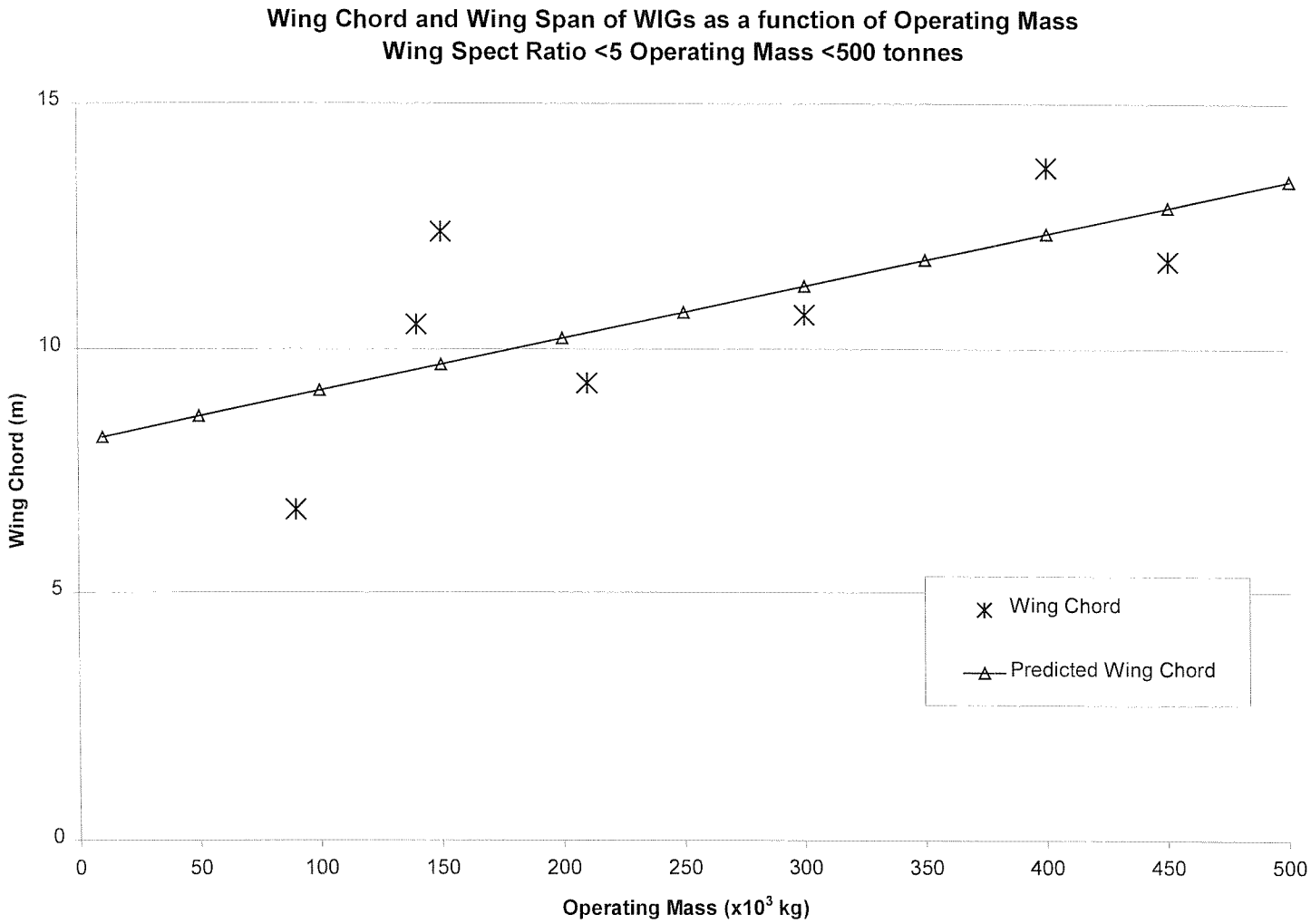

Figure 3-1: WIG wing chord as a function of operating mass

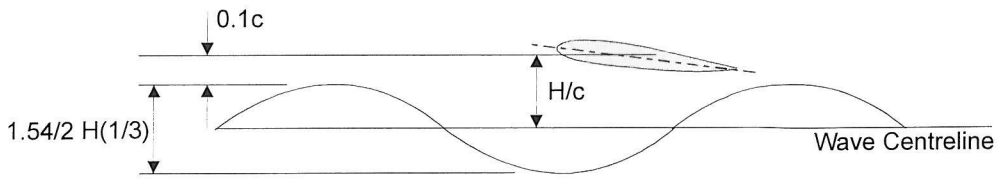

Figure 3-2: Cruising Height Definitions

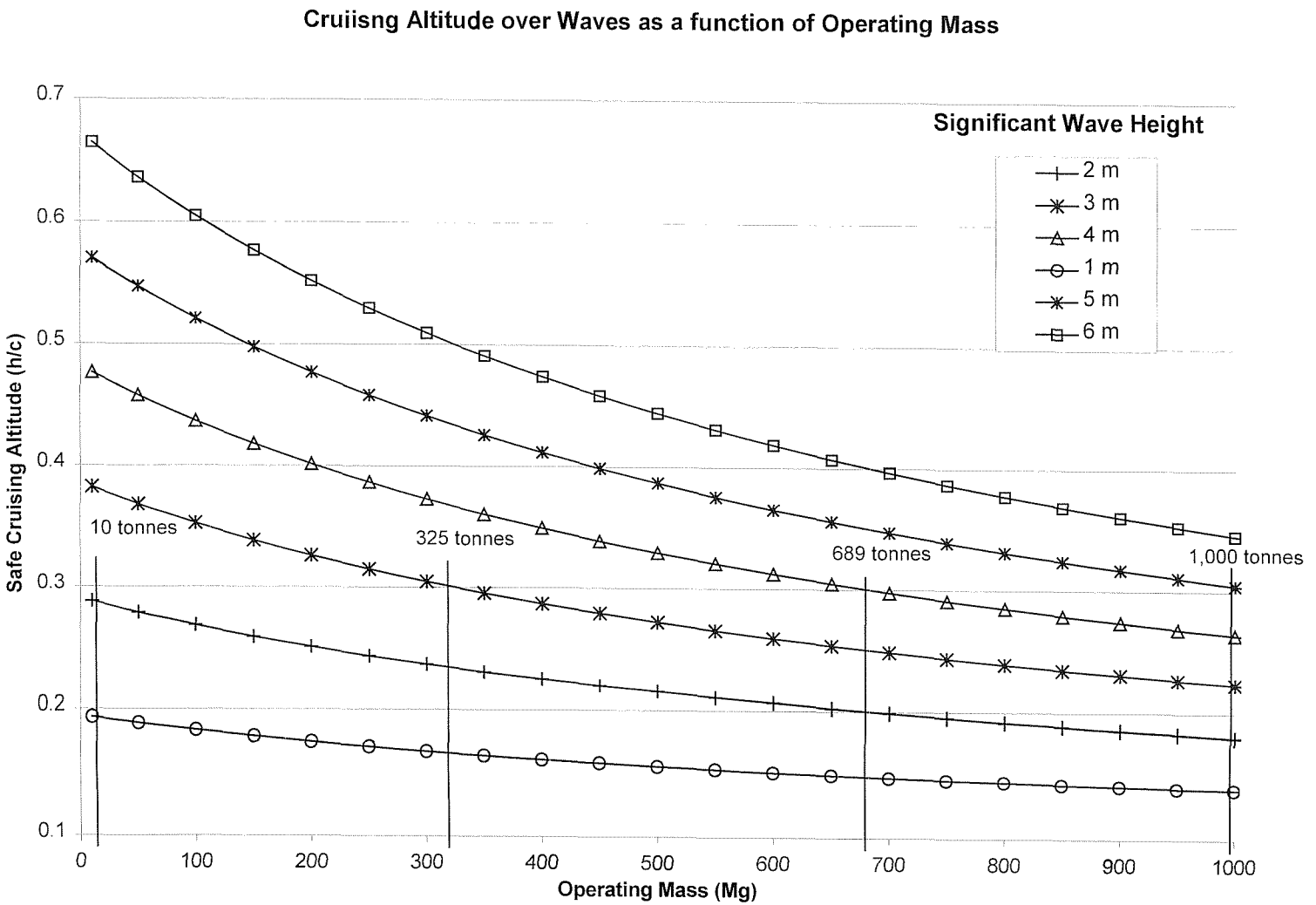

Figure 3-3: WIG cruising altitude as a function of operating mass for varying significant wave height

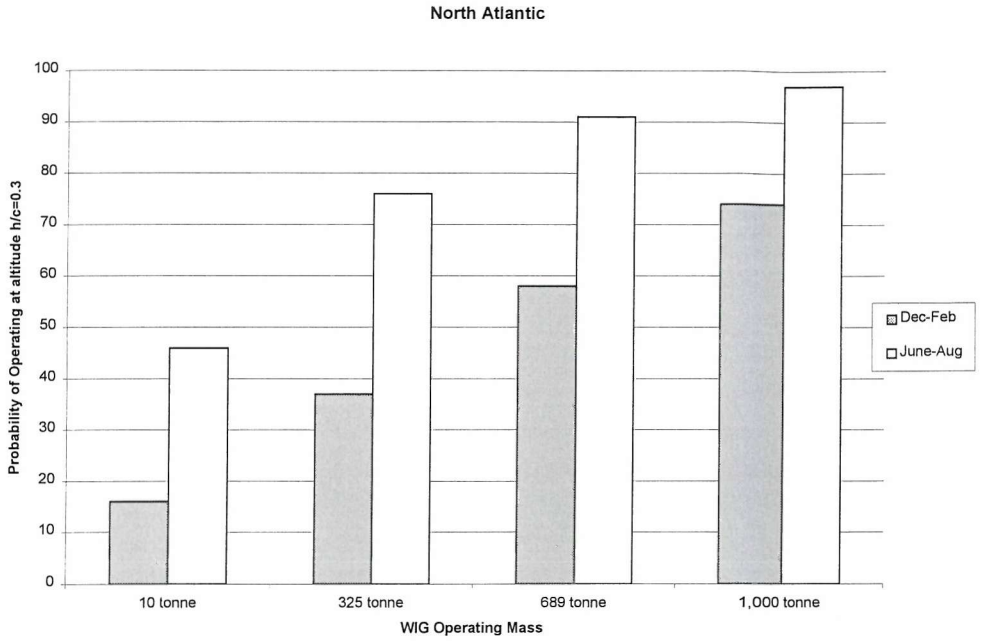

Figure 3-4: Probability of operating at altitude h/c 0.3 for various WIG operational masses in the North Atlantic

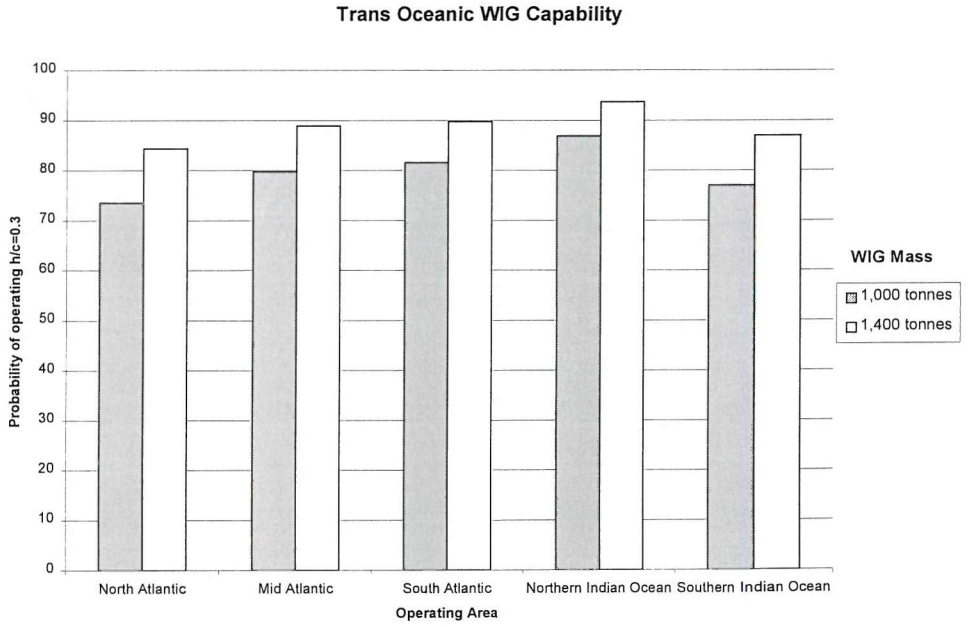

Figure 3-5: Probability of 1,000-1,400 tonne WIG operating at an altitude of h/c 0.3 in a selection of Oceans

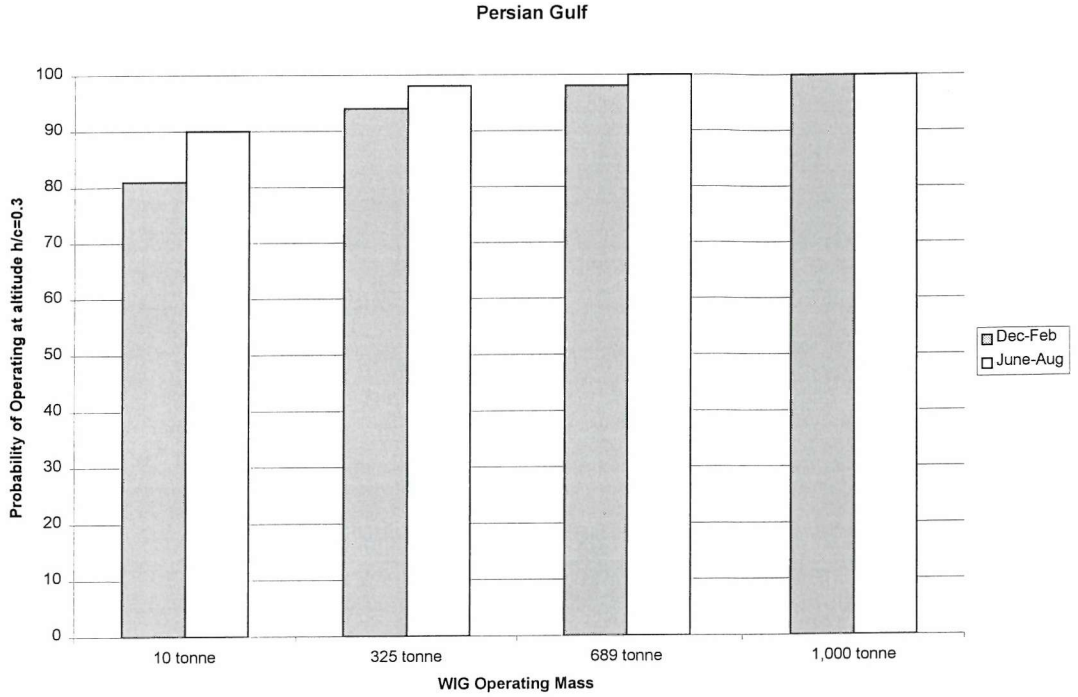

Figure 3-6: Probability of operating at altitude h/c 0.3 for various WIG operational masses in the Persian Gulf

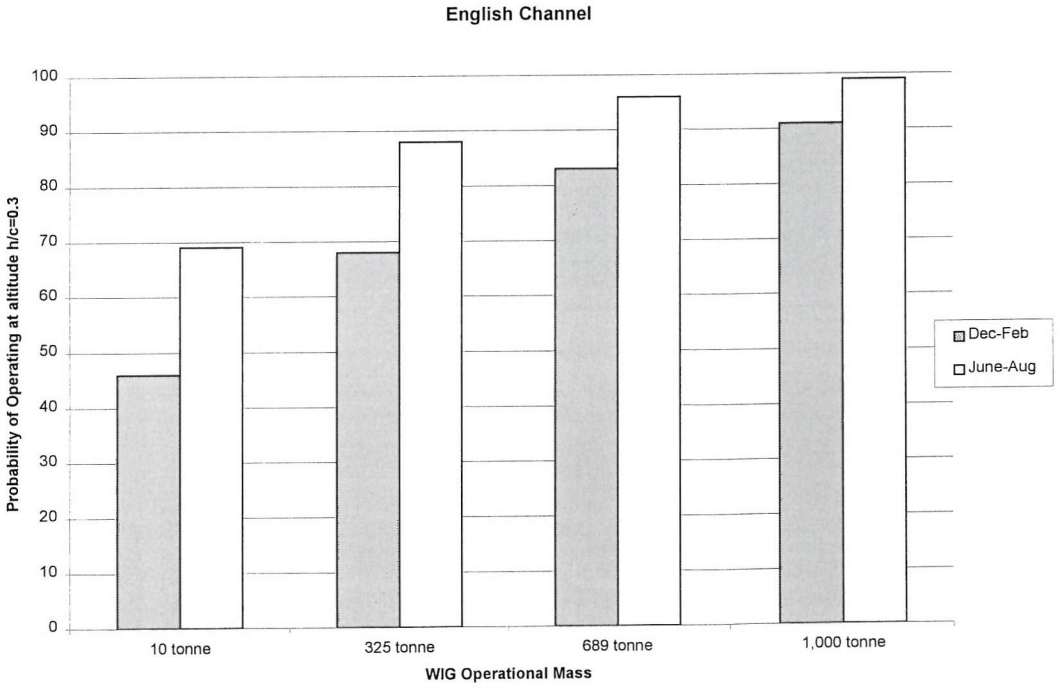

Figure 3-7: Probability of operating at altitude h/c 0.3 for various WIG operational masses in the English Channel

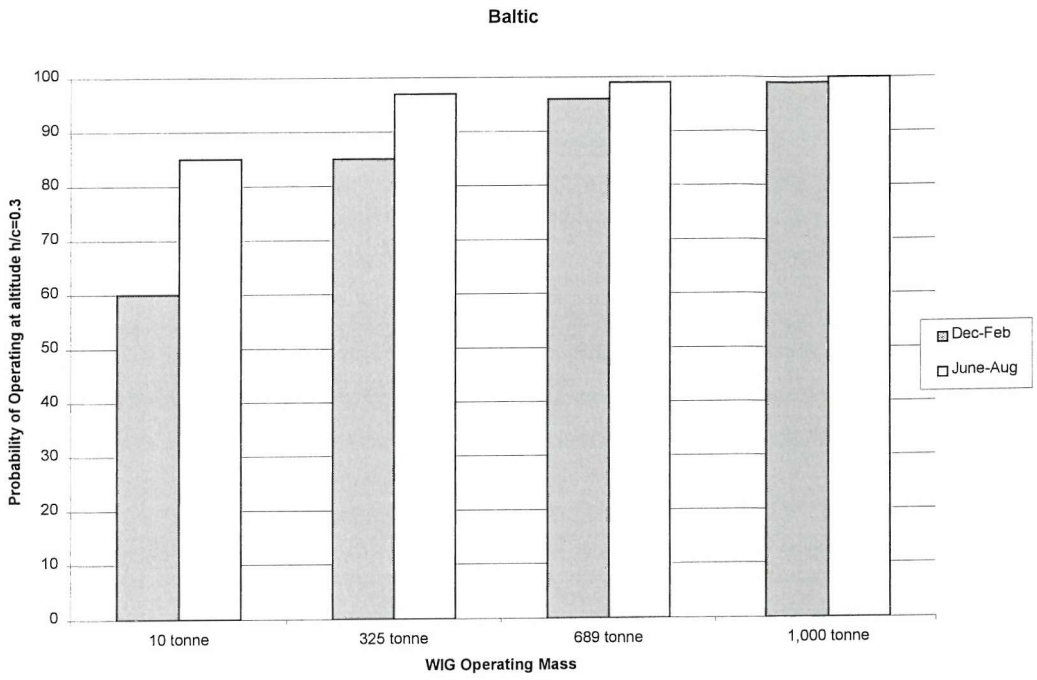

Figure 3-8: Probability of operating at altitude h/c 0.3 for various WIG operational masses in the Baltic

4 Methodology

4.1 Overview

The methodology selected has been to obtain experimental data and behaviour for aerofoil sections in wind tunnels and water tanks. This data forms the basis of the investigative analysis presented in the following chapters.

The approach taken has been to reverse engineer a Russian DHMTU section to investigate the performance of a ground effect aerofoil over flat and wavy surfaces. During the initial stages of the research very little was known about the characteristics of practical dedicated ground effect sections. The choice made in deciding the DHMTU section geometry was based upon minimal experience with the DHMTU family.

4.2 Research Assumptions

The following assumptions have been made in the experimental research:

- A rectangular planform of fixed aspect ratio is used
- No leading or trailing edge wing sweep considered
- Data only applies upto Reynolds Number of 8.3×10^5
- Wing is applicable to aircraft type WIG configuration as discussed in Appendix D
- Compound wing geometry is not considered
- Leading and trailing edge devices are not considered

4.3 Experimental Setup

4.3.1 Equipment

The measurements were taken in University of Southampton 2.1 x 1.7 m rolling road wind tunnel. The flow is driven by six 3 m rotating fans and regulated by controlling the speed of the DC motors that drive the fans. The maximum airflow and road speed produced by the tunnel is 40 ms^{-1} in the working section. The outputs from the wind tunnel balance were connected to an analogue to digital converter that inputted into a standard PC running data acquisition software.

4.3.2 Experimental Procedure

The wing was attached to the supporting arms of the wind tunnel balance in the working section of the wind tunnel (Figure 4-1). The wing was levelled in pitch and roll by the using a digital level. Any yaw present was minimised by checking the position of the vertical support struts and wing when in place. The altitude of the wing was set by lowering the vertical struts and measuring the distance from the wind tunnel floor to the wing rotation point. This was located at a distance of c/3 from the wing leading edge along the chordline of the section. The angle of attack of the wing is varied using balance stepper motors that raised and lowered the sting attachment. The wing was set at an angle of attack of 0 degrees and the Lift and Drag channels were zeroed.

The speed of the wind and road were gradually increased until the working speed of 38 ms^{-1} was reached. Once the working speeds were achieved a settling period of 1 minute was allowed in order to allow the conditions to settle. While the runs were in progress the dynamic pressure, rather than the tunnel free stream velocity was kept constant. This meant that the temperature/pressure variation was taken into account in the readings and no further calculation would be necessary to account for this later.

All the wind tunnel runs were conducted at a free stream velocity of 38 ms^{-1} unless otherwise stated. This corresponds to a Reynolds's Number of 8.3×10^5 based upon wing chord. To simulate the actual flow conditions encountered when a wing flies close to the ground the road surface was run at 38 ms^{-1}. The sections were tested at angles of attack ranging from –5 to +13 degrees, with readings being taken at every 1 degree step. The section was tested at a height of h/c 2.3 which is considered to be operating OGE and between h/c 1.0 to 0.08. The variables for the experiments are summarised in Table 4-1 and accuracy of setting up in Table 4-4.

After data had been obtained at all the required angles of attack the wing was removed and tare measurements were taken at each height and angle of attack (Figure 4-2).

To provide a baseline section for comparison with the DHMTU a symmetrical NACA 0012 airfoil section was used (Figure 4-3). This was selected as it provides conventional aerodynamic performance to act as a datum for the DHMTU used in this research.

4.3.3 Accuracy and Sources of Error

The presence of the wing in the tunnel reduces the area through which the airflow must pass resulting in an increase in the velocity of the air flowing over the wing. This is known in standard texts as 'flow constraint' or 'blocking'. Pope [40] states that conventional tests in the wind tunnel, as opposed to wings that span the whole width of the tunnel, should use the 3 dimensional blocking correction. The change in velocity due to model blockage in the wind tunnel is given by:

$$\frac{u_1}{V} = 0.68\left(\frac{\text{Volume}}{h_t^{\,2} b_t}\right) \qquad \text{Equation 4-1}$$

Where u_1 is velocity due to model blockade, V is the original velocity in the wind tunnel, Volume is the wing volume, b_t is the length of the tunnel side parallel to the wing span and h_t is the length of the other side of the tunnel. Table 4-3 details the definition of the components of the blockage correction equation.

The resulting change in velocity $\frac{u_1}{V}$ is 7.38 x 10^{-5} which is considered to have negligible effect on the results.

The sources and magnitude of the experimental error for the wind tunnel measurements are presented in Table 4-4. Appendix A discusses the uncertainty and repeatability of the wind tunnel results in more detail.

4.4 DHMTU Aerofoil Selection

This research has utilised the Russian DHMTU (Department of Hydromechanics of the Marine Technical University) aerofoil family as the basis for the experimental investigations. The DHMTU aerofoil family was selected because it has and is being employed on WIG craft. Very little information is available in open sources about the DHMTU aerofoil family. The DHMTU aerofoil used in this research was based upon a DHMTU used by the South Koreans [21]. Tothill conducted a small quantitative investigation into potential DHMTU aerodynamics performance [41]. This study employed an aerofoil analysis program known as XFOIL [42] and is detailed in Appendix I.

DHMTU sections are characterised by a flat undersurface and an S-shaped mean line. A DHMTU section is described by 8 numbers, which define the geometry of the upper and lower surfaces. The format being DHMTU a-b.c-d.e-f.g.h, each prefix denoting a parameter of the aerofoil as detailed in Table 4-5. The South Koreans have used a DHMTU 12-35.3-10.2-80.12.1 in their studies, this research has employed a DHMTU 12-35.3-10.2-80.12.2 which is a nearly identical section.

The thickness of the DHMTU section was set to a thickness to chord ratio (t/c) of 12%. This was set to be the same as the NACA 0012 control section and is considered typical of a subsonic aerofoil. The position of the maximum thickness of an aerofoil can be anywhere between 30 to 60% of the aerofoil chord [44]. The candidate DHMTU sections had their maximum thickness varied between 30 to 35% of the chord. The maximum thickness was set at 35% of the chord based upon South Korean experience [21].

The start of the planar underside of the section was maintained at 10% of the chord from the leading edge. Similarly the termination of the planar undersurface was kept constant at a distance of 80%. The angle of the planar surface below the horizontal can either be positive or negative. To produce a restoring pitching

moment the planar undersurface has to possess a negative angle or be parallel to the chord line.

When operating out of ground effect some engineering guidelines can be followed to aid in the design process. The leading edge of the aerofoil should be rounded with a radius of curvature sufficiently large to avoid excessive suction. if high suction were present it would be followed by an adverse pressure gradient that could lead to flow separation. The nose radii of the candidate sections were varied between a nose radius parameter of 2 to 4 as specified in the DHMTU aerofoil generator.

A DHMTU 12-35.3-10.2-80.12.2 was selected for experimental testing. The geometry of this profile is illustrated in Figure 4-4. The co-ordinates of this section are tabulated in Appendix H.

Variable	Experimental Range
Angle of Attack	-5 to 13 degrees (1 degree steps)
Wing Height (h/c)*	2.3, 1.0 to 0.1 (0.1 steps) and 0.08
Reynolds's Number	8.3×10^5, 4.3×10^5, 1.3×10^5

Table 4-1: Test Variables

*Wing height was measured at c/3 to a chordline connecting the leading and trailing edges

	NACA 0012	DHMTU 12-35.3-10.2-80.12.2
Span	0.96 m	0.96 m
Aspect Ratio	3.02	3.01
thickness/chord ratio	12%	12%
Chord	0.317 m	0.319 m
Area	0.303 m^2	0.306 m^2
Wing Sweep	0 degrees	0 degrees

Table 4-2: DHMTU and NACA 0012 Parameters

Nomenclature	Description	Value
Volume (wing volume)	0.7 x chord x thickness x span	(0.7 x 1.06 ft x 0.13 ft x 3.2 ft) 0.019 ft^3
h_t	Length of other side of tunnel	5 ft
b_t	Length of tunnel side parallel to wing span	7 ft

Table 4-3: Nomenclature and values for wind tunnel blockage corrections

Sources of Error	Magnitude
Wind tunnel balance accuracy	See Appendix A
Wing Bank Angle	±0.1 degree
Wing Angle of Attack	±0.1 degree
Wing Height	±0.006 h/c

Table 4-4: Wind Tunnel sources of error

Prefix	Definition	Experimental Value
a	Maximum ordinate of the upper surface (%c)	12
b	Position of the maximum ordinate (%c)	35
c	Ordinate of the start of the flat section (%c, below the horizontal is positive)	3
d	Position of the start of the flat section (%c)	10
e	Ordinate of the end of the flat section (%c, below the horizontal is positive)	2
f	Position of the end of the flat section (%c)	80
g	Slope parameter of the upper trailing edge	12
h	Nose radius parameter	2

Table 4-5: DHMTU Properties

Figure 4-1: DMTU section in 2.1 x 1.7 m rolling road wind tunnel

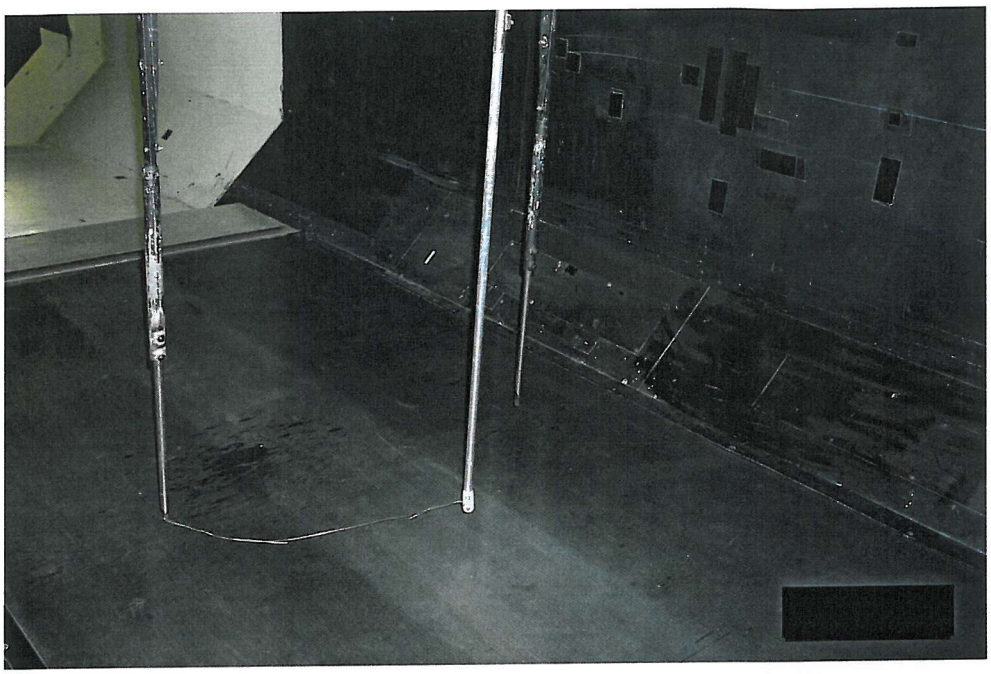

Figure 4-2: Tare measurement arrangement

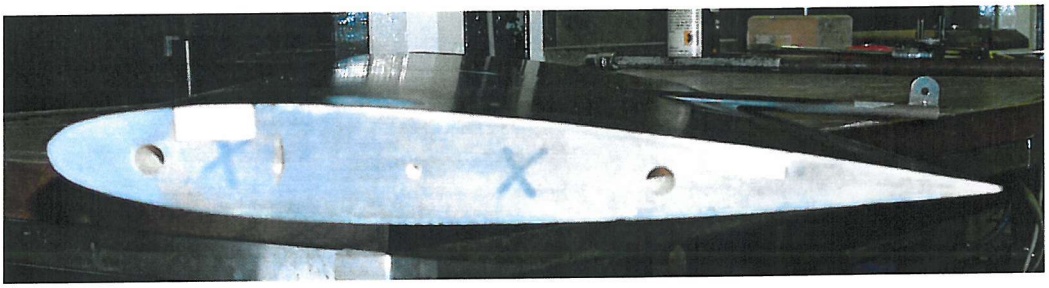

Figure 4-3: NACA0012 baseline section

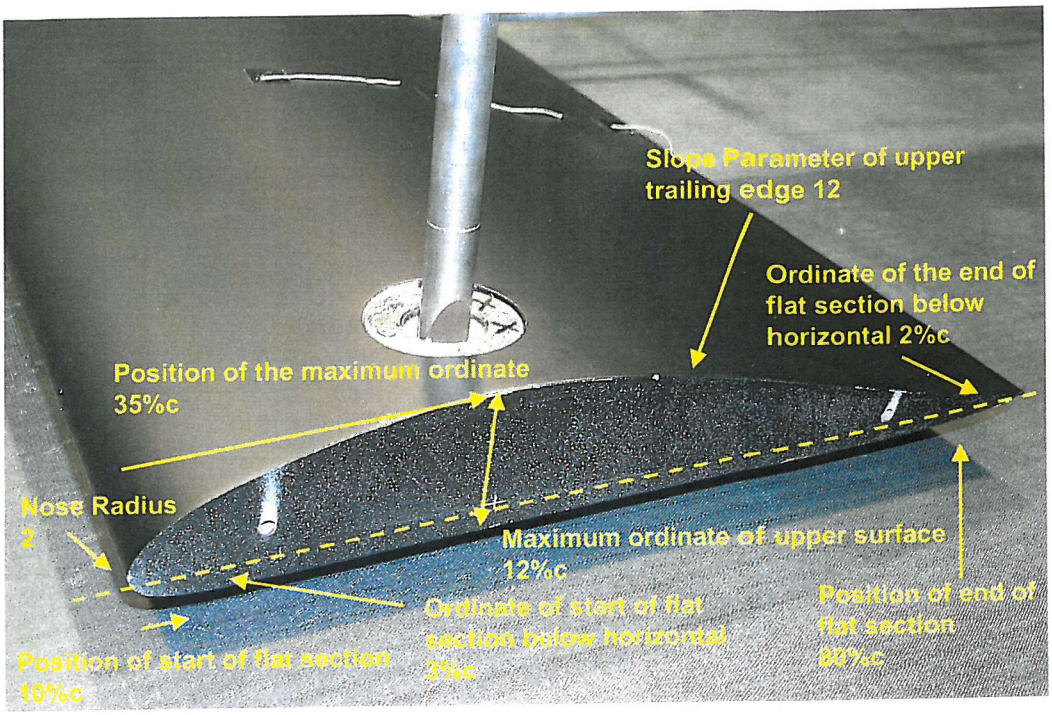

Figure 4-4: DHMTU 12-35.3-10.2-80.12.2 Profile

5 Lift and Drag In Ground Effect

5.1 Overview

This chapter presents the results and analysis of experimental trials conducted during this research program in the 2.1 x 1.7 m rolling road wind tunnel. The experimental procedure and set up were detailed in Chapter 4. The aim of this chapter is to analyse the aerodynamic behaviour of the DHMTU 12-35.3-10.2-80.12.2 flying over a flat surface in ground effect operating at low Reynolds Number. The aerodynamic data obtained in the rolling road wind tunnel allows a comparison to be made with operation over wavy surfaces (Chapter 7).

5.2 Background to Behaviour of Drag in Ground Effect

The total drag coefficient C_D of a 3D wing comprises a zero lift drag component C_{D0} and a lift dependent drag component C_{DV} as shown in equation 5-1

$$C_D = C_{D0} + C_{DV} \qquad \text{Equation 5-1}$$

When operating in ground effect the vortex drag component C_{DV} is equal to

$$C_{DV} = \Phi k C_L^{\,2} \qquad \text{Equation 5-2}$$

The term Φ is a ground effect vortex drag reduction factor that makes allowance for the effect that the proximity of the ground has on the wingtip vortices and the downwash across the wingspan. C_L is the lift coefficient and k is a constant of proportionality that is given by equation 5-3.

$$k = \frac{1}{\pi AR e} \qquad \text{Equation 5-3}$$

This constant k is dependent upon the wing's aspect ratio (AR) and a parameter known as the span efficiency factor (e). This efficiency factor describes how close the lift distribution across the wingspan is to the theoretically ideal elliptical distribution. If the spanwise lift distribution is elliptical e is unity, but in practice it

is usually less, due to the wing planform geometry and wing-fuselage interference effects. The product ARe is referred to as the 'effective aspect ratio' and expresses the aspect ratio that the wing would posses if operating out of ground effect (OGE) [44]. It is a useful metric in illustrating the decrease in vortex drag as the wing descends in altitude.

5.3 Experimental Results of Drag IGE

5.3.1 Behaviour of Overall Drag In Ground Effect

Figure 5-1 presents the ratio of the total drag coefficient (C_D) in ground effect (h/c 1 to 0.1) to the drag when out of ground effect (h/c 2.3). This data applies for an angle of attack of 5 degrees where the maximum aerodynamic efficiency is achieved. The total drag of both sections increases as they enter moderate ground effect at h/c 1. The increase is greater for the DHMTU where the drag is 1.45 times its OGE value. The contrast with the NACA 0012 drag can be seen where it only increases by 1.06 times it OGE value. With a decrease in altitude the DHMTU exhibits a decrease in drag until in extreme ground effect (h/c 0.1) the drag has reduced to just above its OGE value. Similarly the NACA 0012 exhibits an increase in drag with decreasing altitude, until at h/c 0.1 the drag is 1.15 times its OGE value. Figure 5-2 shows that the overall drag of the DHMTU does decrease over the ground effect regime (h/c<1) but is still greater than when the wing is operating out of ground effect.

The above results illustrate that the overall drag of these two aerofoils operating in ground effect increases over the OGE value and does not reduce. This is an important finding as the main merit for WIG flight is an increase in the aerodynamic efficiency that is the ratio of Lift to Drag. If the overall drag remains nearly constant or increases the efficiency of a wing in ground effect will have to rely upon the increase in lift alone to improve the aerodynamic efficiency.

The results indicate that the DHMTU section possesses approximately twice the overall drag of the NACA 0012 section throughout the altitude range h/c 2.3 to h/c 0.1. Figure 5-3 illustrates this presenting the overall drag for the NACA 0012 and DHMTU at an angle of attack of 5 degrees.

At an altitude of h/c 0.1 the drag polar exhibits very different behaviour than at higher altitudes (Figure 5-4). This is due to a large reduction in vortex drag as discussed later in section 5.3.3.

Figure 5-5 shows the comparison between experimental data obtained for this research and data obtained by NACA for a NACA 0012 aerofoil [45]. The NACA data was obtained experimentally in a wind tunnel at a Reynolds Number of 3.23 x 10^6 and has been corrected to reflect the performance of a NACA 0012 of infinite aspect ratio.

When the NACA 0012 is OGE and not producing any lift, the performance between the data obtained for this research and the NACA data is very small. This provides an independent verification of the lift and drag data obtained for this research. As the angle of attack of the section increases the drag of the NACA 0012 with an aspect ratio of 3 is significantly greater than the data obtained by NACA of infinite aspect ratio. This is a result of the production of vortex drag of the finite wing (AR=3). In contrast this is not seen in the NACA data where vortex drag is not present for a wing of infinite span.

As the altitude of the NACA 0012 decreases the ground effect data starts to resemble the infinite aspect ratio data obtained by NACA. This illustrates how the flow around the NACA 0012 is becoming two dimensional with a reduction in altitude.

5.3.2 Behaviour of Zero Lift Drag In Ground Effect

The drag polar for the DHMTU section is shown in Figure 5-4, for clarity not all the altitudes between h/c 2.3 to 0.1 are shown. This graph illustrates that the zero lift drag (C_{D0}) increases as altitude decreases from an OGE altitude of h/c 2.3. The zero lift drag coefficient can be read from Figure 5-4 where the value of the lift of the section is zero. This change in C_{D0} would be due to the increase in skin friction and pressure drag as a result of ground proximity. The data obtained

for the NACA 0012 confirms this trend where the zero lift drag also increases with decreasing altitude (Figure 5-5).

A comparison between the DHMTU and NACA 0012 sections show that the DHMTU generates greater values of zero lift drag (Figure 5-6). The trough at h/c 0.3 for the NACA 0012 is the result of experimental error. It is otherwise unclear why CD_0 would suddenly decrease at this altitude. As the extreme ground effect altitude of h/c 0.1 is approached the NACA 0012 can be seen to possess a much greater increase in the rate of CD_0 than the DHMTU section.

Compared to the NACA 0012 the DHMTU possesses between 1.3 to 2.8 times CD_0 throughout the whole altitude range tested. This is not unsurprising, as the NACA 0012 is a much more streamlined aerofoil section and the DHMTU profile is quite bluff. The greatest difference occurs at h/c 1.0 where the DHMTU produces 2.8 times more zero lift drag than the NACA 0012. The general trend is for the difference in CD_0 between the two sections to narrow as altitude decreases. This results in the DHMTU only producing 1.3 times CD_0 than the NACA 0012 in extreme ground effect (h/c 0.1). This can be explained by the differences in CD_0 behaviour between the two sections as altitude decreases. The values of CD_0 for the NACA 0012 increase by a factor of two between moderate (h/c 1.0) and extreme ground effect (h/c 0.1). Conversely in extreme ground effect (h/c 0.1) the DHMTU possesses 90% of CD_0 obtained at h/c 1.0.

The ratios of zero lift drag in ground effect to the out of ground effect for both aerofoils are shown in Figure 5-7. It can be seen that the zero lift drag increase for the DHMTU varies much less than the NACA 0012 with decreasing altitude. This is especially noticeable as the NACA 0012 approaches the extreme ground effect regime (h/c 0.1) where a rapid increase in the CD_0 of the NACA 0012 occurs below an altitude of h/c 0.2. As in Figure 5-6 the value at h/c 0.3 is most likely a result of experimental error. Compared to operation out of ground effect the zero lift drag of the NACA 0012 and DHMTU increase by a peak factor of 2.2 and 1.5 respectively when in extreme ground effect (h/c 0.1).

At low angles of attack the DHMTU aerofoil operating out of ground effect produces less overall drag than when it is in ground effect. This can be seen in Figure 5-8 where even when in extreme ground effect (h/c 0.1) the overall drag is still greater than compared to OGE. The data at h/c 0.1 does not exceed an angle of attack of 5 degrees due to the proximity of the ground. It can be seen from Figure 5-8 that above an altitude of h/c 0.2 and angle of attack of 6 degrees, less overall drag is produced than when OGE. As the altitude increases the angle of attack that this occurs at increases. Until at h/c 0.8 the drag is greater in ground effect over the whole angle of attack range tested. This behaviour is a result of the zero lift drag increasing and a decrease in the vortex drag reduction factor. When the NACA 0012 is operating in extreme ground effect (h/c 0.1) a rapid rise in overall drag results below an angle of attack of 2 degrees (Figure 5-9).

Figure 5-10 depicts the fraction of the drag that comprises C_{D0} for both sections as a function of altitude for an angle of attack of 5 degrees. When the DHMTU is OGE (h/c 2.3) 73% of the drag comprises C_{D0} the remaining 27% vortex drag. The NACA 0012 exhibits the opposite distribution with 38% C_{D0} and 62% vortex drag. The fact that the DHMTU possesses a greater proportion of C_{DO} is not unsurprising, as the NACA 0012 is a more streamlined section. When the DHMTU section moves into moderate ground effect (h/c 1.0 to 0.2) this distribution of drag is equally divided between the zero lift and vortex drag. The NACA 0012 exhibits a similar pattern with 40-50% of the drag comprising zero lift drag.

The division between zero lift and vortex drag exhibits a mild fluctuation down to an altitude of h/c 0.3 for both sections. Once the sections enter the extreme ground effect regime there is a distinct increase in the proportion of C_{DO} with peak values being obtained at h/c 0.1. Upon entering extreme ground effect (h/c 0.1) the proportion of C_{D0} increases to 60% for the DHMTU and 74% for the NACA 0012. This illustrates the increasing proportion of CD_0 in the overall drag and a significant reduction of vortex drag when operating at altitudes at or less than h/c 0.3.

5.3.3 Behaviour of Vortex Drag In Ground Effect

Figure 5-4 illustrates that though the zero lift drag is lower when the DHMTU operates OGE, the value of the vortex drag is much greater with increasing lift when OGE. This can be seen by comparing the gradient of the curve when h/c 2.3 and h/c 0.1. The behaviour of the vortex drag for each section is presented in Figure 5-11. Evident from these results is the reduction in vortex drag with decreasing altitude for both aerofoils. To illustrate the reduction in vortex drag whilst operating in ground effect a vortex drag reduction factor Φ is introduced as shown in equation 5-2.

Figure 5-12 illustrates the experimental drag reduction factors as a function of altitude for the DHMTU and NACA 0012 aerofoil sections. It can be seen that a significant reduction in vortex drag is achieved when operating in ground effect. An important result is that the drag reduction factor is independent of the aerofoil section. This allows the theoretical predictions of vortex drag reduction discussed below, to be employed with confidence.

At h/c 1.0 no reduction in vortex drag is experienced by the section compared to OGE operation. As the wing reduces in altitude to h/c 0.5 the aerofoils are only experiencing 70% of OGE vortex drag. When the altitude decreases down to extreme ground effect (h/c 0.1) the DHMTU only experiences approximately 20% of OGE vortex drag. The NACA 0012 aerofoil also conforms to this behaviour with little appreciable difference between the sections.

A theoretical method to analyse this reduction in vortex drag is to consider the horseshoe vortex model in close proximity to the ground. The horseshoe vortex is a representation of a wing in flight; the circulation around the wing that results in lift is represented by a bound vortex with the trailing vortices due to spanwise flow originating from the end of the bound vortex. The bound vortex is a theoretical representation that replaces the wing whilst the trailing vortices physically exist. A vortex represents circulatory flow and is a fundamental tenet of aerodynamics; the reader unfamiliar with this subject area is referred to the standard aerodynamic texts such as Houghton [43].

It should be noted that there is a starting vortex associated with the initial acceleration of an aerofoil. This starting vortex is soon left behind and the trailing vortices effectively stretch to infinity as steady flight proceeds. In practice only the bound and trailing vortices are considered in analysis.

To analyse the effect of the ground on the vortex drag a horseshoe vortex is placed at a height 'h' with the ground replaced by an inverted horseshoe vortex at a distance h below ground level (Figure 5-13). Note that the vortices of the image wing are of opposite direction to the 'real' horseshoe vortex.

The circulation from each vortex acts along the wing's upper surface in an opposite manner to the real wing's vortices. This is shown in Figure 5-14 where the trailing vortices of the image wing are acting on the real wing at a position y from the centre span.

There are two main approaches considered in literature that employs the horseshoe vortex model, McCormick [44] and Houghton [43]. McCormick considers the ratio of downwash on the real wing due to the real wing's vortices at midspan with the downwash produced by the image trailing vortices at centre span. This leads to McCormicks vortex drag factor

$$\Phi_{\text{McCormick}} = \left[\frac{\left(\frac{16h}{\pi b}\right)^2}{1+\left(\frac{16h}{\pi b}\right)^2} \right] \qquad \text{Equation 5-4}$$

Where h is the wing's height above the ground and b is the wingspan.

This expression is found in many aeronautical textbooks on discussions of vortex drag reduction. The reader should note that in McCormick's textbook [44] a misprint has resulted in the π term being left out of the equation. This can be checked by comparing the drag reduction factor in equation 5-4 with the graph

(Figure 7.4) in McCormicks book. The correct derivation of McCormick's drag reduction factor is presented in Appendix B of this thesis.

The advantage of McCormick's drag reduction factor is that it is relatively straightforward to derive but only considers the change in downwash at the midspan of the wing. The alternative approach presented by Houghton considers the downwash along the whole wingspan (equation 5-5). It is a rather more involved process to derive this equation and is also presented in Appendix B.

$$\Phi_{\text{Houghton}} = \left[1 - \frac{2}{\pi^2} \ln\left[1 + \left(\frac{\pi b}{8h}\right)^2\right]\right] \qquad \text{Equation 5-5}$$

Figure 5-15 compares McCormicks and Houghton's drag reduction factor as a function of h/b (height/wingspan) with experimental data obtained during this research. It can be seen that compared to the experimental data both of the expressions overestimate the reduction in vortex drag. McCormick provides the greatest overestimation of the reduction in drag. This is because McCormick's formulation only considers the downwash acting at the centre of the wingspan. He does not take into account the spanwise distribution of the load. As the altitude reduces below half the wingspan McCormick and Houghton start to show a strong variation. It can be seen from the graph that when h/b is less than 0.04 Houghton's drag reduction factor becomes negative. This is physically impossible and must be borne in mind if applying Houghton's formulation at very low altitudes.

Suh and Ostowari [46] have modified Houghton's drag reduction formulation by including a span efficiency factor 'e' resulting in equation 5-6. The value of e is 1 for elliptical wings and between 0.5 to 1 for most common wing shapes. The wing efficiency factor is an adjustment for the spanwise loading due a non-ideal wing planform. An elliptical spanwise lift distribution is produced by an elliptical wing planform but this is expensive to manufacture and a taper is introduced into the planform instead.

$$\Phi_{\text{Suh+Ostowari}} = \left[1 - \frac{2e}{\pi^2} \ln\left[1 + \left(\frac{\pi b}{8h}\right)^2\right]\right]$$ Equation 5-6

It can be seen from Figure 5-15 that when e is set to 0.8 it produces a close approximation to the experimental results below h/c 0.8. The problem with including the span efficiency factor is that it can only be evaluated by flight, CFD or wind tunnel tests. The value of e will vary with wing planform shape as well as proximity to the ground.

In summary Houghton's method (equation 5-5) provides a more accurate description of the reduction in vortex drag than McCormick (equation 5-4). It is recommended that this formulation be applied to assess vortex drag reduction in any study. Though Houghton's method should be treated with caution if applied to altitudes less than h/b 0.04. Suh and Ostowari's modification of Houghton's equation (equation 5-6) does match experimental data when e=0.8 for the wing tested but this will vary with wing planform. This modification of Houghton is applicable if a priori knowledge of the span efficiency factor 'e' is available.

As a wing reduces in altitude the magnitude of the downwash velocity from the wingtip vortices is reduced due to the constraining influence of the ground plane. This results in a reduction of vortex drag and a resultant increase in wing planform efficiency. This increase in planform efficiency can be quantified by an increase in the effective aspect ratio (ARe) of a wing. From equations 5-2 and 5-3 it can be seen that a reduction in vortex drag results in an increase in the effective aspect ratio. As the vortex drag is reduced the effective aspect ratio is increased indicating that the flow is becoming more two-dimensional.

5.3.4 Behaviour of Effective Aspect Ratio In Ground Effect

Figure 5-16 illustrates the effect that decreasing altitude has on the effective aspect ratio of the DHMTU and NACA 0012 sections. The trend for increasing aspect ratio as the altitude decreases can be seen. The effective aspect ratio at h/c 1.0 is approximately equal to the geometric value of the wing when it is

operating OGE. It can be seen that the NACA 0012 possesses lower effective aspect ratio than the DHMTU aerofoil.

When operating in extreme ground effect (h/c 0.1) both sections posses effective aspect ratios of around 14. This is nearly five times the geometric aspect ratio of the sections. The DHMTU was also tested at an altitude of h/c 0.08 where an effective aspect ratio of 20 was achieved, nearly 7 times that of the geometric value.

5.4 Effect of Ground Conditions and Reynolds Number on Drag In Ground Effect

As discussed in chapter 2 previous research showed that the correct ground conditions at low altitudes is important. Though no mention was made of the effect that this had on the drag. Figure 5-17 illustrates the effect of turning the wind tunnel road off on the drag at an altitude of h/c 0.1. The stationary surface has a negligible effect on the zero lift drag coefficient, it increases by only 0.2% of the moving ground value. At higher lift coefficients the vortex drag increases when the road is stationary. This leads to a reduction of the effective aspect ratio from 13.7 to 10.9. This translates to a 20% reduction in effective aspect ratio and increase in vortex drag due to the stationary ground.

The reduction in Reynolds Number produces an increase in the drag characteristics of the DHMTU (Figure 5-17). When the Reynolds number is reduced by 50% to 430,000 the zero lift drag coefficient increases by 1%. Even when the Reynolds number is reduced down to 130,000 CD_0 only increases by 4% (Table 5-1).

As can be seen from Figure 5-17 the vortex drag of the DHMTU at Reynolds Number 130,000 exhibits a rapid increase in vortex drag. This reduces the effective aspect ratio of the wing in extreme ground effect near to the actual geometric aspect ratio (Table 5-2). The general trend is that a decrease in Reynolds Number results in an increase in the zero lift and vortex drag components of the wing.

5.5 Lift in Ground Effect

On approaching the ground the magnitude of the lift produced by both the DHMTU and NACA 0012 aerofoil increases. The proximity of the ground also has the effect of increasing the gradient of the lift curve $dC_L/d\alpha$ of both sections. There is indirect evidence that the stall angle of the sections reduces with a decrease in altitude. This is a result of the effective aspect ratio of the wing increasing with a reduction in altitude (see section 5.3.3). As the aspect ratio of a wing increases the gradient of the lift curve slope decreases and the angle of maximum lift (stall angle) reduces. This can be seen in Figure 5-18 where at an altitude of h/c 0.4 maximum C_L is obtained at 11 degrees AoA, by implication the stall angles for higher altitudes were not seen as they occurred at higher angles of attack. Stall behaviour was not observed at lower altitudes due to the ground clearance constraint on angle of attack.

The lift behaviour of the NACA 0012 in ground effect is presented in Figure 5-19. A major difference between the two aerofoils is that at low angles of attack the NACA 0012 produces a downward force. The angle of attack below that this downward force occurs increases with decreasing altitude (Table 5-3).

As both sections approaches the ground the lift curve slope gradient ($dC_L/d\alpha$) increases (Table 5-4). At h/c 1 a value of $dC_L/d\alpha$ of 4 is obtained for the DHMTU, as the section reaches extreme ground effect this increases to 10 radian^{-1} to 15 radian^{-1}. This can be compared to the lift curve slope gradient of the NACA 0012 that possesses similar values except in extreme ground effect (h/c<0.1).

One consequence of the increase in lift curve slope gradient at very low altitudes (h/c<0.1) is large variation in lift that results from small variations in angle of attack. This would be a major consideration in the design of the flight control system of a WIG vehicle.

Figure 5-20 presents the ratio of lift in ground effect to the lift out of ground effect (h/c 2.3) as a function of altitude for both aerofoils. At the margin of moderate ground effect (h/c 0.9-1.0) both aerofoils generate a marginal increase in lift over

the OGE value, typically a value of 1.05 CL_{OGE} is achieved. As the altitude decreases the lift increases relatively steadily for both sections. The data at h/c 0.7 and 0.8 for the NACA 0012 indicates that the lift reduces below the OGE value.

From the small increase in lift at h/c 0.9 to 1.0 the lift of the DHMTU increases to $1.64CL_{OGE}$ at an altitude of h/c 0.2. In the extreme ground effect regime of h/c 0.1 the DHMTU lift doubles over its OGE value to $2.1CL_{OGE}$. It is evident fromFigure 5-20 that the DHMTU aerofoil consistently produces a greater increase in lift when in ground effect compared to the NACA 0012 aerofoil. This indicates that aerofoil geometry determines the increase in ground effect lift.

Figure 5-21 illustrates the comparison in lift performance of the NACA 0012 and DHMTU sections between h/c 0.2 to 0.1. The DHMTU section has superior lift characteristics between altitudes of h/c 0.1 to 1. As discussed earlier when the NACA 0012 is at h/c 0.1 large downward forces are produced when the angle of attack reduces below 3 degrees. These large downward coefficients are probably a result of the suction effect caused by the lower surface and the flat ground surface. These suction forces can be seen to be present at h/c 0.2 and 0.3 but they are less dominant. The superior lift performance of the DHMTU IGE can be ascribed to the favourable interaction between the geometry of the lower section and ground. This illustrates the importance of optimally designing the aerofoil geometry of the section for operation IGE.

Table 5-5 illustrates the superior lift producing capability of the DHMTU over the NACA 0012 at an AoA of 5 degrees. It can be seen that the DHMTU generates between 1.4 to 2.1 times the lift of the NACA 0012 when operating IGE.

One of the requirements for a ground effect section is for dC_L/dH to be gradual. Figure 5-22 and Figure 5-23 illustrates the variation in C_L with altitude for the DHMTU and NACA 0012. In extreme ground effect the NACA 0012 produces a reduction of lift with decreasing altitude at AoA less than 3 degrees. The magnitude of dC_L/dH for the NACA 0012 becomes more negative with decreasing angle of attack. At AoA of 1 degree C_L decreases by a factor of 5.3

between h/c 0.2 to 0.1. At AoA of 4 and 5 degrees the ram ground effect produces an increase in C_L. The DHMTU produces a negative gradient only at AoA 1 degree. As the AoA increases dC_L/dH for the DHMTU increases in magnitude at the operating AoA C_L increases by 1.3 times between h/c 0.2 to 0.1.

No discernible effect of Reynolds Number on the lift of the sections can be quantified (Figure 5-24).

5.6 Aerodynamic Efficiency

The lift to drag (L/D) ratio or aerodynamic efficiency of the DHMTU aerofoil operating in ground effect is shown in Figure 5-25. A decrease in operating altitude results in a significant increase in the L/D ratio. When operating out of ground effect the DHMTU aerofoil possesses a L/D of 8.4. When the wing is in the moderate ground effect height regime the peak L/D increases between 12.7 (h/c 0.5) to 16.5 (h/c 0.2). As the aerofoil descends to the extreme ground effect altitude of h/c 0.1 the peak L/D ratio has nearly doubled to 22. Reducing the altitude to h/c 0.08 results in a further increase in L/D to 23.1 though the maximum angle of attack that could be achieved at this height was 3 degrees. It is also of interest to note that when the altitude is h/c 0.08 no useful performance is obtained below an angle of attack of 0.5 degree.

The data also illustrates that when the DHMTU is operating in extreme ground effect the L/D reduces at a much greater rate with AoA than when in moderate ground effect. When a WIG craft is cruising in extreme ground effect large variations in the L/D will be produced for small changes in angle of attack. For example if cruising at an altitude of h/c 0.08 a L/D of 18 is achieved at 2 degrees angle of attack. If the angle of attack were reduced to 1 degree the L/D would reduce to approximately 5, a 72% reduction in aerodynamic efficiency.

This illustrates a disadvantage for a WIG craft cruising in extreme ground effect. To maintain the beneficially high L/D obtained within this altitude regime the aerofoils angle of attack would have to be maintained within very fine tolerances. It can be seen from Figure 5-25 that if a WIG craft were operating in moderate

ground effect, say h/=0.4, very accurate maintenance of angle of attack would not be such a prerequisite.

The aerodynamic efficiency of the NACA 0012 aerofoil operating in ground effect is shown in Figure 5-26. The NACA 0012 produces peak L/D in excess of the DHMTU at h/c 0.2 and 0.3 and comparable at 0.1 (Table 5-7). This however is not the only measure of performance of the sections as an inspection ofFigure 5-27 reveals. The efficiency curves of the NACA 0012 shows that the section provides little or no performance at small angles of attack. This is of significance as at low altitudes only small angle of attacks are realisable due to the proximity of the ground. At h/c 0.1 the NACA 0012 L/D provides no performance below AoA of 2.5 degrees. This also occurs at h/c 0.2 where below AoA of 1.5 degrees the NACA 0012 possesses no performance. Slight changes in AoA for NACA 0012 when operating in extreme ground effect will result in radically different performance.

At the low Reynolds Number aerodynamic efficiency is reduced from 22 at Re 8.3 x 10^5 to 10.5 at Re 1.3 x10^5 (Figure 5-28). This is a result of the rapid increase in drag at AoA 1 degree as illustrated in Figure 5-17.

5.7 Summary

1. The overall drag (C_D) of both the DHMTU and NACA 0012 aerofoils is greater in ground effect than out of ground effect. This is an important result, as wing in ground effect flight does not result in the reduction of overall drag for the two sections tested. The reason for this is the increase in the zero lift component of drag (C_{D0}). The ground effect values of zero lift drag of the NACA 0012 and DHMTU increase by a factor of 2.2 and 1.5 respectively over there out of ground effect values. This research has shown that the CD_0 of an aerofoil section operating in the ground effect regime can be upto double its out of ground effect value.

2. A significant reduction in the vortex drag (CD_V) of the aerofoils is produced as a result of flying in ground effect. When operating in the extreme ground effect regime (h/c 0.1) the aerofoil sections tested will typically possess only 20% of the out of ground effect vortex drag. Even flying in moderate ground effect will result in considerable vortex drag reduction. Flying at an altitude of h/c 0.5 will result in a wing possessing 70% of OGE vortex drag. These experiments have indicated that the vortex drag reduction factor is independent of aerofoil geometry. With the knowledge of a sections OGE drag characteristics accurate estimates of the magnitude of IGE vortex drag can be obtained. Unfortunately the significant reduction in vortex drag coupled with the increase in the zero lift drag is not sufficient enough to reduce the overall drag of the trial sections in ground effect.

3. When operating in extreme ground effect (h/c 0.1) both aerofoils posses an effective aspect ratio of approximately 14 compared to their geometrical aspect ratio of 3. As the altitude of the DHMTU reduced to h/c 0.08 the effective aspect ratio increased to 20.

4. When the DHMTU is out of ground effect 73% of the overall drag is composed of zero lift drag and 27% is vortex drag. As the altitude of the section decreases to the upper limit of moderate ground effect regime

(h/c 1) this division reduces to 50% zero lift and vortex drag. When the section is operating in extreme ground effect (h/c 0.1) the zero lift drag increases to 61% of the overall drag with the vortex component reducing to 39% of the total drag. The reduction in vortex drag is compensated for by an increase in zero lift drag. This illustrates that a WIG craft designer cannot expect a reduction in overall drag when flying in ground effect.

5. As the altitude of both the aerofoils decreases the lift increases. There is a noticeable demarcation between the moderate ground effect regime of h/c 1.0–0.2 and operating in extreme ground effect (h/c<0.1). This is indicated by an increase in the gradient of the lift curve slope $dC_L/d\alpha$ with a reduction in altitude. The DHMTU and NACA 0012 exhibit similar values of $dC_L/d\alpha$ in moderate ground effect, with the DHMTU possessing higher $dC_L/d\alpha$ in extreme ground effect. A dramatic increase in the lift curve slope gradient is evident when the altitude reduces to h/c 0.1. At this altitude the value of $dC_L/d\alpha$ for the DHMTU has increased to 10 units/radian from 5 units/radian at h/c 0.3.

6. In the moderate ground effect region the lift of the DHMTU increases from $1.05CL_{OGE}$ (h/c 1.0) to 1.64 CL_{OGE} (h/c 0.2). When operating at extreme ground effect altitudes h/c<0.1 the lift increases by over twice the lift generated out of ground effect. The DHMTU aerofoil generates greater lift than the NACA 0012, upto 1.6 times the lift in extreme ground effect. A distinct advantage of the DHMTU aerofoil is that it generates lift at low angles of attack (<3 degrees) and extreme ground effect (h/c 0.1). This is in contrast to the NACA 0012 that generates a downward force under these conditions making it unsuitable for applications in ground effect craft.

7. The aerodynamic efficiency of both the DHMTU and NACA 0012 aerofoils increase with a reduction in altitude. When operating out of ground effect the DHMTU aerofoil produced a peak aerodynamic efficiency of 8.4. As the DHMTU enters the moderate ground regime the peak L/D is 12.7 at an altitude of h/c 0.5 increasing to 16.5 at h/c 0.2. As the DHMTU

descends to the extreme ground effect altitude of h/c 0.1 the peak aerodynamic efficiency doubles compared to the out of ground effect value to 22. In extreme ground effect at low angles of attack the L/D reduces at a much higher rate than when operating in moderate ground effect. The angle of attack of the peak aerodynamic efficiency varies between 5 to 6 degrees. The advantage of the DHMTU over the NACA 0012 is that it provides useful performance at low angles of attack when operating in extreme ground effect. The NACA 0012 aerofoil is particularly unsuited to operation in extreme ground effect due to its poor lift and drag performance at low angles of attack.

8. When operating in the extreme ground effect regime (h/c<0.1) as has been suggested by some authors the WIG craft designer needs to be aware that small changes in altitude or angle of attack result in significant variations in lift, drag and aerodynamic efficiency.

9. An increase in Reynolds Number results in an increase in zero lift and vortex drag. The variation in Reynolds Number results in no discernible effect on the lift of the DHMTU aerofoil.

Reynolds Number	CD_0
130,000	0.2952
430,000	0.2863
830,000	0.2833

Table 5-1: Zero lift drag coefficients for DHMTU at h/c 0.1

Reynolds Number	K	Effective Aspect Ratio (Ae)
130,000	0.0975	3.26
430,000	0.0242	13.15
830,000	0.0226	14.08

Table 5-2: k factor dependency on Reynolds Number

Altitude (h/c)	Angle of Attack (degrees)
1.0	0.60
0.4	1.25
0.2	1.60
0.15	2.35
0.1	2.65

Table 5-3: Angle of Attack at which downward force produced for the NACA 0012 as a function of altitude

h/c	DHMTU $dC_L/d\alpha$ (units of lift per radian)	NACA 0012 $dC_L/d\alpha$ (units of lift per radian)
2.3	3.9	3.5
1.0	4.0	3.7
0.9	4.1	3.8
0.8	4.2	3.9
0.7	4.3	4.0
0.6	4.5	4.2
0.5	4.6	4.4
0.4	4.8	4.8
0.3	5.3	5.2
0.2	6.3	7.3
0.1	9.9	12.5
0.08	15.0	N/O

Table 5-4: DHMTU and NACA 0012 Lift Curve Slope Gradient In Ground Effect

N/O Not Obtainable

H/c	DHMTU C_L/NACA 0012 C_L
1	1.5
0.9	1.4
0.8	2.0
0.7	2.1
0.6	1.6
0.5	1.7
0.4	1.8
0.3	1.7
0.2	1.6
0.1	1.6

Table 5-5: Ratio of DHMTU C_L/NACA C_L at AoA 5 degrees

Angle of Attack (degrees)	NACA 0012 $\frac{dC_L}{dH}$	DHMTU $\frac{dC_L}{dH}$
1	-3.10	-0.20
2	-2.04	0.58
3	-1.01	1.56
4	-0.74	1.47
5	-0.28	1.77
6	0.12	N/O*

Table 5-6: Variation of dC_L/dH between h/c 0.1 and h/c 0.2

*N/O Not Obtainable

h/c	DHMTU L/D	AoA (degrees)	NACA 0012 L/D	AoA (degrees)
1	8.4	6	12.9	5
0.9	9.2	6	12.0	6
0.8	10.0	5	12.3	6
0.7	11.0	5	15.1	5
0.6	11.9	5	13.8	6
0.5	12.7	6	13.9	5
0.4	12.8	6	14.3	6
0.3	14.1	5	18.7	5
0.2	16.5	6	18.4	7
0.1	22.0	5	21.5	5

Table 5-7: Comparison of peak L/D for DHMTU and NACA 0012 Sections

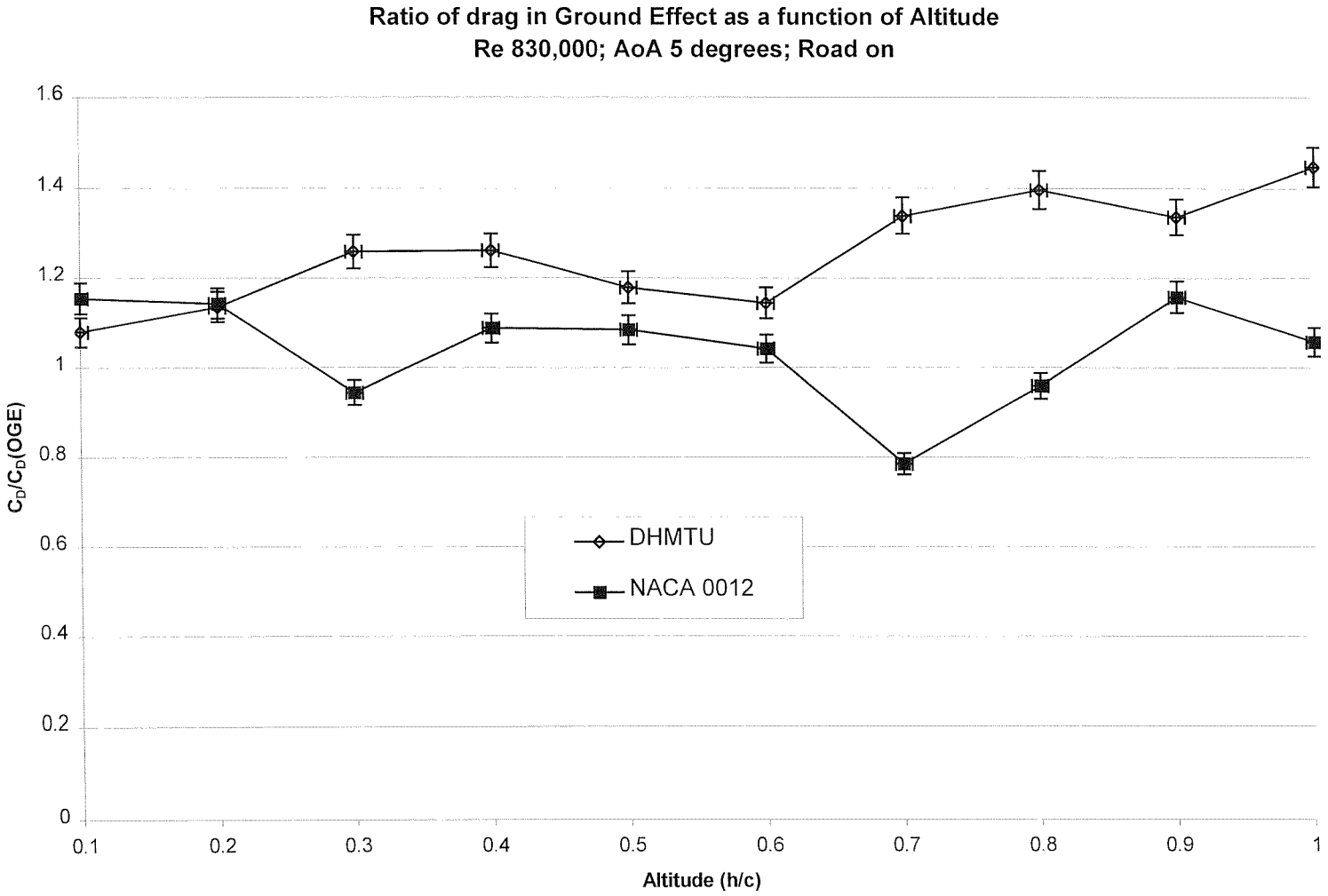

Figure 5-1: Ratio of total drag in ground effect to out of ground effect as a function of altitude

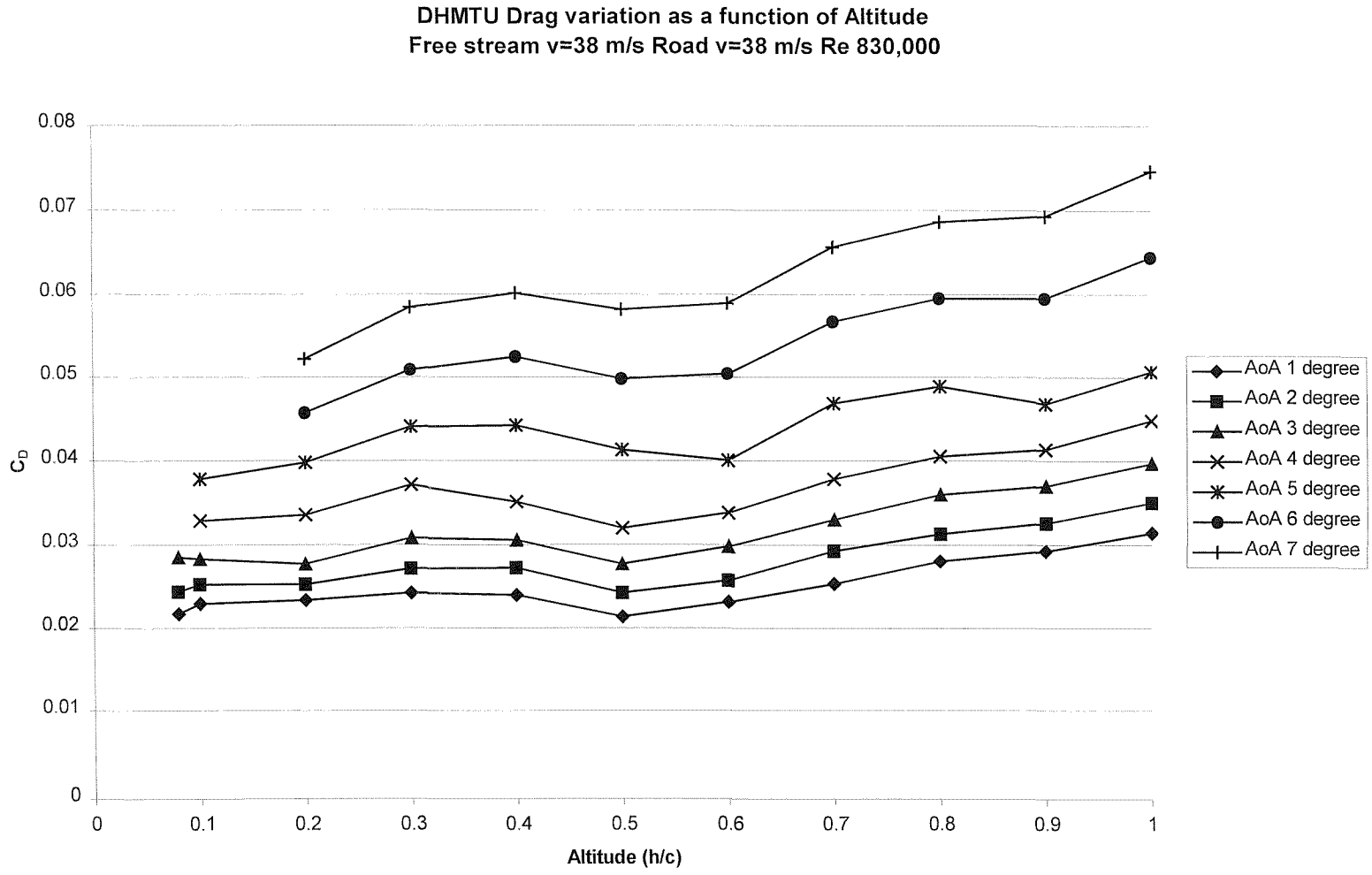

Figure 5-2: DHMTU Drag variation as a function of Altitude

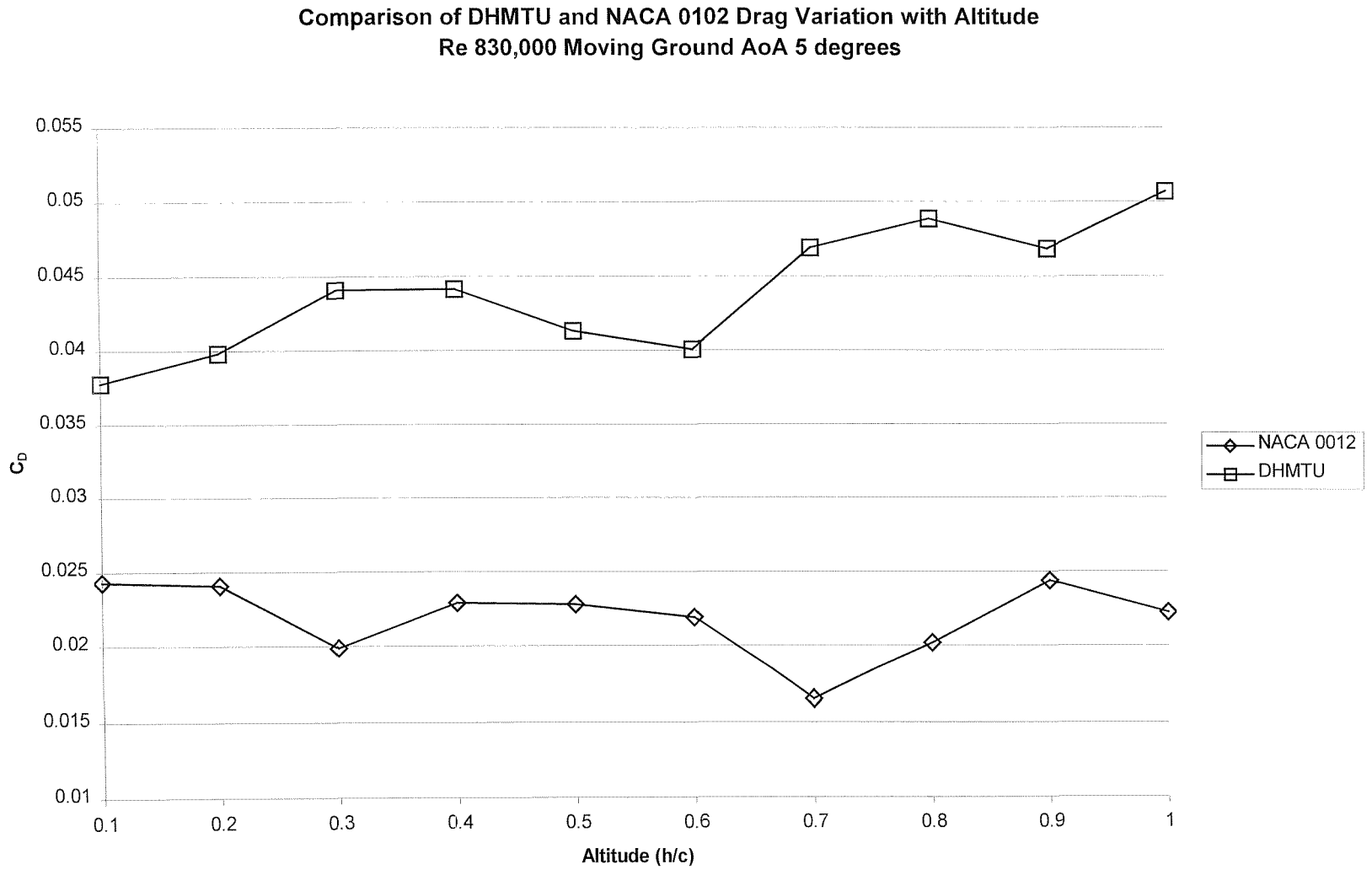

Figure 5-3: Comparison of Total Drag for DHMTU and NACA 0012 as a function of Altitude

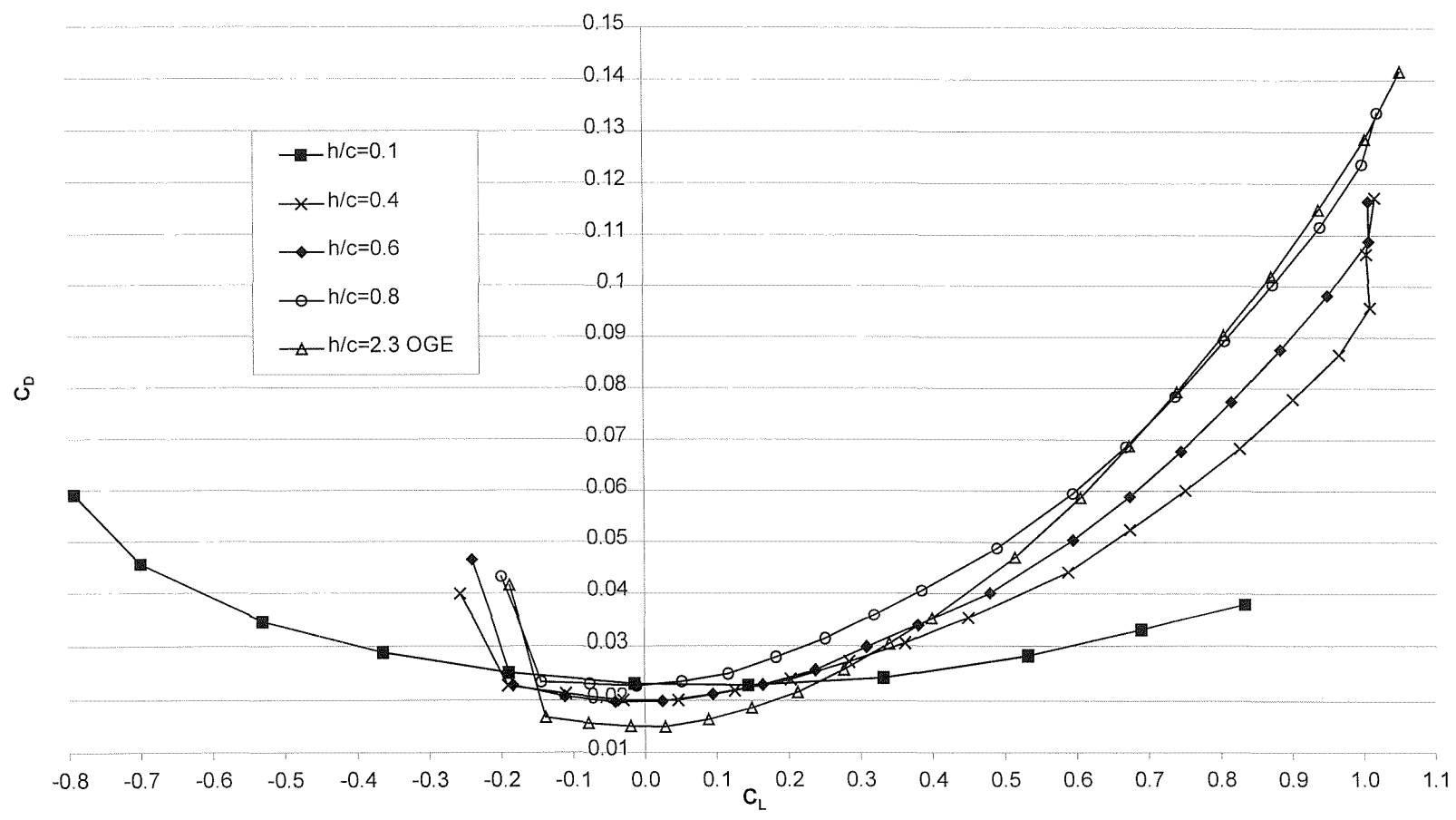

Figure 5-4: Drag Polar for DHMTU between altitude h/c 2.3 to 0.1

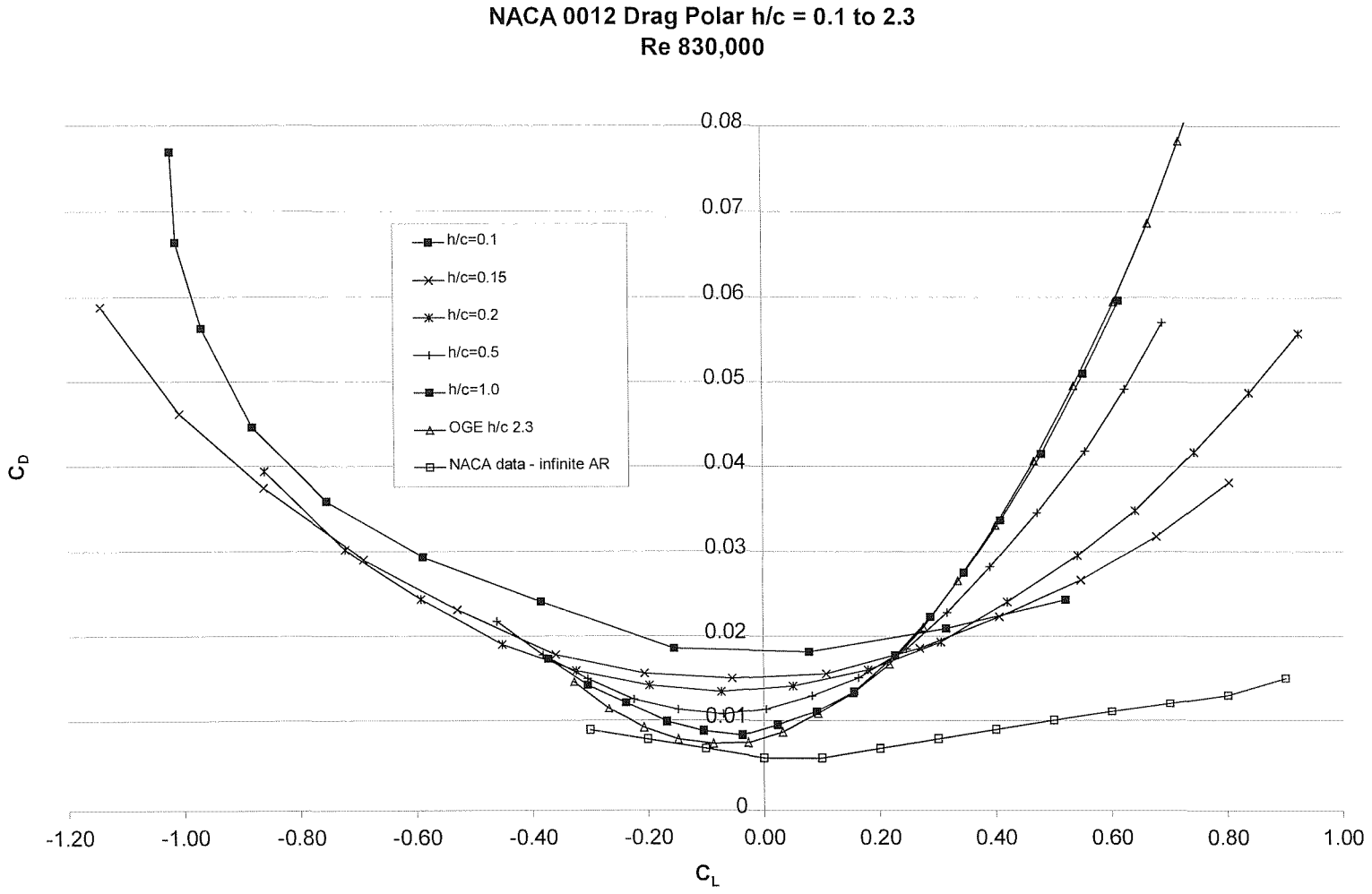

Figure 5-5: NACA 0012 Drag Polar with variation in altitude (h/c)

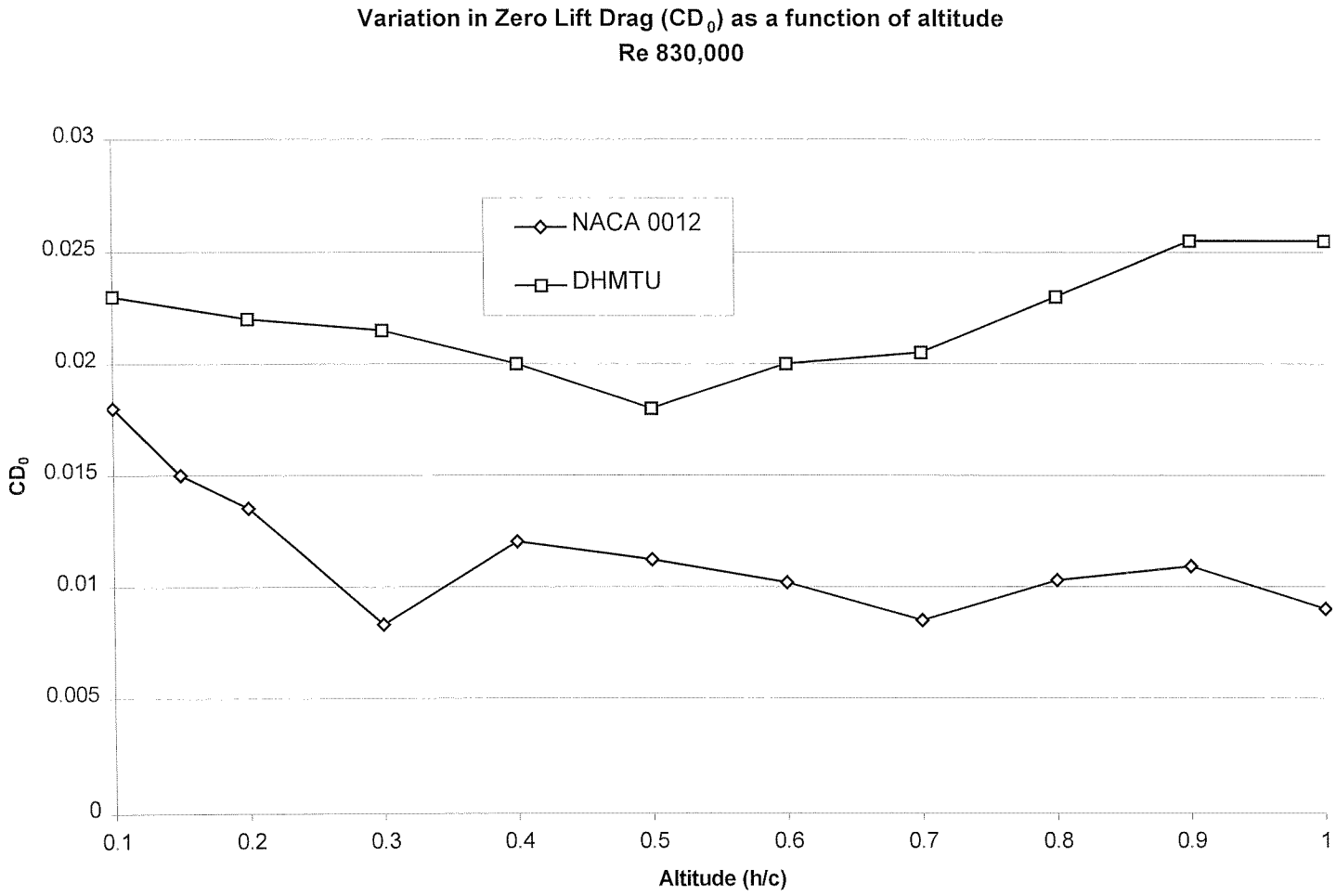

Figure 5-6: Zero lift drag factor as a function of altitude

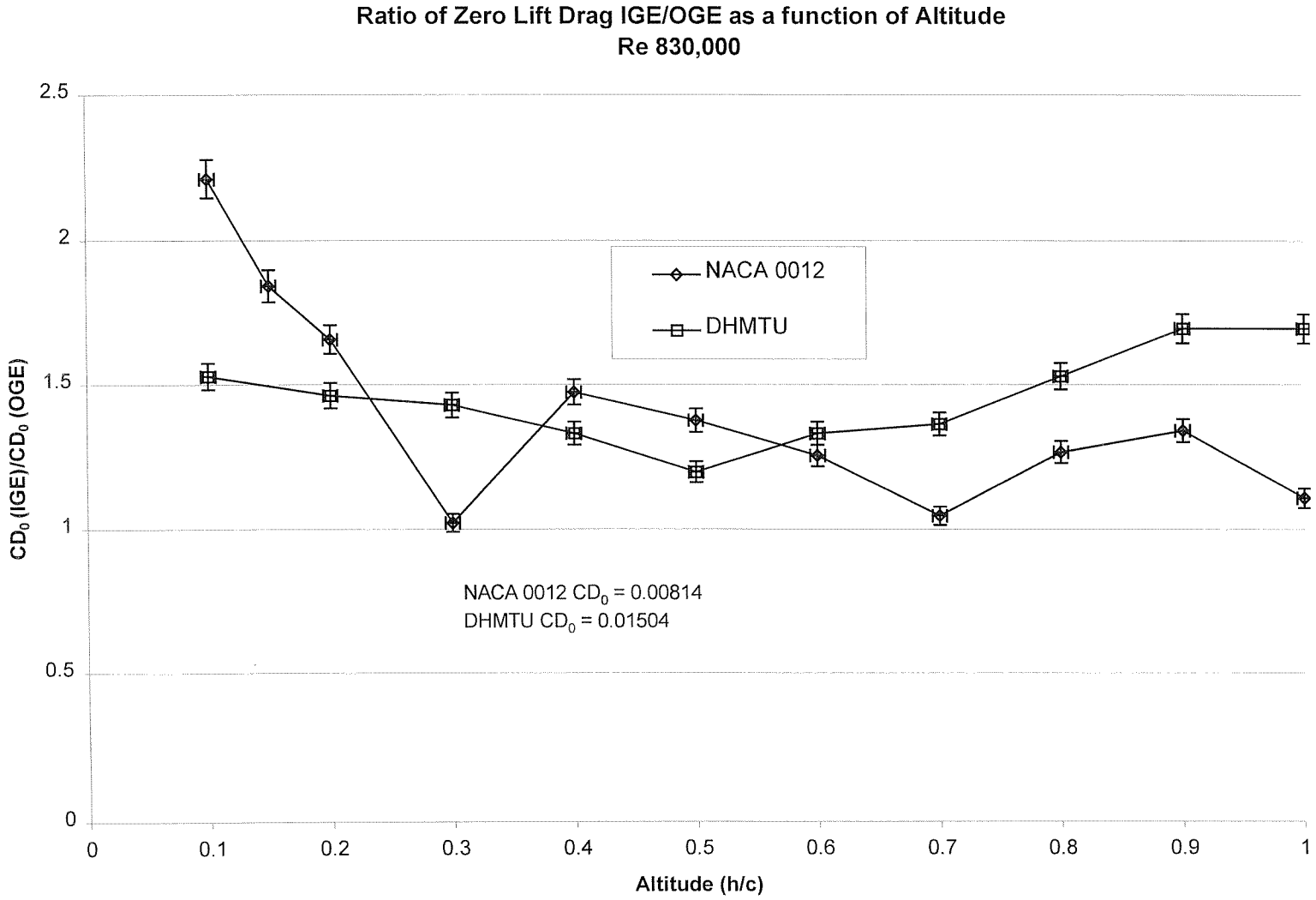

Figure 5-7: Ratio of zero lift drag in ground effect/out of ground effect as a function of altitude

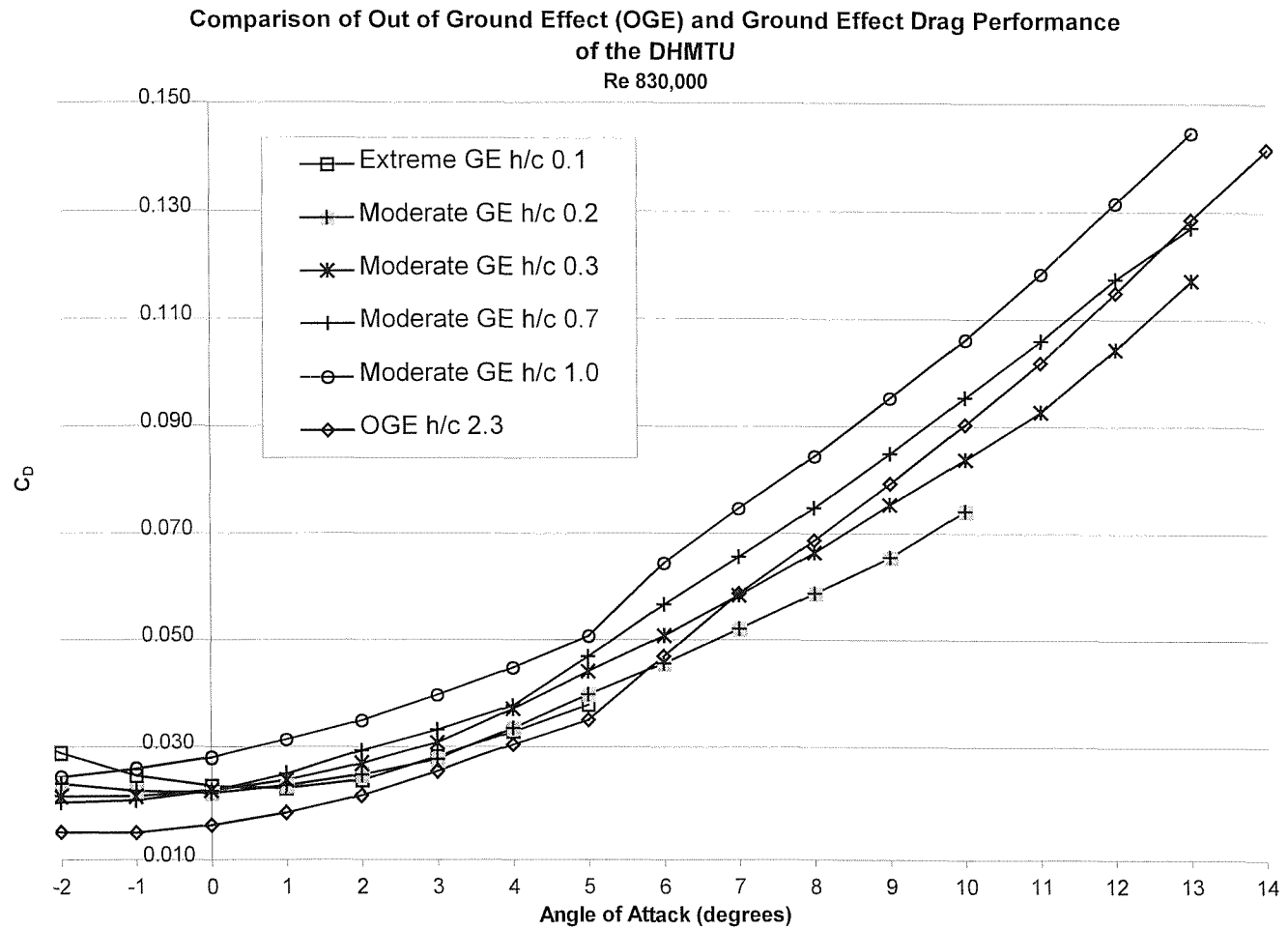

Figure 5-8: Overall drag Vs angle of attack for the DHMTU aerofoil at various altitudes

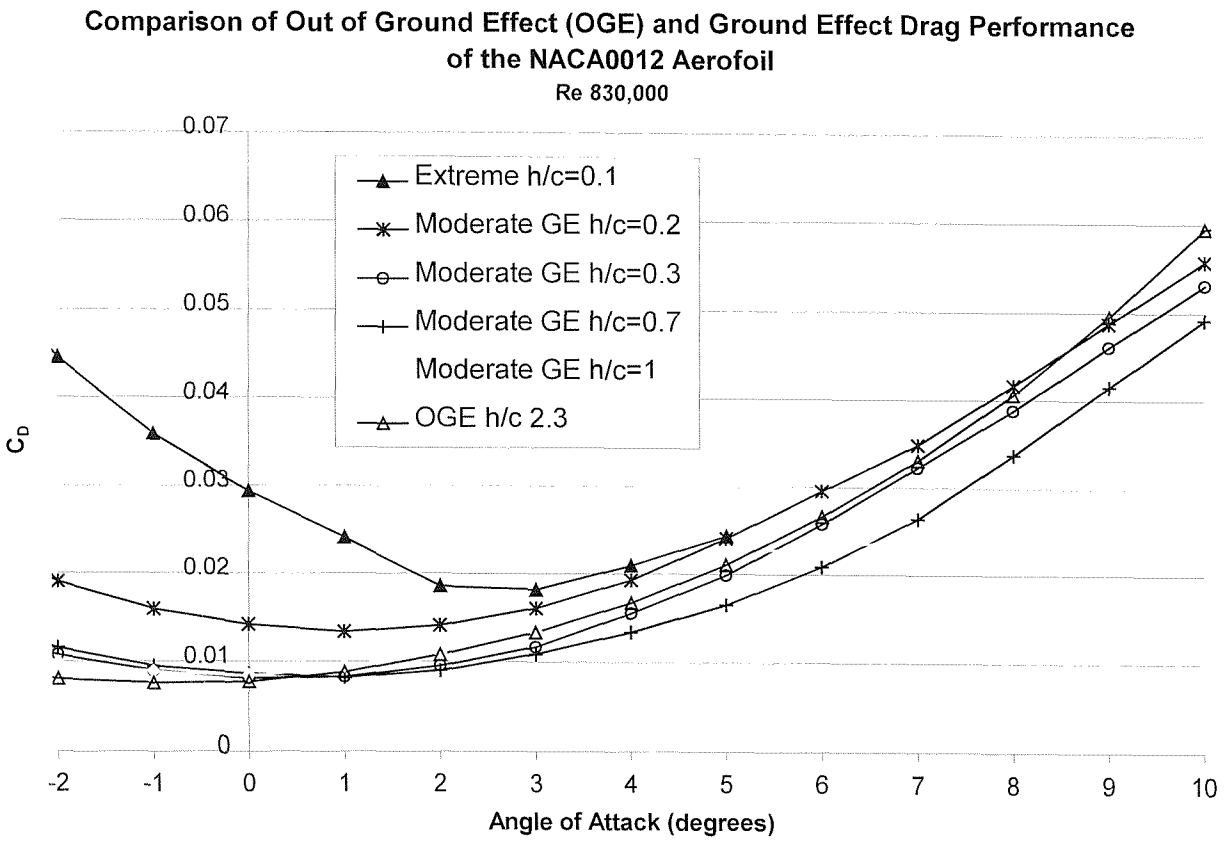

Figure 5-9: Overall drag Vs angle of attack for the NACA 0012 aerofoil at various altitudes

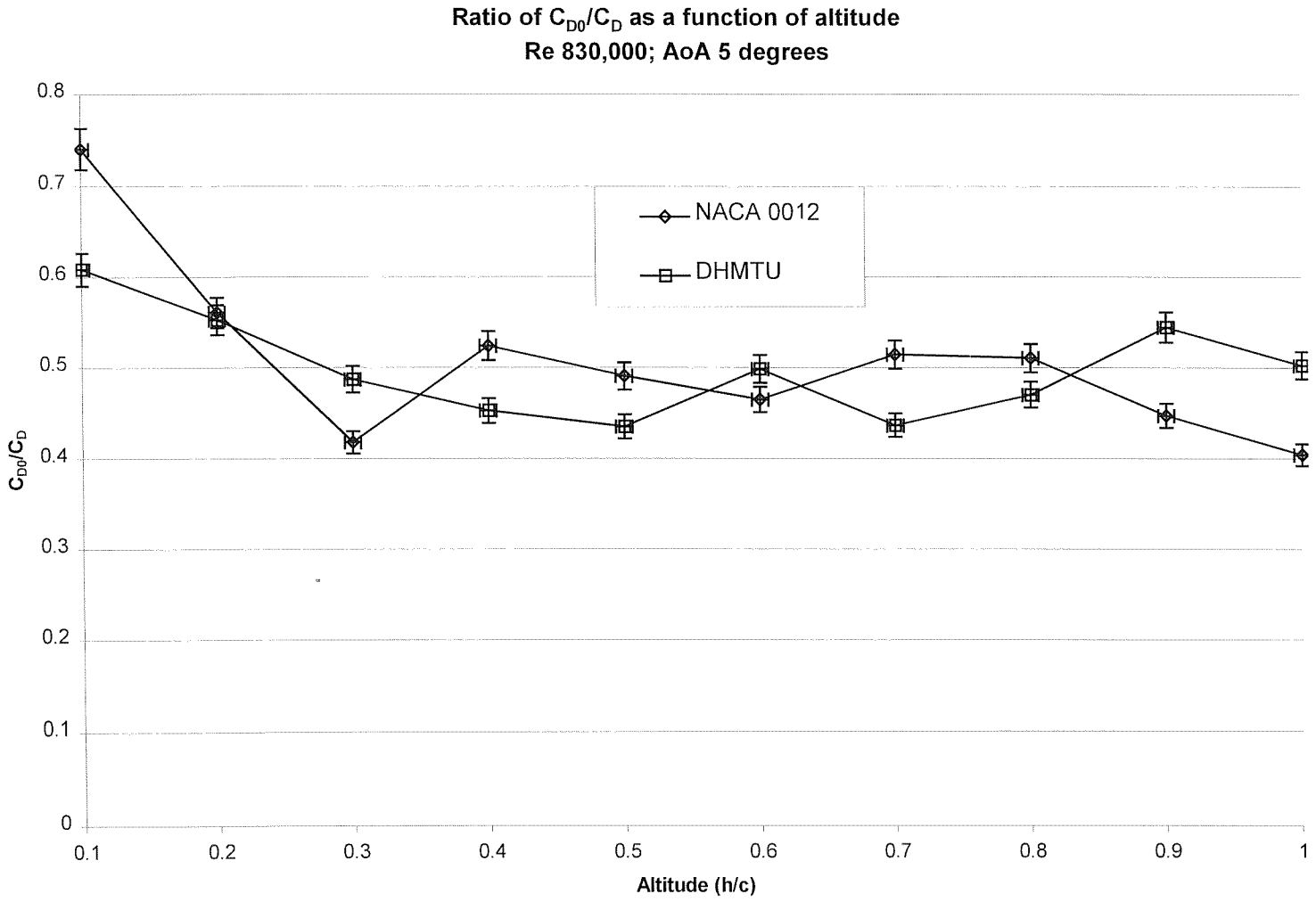

Figure 5-10: Ratio of C_{D0} to C_D as a function of altitude at an angle of attack of 5 degrees

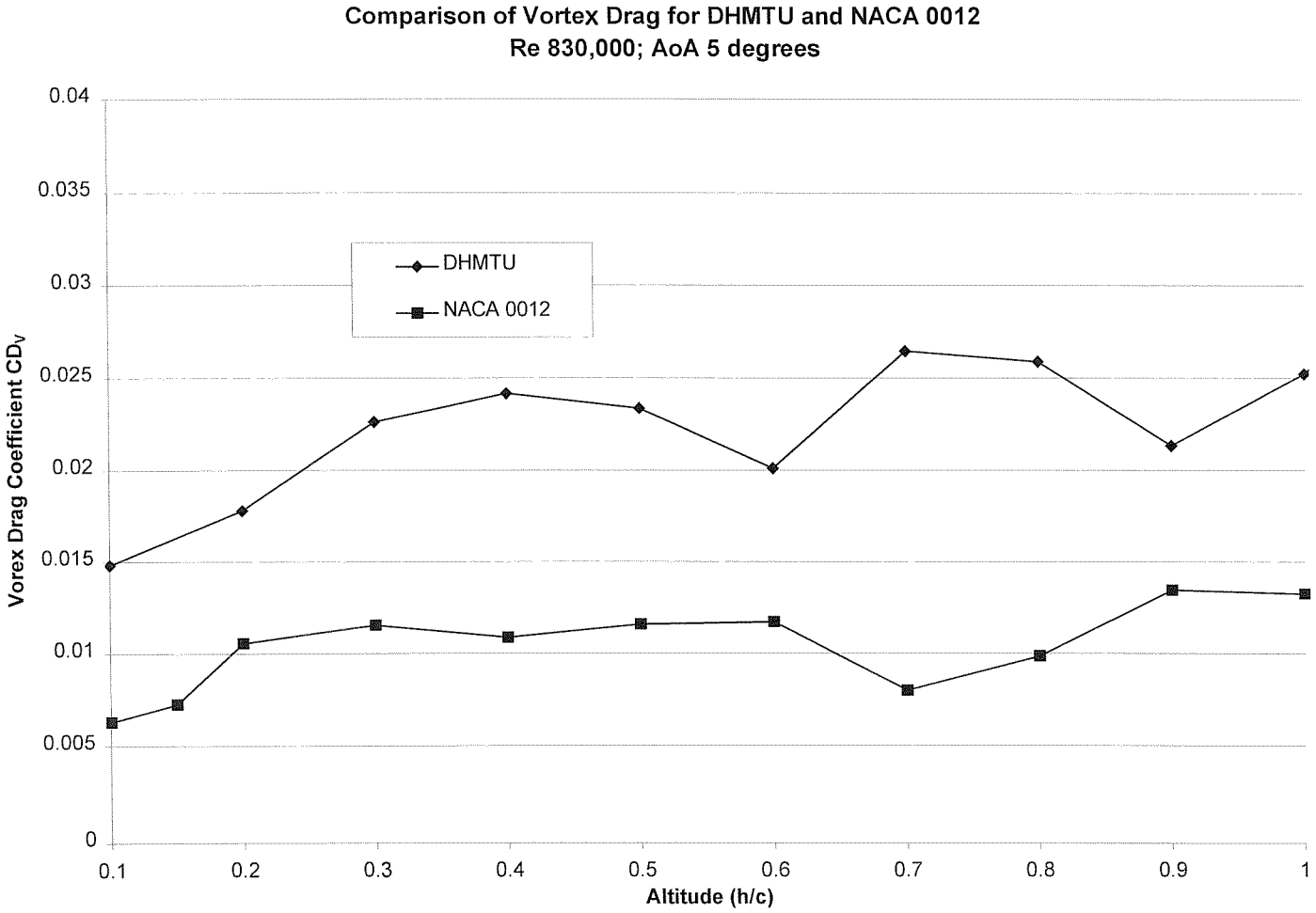

Figure 5-11: Comparison of DHMTU and NACA 0012 Vortex Drag Coefficients

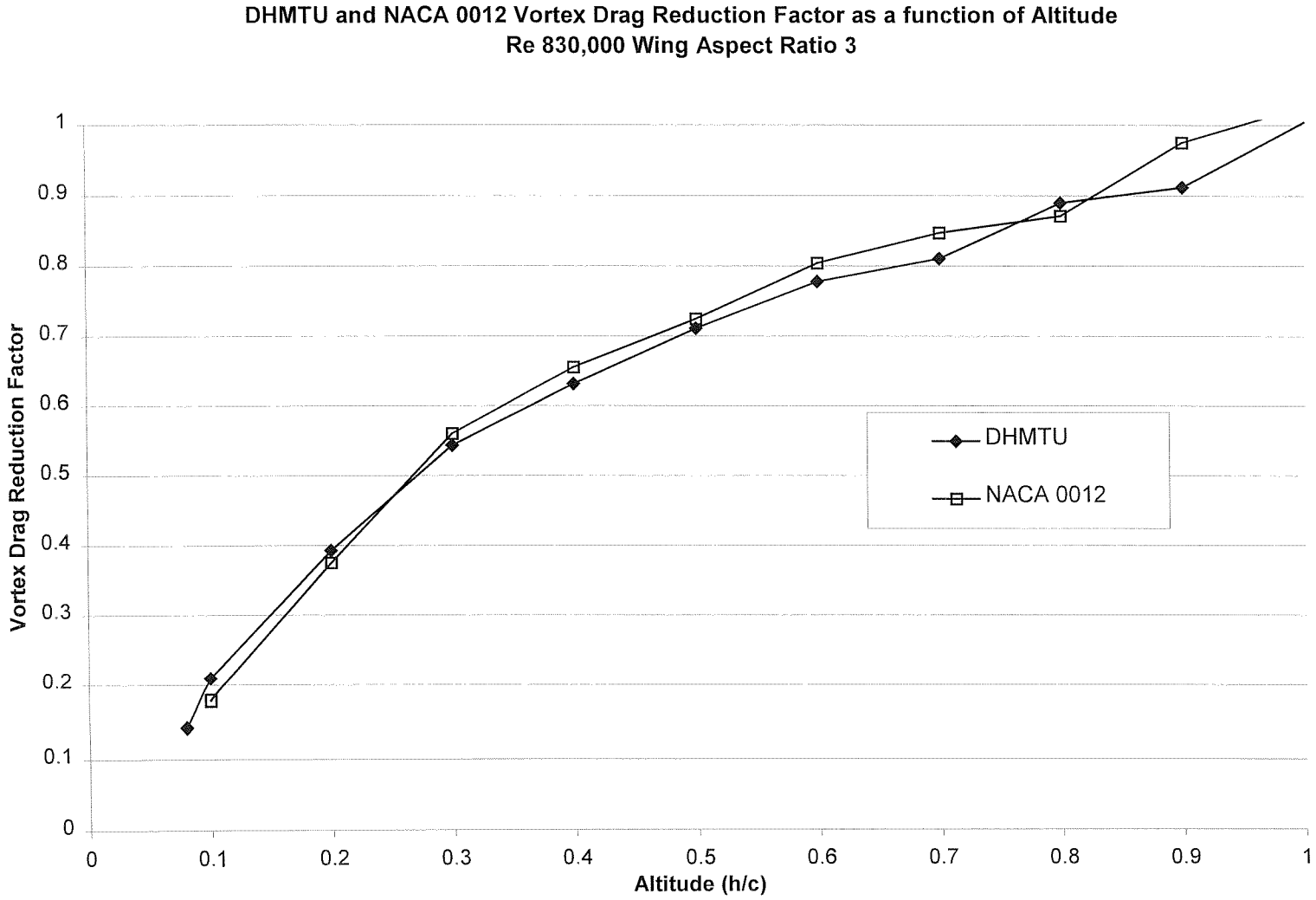

Figure 5-12: Vortex Drag Reduction Factor as a function of Altitude

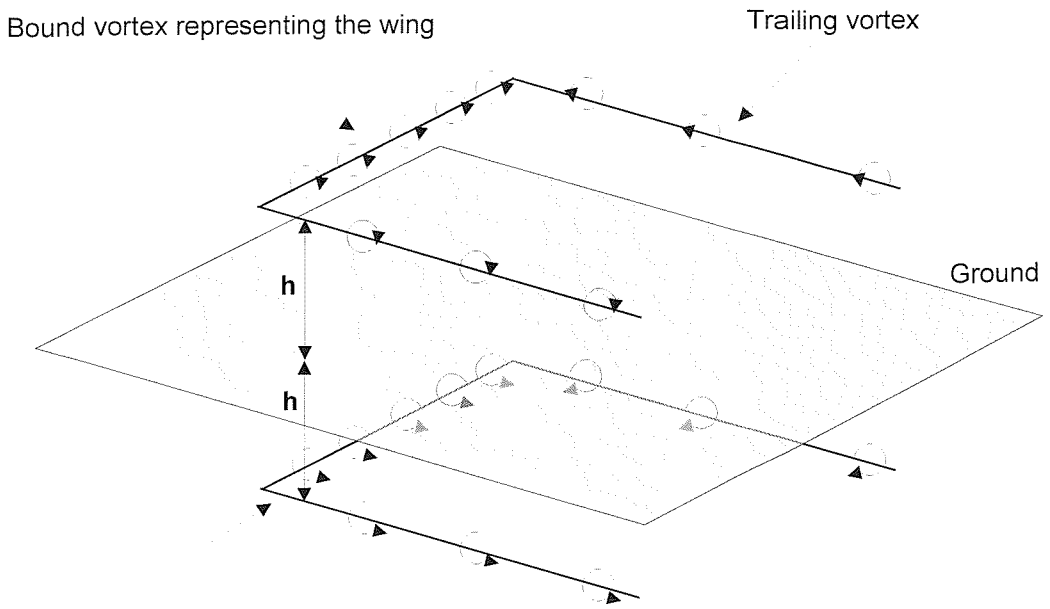

Figure 5-13: Horseshoe vortex arrangement illustrating the image horseshoe vortex that replaces the ground

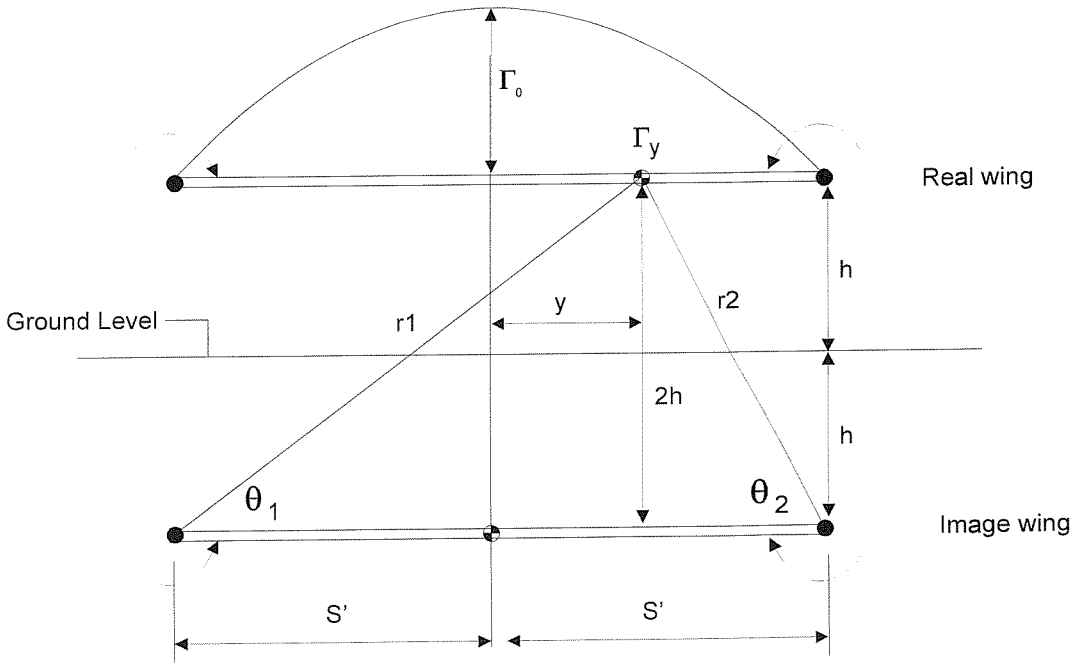

Figure 5-14: Geometry for calculation of drag reduction factors

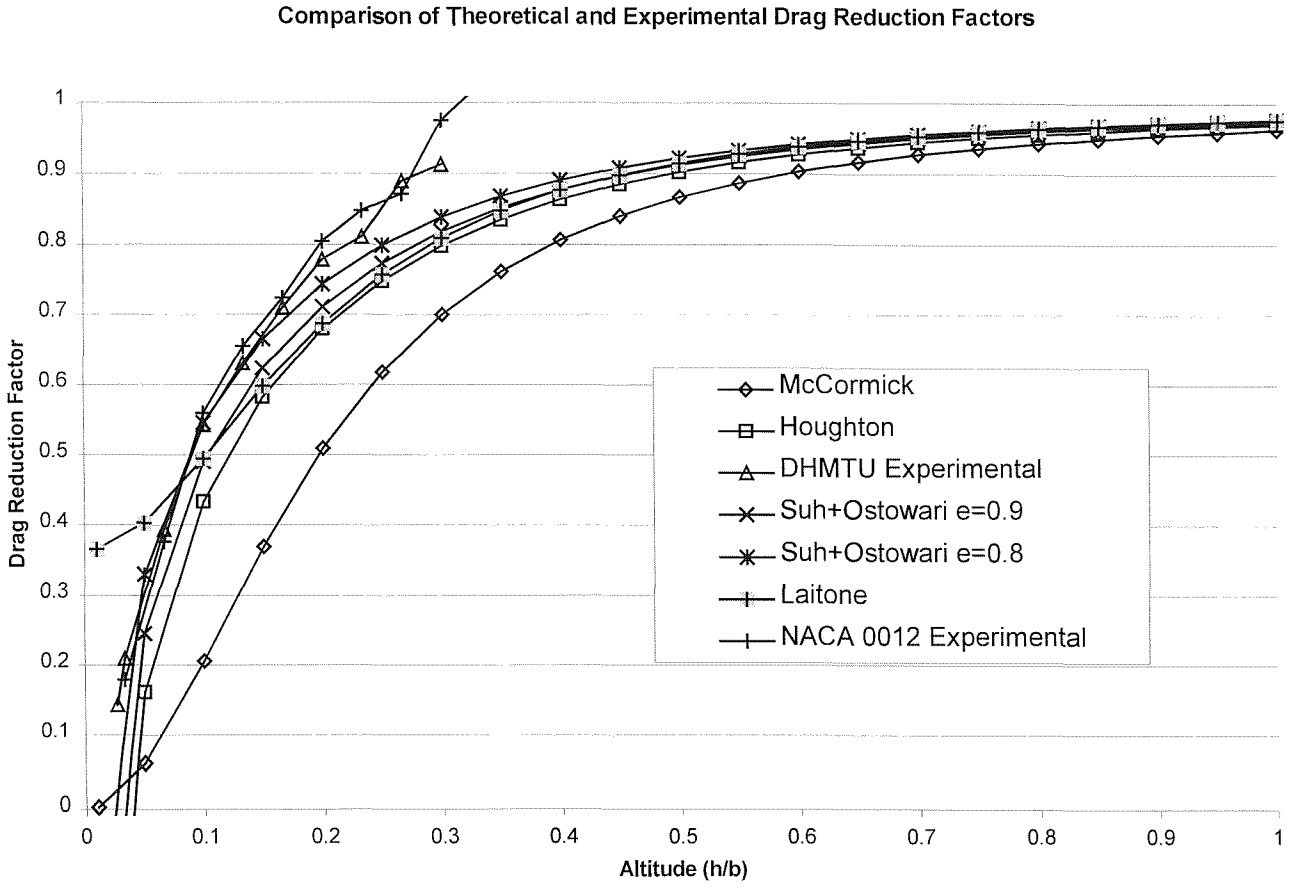

Figure 5-15: Graph illustrating the behaviour of various vortex drag reduction approximations

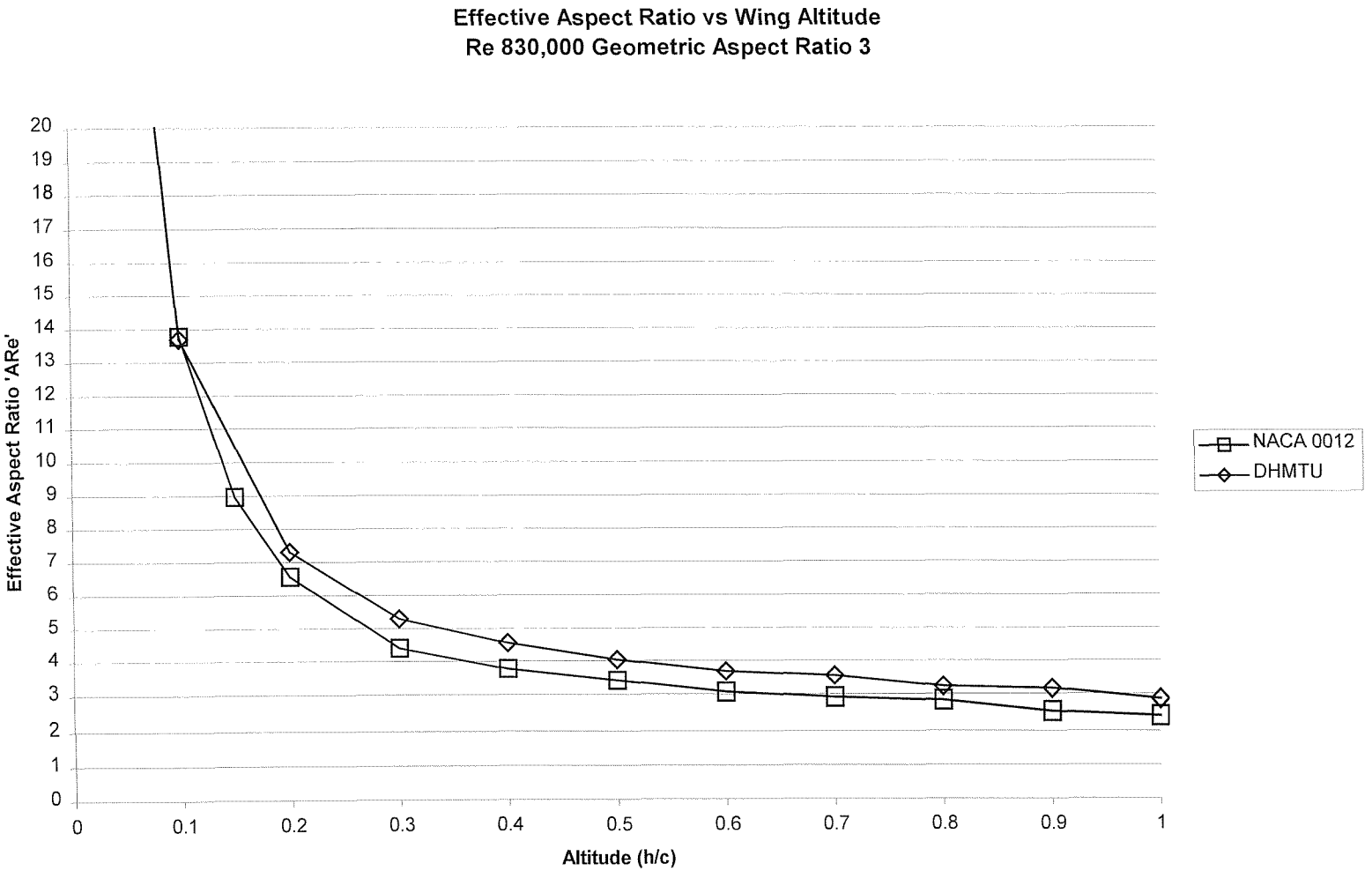

Figure 5-16: Increase in Effective Aspect Ratio with decreasing altitude

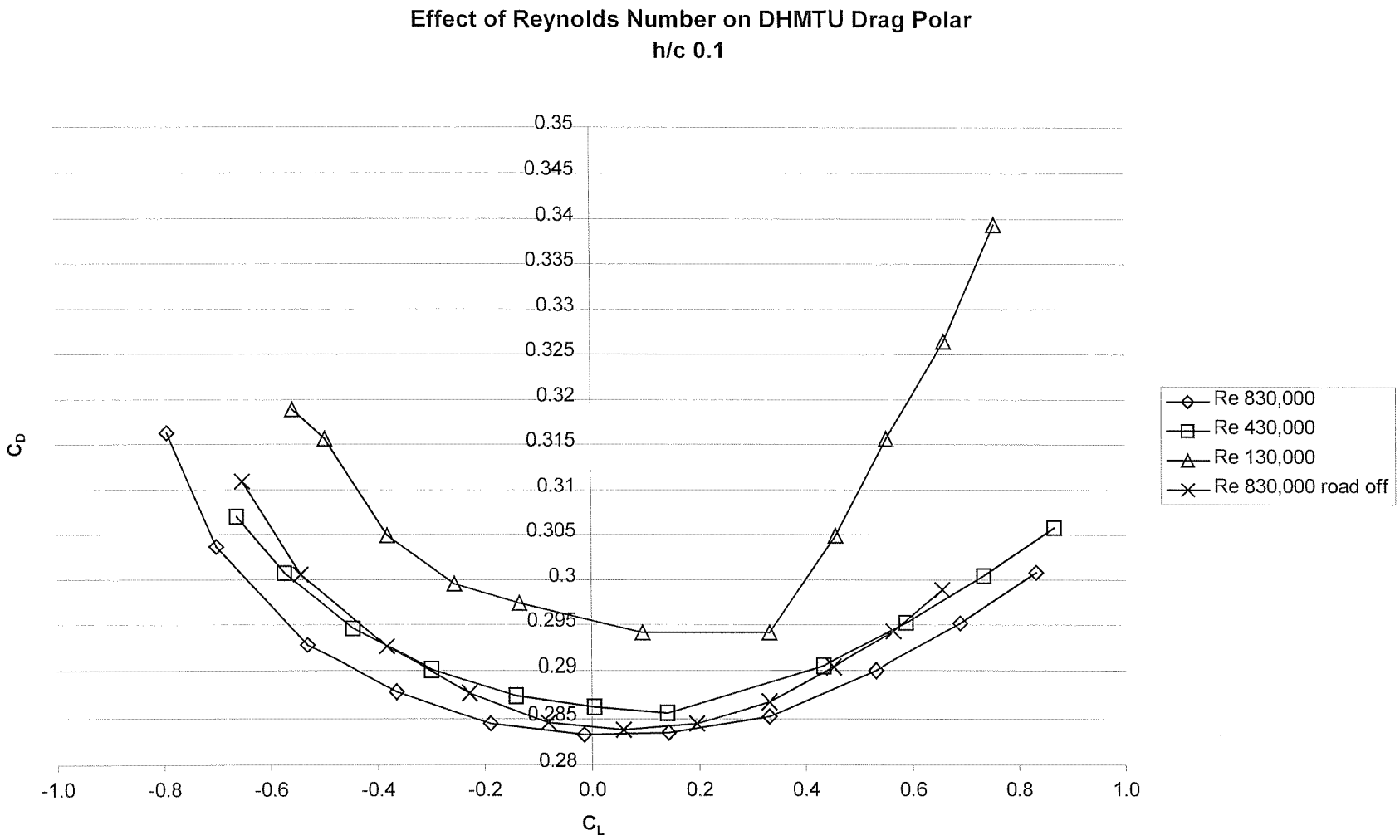

Figure 5-17: Effect of Reynolds Number variations on DHMTU Drag Polar

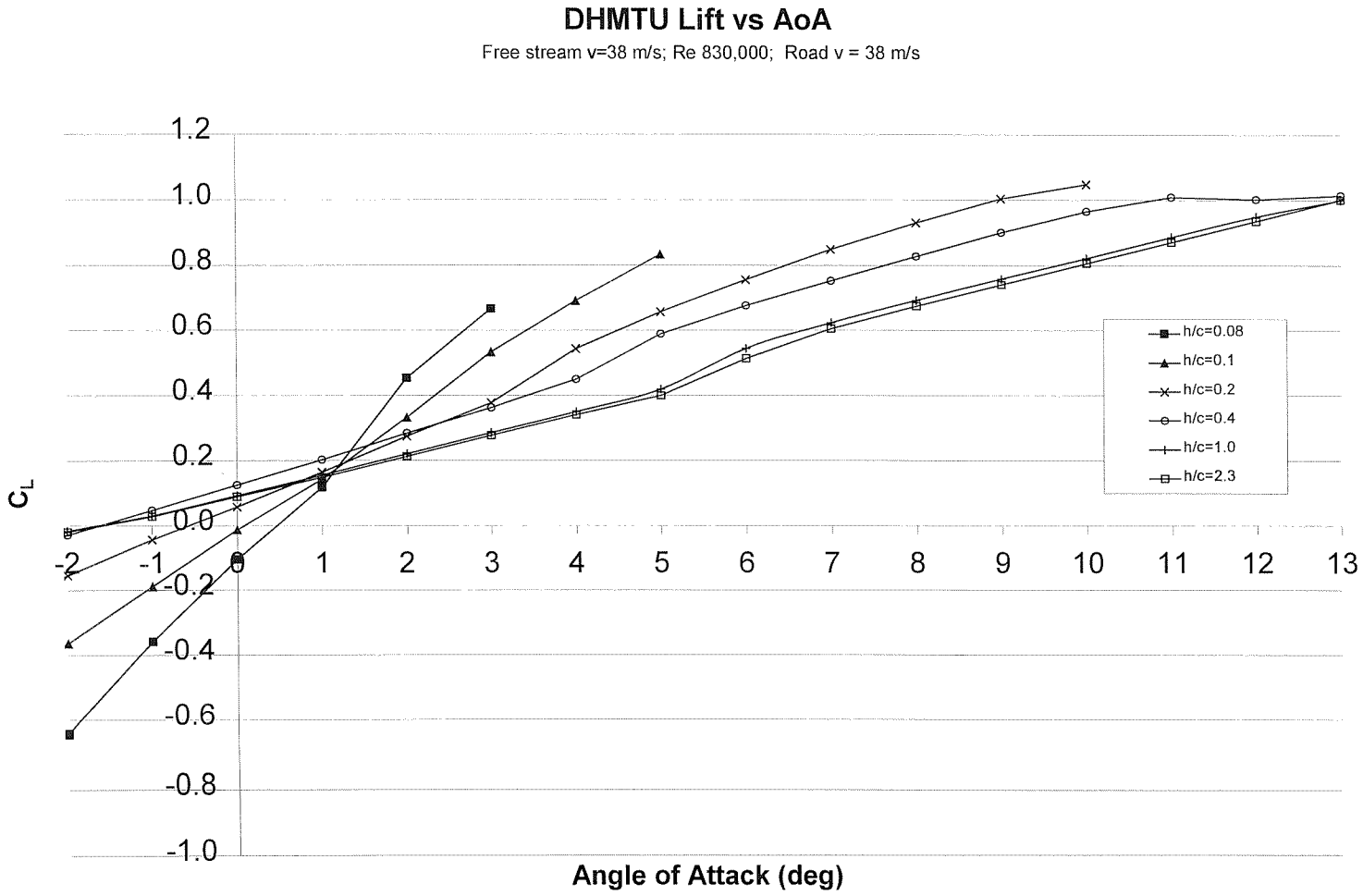

Figure 5-18: DHMTU Lift vs AoA as a function of altitude

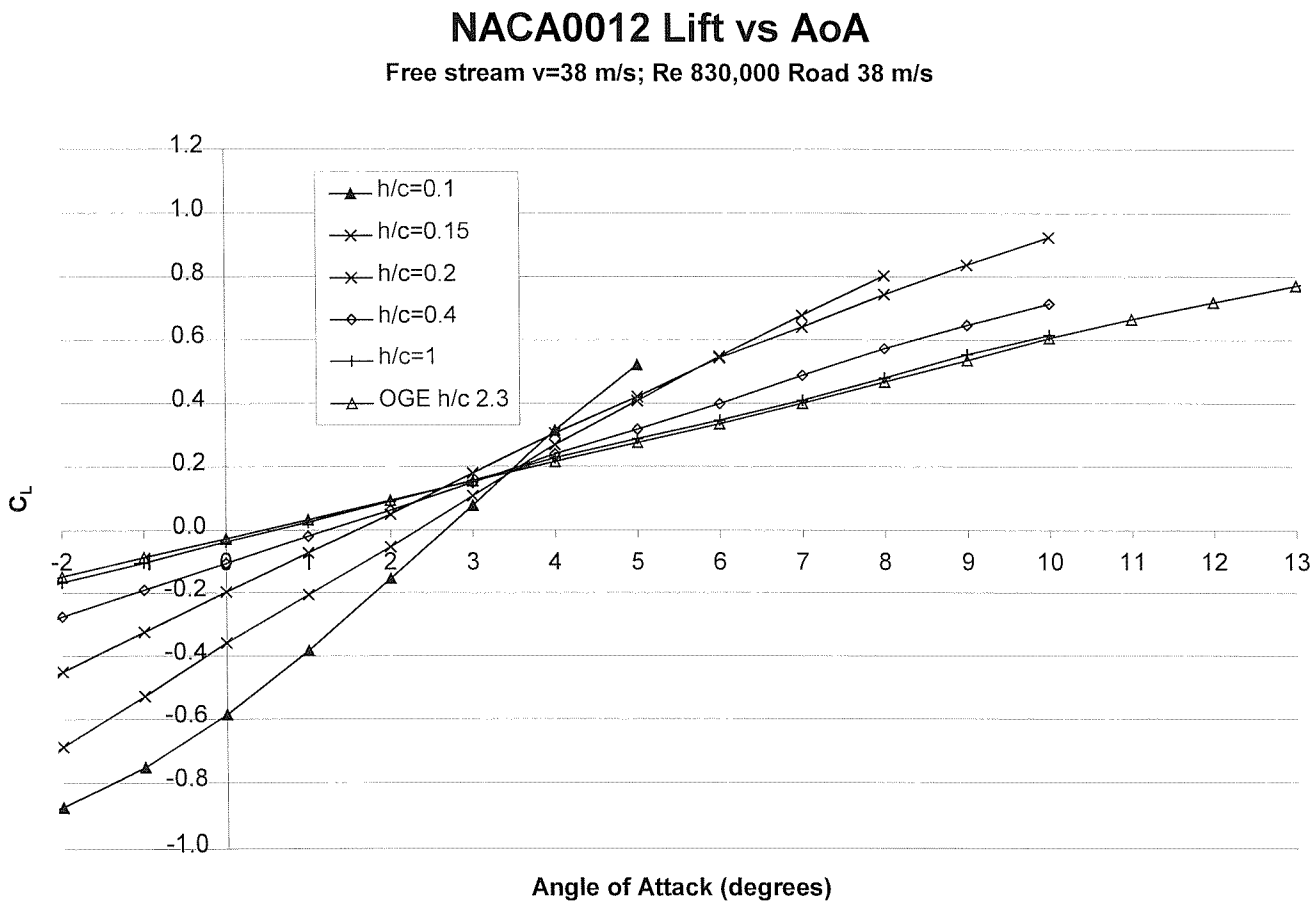

Figure 5-19: NACA 0012 Lift vs AoA as a function of altitude

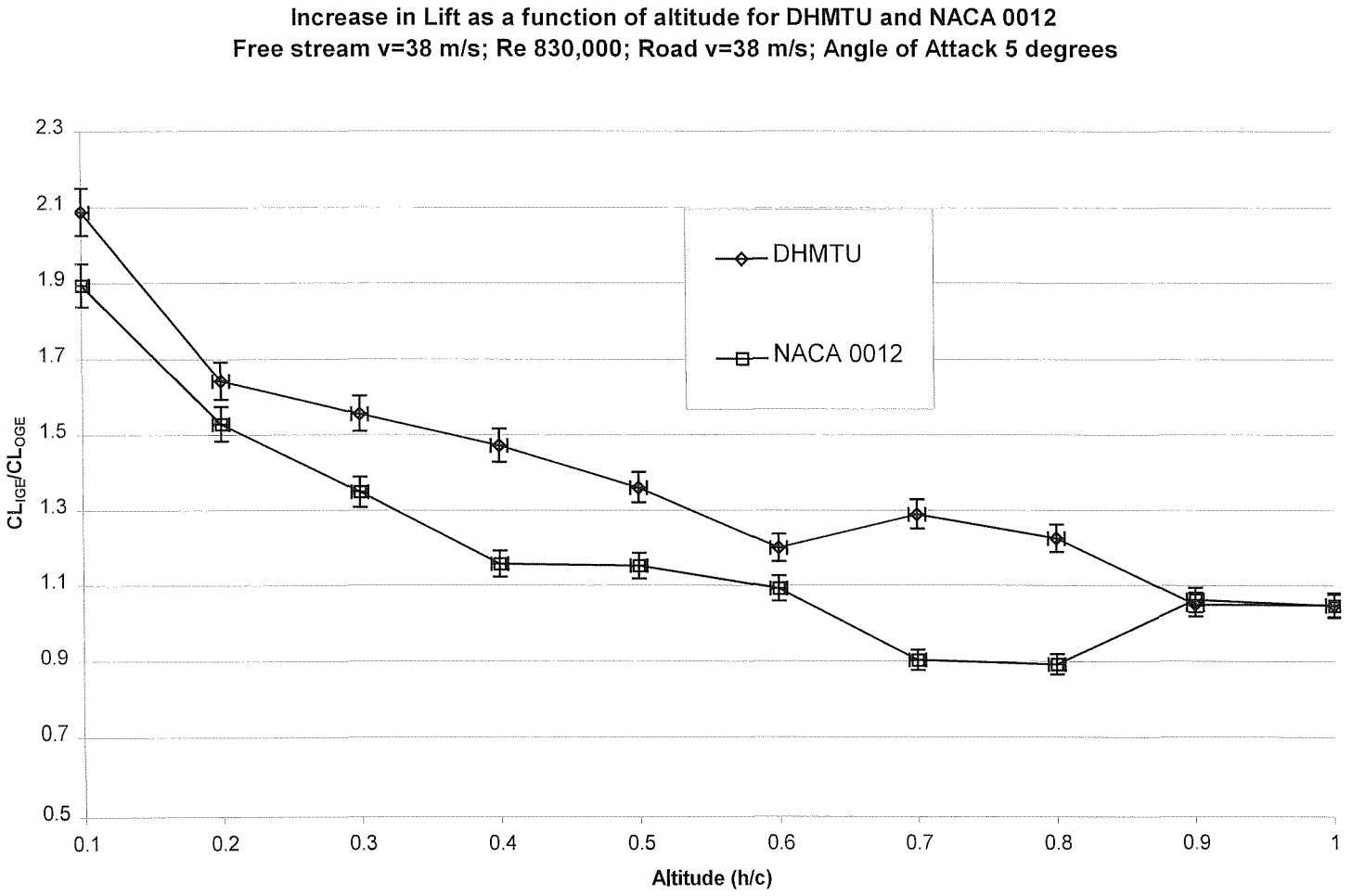

Figure 5-20: Graph illustrating the ratio of lift IGE/lift OGE as a function of altitude for the DHMTU and NACA 0012

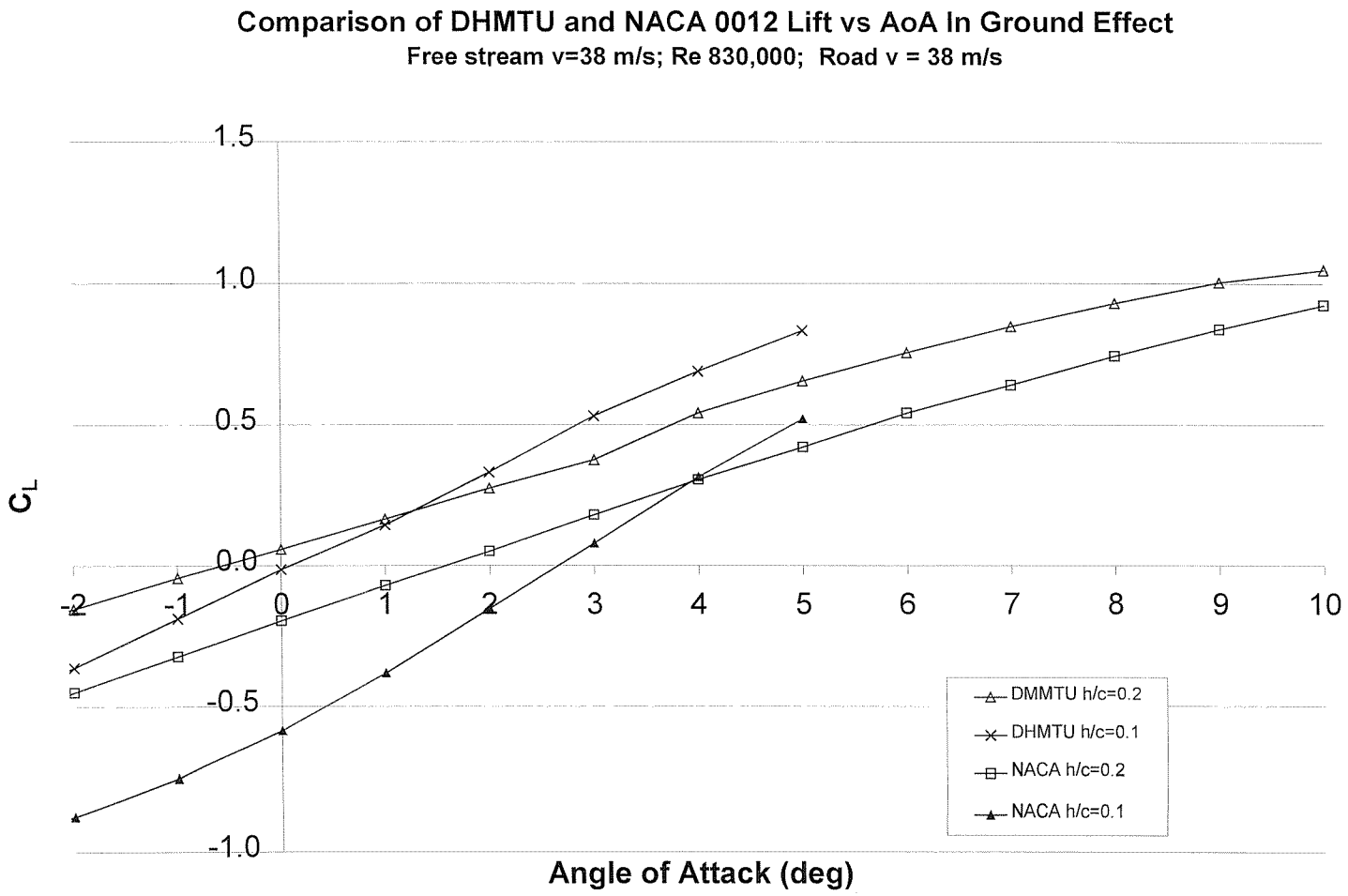

Figure 5-21: Comparison of Lift vs AoA for DHMTU and NACA 0012

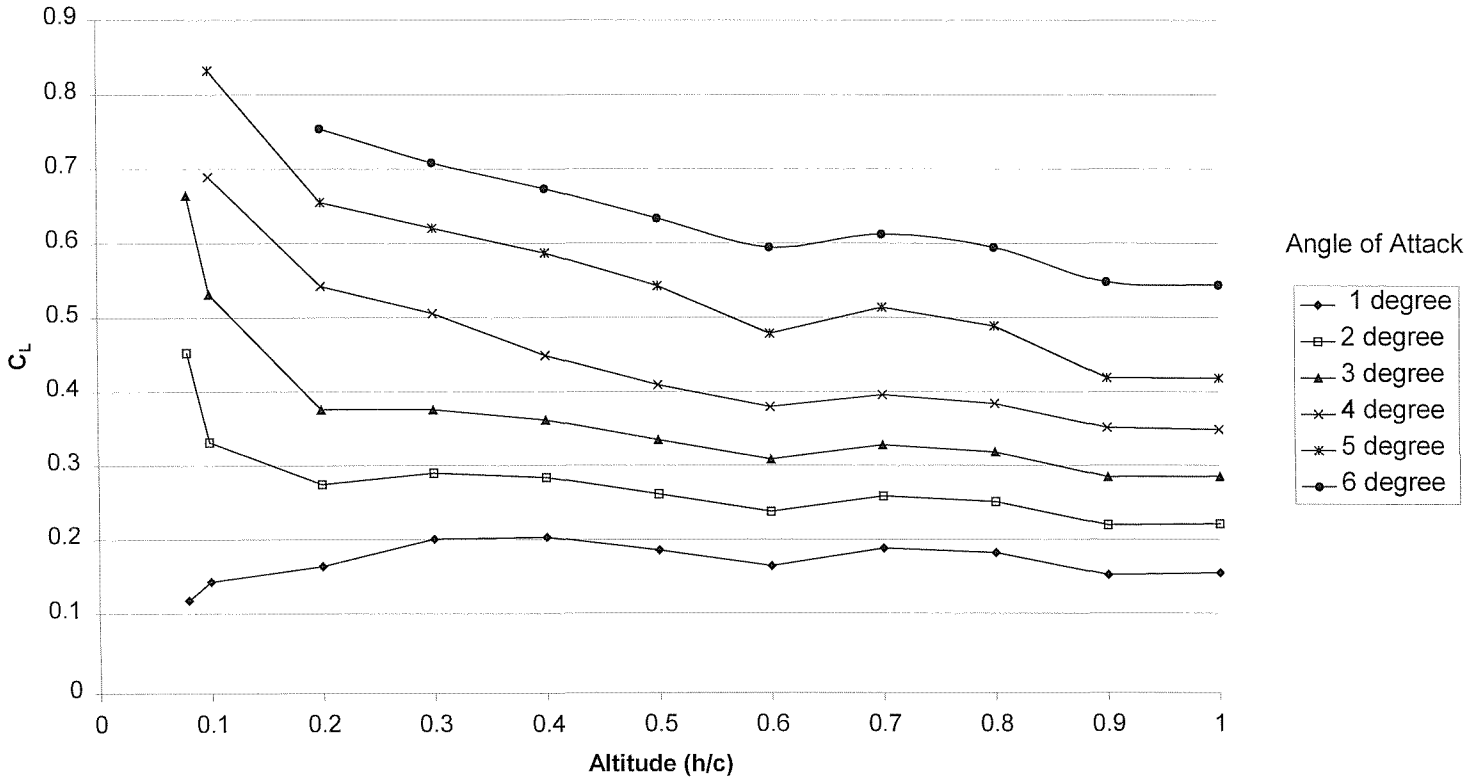

Figure 5-22: Variation of C_L with altitude for DHMTU

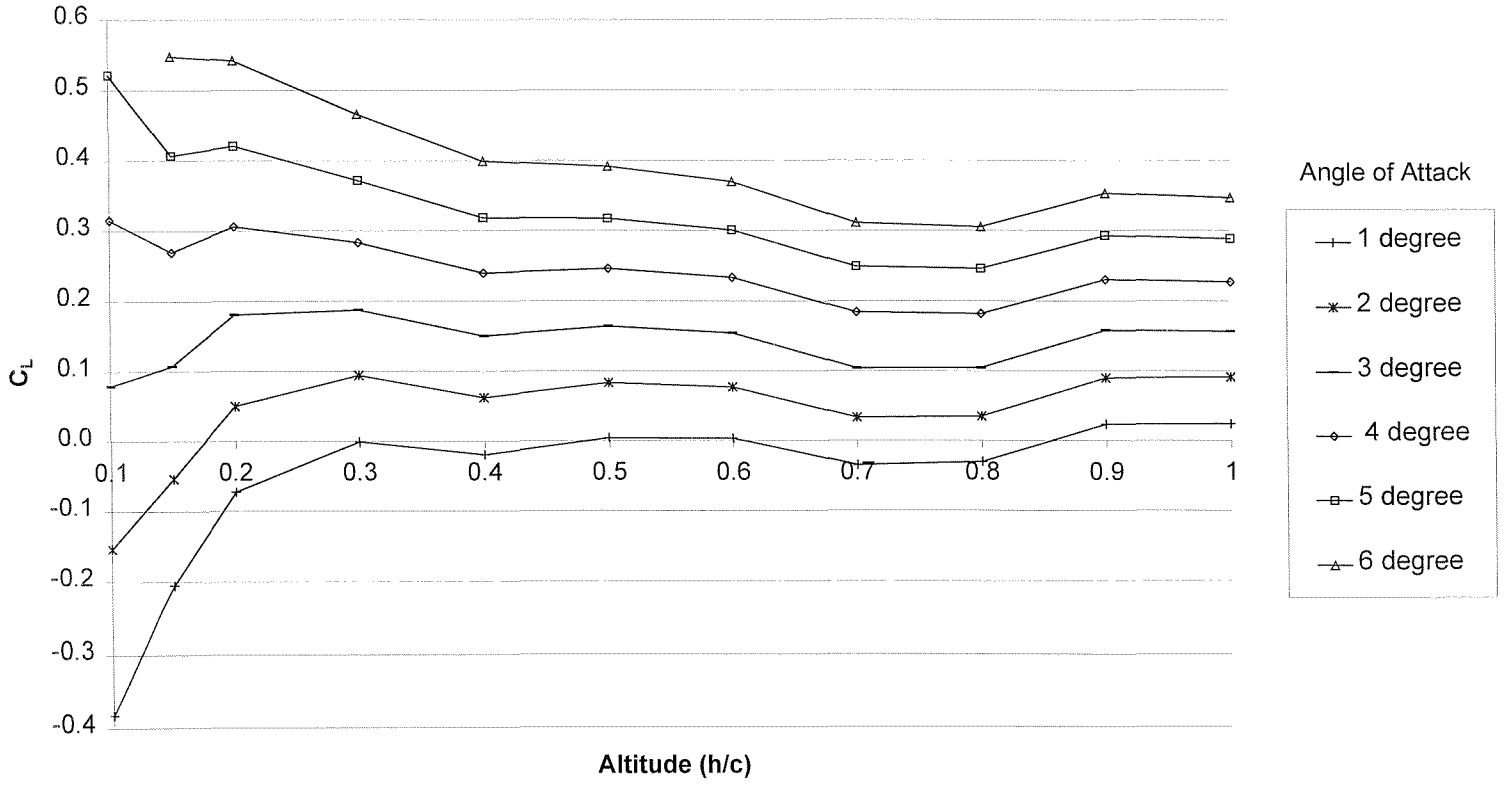

Figure 5-23: Variation of C_L with altitude for NACA 0012

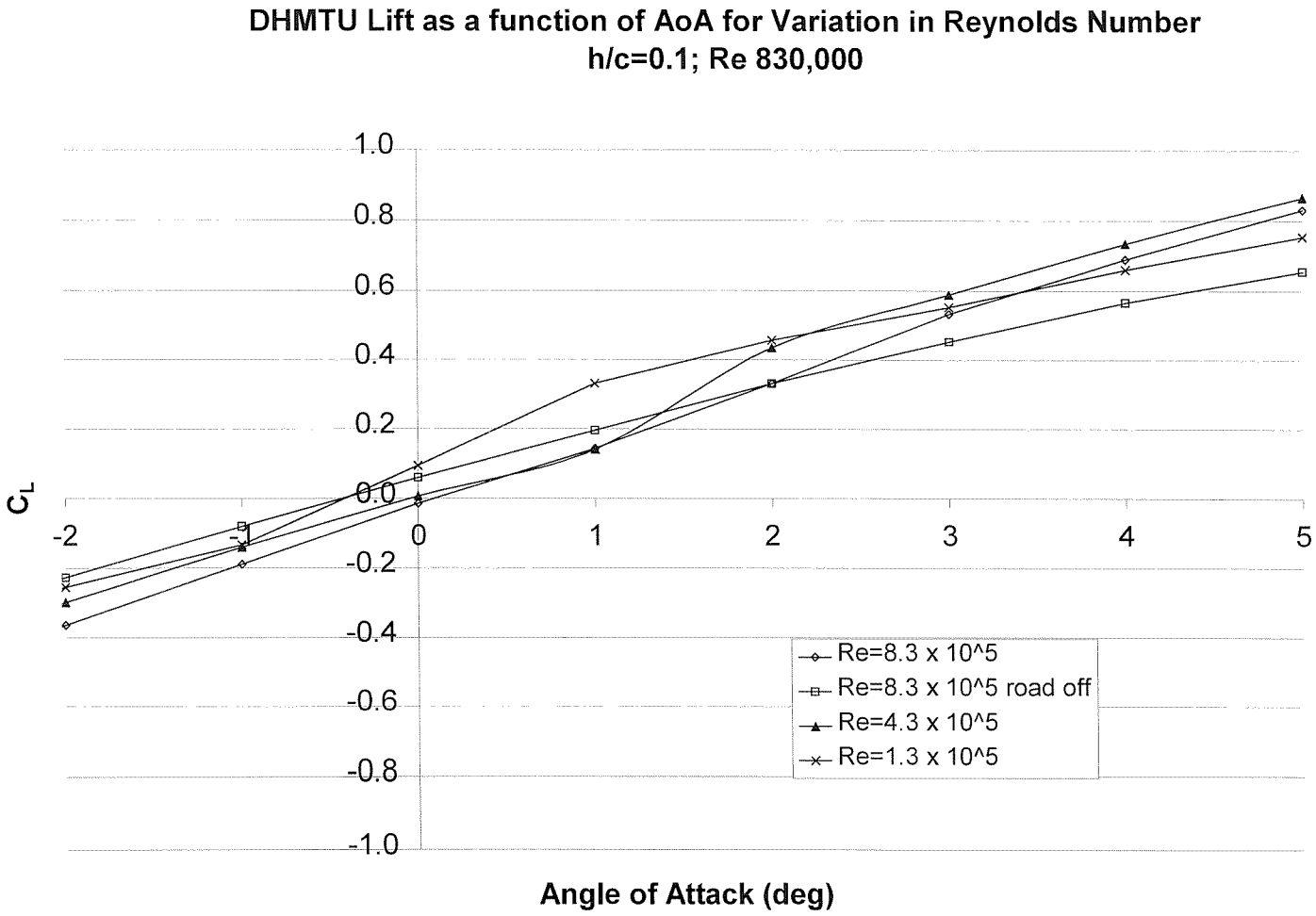

Figure 5-24: Effect of Reynolds Number variation and stationary ground on DHMTU lift characteristics

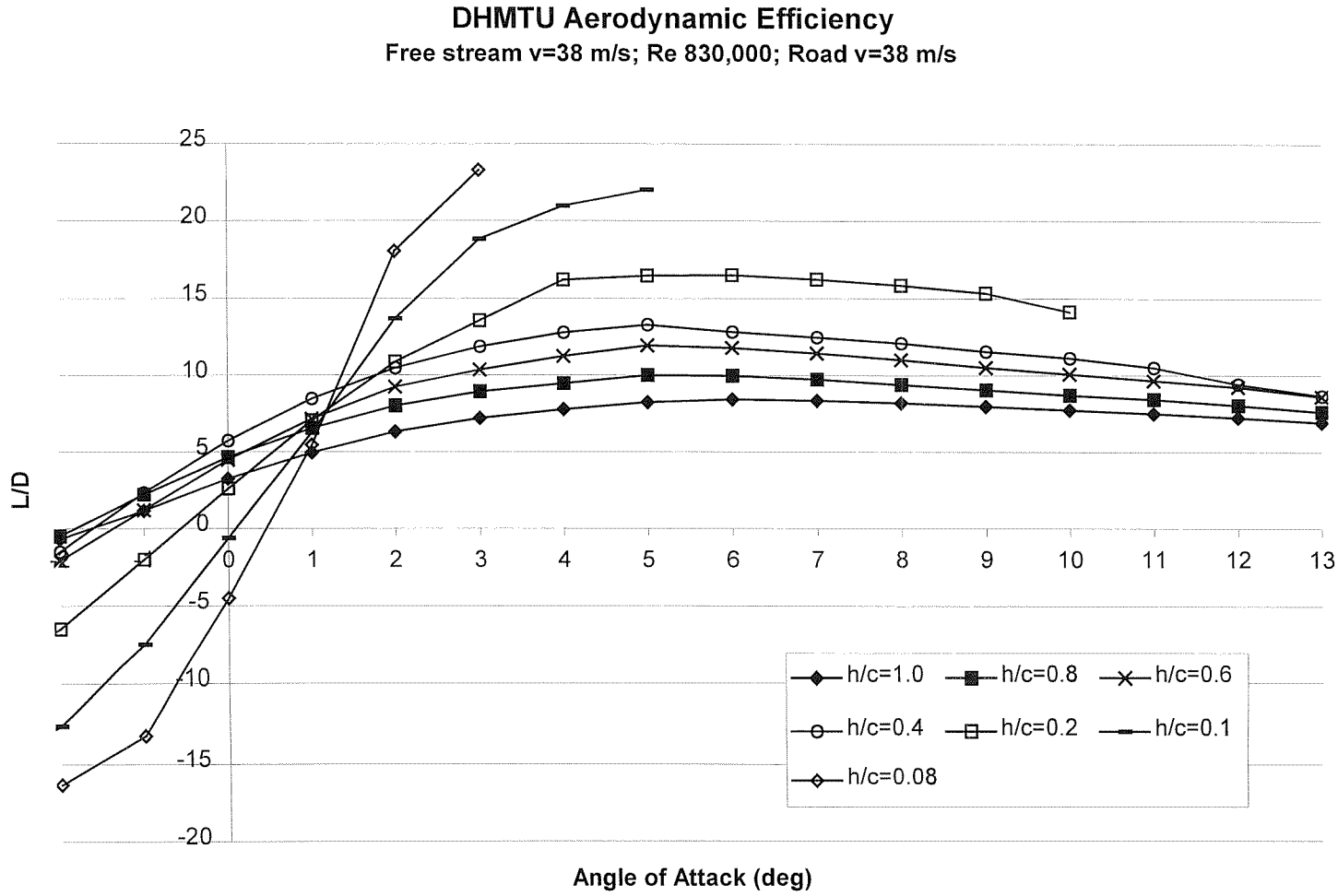

Figure 5-25: DHMTU Aerodynamic Efficiency

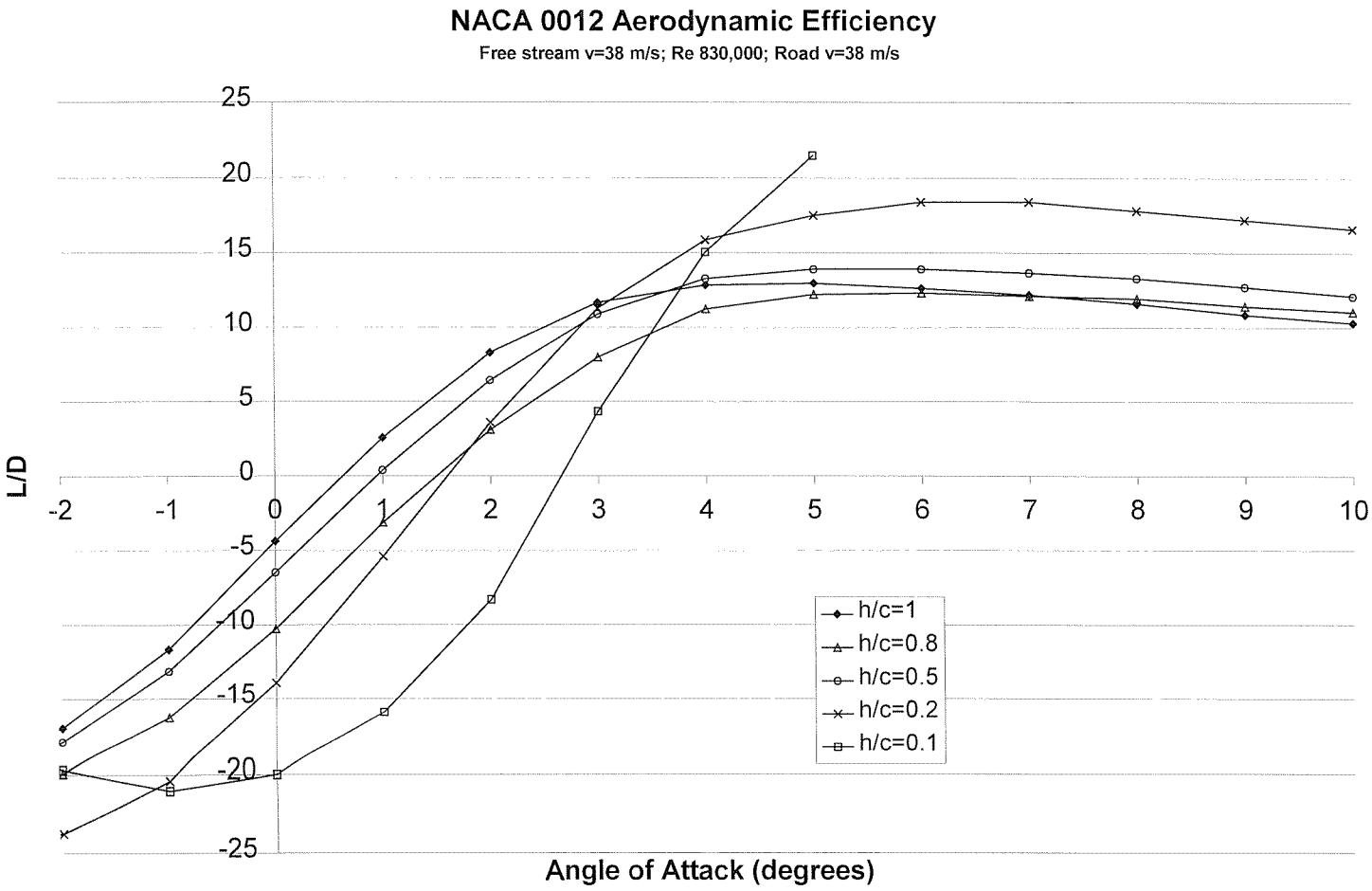

Figure 5-26: NACA 0012 Aerodynamic Efficiency

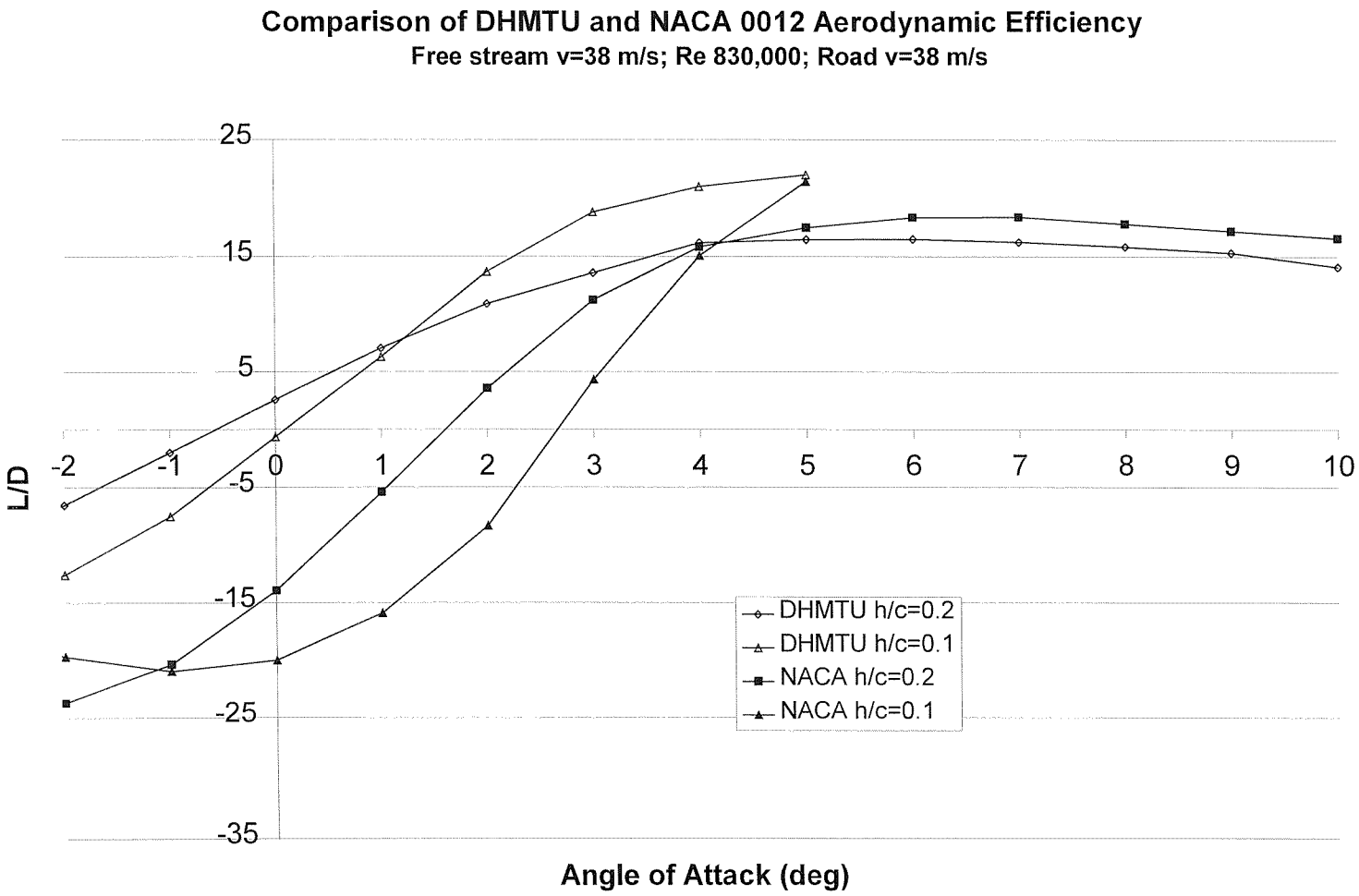

Figure 5-27: Comparison of DHMTU and NACA 0012 Aerodynamic Efficiencies

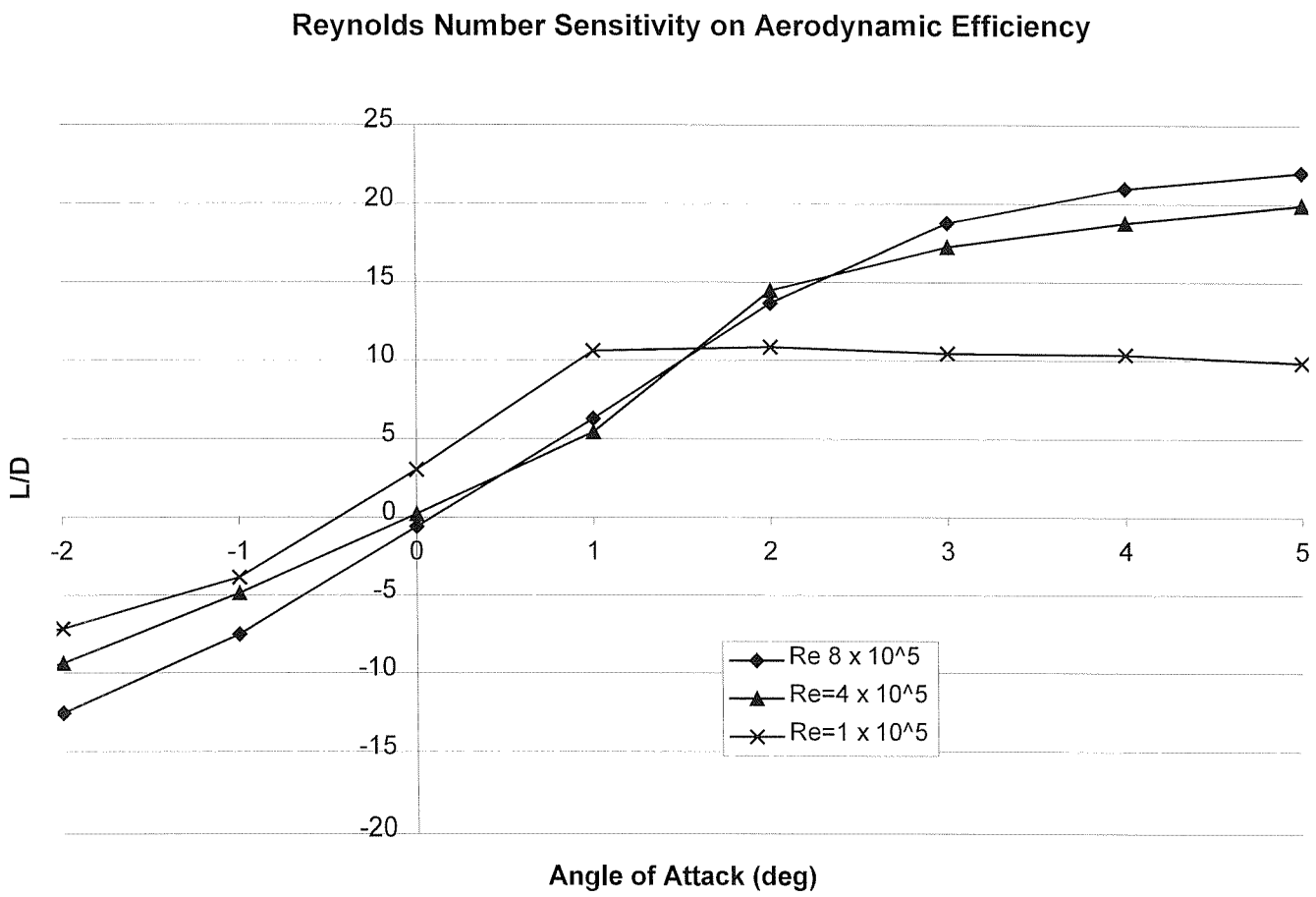

Figure 5-28: Effect of Reynolds Number on Aerodynamic Efficiency for DHMTU aerofoil

6 Longitudinal Stability In Ground Effect

6.1 Introduction

This chapter illustrates the effect of ground proximity on the pitching moment and position of aerodynamic centre for the NACA 0012 and DHMTU aerofoils as they operate in ground effect. The data was acquired in the rolling road wind tunnel experiments detailed in Chapter 5.

6.2 Overview of Longitudinal Stability and Requirements

The longitudinal stability of a wing is its ability to generate a restoring moment in pitch to an external disturbance. If the angle of attack of a wing is increased by a disturbance a longitudinally stable wing will produce a downward pitching moment to restore the wing to the original Angle of Attack (AoA). Similarly if a disturbance reduced a wings AoA a longitudinally stable wing would generate an upward pitching moment to restore the original AoA. A longitudinally stable wing will produce a restoring pitching moment in the opposite direction of the disturbance returning the wing to its original equilibrium condition.

The relevant aerodynamic characteristic to investigate static longitudinal stability is the variation in pitching moment coefficient C_m. The wing's pitching moment is generated as a result of the pressure and shear stress distributions over an aerofoil. Anderson provides a detailed explanation of the cause of an aerofoils pitching moment [55]. The pitching moment coefficient C_m is defined as:

$$C_m = \frac{2M}{\rho V^2 S c}$$ Equation 6-1

Where M is the pitching moment, ρ is the density of air, V is the free steam velocity, S is the wing area and c is the wing chord. The sign convention adopted throughout aeronautics is that nose down pitching moments are negative.

The reader should note that the pitching moment measurements were taken at the rotation point of both the NACA 0012 and DHMTU. This corresponds as a distance c/3 from the wing leading edge.

For an aerofoil to be statically stable in pitch and in trim the following two conditions have to be fulfilled [44]

$$\frac{dC_L}{d\alpha} > 0 \qquad \text{Equation 6-2}$$

$$M > 0 \text{ for } \alpha = 0 \qquad \text{Equation 6-3}$$

When operating in ground effect an aerofoil must fulfil the above conditions at each altitude of operation. Additionally as the wing descends in altitude the variation of the pitching moment (dC_m/d_H) should be a minimum. In order not to require large stabilising forces to be generated with small changes in altitude. Finally the movement of the aerodynamic centre should also be a minimum.

The stability of a wing section can be investigated by looking at the pitching moment versus angle of attack (C_m vs AoA) and lift versus pitching moment curves (C_L vs C_m). A stable wing is indicated by a curve that possesses a negative $dC_m/d\alpha$ and dC_m/dC_L gradient. The magnitude of longitudinal stability is defined as the value dC_m/dC_L. The more positive the value of the gradient dC_m/dC_L the less stable the wing is in pitch.

6.3 Pitching Moment Characteristics In and Out of Ground Effect

Figure 6-1 shows the pitching moment behaviour of the NACA 0012 operating in and out of ground effect. The curve at an altitude of h/c 2.3 illustrates typical stability characteristics of an aerofoil operating out of ground effect. It is a linear curve possessing a constant negative gradient, indicating pitch stability, between –5 to +6 degree angles of attack. At angles of attack greater than 6 degrees a reduction in the gradient occurs indicating a reduction in stability. As the NACA 0012 is a symmetrical aerofoil the pitching moment at an angle of attack of 0 degrees should be zero. Due to inaccuracies in the experimental results this is not the case and zero pitching moment occurs at an AoA of 0.4 degree.

As the NACA 0012 enters the moderate ground effect regime the gradient of the pitching moment ($dC_m/d\alpha$) increases down to an altitude of h/c 0.3 (Table6-1). A transition in the behaviour of the pitching moment occurs below an altitude of h/c 0.3. The gradient $dC_m/d\alpha$ increases and the curve is non-linear in the positive angle of attack region. At an altitude of h/c 0.15 and above an angle of attack of 5 degrees the pitching moment becomes less negative. This results in the NACA 0012 becoming unstable. As the altitude reduces to h/c 0.1 this unstable behaviour occurs earlier at an angle of attack of 3 degrees. This is a significant disadvantage of the NACA 0012 when operating in the extreme ground effect regime.

As the altitude decreases the magnitude of the NACA 0012 pitching moment increases. This can be seen in Figure 6-2 that presents the magnitude of the pitching moment as a function of altitude between angles of attack of 1 to 5 degrees. In extreme ground effect the pitching moment is nearly 4 times the out of ground effect value (Figure 6-10).

When the NACA 0012 is operating between altitudes of h/c 1 and 0.3 the variation in pitching moment with altitude is linear. Figure 6-2 illustrates that below an altitude of h/c 0.3 a much more rapid non linear change in pitching moment with altitude occurs. This is due to the significant increase in lift, and hence pitching moment, that is obtained below this altitude as illustrated in Figure 5-19.

Figure 6-3 plots the lift as a function of pitching moment from OGE (h/c 2.3) to extreme ground effect (h/c 0.1). It can be seen that when operating OGE and in moderate ground effect the gradient dC_m/dC_L is steadily increasing (Table 6-1). This indicates that the NACA 0012 is becoming increasingly unstable with a decrease in altitude. As the section approaches extreme ground effect ($h/c<0.2$) a distinct change in behaviour is exhibited. The C_m-C_L curve becomes distinctly non-linear. Note that the NACA 0012 produces negative lift at small angles of attack below an altitude of h/c 0.4 (Figure 6-3 and Figure 5-19).

The variation in C_m with angle of attack and lift coefficient for the DHMTU is shown in Figure 6-4 and Figure 6-5 respectively. It can be seen that the DHMTU exhibits a stable negative $dC_m/d\alpha$ gradient over the ground effect altitude range tested. As the altitude of the section decreases the magnitude of the pitching moment increases. The stability of the DHMTU decreases with altitude as can be seen by the increase in the gradient dC_m/dC_L (Figure 6-5).

An interesting feature of the DHMTU is the positive step in the curves indicating a region of reduced stability. Figure 6-5 illustrates the instability as a reversal in dC_m/dC_L gradient on the curve. The differences in dC_m/dC_L can be quite clearly seen. Table 6-2 presents the pitch stability of the DHMTU before and after the step change in behaviour. After the step the gradient dC_m/dC_L increases resulting in reduced pitch stability.

The position that this change in behaviour occurs corresponds to a step change in the lift curve slope. Figure 6-6 graphically illustrates this correlation for h/c 0.1 to 0.3. The position of this region of relative instability decreases with reduced altitude and for altitudes between h/c 1 to 0.1 lies within 5 to 1 degrees AoA. This region of instability lies just below the optimum operating angle of attack for the DHMTU of 5 to 6 degrees.

Figure 6-7 illustrates the pitching behaviour of both sections in ground effect between h/c 1.0 to 0.5. As the altitude is decreased the respective behaviour of the NACA 0012 and DHMTU curves do not radically alter. The NACA 0012 exhibits linear behaviour upto 6 degrees AoA, whilst the DHMTU exhibits the characteristics step change in gradient as discussed above. The NACA 0012 develops a greater magnitude of downward pitching moment than the DHMTU section. This is presented in Table 6-3 where it can be seen as the altitude decreases from h/c 1 to h/c 0.5 the NACA 0012 produces from 2.1 to 7.1 times the pitching moment as the DHMTU.

Figure 6-8 depicts the performance of both sections between h/c 0.4 and 0.1. In extreme ground effect (h/c 0.1) a noticeable change in behaviour can be seen for the NACA 0012. This is manifest in the significant increase in pitching moment

magnitude and behaviour of the curve as its gradient reduces compared to higher altitudes. In contrast when the DHMTU is at an altitude of h/c 0.1 the increase in pitching moment is not as significant.

It can be seen from Table 6-4 that the DHMTU section posses a higher $dC_m/d\alpha$ than the NACA 0012. In other words the DHMTU produces a greater rate of restoring moment than the NACA 0012.

The DHMTU section possesses a more gradual variation in pitching moment with altitude than the NACA 0012 section (Figure 6-9). Another feature that stands out from Figure 6-9 is that the NACA 0012 produces significantly greater pitching moment than the DHMTU at all altitudes, especially in extreme ground effect. The increase in pitching moment above the OGE value can be seen in Figure 6-10. In extreme ground effect the pitching moment produced by the DHMTU is only 1.6 greater than its OGE value. In contrast the NACA 0012 is 3.8 times its OGE value.

The angle of attack at which the pitching moment of a section is zero and hence stable is known as the 'trim angle'. The trim angle can be obtained from the pitching moment angle of attack graphs where the curve intercepts the x-axis. The values are shown in Table 6-5 and illustrated in Figure 6-11 for both the DHMTU and NACA 0012. The DHMTU possesses a positive trim angle with decreasing altitude resulting in it producing usable lift throughout the altitude range. The NACA 0012 by comparison requires a negative angle of attack below an altitude of h/c 0.65 for stability.

6.4 Variation of Aerodynamic Centre in Ground Effect

The aerodynamic centre is a position along the aerofoil's chord where the pitching moment C_m is virtually constant with changes in angle of attack [55]. The aerodynamic centre is a useful concept for the study of stability and control. The location of the aerodynamic centre X_0 is give by [44]:

$$X_0 = x_w + \left[\frac{C_m - C_{m0}}{C_L}\right]$$ Equation 6-4

Where x_w is the rotation point of the wing (c/3 from leading edge), C_m and C_L are the pitching moment and lift coefficient respectively at an angle of attack. C_{m0} is the pitching moment coefficient at zero lift. The values of C_{m0} for the NACA 0012 and DHMTU sections are presented in Table 6-6.

The movement of the aerodynamic centre for both the NACA 0012 and DHMTU are presented in Figure 6-12. This graph depicts the distance of the aerodynamic centre from the aerofoils leading edge in x/c as a function of altitude. It can be seen that with a decrease in altitude the aerodynamic centre of both sections moves rearwards, further away from the leading edge. Between the moderate ground effect altitudes of h/c 1.0 to 0.2 the aerodynamic centre of both sections has moved 0.06c. The main difference occurs when the sections move into the extreme ground effect regime below an altitude of h/c 0.2. In this region the aerodynamic centre of the NACA 0012 moves rearwards the same amount as it did between the much greater altitude band of h/c 1.0 to 0.2. In contrast the DHMTU has moved nearer to the leading edge by 0.009c.

6.5 Summary

When the NACA 0012 enters ground effect there is an increase in the magnitude of the pitching moment at all angles of attack compared to out of ground effect operation. On entering moderate ground effect the pitching moment is approximately its OGE value. As the altitude decreases the magnitude of the pitching moment steadily increases until at an altitude of h/c 0.3 it is 1.4 times its OGE value. As the extreme ground effect region is entered a rapid rise in the magnitude of the pitching moment occurs so that at an altitude of h/c 0.1 it is nearly 4 times its OGE value. The experimental data reveals that there is a distinct difference between the pitching moment behaviour when in moderate (h/c 1.0 to h/c 0.3) and when operating in or near extreme ground effect (h/c<0.2). In the moderate ground effect regime the NACA 0012 is stable over a wide range of positive angles of attack. As the section nears extreme ground effect (h/c 0.2) the

pitching moment curve becomes non-linear at angles of attack above 3 degrees. This reduces to 1 degree when operating in extreme ground effect (h/c 0.1).

The gradient of the pitching moment angle of attack curve ($dC_m/d\alpha$) is increasing down to an altitude of h/c 0.3. When the NACA 0012 is below h/c 0.15 the pitching moment angle of attack curve is non-linear. A general observation is that over positive ranges of angles of attack the stability of the NACA 0012 decreases with a reduction in altitude, becoming unstable in extreme ground effect.

The DHMTU produces similar trends with an increase in the magnitude of the pitching moment and a reduction in longitudinal stability occurring with a decrease in altitude. As with the NACA 0012 a distinction can be seen in the experimental data between moderate and extreme ground effect. A feature not present with the NACA 0012 is a reduction in stability as a result of flow separation occurring at low angles of attack.

The DHMTU possesses significant longitudinal stability advantages when operating in extreme ground effect. The NACA 0012 generates a much greater magnitude of pitching moment than the DHMTU. In moderate ground effect this is between 2 to 7 times the DHMTUs value. The increase in pitching moment when operating in extreme ground effect is much more significant for the NACA 0012 than the DHMTU. The DHMTU possesses a higher $dC_m/d\alpha$ than the NACA 0012 resulting in a greater rate of restoring moment. The DHMTU possesses a more gradual variation in C_m with decreasing altitude than the NACA 0012. Compared to operating OGE the pitching moment increases by 1.6 for the DHMTU and 3.8 for the NACA 0012.

As altitude reduces the trim angle of both sections reduces. The DHMTU possesses the advantage of a positive trim angle over the whole ground effect range resulting in the production of lift. The NACA 0012 in contrast produces a negative trim angle below an altitude of h/c 0.6 resulting in a downward force being produced. This is further evidence that the NACA 0012 is unsuited to operation in ground effect.

Altitude (h/c)	$\frac{dC_m}{dC_L}$ per radian	$\frac{dC_m}{d\alpha}$ per radian
2.3 (OGE)	-10.7	-0.0060
1.0	-12.4	-0.0053
0.9	-12.5	-0.0054
0.8	-12.3	-0.0055
0.7	-13.0	-0.0055
0.6	-13.3	-0.0056
0.5	-13.9	-0.0056
0.4	-15.2	-0.0057
0.3	-15.2	-0.0059
0.2	N/O	N/O
0.1	N/O	N/O

Table 6-1: dC_m/dC_L and $dC_m/d\alpha$ for NACA 0012 out of and in ground effect

N/O Not Obtainable

Altitude (h/c)	Pre step dC_m/dC_L	Post Step dC_m/dC_L
2.3 (OGE)	-9.94	-15.1
1	-8.85	-13.5
0.9	-9.10	-13.8
0.8	-9.0	-15.4
0.7	-9.1	-15.0
0.6	-9.3	-14.9
0.5	-9.2	-15.7
0.4	-10.1	-18.3
0.3	-9.6	-20.0
0.2	-8.6	-36.0
0.1	-6.2	-116.8

Table 6-2: Pre and Post step dC_m/dC_L for DHMTU

h/c	NACA C_m/DHMTU C_m
2.3	1.73
1	2.15
0.9	2.14
0.8	3.00
0.7	3.58
0.6	2.61
0.5	4.16
0.4	7.09
0.3	5.61
0.2	4.37
0.1	4.02

Table 6-3: Ratio of NACA 0012 and DHMTU C_m at AoA 5 degrees

	$\frac{dC_m}{d\alpha}$ per radian	
h/c	NACA 0012	DHMTU
2.3	-0.34	-0.32
1	-0.30	-0.41
0.9	-0.31	-0.41
0.8	-0.32	-0.42
0.7	-0.32	-0.42
0.6	-0.32	-0.44
0.5	-0.32	-0.44
0.4	-0.33	-0.44
0.3	-0.34	-0.49
0.2	N/O	-0.68
0.1	N/O	N/O

Table 6-4: Comparison of Cm-AoA gradient of NACA 0012 and DHMTU in linear region

* N/O Not Obtainable

	Trim Angle (degrees)	
Altitude (h/c)	**DHMTU**	**NACA 0012**
2.3	2.34	0.40
1	3.27	0.94
0.9	3.32	0.80
0.8	2.64	0.92
0.7	2.37	0.40
0.6	2.47	-0.45
0.5	2.02	-0.56
0.4	1.81	-0.93
0.3	1.38	-1.70
0.2	0.99	-2.70
0.1	0.94	-2.68

Table 6-5: Trim Angles for DHMTU and NACA 0012 as a function of altitude

	C_{m0}	
Altitude (h/c)	**NACA 0012**	**DHMTU**
2.3	0.002186	0.0147
1	0.0016	0.0345
0.9	0.0008	0.0336
0.8	-0.0032	0.0336
0.7	-0.0610	0.0316
0.6	-0.0740	0.0293
0.5	-0.0780	0.0281
0.4	-0.0118	0.0255
0.3	-0.0166	0.0228
0.2	-0.0376	0.0162
0.1	-0.1133	0.0185

Table 6-6: Zero lift pitching moment coefficients for NACA 0012 and DHMTU sections as a function of altitude

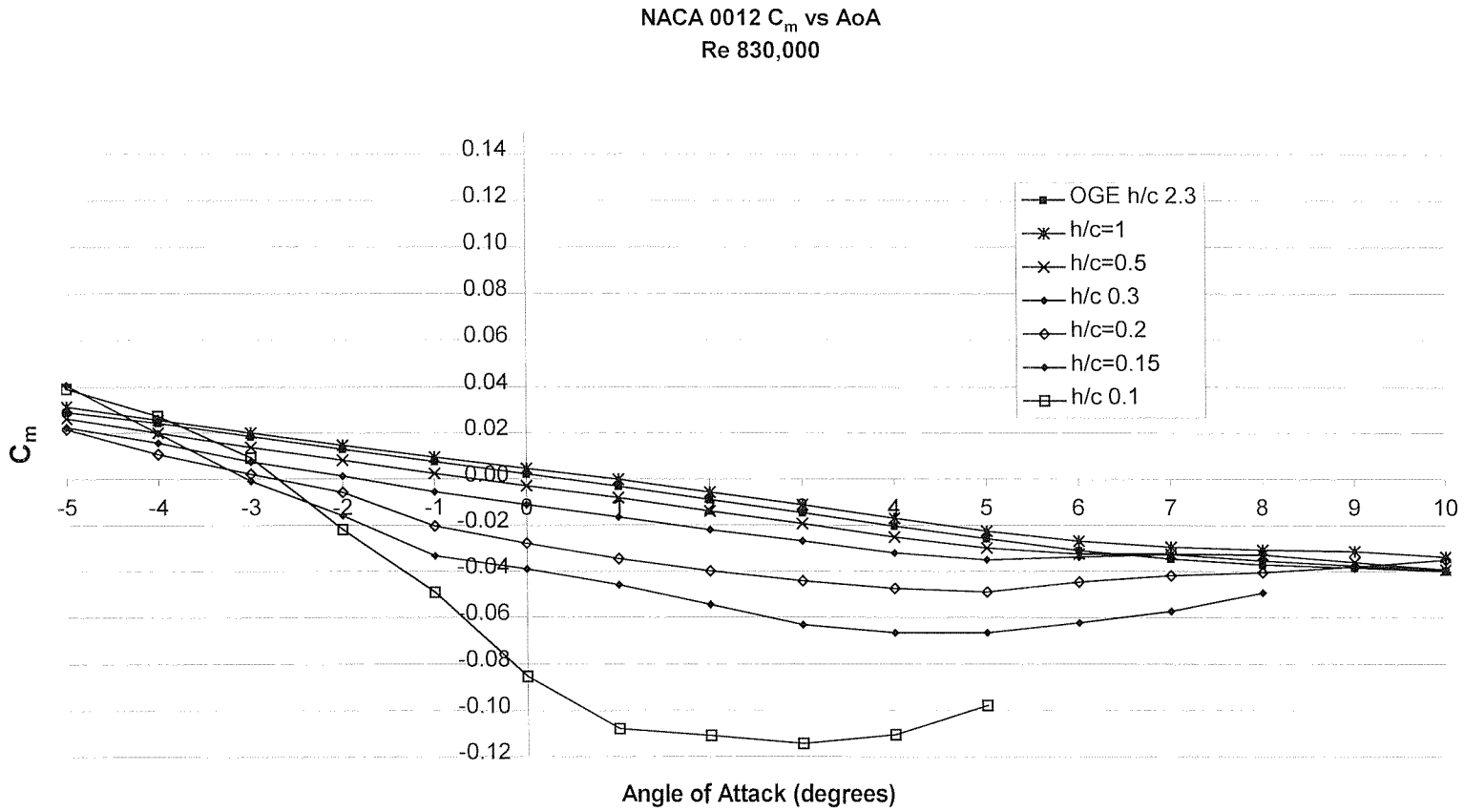

Figure 6-1: NACA 0012 Pitching Moment vs Angle of Attack

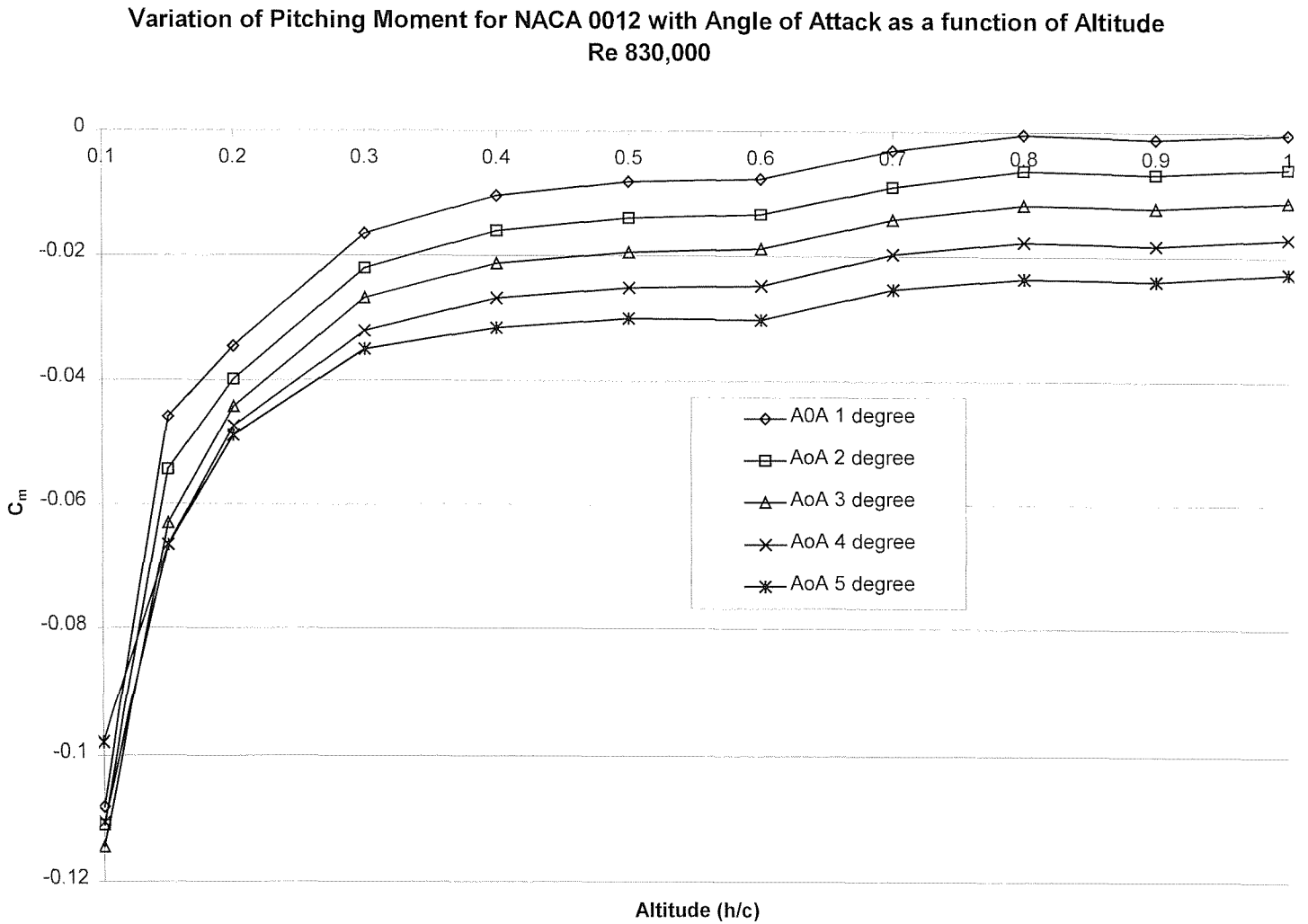

Figure 6-2: Variation of Pitching Moment with Angle of Attack for the NACA 0012 for various Altitudes

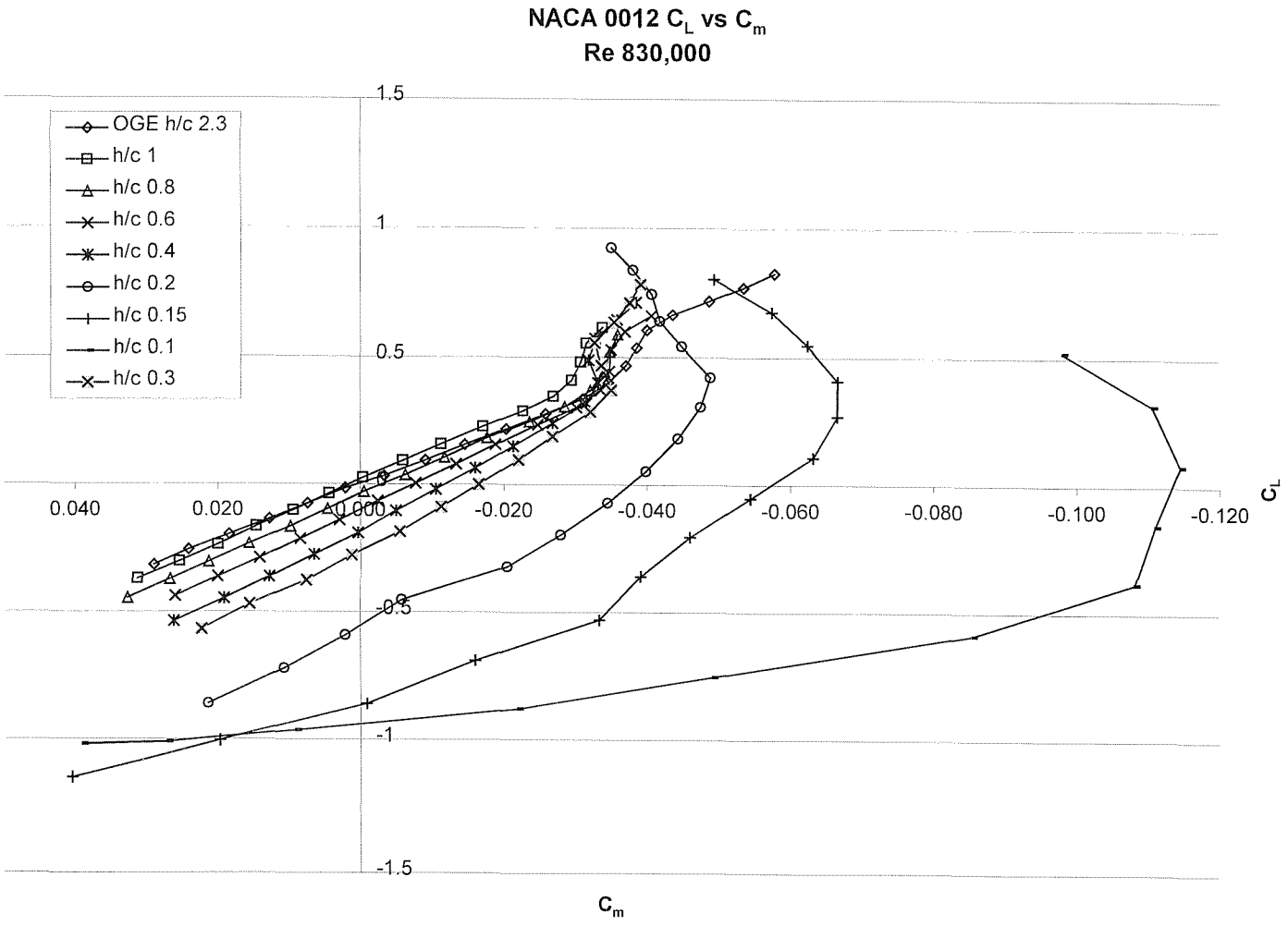

Figure 6-3: NACA 0012 C_L vs C_m

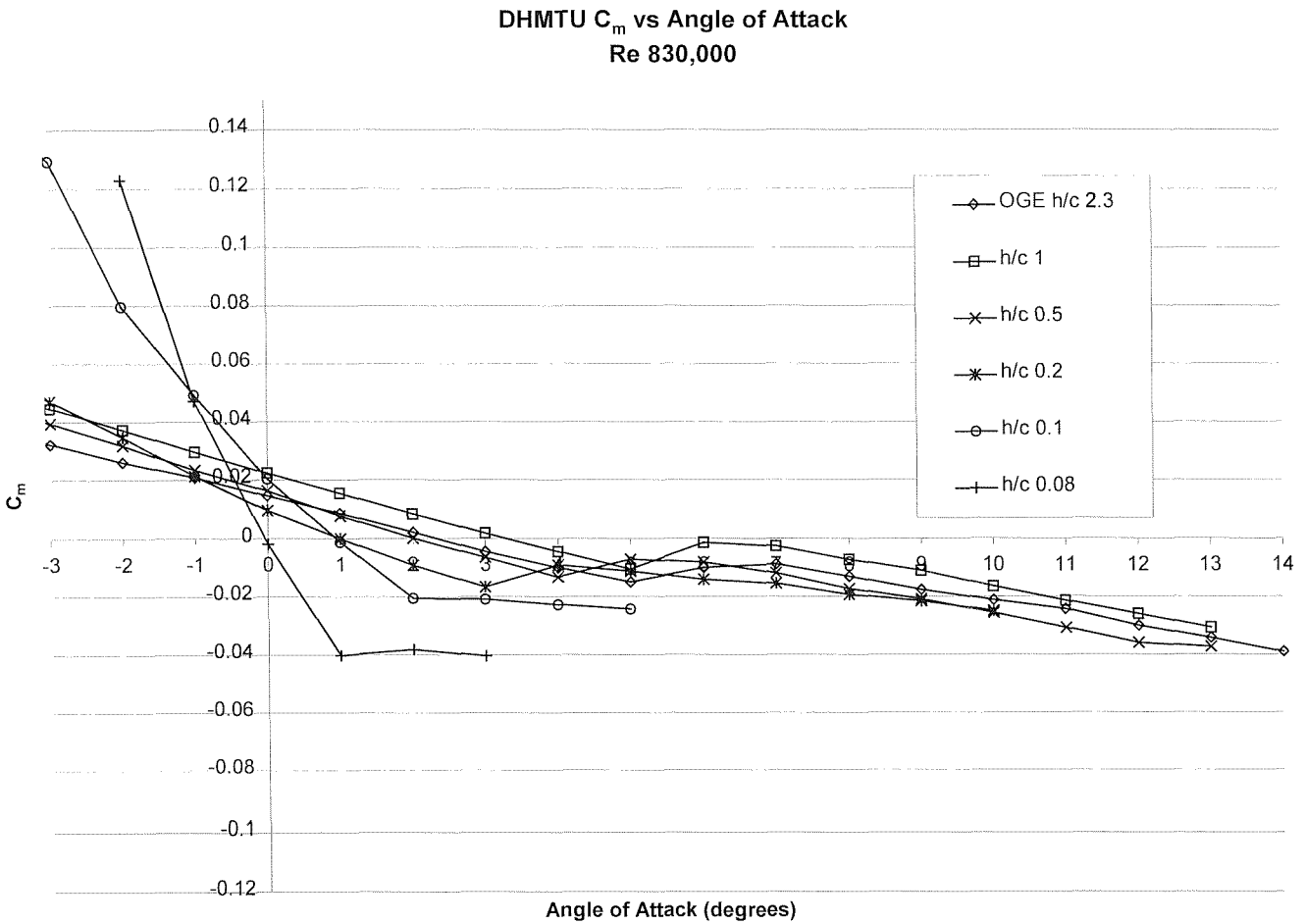

Figure 6-4: DHMTU Pitching Moment vs Angle of Attack

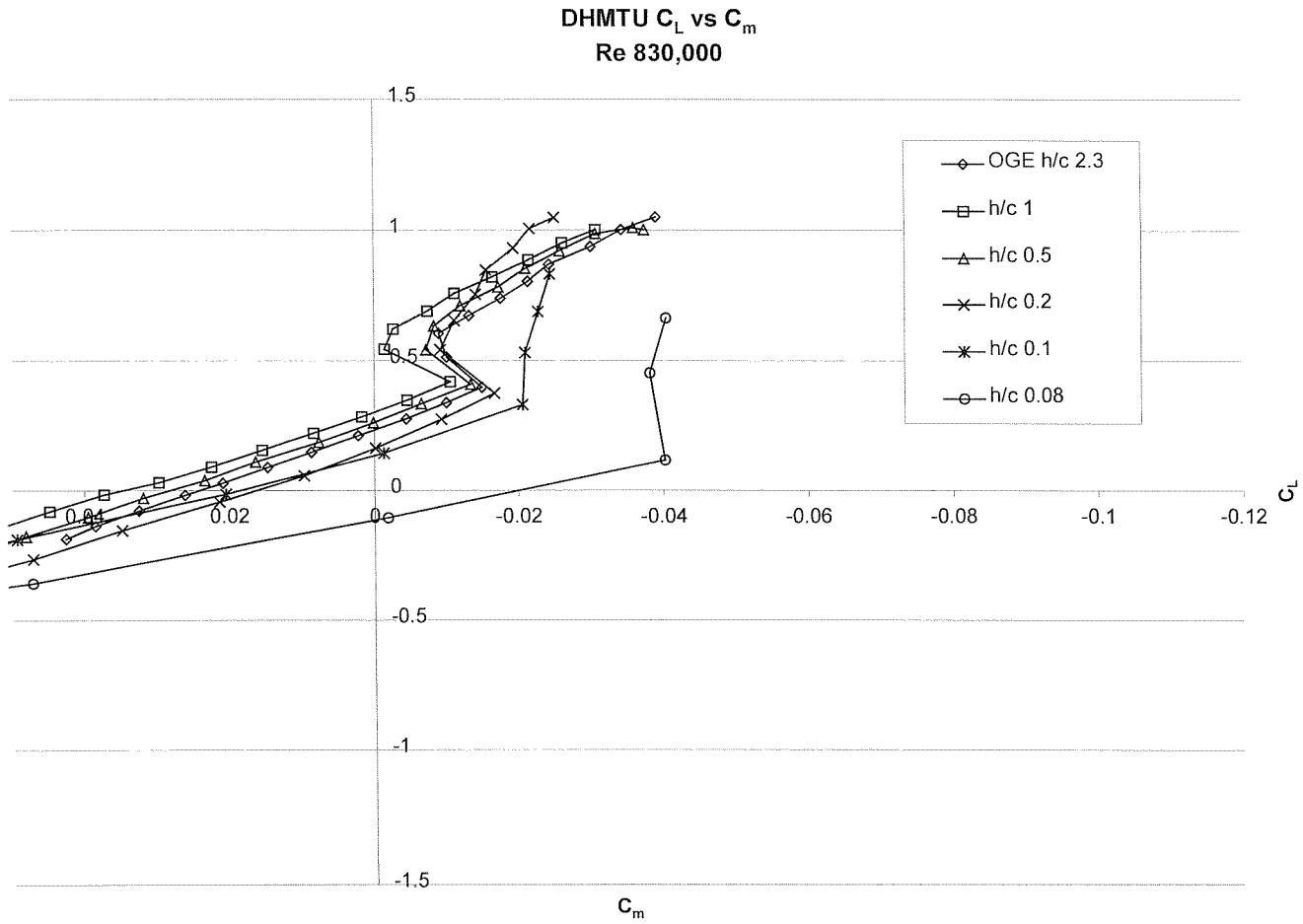

Figure 6-5: DHMTU C_L vs C_m

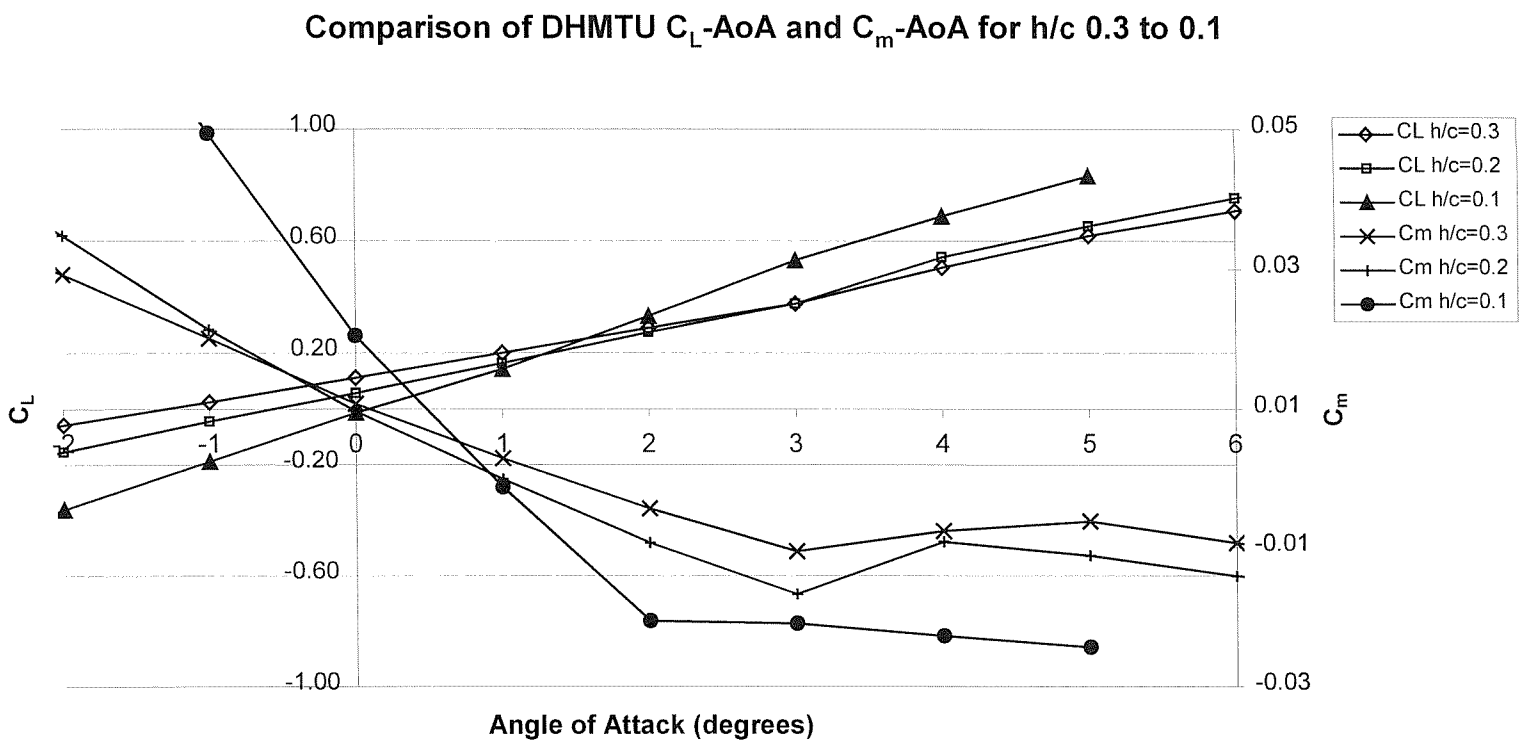

Figure 6-6: Comparison of Lift and Pitching Moment Curves for DHMTU at altitudes h/c 0.1 to 0.3

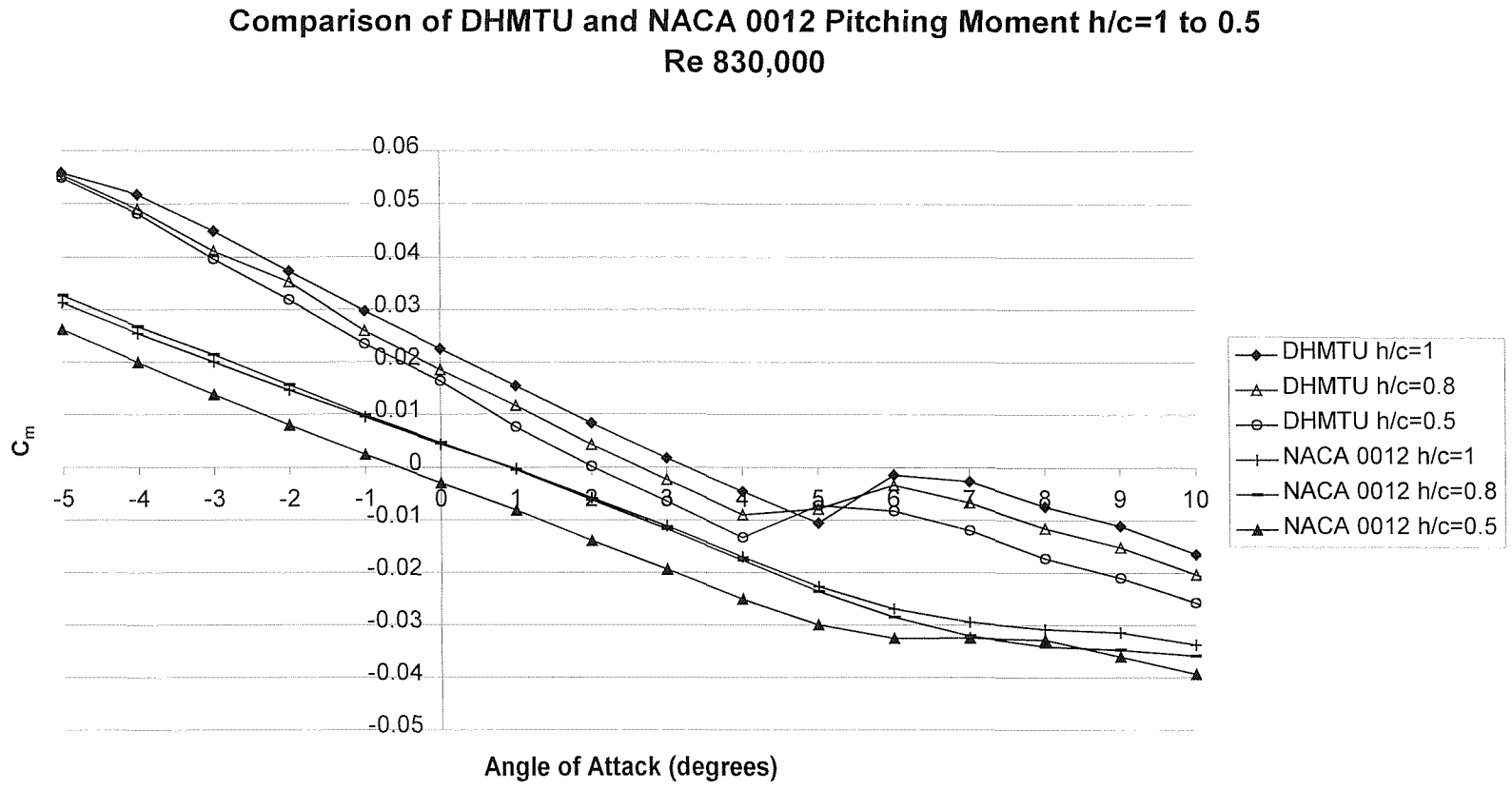

Figure 6-7: Pitch behaviour of NACA 0012 and DHMTU (upper set of lines) sections between altitudes h/c 1.0 to 0.5

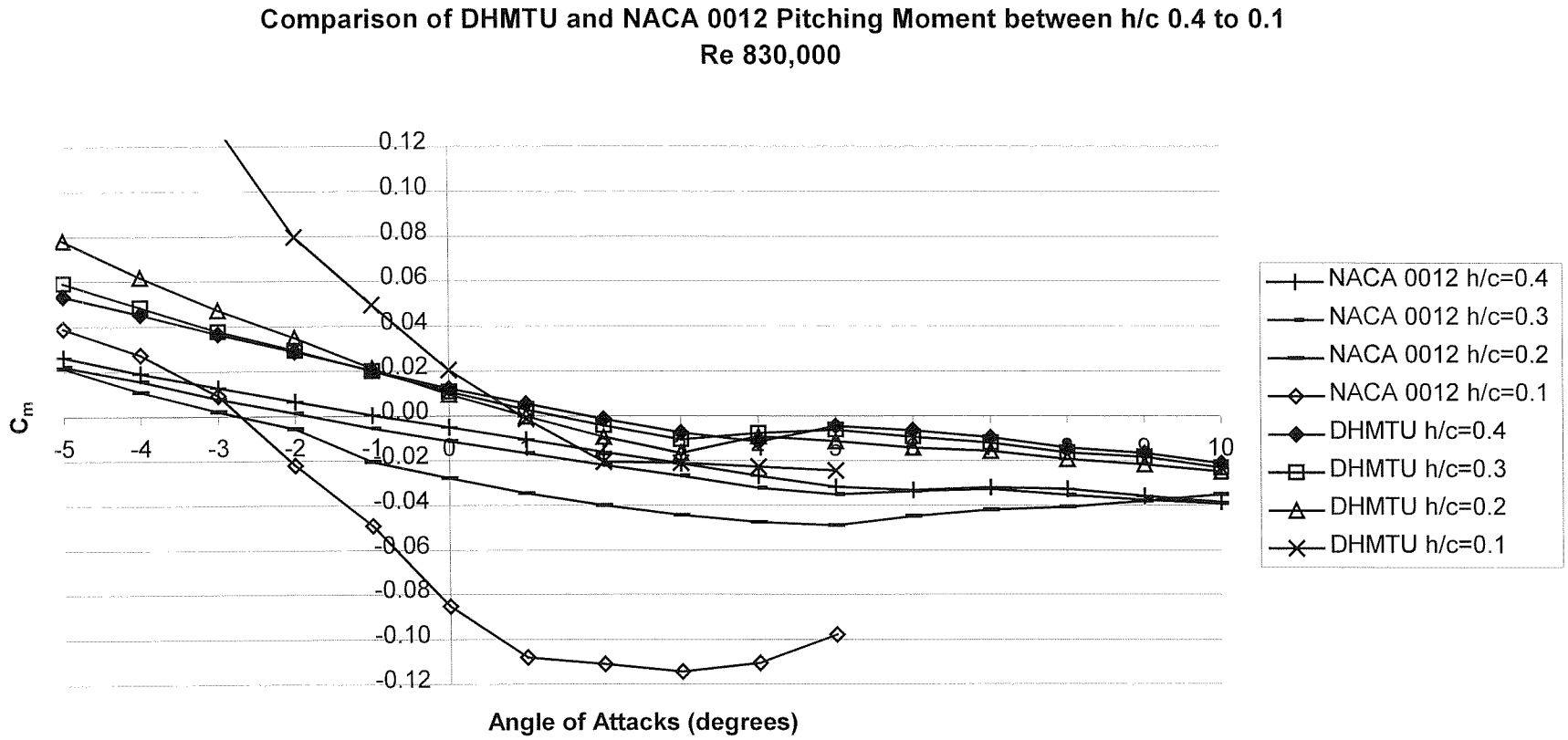

Figure 6-8: Pitch behaviour of NACA 0012 and DHMTU sections between altitudes h/c 0.4 to 0.1

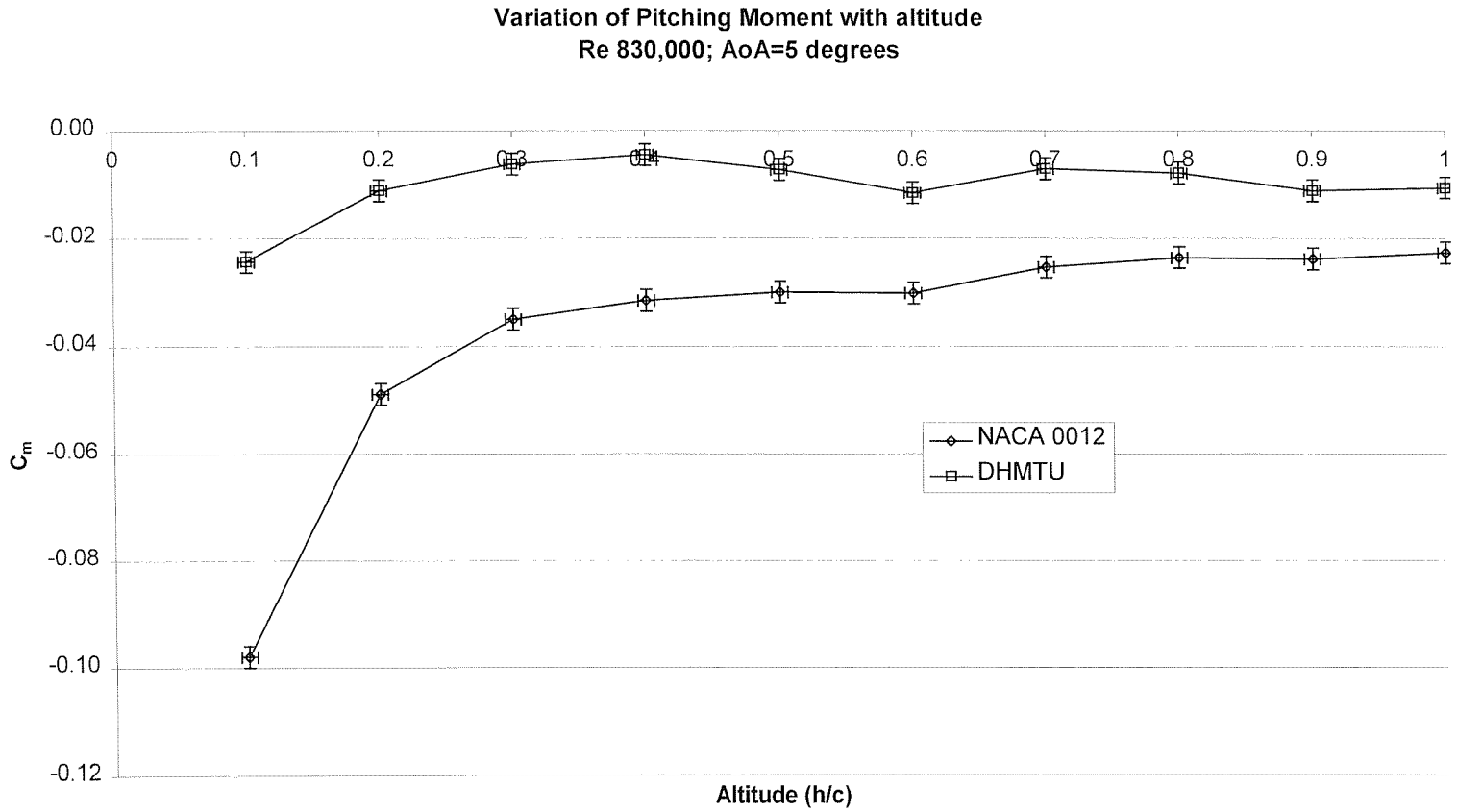

Figure 6-9: Variation of Pitching Moment as a function of altitude

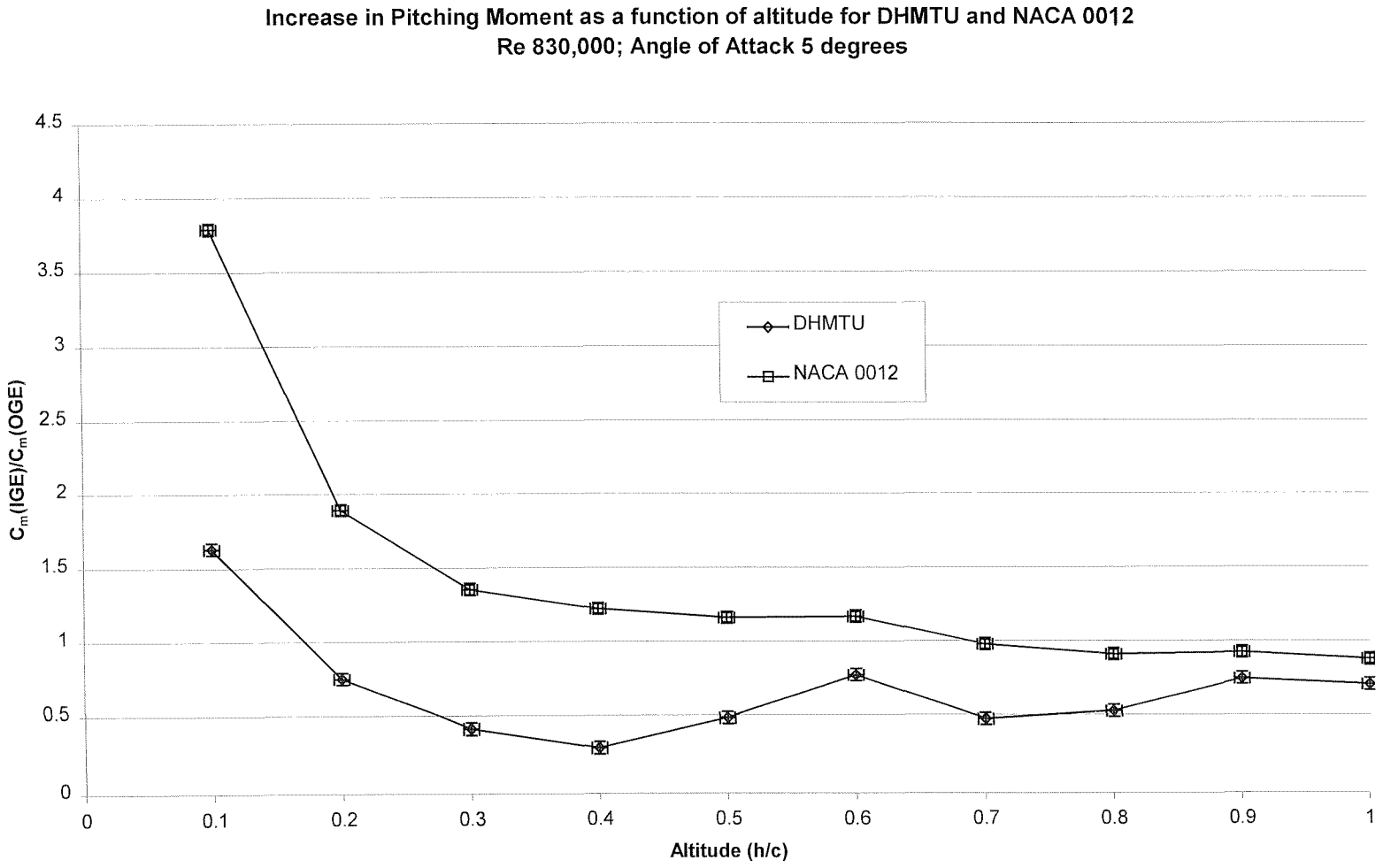

Figure 6-10: Graph illustrating the ratio of C_m IGE/C_m OGE as a function of altitude

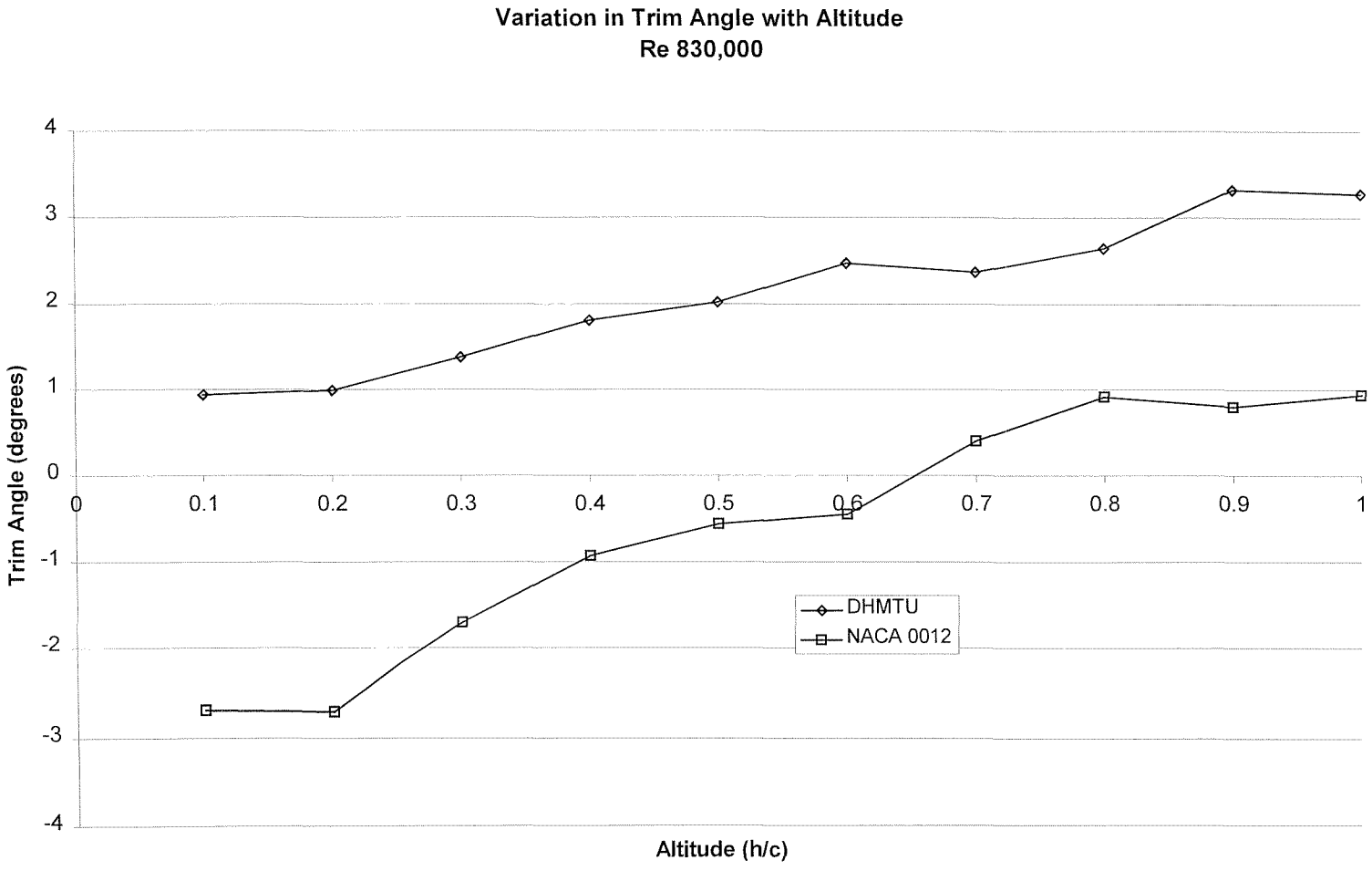

Figure 6-11: Variation of trim angle with altitude

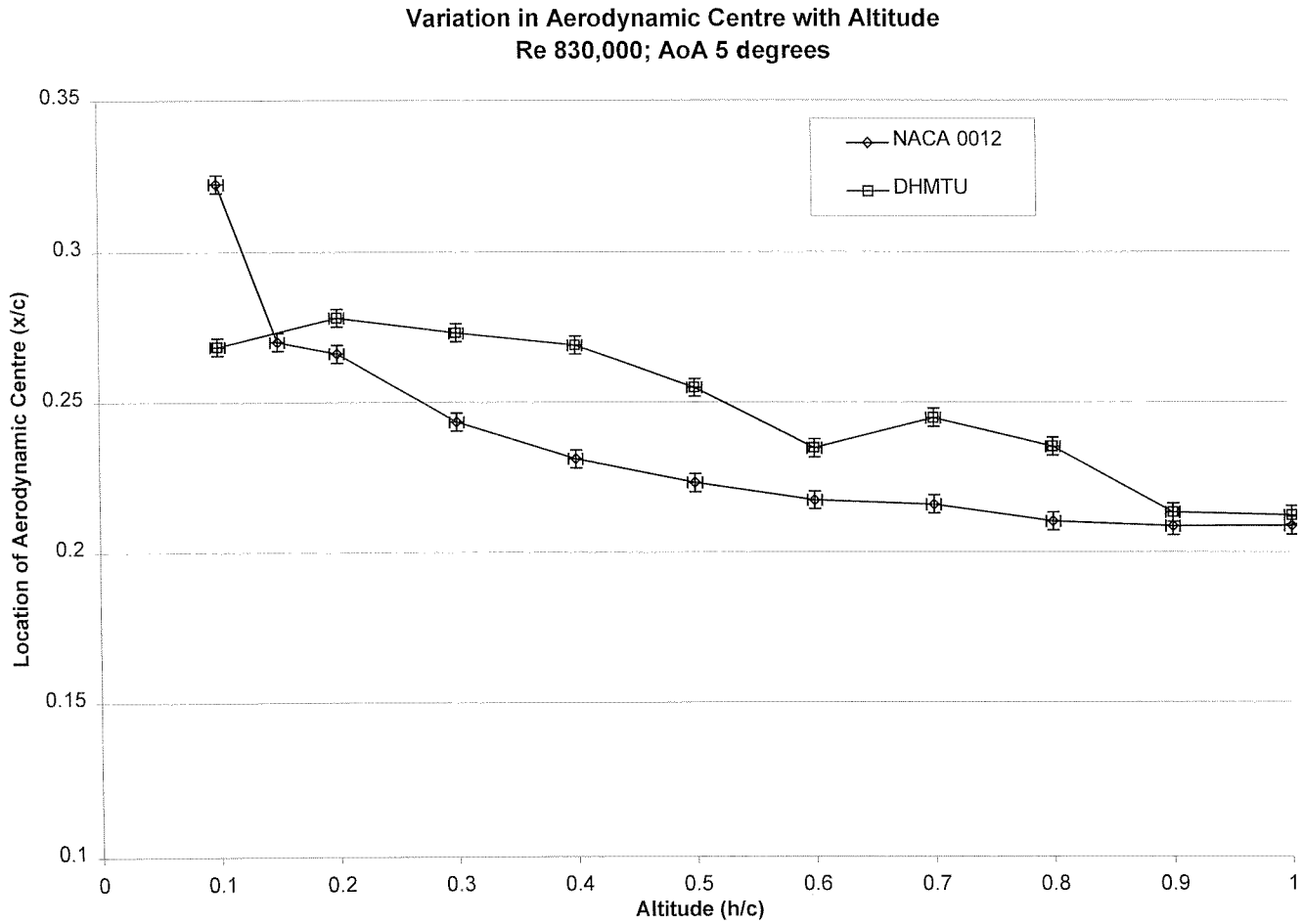

Figure 6-12: Variation of Aerodynamic Centre with altitude for NACA 0012 and DHMTU

7 Pressure Tapping and Flow Visualisation Analysis

7.1 Overview

The previous chapter illustrated the bulk changes in aerodynamic lift and drag forces that occur when the DHMTU 12-35.3-10.2-80.12.2 and NACA 0012 aerofoils operate in ground effect. This chapter presents the pressure profiles over the DHMTU aerofoil at various ground effect altitudes.

In order to investigate the pressure distribution around the DHMTU aerofoil in ground effect a total of 30 pressure tappings were made down the centre of the sections span. The location of these and their identifying number are shown in Figure 7-1, Figure 7-2 and Figure 7-3. The positions of the pressure tappings are given as a ratio of the wingchord (x/c). The dimensions of the trial DHMTU wing are given in Table 4-2 and the test variables are presented in Table 7-1. The measurements were taken in the University of Southampton 2.1 x 1.7 m rolling road wind tunnel. Further details of this facility are contained in Chapter 4. The measurement uncertainty and repeatability of the pressure tapping measurements are located in Appendix A.

7.2 Variation in Pressure Profiles with Altitude

7.2.1 Lower Surface Pressure Distribution

The pressure distribution along the underside of the DHMTU aerofoil as a function of altitude is shown in Figure 7-4. The data presented is for an angle of attack of 3 degrees as this was the maximum that could be achieved at the lowest tested altitudes. To assist the reader in understanding the following analysis the DHMTU aerofoil has been annotated with the key pressure tapping locations (Figure 7-3). Though this chapter is discussing the chordwise pressure distribution along the centre span of the DHMTU wing, the wingtip is shown to allow the reader to associate the location of pressure tappings to the aerofoil geometry.

The data in Figure 7-4 shows that as the altitude decreases the pressure on the lower surface increases. As the altitude reduces from h/c 1.0 to 0.6 the increase

in pressure on the lower surface is slight. Below an altitude of h/c 0.6 greater increases in pressure result for every additional h/c 0.1 decrease in altitude. The results presented in Figure 7-4 superbly illustrate the difference between moderate (h/c>0.1) and extreme (h/c<0.1) ground effect. It is noticeable that when the altitude falls below h/c 0.2 the pressure under the section greatly increases. Also the rate at which the pressure increases is particularly evident when h/c is 0.1 and 0.08. Compare the near linear nature of the pressure increase above an altitude of h/c 0.2 to the extreme ground effect pressure profiles where the pressure gradient across the lower section profile shows a rapid increase up to x/c 0.48. This corresponds to a distance of 0.5 chord from the section leading edge. Another feature that can be seen in this data is the increase in pressure at the trailing edge of the aerofoil as the altitude decreases.

As the altitude increases above h/c 0.6 suction is present near the leading edge on the lower surface from x/c 0.06 to 0.18. As the altitude decreases below h/c 0.5 this changes and pressure is present along the whole length of the lower surface. Note that at x/c 0.06 when the altitude of the DHMTU is h/c 0.08 the pressure reduces below that for when the aerofoil is at h/c 0.5. When the DHMTU is operating out of ground effect (h/c 2.9) suction is present on the lower surface from the x/c 0.06 to 0.48.

The total pressure coefficient on the lower surface of the DHMTU as a function of altitude is shown in Figure 7-5. It can be seen that there is a continual increase in pressure as the altitude decreases. When the wing is at an altitude of h/c 0.2 and an angle of attack of 3 degrees the pressure under the wing is 13 times that experienced at a moderate ground effect altitude of h/c 0.8. When the DHMTU is at the extreme ground effect altitude of h/c 0.1 the pressure under the lower surface is 21 times greater than at h/c 0.8. Reducing the altitude by even h/c 0.02 to h/c 0.08 increases the pressure to 26 times that produced at h/c 0.8.

Figure 7-6 provides a graphical depiction of the airflow on the undersurface of the DHMTU at an altitude of h/c 0.15 and 5 degrees angle of attack. The effect of the spanwise component of the flow due to wingtip circulation is very evident. This

can be seen in the deflection of the chordwise flow towards the wingtip. Another feature that can be discerned is the flow separation at the trailing edge.

As shown in Chapter 5 when the ground does not constrain the DHMTU aerofoil's angle of attack its highest aerodynamic efficiency is achieved between 5 to 6 degrees AoA. Figure 7-7 presents the pressure profiles on the lower surface of the DHMTU aerofoil at an angle of attack of 5 degrees. It can be seen that there are three distinct groups of curves on this graph. The out of ground effect curve at h/c 2.9 possessing the lowest pressure on the aerofoil under surface. Than there are the group of moderate ground effect curves covering the altitudes between h/c 0.9 and 0.4. The curves at h/c 0.2 and 0.3 stand apart possessing much higher-pressure profiles than the curves between h/c 0.9 to 0.4. The curve at h/c 0.3 exhibits the linear increase in pressure along the surface displayed at higher altitudes. In contrast the h/c 0.2 curve exhibits the rapid increase associated with the extreme ground effect curves at an angle of attack of 3 degrees (Figure 7-4).

At the optimum angle of attack of 5 degrees the pressure under the DHMTU lower surface is approximately 7.5 times greater at h/c 0.2 compared to operating out of ground effect. Even when operating at moderate ground effect altitudes the pressure on the lower surface is over 2.5 times that experienced out of ground effect.

A comparison between the total pressure on the lower and upper surface of the DHMTU wing is shown in Figure 7-5. It can be seen that when the DHMTU is operating out of ground effect the contribution of lift from the upper surface is much greater than that from the lower surface. This is a standard and well known result and there is nothing remarkable about this. What is interesting is that as the altitude decreases the contribution of lift from the upper surface increases only slightly compared to the large increases recorded on the lower surface. Quantitatively the total pressure on the upper surface when the wing is at an altitude of h/c 0.1 is only 13% greater than at h/c 2.9. In contrast when the wing is OGE suction is present on the lower surface, but when the altitude has reduced to h/c 0.1 the total pressure on the lower surface is now equal to that on the

upper. This illustrates that when in ground effect the variation in total pressure on the upper surface with a decrease in altitude is much less than the increase in pressure on the lower surface.

7.2.2 Upper Surface Pressure Distribution

The trends in the flow over the upper surface of the DHMTU aerofoil can be seen in Figure 7-8. The key chordwise tapping positions described below can be seen on the annotated DHMTU aerofoil in Figure 7-9. The points are illustrated near the wingtip to provide the reader with reference features on the aerofoil section.

Increasing suction can be seen to occur between x/c 0 to 0.06 as the flow accelerates over the section's nose. As the altitude decreases the magnitude of this suction near the leading edge increases. The pressure over the whole of the upper surface decreases with decreasing altitude.

The suction remains high between x/c 0.06 to 0.36 over increasing section camber. A reduction in suction is produced after x/c 0.36 as a result of flow separation. This separation can be seen in an image recorded during flow visualisation experiments (Figure 7-10). A pooling of the flow visualisation mixture indicates that the flow has separated. As can be seen from Figure 7-10 the flow has reattached itself but this flow separation bubble has reduced the lift and increased the drag of the DHMTU aerofoil. This phenomenon of flow separation is a low Reynolds Number effect and is the result of the increasing camber of the upper section.

The gradual decrease in suction is present until after x/c 0.72 when positive pressure is present on the upper surface. The greatest changes with altitude occur over the first half of the section upto x/c 0.36. The pressure distribution reveals that when operating in ground effect the most scope for increasing the suction and thereby performance over the upper surface is by optimising the front half of the section. This includes parameters such as the leading edge nose radius and camber of the front of the section.

A major finding is the large differences in pressure coefficient on the upper and lower surfaces with small changes in altitude between h/c 0.3 and 0.08. If we consider the postulated UWIGV with a chord of 0.319 m, a translation in altitude of just 0.03 m in this altitude regime will produce a significant variation in the lift characteristics of the wing. This will require the vehicles flight control system to be able to provide rapid stabilising responses. Alternatively the UWIGV could operate above an altitude of h/c 0.3.

7.3 Angle of Attack change on pressure distribution

This section discusses the performance of the DHMTU aerofoil at various altitudes as a function of angle of attack. The following altitudes are presented:

- h/c 0.9 this allows the DHMTU performance over a large range of AoA to be investigated
- h/c 0.4 and 0.2 typical moderate ground effect altitudes
- h/c 0.08 illustrating the behaviour of the section in extreme ground effect, though this only allows a small range of AoA to be investigated.

Figure 7-11 depicts the pressure profile over the upper surface of the DHMTU at h/c 0.9 for AoA between 1 to 11 degrees. At an angle of attack of 9 degrees the suction over the upper surface between x/c 0.18 to 0.48 reduces and has become significant at 10 degrees. When the altitude has reduced to h/c 0.4 the reduction in suction occurs at an angle of attack of 10 degrees (Figure 7-12). A further reduction in altitude to h/c 0.2 results in this reduction in suction being observed at an angle of attack of 8 degrees (Figure 7-13). This shows that with a decrease in altitude the angle of attack at which a reduction in suction over the upper surface takes place occurs at a smaller angle of attack.

When the DHMTU aerofoil is in extreme ground effect this reduction in suction is not seen as the ground constrains the maximum angle of attack that can be achieved. At h/c 0.1 the maximum achievable angle of attack is 4 degrees (Figure 7-19) reducing to 3 degrees at h/c 0.08 (Figure 7-20).

As with any aerofoil section an increase in angle of attack results in an increase in pressure over the lower surface. As the DHMTU operates in ground effect the

increase in pressure with angle of attack increases with decreasing altitude. This can be clearly seen by comparing the range of pressure profiles when the DHMTU is out of ground effect (Figure 7-14) with those in moderate ground effect (Figure 7-16) and extreme ground effect (Figure 7-19 and Figure 7-20).

An angle of attack is reached where the pressure near the leading edge on the lower surface is lower than that of the preceding angle. When the DHMTU is at a moderate ground effect altitude of h/c 0.9 the pressure on the lower surface decreases when the angle of attack exceeds 10 degrees (Figure 7-15). This angle remains constant throughout the moderate ground effect regime down to an altitude of h/c 0.4 (Figure 7-16). As the altitude reduces to h/c 0.3 the pressure near the leading edge decreases when the AoA is above 7 degrees (Figure 7-17). A further reduction in altitude to h/c 0.2 reduces this angle to 6 degrees (Figure 7-18). This demonstrates that as the altitude reduces the angle of attack at which this drop in pressure on the lower surface occurs becomes progressively smaller below h/c 0.4.

The proximity of the ground has the effect of decreasing the angle of attack that pressure is present over the whole lower surface. When the DHMTU is out of ground effect pressure is present over the whole lower surface at an angle of attack of 5 degrees. As the section descends to a moderate ground effect altitude of h/c 0.4 this reduces to 4 degrees. In extreme ground effect this reduces to 1 degree at h/c 0.1 (Figure 7-20).

7.4 Tripping the Boundary Layer

To investigate the sensitivity of the DHMTU aerofoil to tripping the boundary layer, a wire was stretched across the leading edge of the DHMTU aerofoil. Figure 7-21 presents the resulting pressure profiles over the upper and lower surfaces of the DHMTU at an altitude of h/c 0.2. It can be seen that tripping the boundary layer has resulted in a reduction of suction over the upper surface and suction is now present over the rear part of the DHMTU upper surface from x/c 0.78 (Figure 7-9). Tripping the boundary layer has reduced the lift contribution from the upper surface by 6% of its no trip value.

Like the upper surface tripping the boundary layer has had the effect of reducing the pressure and hence contribution to lift from the lower surface The lift contribution from the lower surface has been reduced by 12% of the untripped value. Near the leading edge the pressure has been reduced to 32% of its no trip value (Figure 7-22). Moving further aft this reduction in pressure is greatly diminished until it's approximately 95% of the no-trip value is produced near the trailing edge.

The overall result of tripping the boundary layer at the leading edge of the DHMTU is to reduce the overall lift coefficient by 8%.

7.5 Sensitivity to Ground Conditions

A series of experiments were carried out to investigate how the pressure distribution over the upper and lower surfaces of the DHMTU aerofoil is effected by operating over a stationary surface. The data obtained when the ground was stationary has been compared to the normal operating case of the moving road running at the wind tunnel airflow speed of 38 ms^{-1}. These results are of particular interest for the validity of the data obtained in the CWC trials (Chapter 7) where the limitations in the testing apparatus result in the wavy surfaces being stationary. The general question that needs to be addressed is what are the effects on the pressure profile of operating over a stationary ground compared to a moving one. More specifically at what altitude are these effects evident and their magnitude.

When the DHMTU is operating out of ground effect (h/c 2.9) there is no significant change on the lower surface pressure distribution whether the ground is stationary or moving (Figure 7-23). This result is to be expected as the section is out of even moderate ground influence.

As the aerofoil descends into the moderate ground effect regime (h/c 1.0-0.2) the effect of the stationary ground conditions become noticeable on the lower surface pressure distribution. This can be seen in Figure 7-24 when the DHMTU aerofoil is operating at an altitude of h/c 0.9. The peak pressure on the under surface reduces to 92% of the Cp value when the road surface on. Down to an altitude of

h/c 0.3 the peak pressure on the under surface reduces by a maximum to 88% of the moving road value (Figure 7-27).

When the aerofoil is at an altitude of h/c 0.2, the lower limit of the moderate ground effect regime, larger reductions in pressure on the lower surface are exhibited. Here the greatest reduction in pressure does not occur near the leading edge but increases to a maximum at the trailing edge of the section (Figure 7-25). This is a result of the trailing edge being closest to the ground and experiencing a greater influence of the ground conditions. At this altitude the pressure at the trailing edge due to the stationary ground is only 67% of the value when the road was on (Figure 7-27).

When the DHMTU aerofoil is operating in extreme ground effect the stationary road has a significant effect on the underside pressure. At h/c 0.1 the pressure coefficients under the wing are only 50-60% of the values when the road was moving. As the aerofoil descends down to h/c 0.08 the pressure coefficients are now only 40-54% of the moving ground values. The large reduction in pressure along the lower surface can be seen in Figure 7-26. With the road stationary at this altitude suction is now present between tappings 16 and 17.

Figure 7-28 to Figure 7-30 illustrates the effect that a stationary surface has on the pressure distribution on the upper surface of the DHMTU aerofoil. At altitudes above h/c 0.2 the stationary surface has no effect on the pressure distribution over the upper surface. Figure 7-28 shows that at h/c 0.2 the stationary surface has little effect on the upper surface pressure distribution. As the altitude reduces to h/c 0.1 and h/c 0.08 the stationary ground does reduce the suction on the upper surface of the DHMTU (Figure 7-29 and Figure 7-30).

A comparison between Figure 7-27 and Figure 7-31 shows that the reduction in suction over the upper surface of the DHMTU aerofoil is much less than the reduction of pressure on the lower surface. At an altitude of h/c 0.2 the difference in pressure coefficient on the upper surface with the road on and off is negligible. The effect of the road being turned off is more noticeable at h/c 0.1 where the pressure coefficient is between 85-96% of the moving ground value.

As the altitude decreases to h/c 0.08 the suction has decreased by 77-93% of the Cp when the road is on.

7.6 Summary

1. As the DHMU aerofoil enters the ground effect regime the pressure on the lower surface and the suction on the upper surface increases. The increase in pressure on the DHMTU lower surface due to ground effect is greater than the increase in suction over the upper surface. With a reduction in altitude the pressure profile on the lower surface of the DHMTU incrementally increases down to an altitude of h/c 0.3. Further reductions in altitude below h/c 0.3 result in significant increases in pressure. This is most evident when the DHMTU enters extreme ground effect (h/c <0.1).

2. On the upper surface of the DHMTU the effect of ground proximity is most evident over the frontal half of the aerofoil. Pressure profile data and flow visualisation show that flow separation and reattachment occurs on the aerofoil's upper surface. This is a result of the combination of low Reynolds Number (830,000) and camber of the upper section.

3. As the altitude decreases the angle of attack that flow separation on the upper surface of the DHMTU aerofoil occurs at reduces. At the higher end of the moderate ground effect regime (h/c 1.0 to h/c 0.4) this angle of attack remains relatively constant around 9-10 degrees. At h/c 0.3 and 0.2 upper surface flow separation occurs at 8 degrees. At these low angles of attack no upper surface flow separation was observed due to the ground constraint on achievable angle of attack.

4. Tripping the boundary layer reduces the suction over the upper surface and pressure on the lower surface of the DHMTU aerofoil. When the boundary layer is tripped the DHMTU wing experiences a 8% reduction in lift coefficient. The pressure profile on the upper surface over the rear part of the DHMTU now experiences suction as a result of tripping the boundary layer.

5. The lower surface of the DHMTU aerofoil is much more effected by a stationary ground than the upper surface. Pressure profiling data has indicated that the lower surface has a noticeable reduction of the pressure coefficient, typically 80% of the peak moving ground value, when operating in the moderate ground effect regime (h/c 1.0-0.3). In contrast the upper surface of the DHMTU is not influenced by the ground speed until an altitude of h/c 0.2. In extreme ground effect the pressure coefficient on the lower surface is reduced to 50-60% of the moving ground value at h/c 0.1. This compares with the pressure coefficient on the upper surface is 85-96% the moving ground value.

6. When the DHMTU is operating at altitudes below h/c 0.2 a stationary ground surface reduces the pressure coefficient on the upper and lower surfaces and as a result the lift of the aerofoil is lower. This indicates that data obtained in the CWC trials below an altitude of h/c 0.2 should be treated with extreme caution.

Variable	Experimental Range
Angle of Attack	1 to 11 degrees (1 degree steps)
Wing height (h/c)	0.08, 0.1 to 1.0 (0.1 steps) and 2.9
Reynolds Number	8.3×10^5

Table 7-1: Pressure profiling variables used in experiments

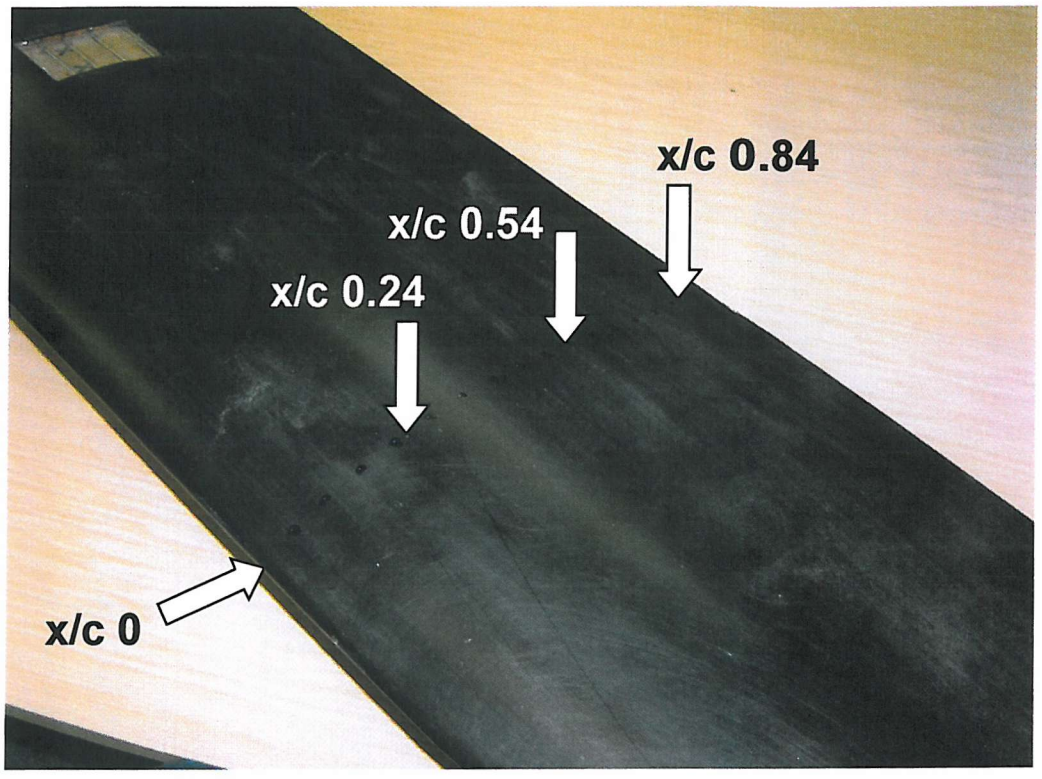

Figure 7-1: Location of Pressure Tappings on the DHMTU upper surface

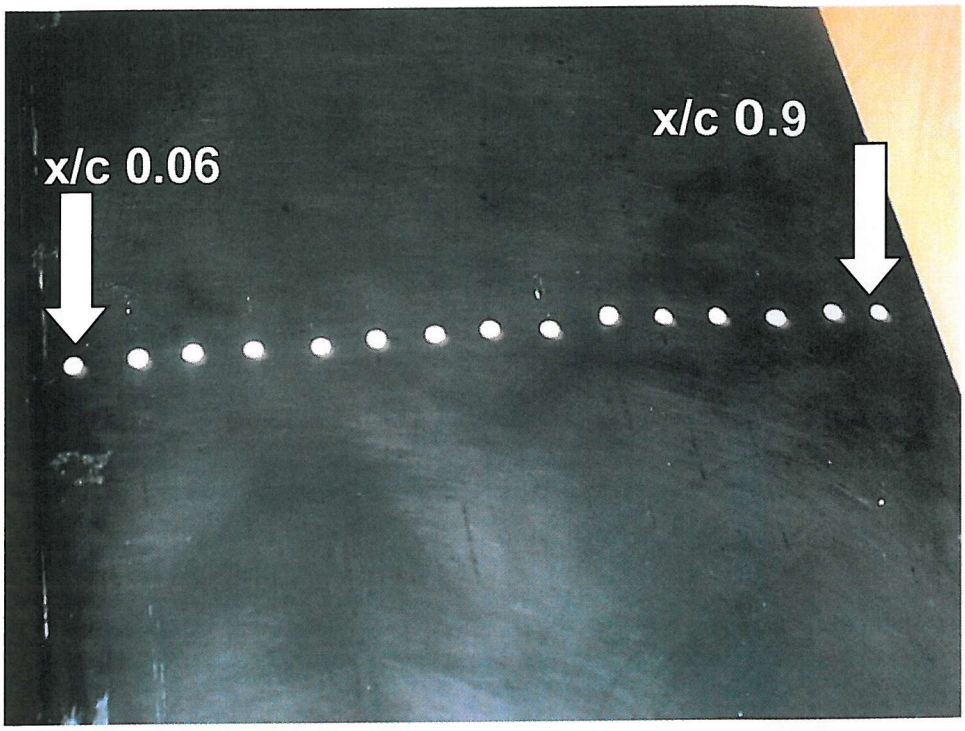

Figure 7-2: Location of Pressure Tappings on the DHMTU lower surface

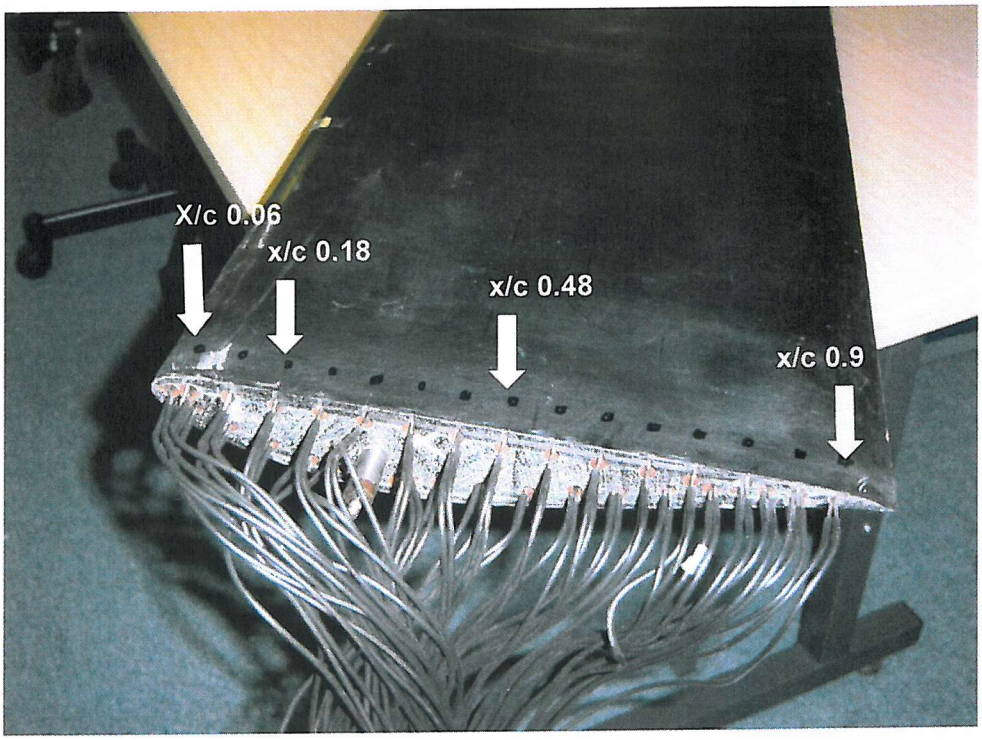

Figure 7-3: Key points on the lower surface of the DHMTU aerofoil

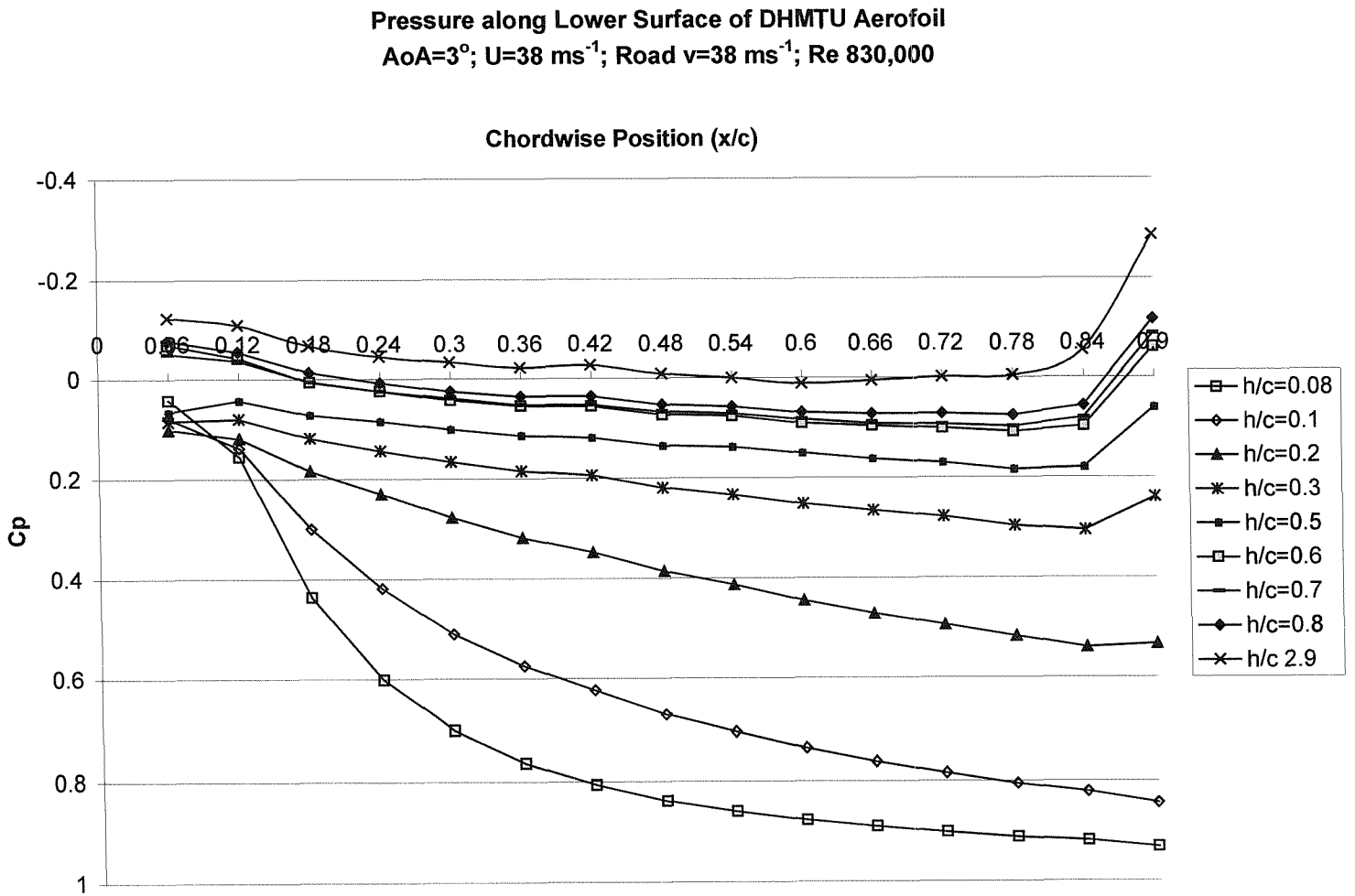

Figure 7-4: Pressure distribution under DHMTU mid span as a function of altitude (AoA 3 degrees)

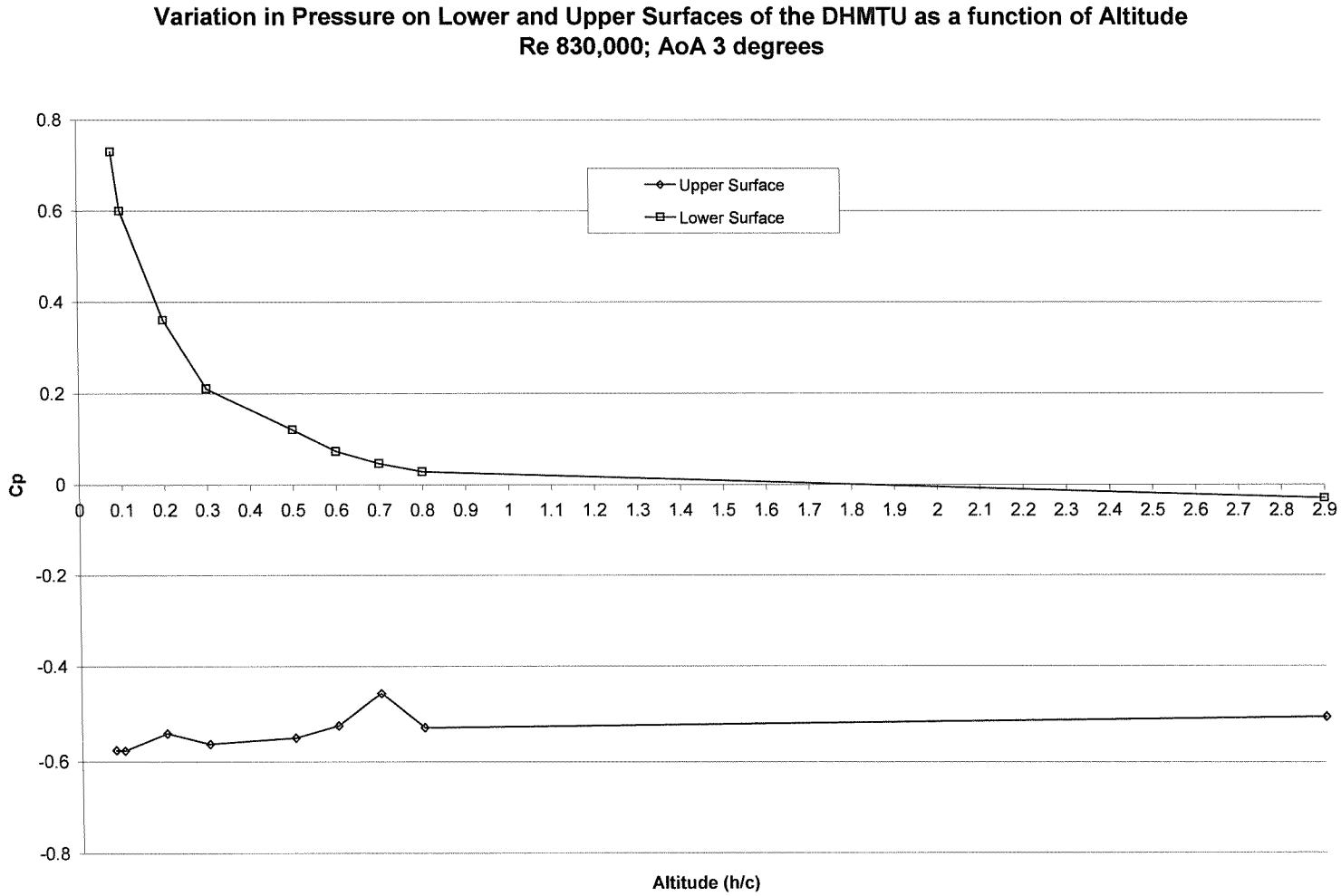

Figure 7-5: Integrated pressure recorded on the DHMTU upper and lower surface as a function of altitude

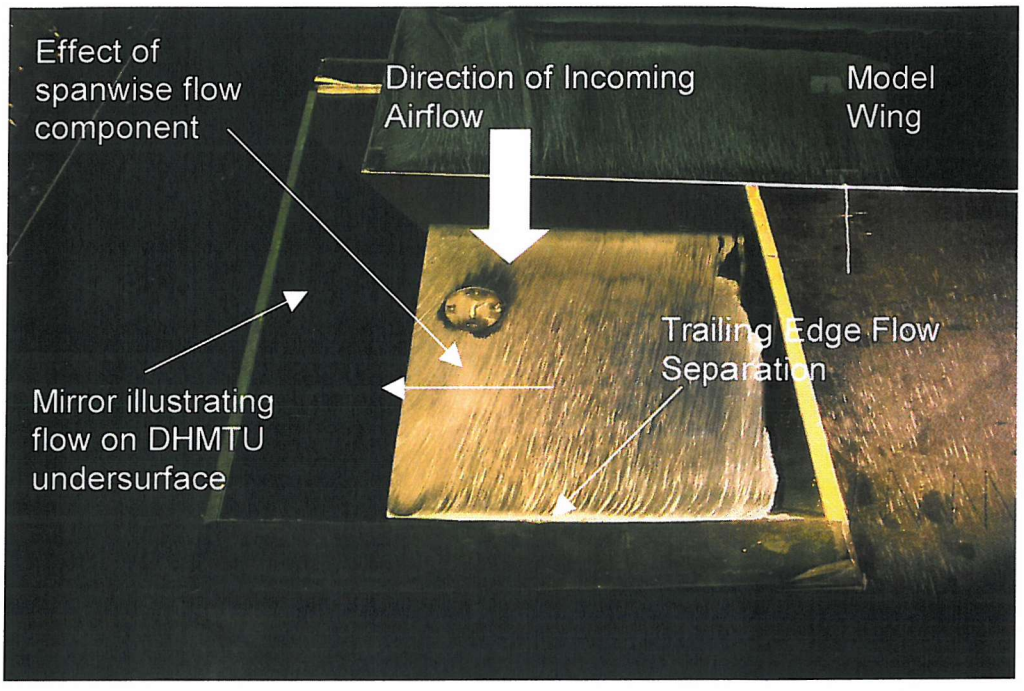

Figure 7-6: The mirror portrays the flow on the underside of DHMTU illustrating trailing edge flow separation and spanwise flow direction due to wing tip circulation at a Reynolds Number of 830,000

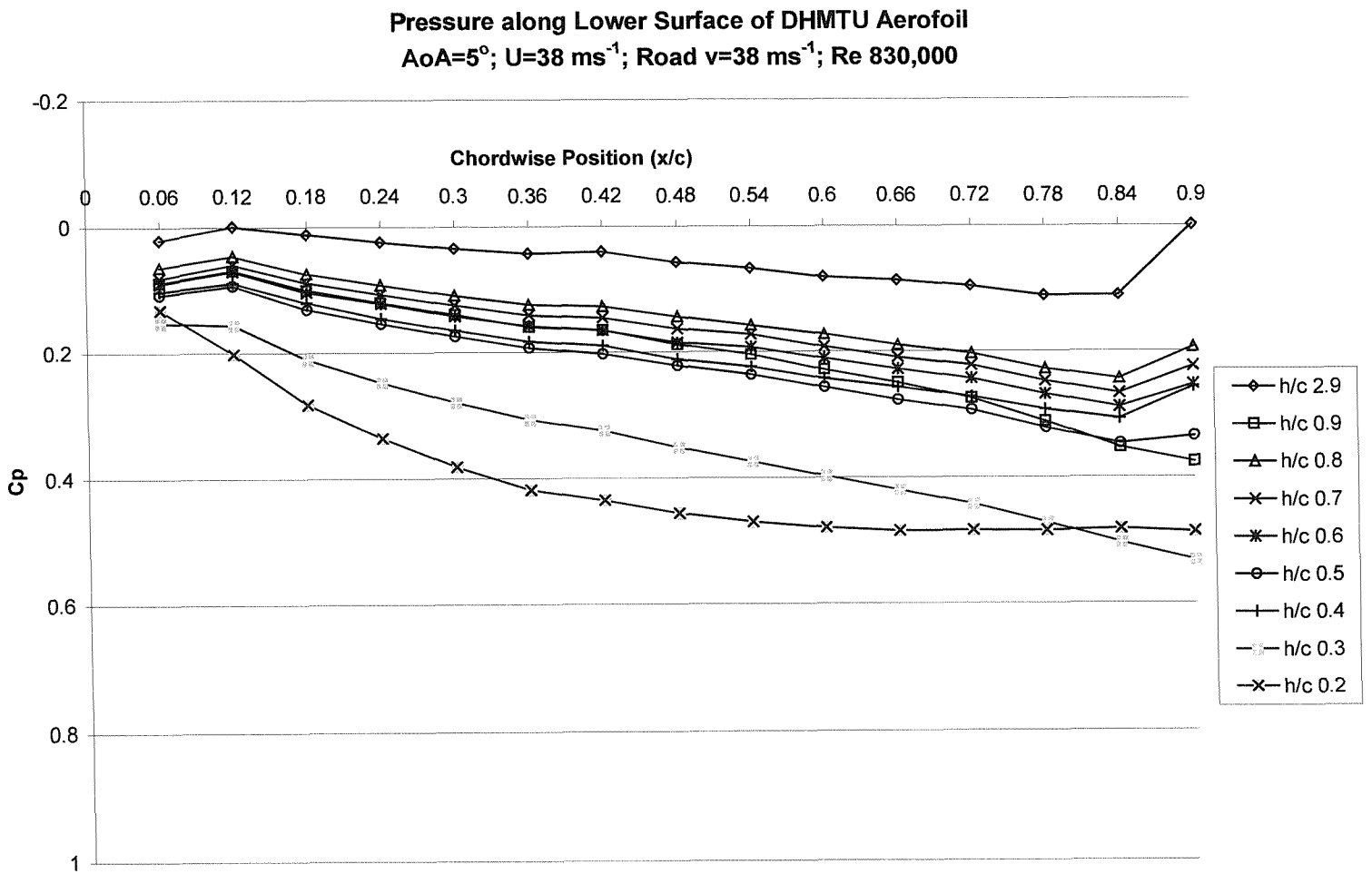

Figure 7-7: Pressure distribution under DHMTU mid span as a function of altitude (AoA 5 degrees)

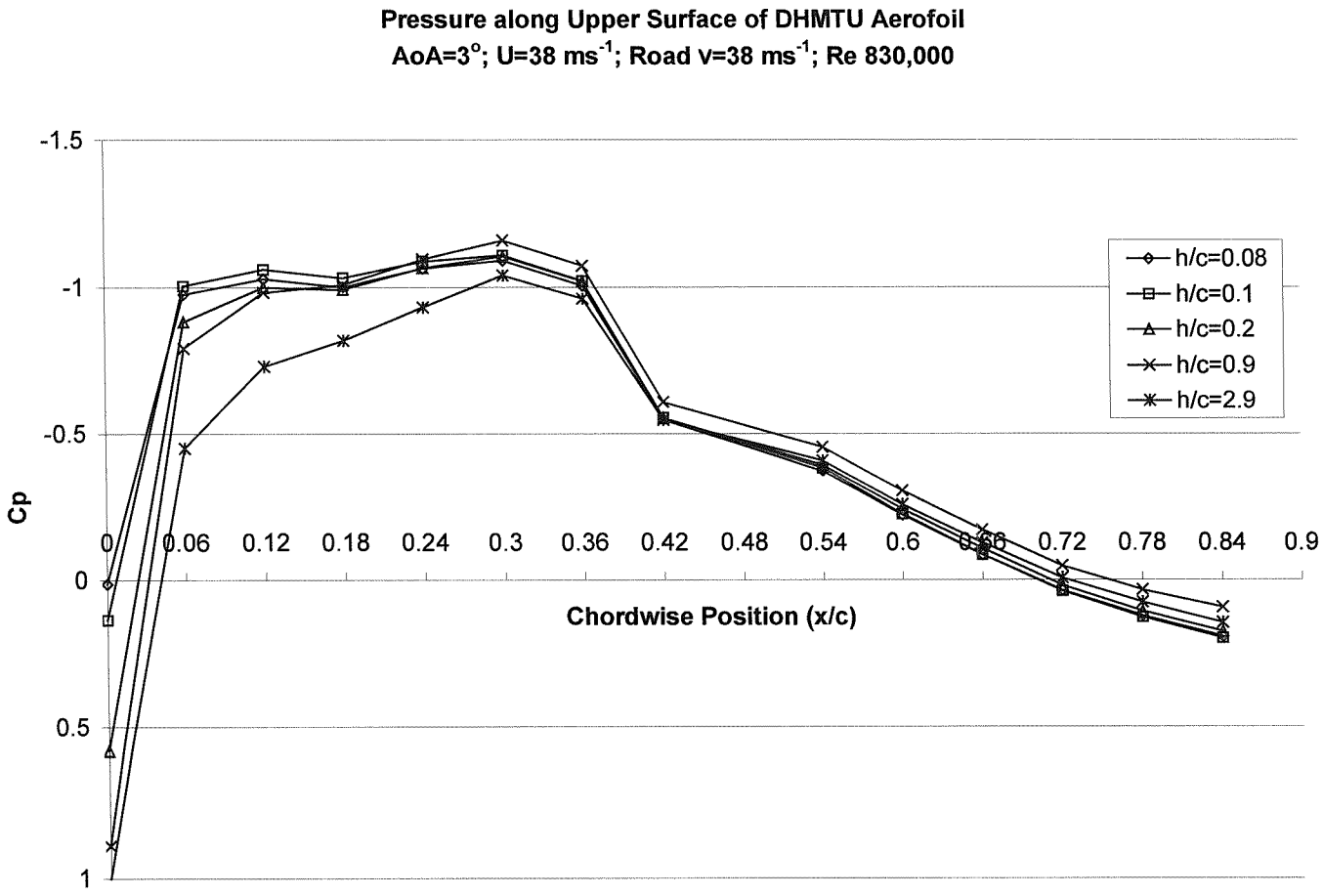

Figure 7-8: Pressure profile over upper DHMTU section as a function of altitude (AoA 3 degrees)

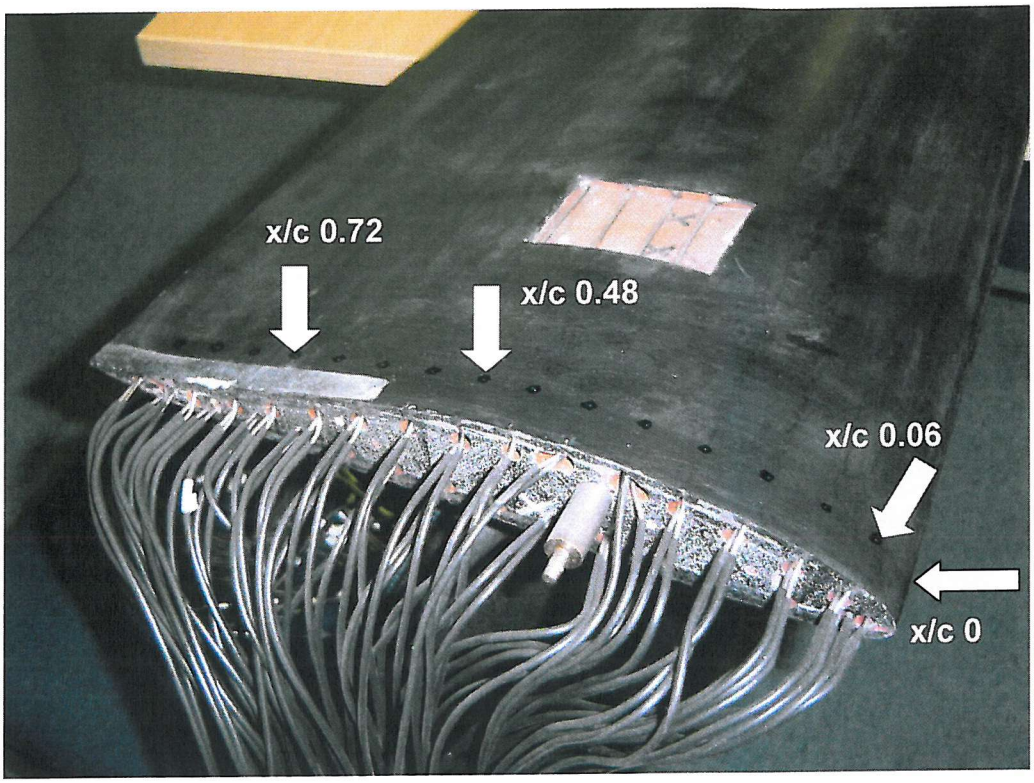

Figure 7-9: Key points on the upper surface of the DHMTU aerofoil

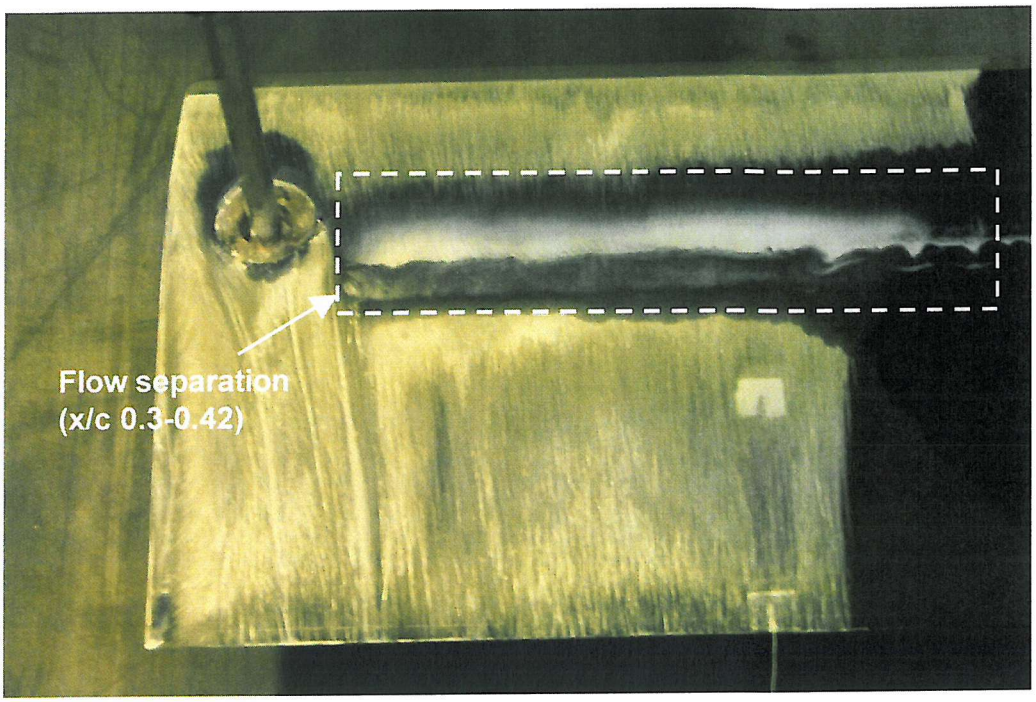

Figure 7-10: Flow over the top of DHMTU h/c 0.15, AoA=5 degrees and Re 830,000

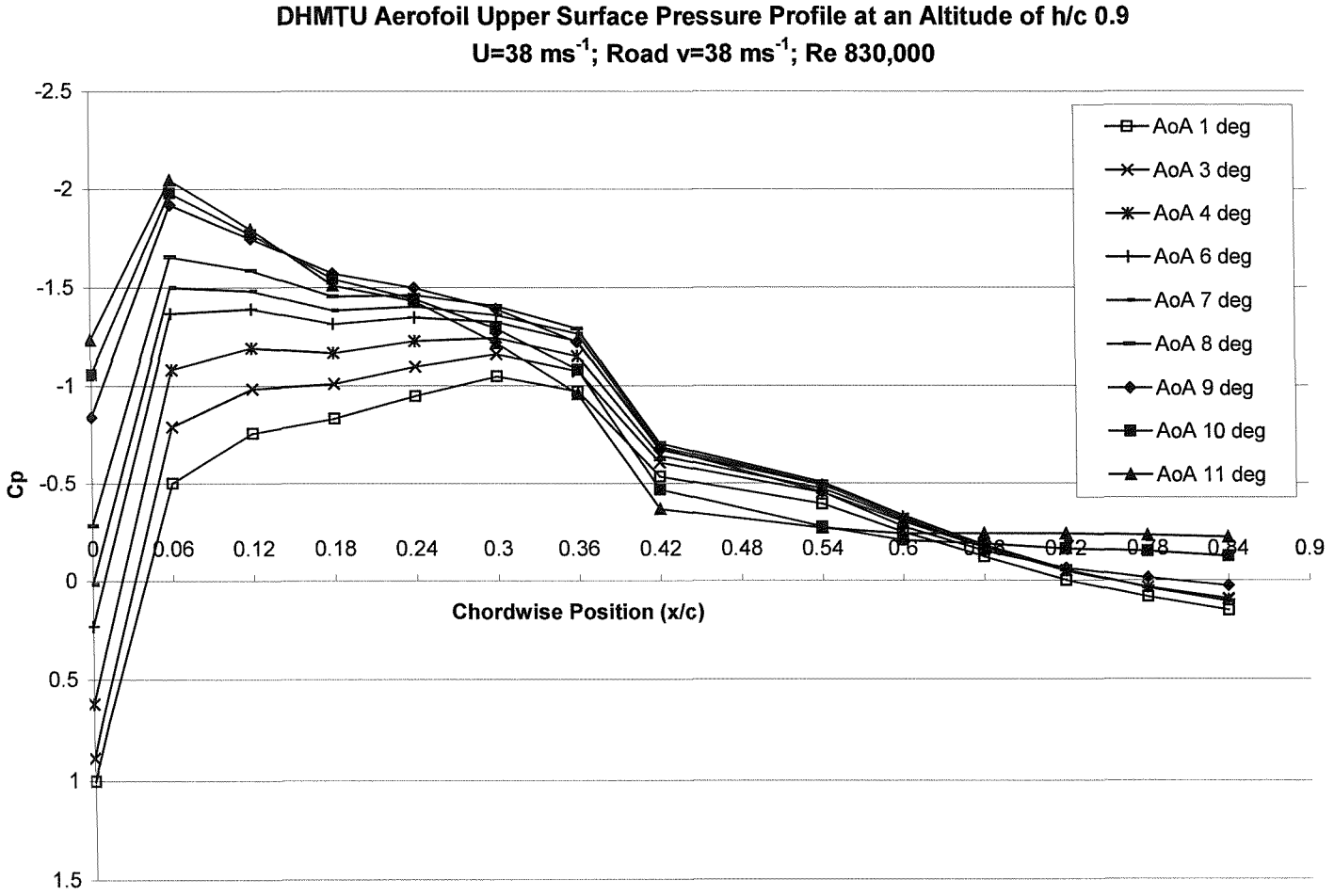

Figure 7-11: Pressure distribution on upper surface of DHMTU aerofoil at h/c 0.9

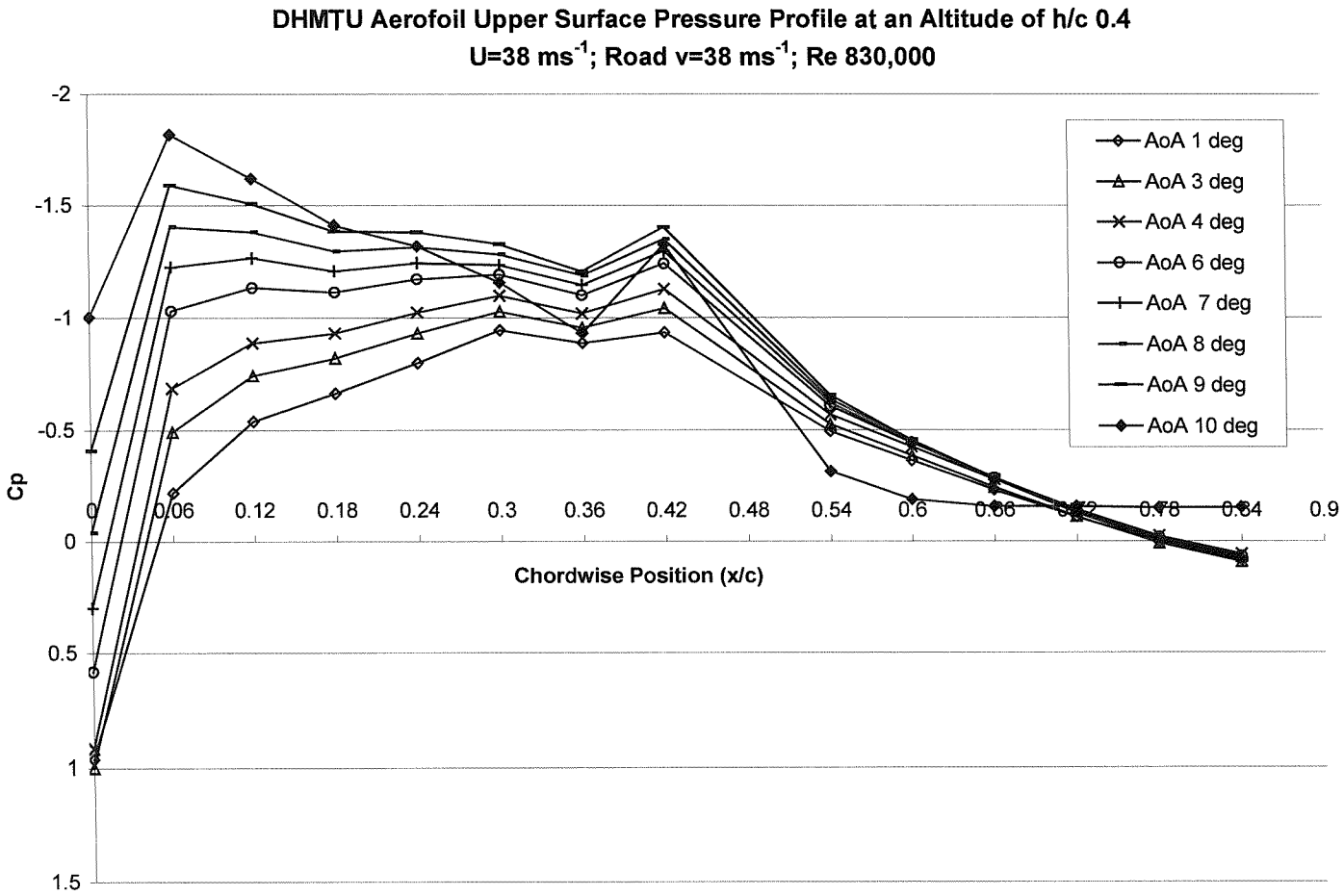

Figure 7-12: Pressure distribution on upper surface of DHMTU aerofoil at h/c 0.4

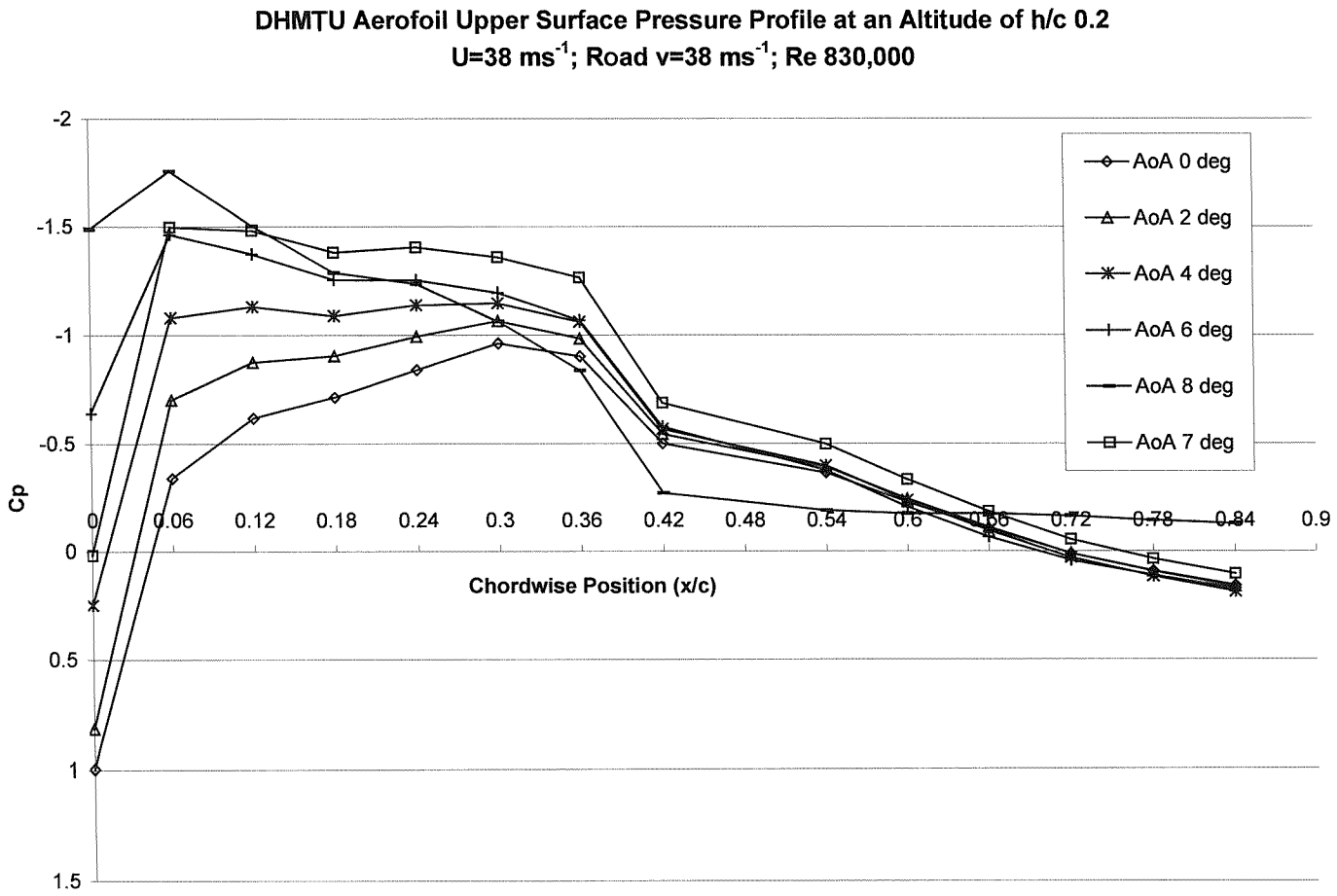

Figure 7-13: Pressure distribution on upper surface of DHMTU aerofoil at h/c 0.2

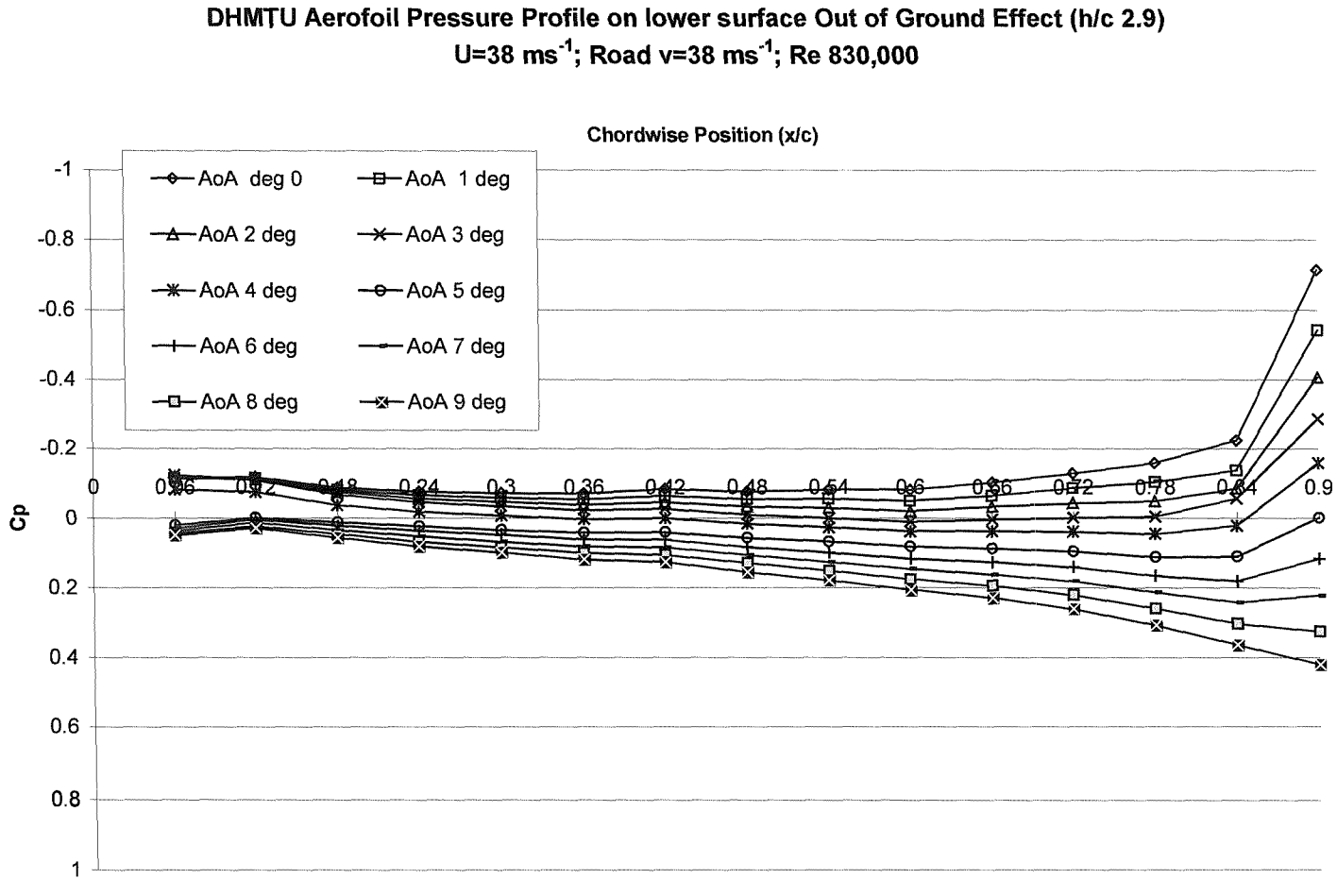

Figure 7-14: Pressure distribution on lower surface of DHMTU as a function of angle of attack out of ground effect

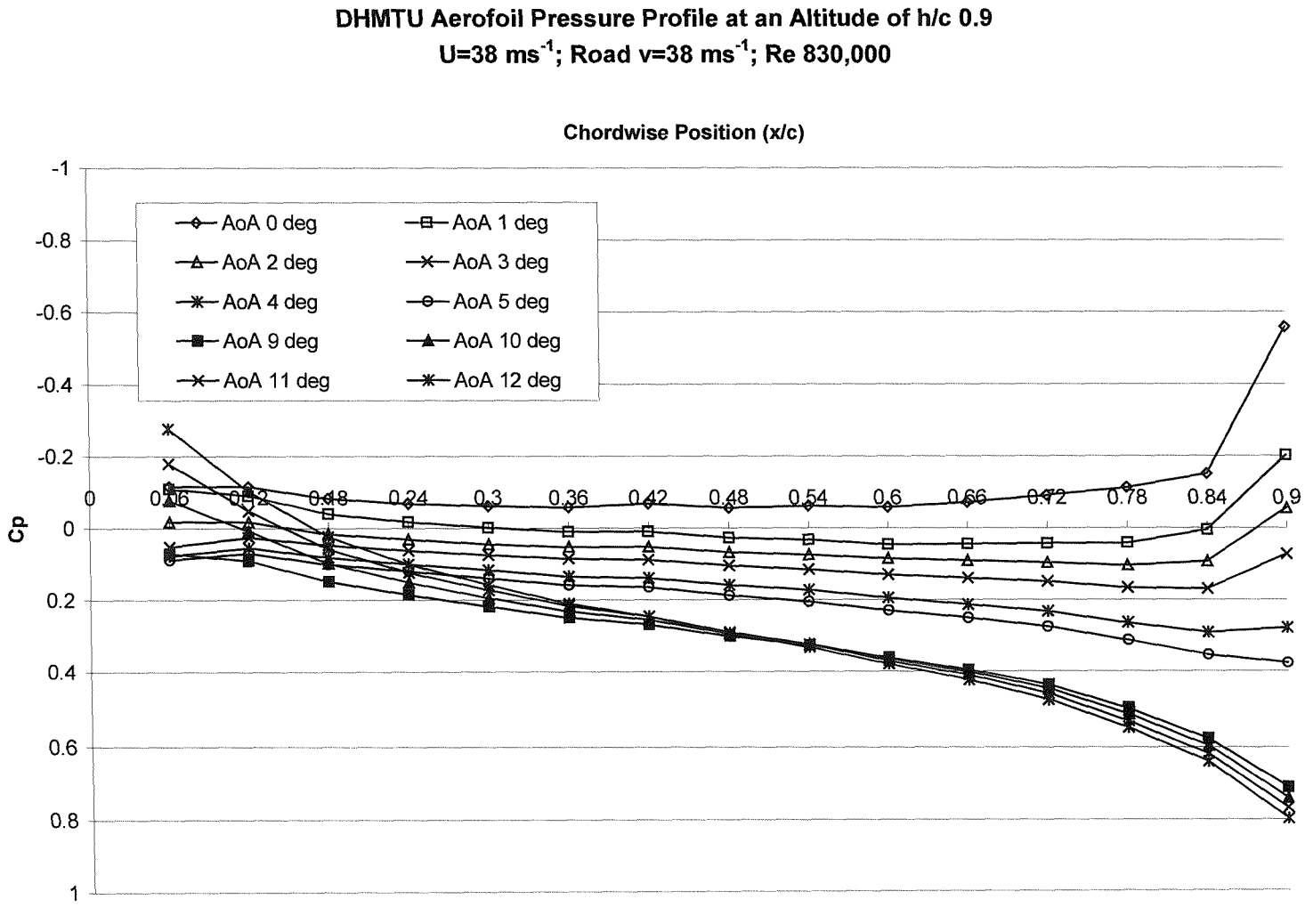

Figure 7-15: Pressure distribution on lower surface of DHMTU as a function of angle of attack at h/c 0.9

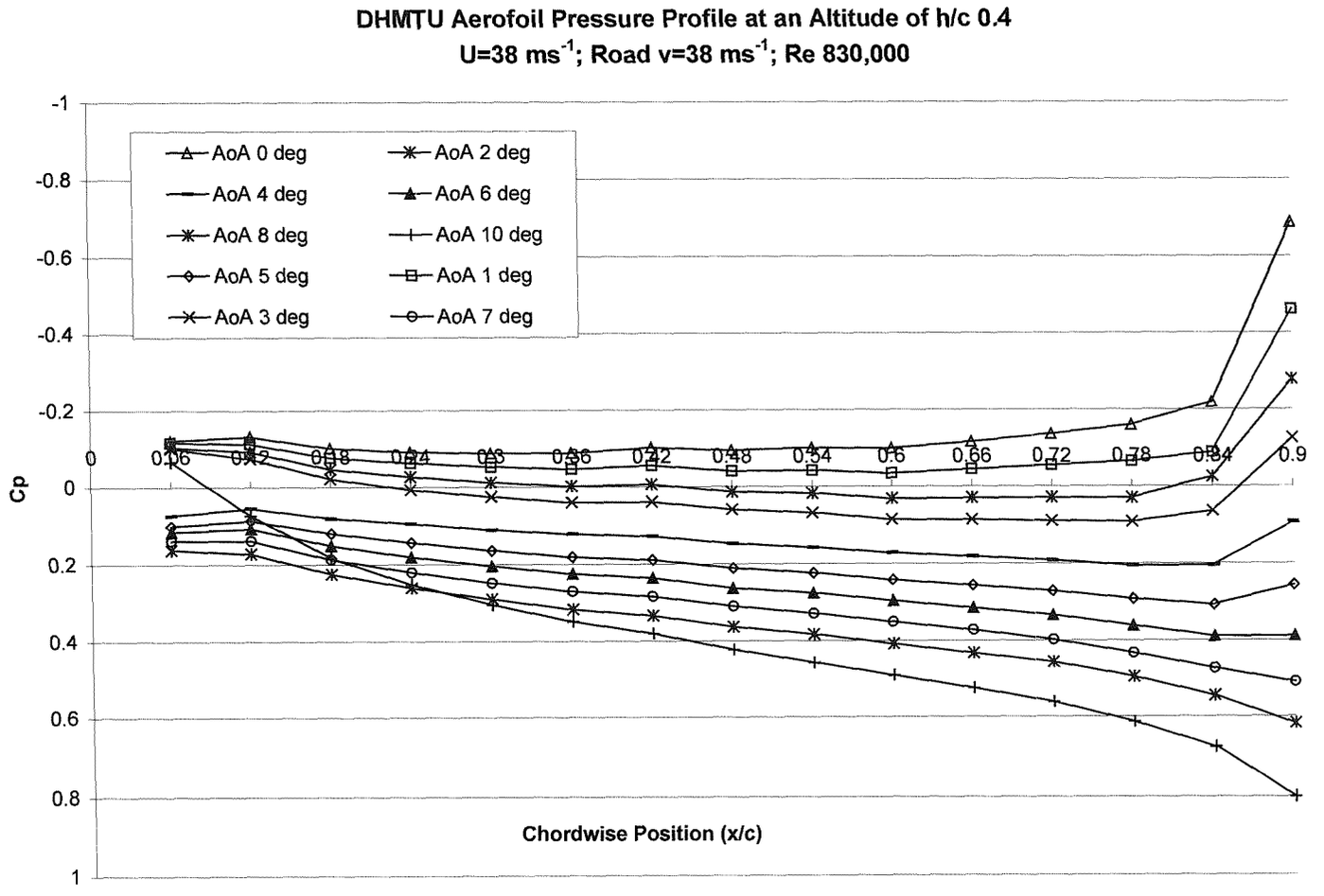

Figure 7-16: Pressure distribution on lower surface of DHMTU as a function of angle of attack at h/c 0.4

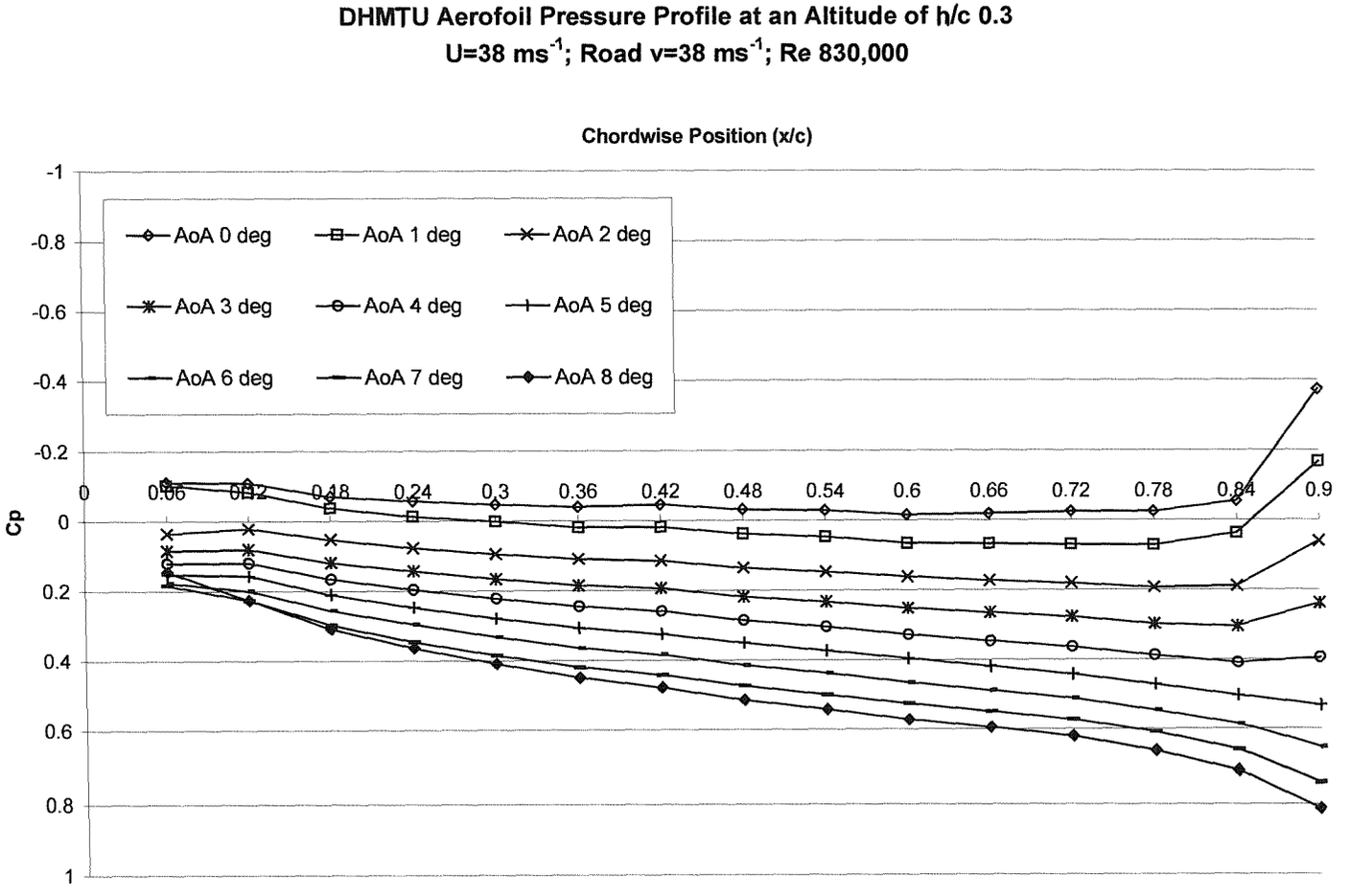

Figure 7-17: Pressure distribution on lower surface of DHMTU as a function of angle of attack at h/c 0.3

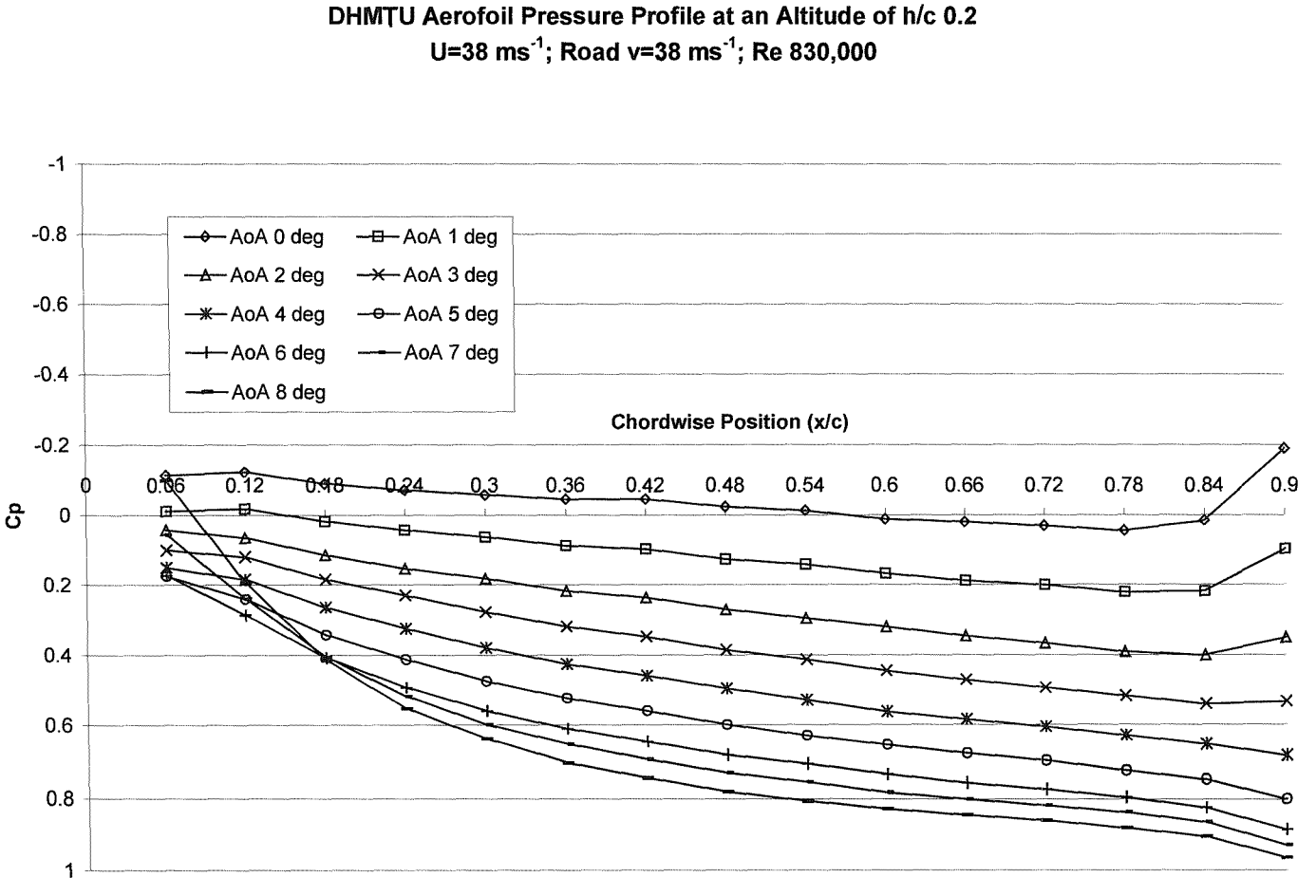

Figure 7-18: Pressure distribution on lower surface of DHMTU as a function of angle of attack at h/c 0.2

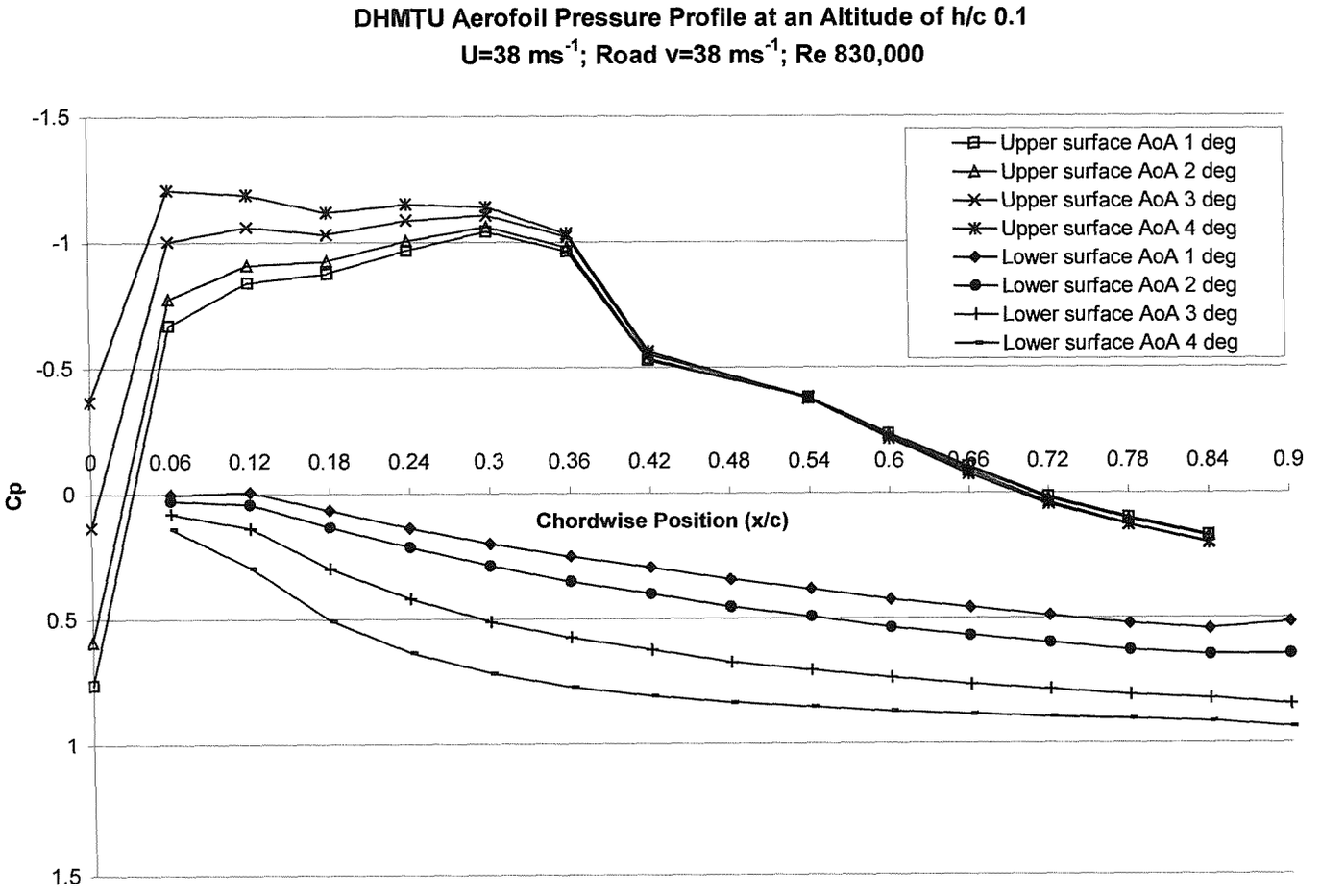

Figure 7-19: Upper and Lower surface pressure distribution over DHMTU at h/c 0.1 for AoA between 0 to 4 degrees

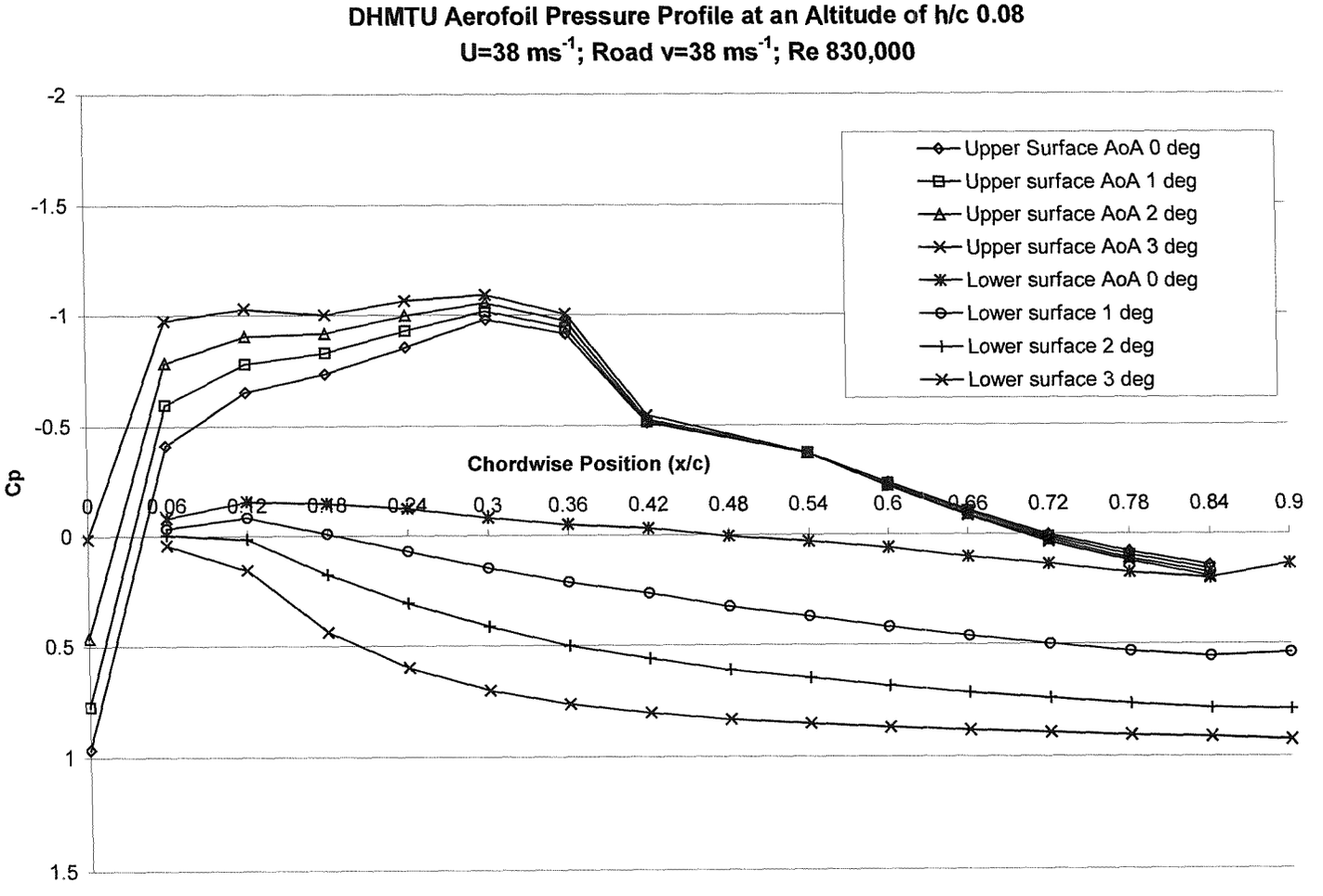

Figure 7-20: Upper and Lower surface pressure distribution over DHMTU at h/c 0.08 for AoA between 0 to 3 degrees

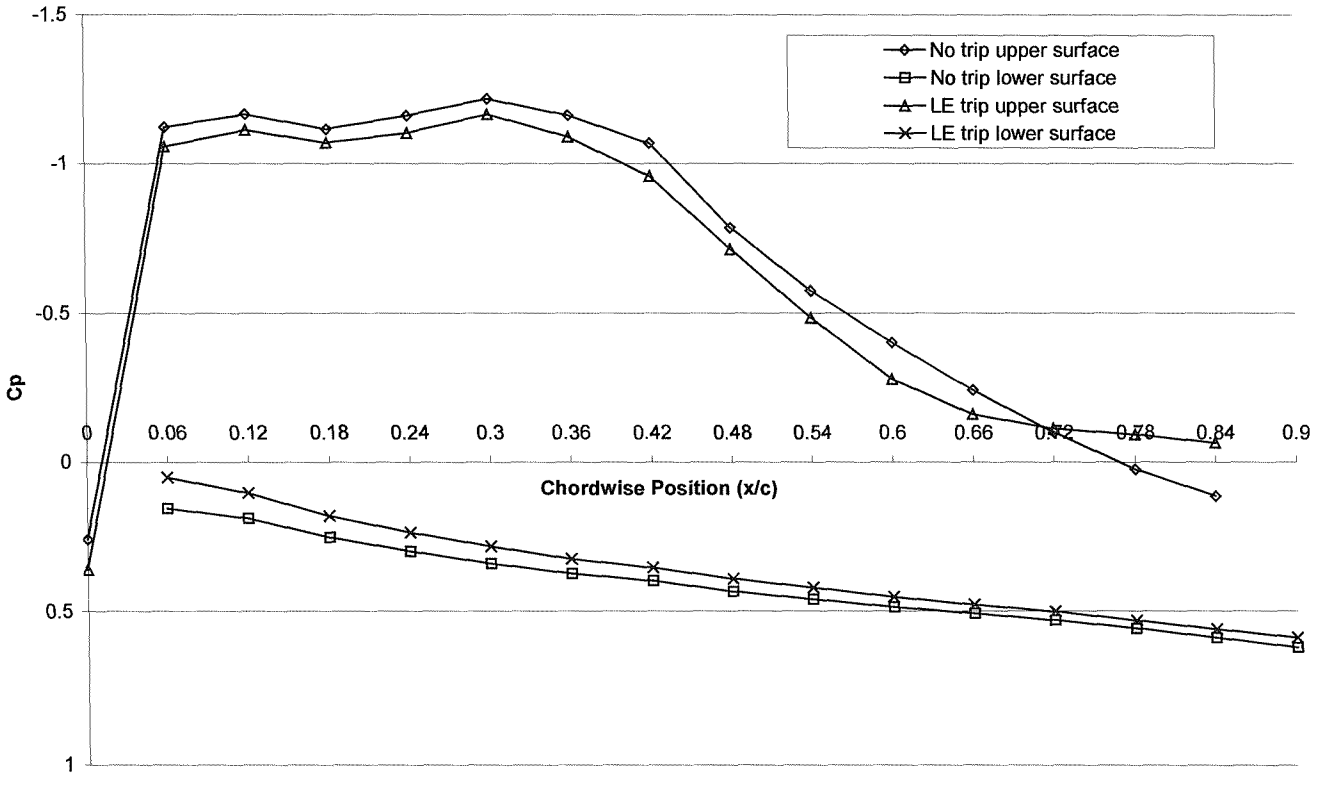

Figure 7-21: Effect on the DHMTU's upper surface of tripping the boundary layer at h/c 0.2

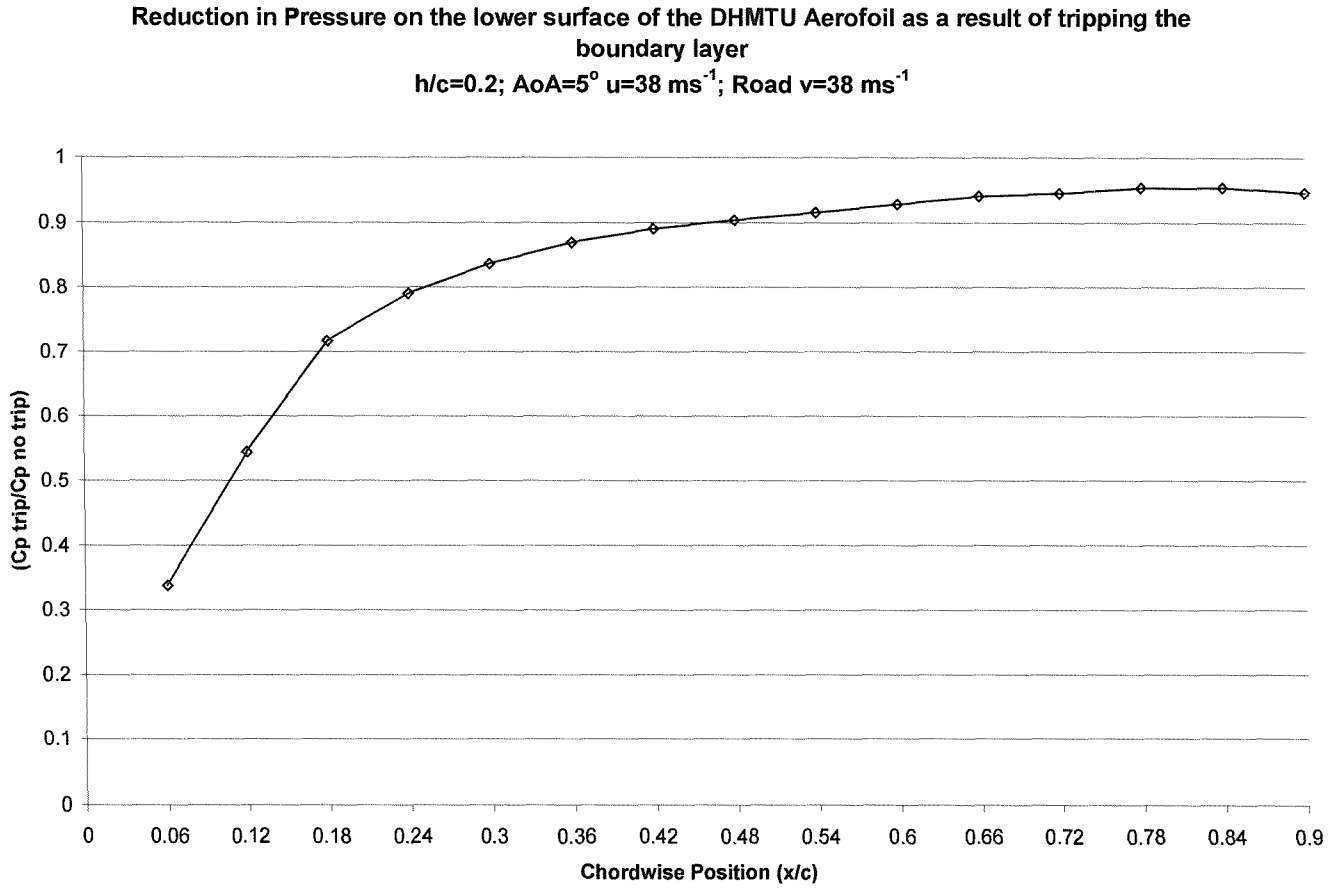

Figure 7-22: Reduction in pressure on the DHMTU lower surface as a result of boundary layer trip at h/c 0.2

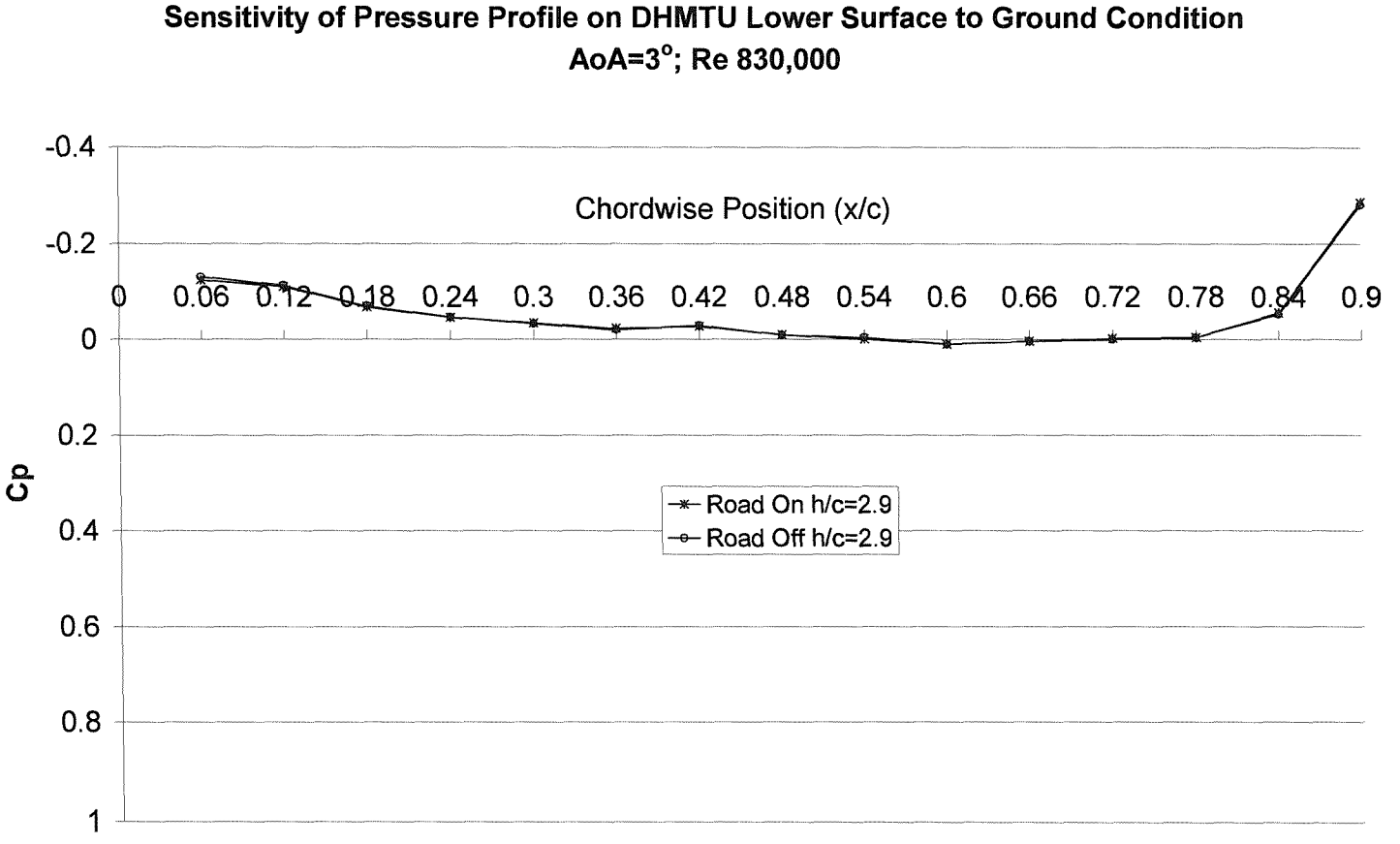

Figure 7-23: Pressure profile on DHMTU lower surface with road on and off h/c 2.9

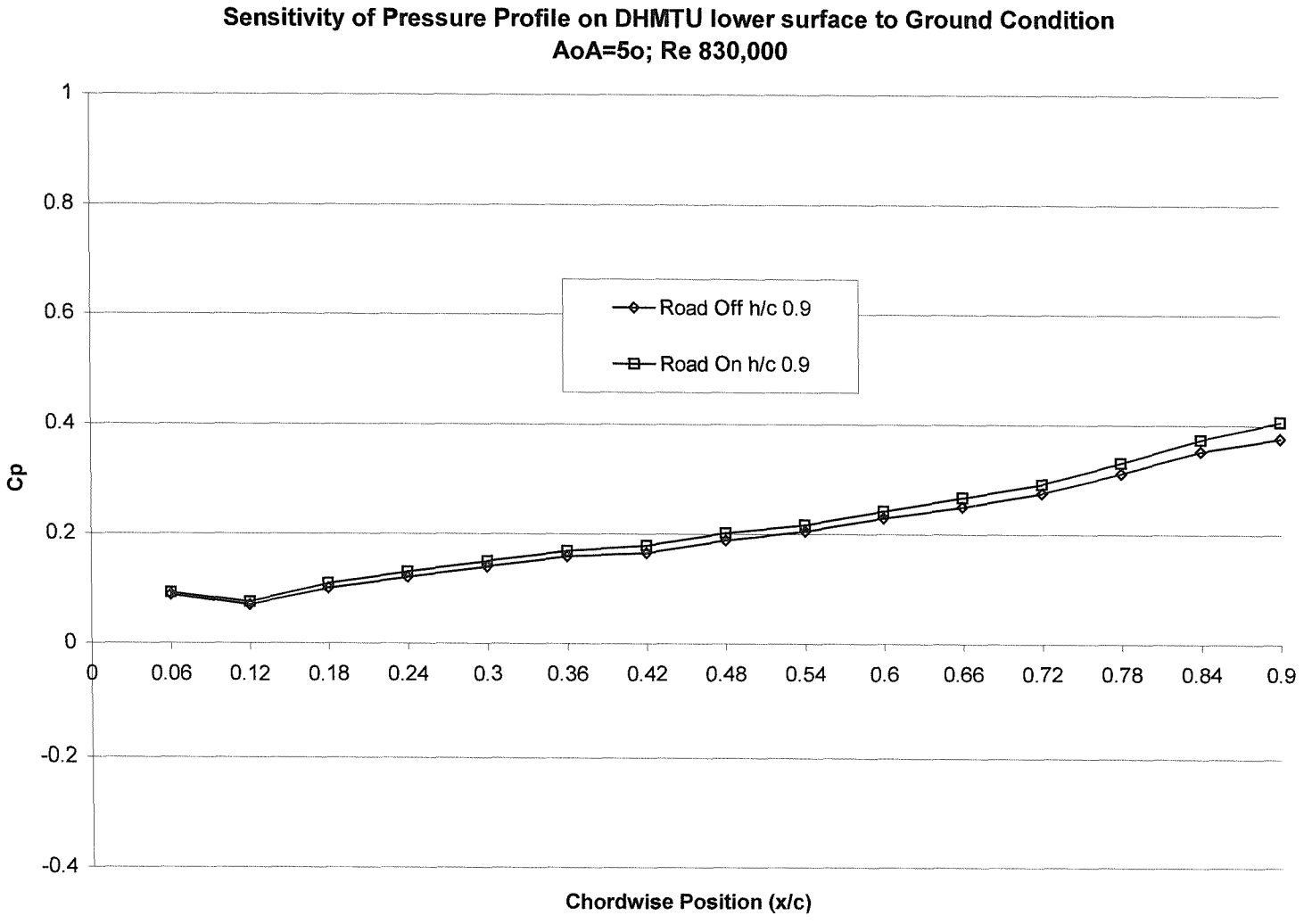

Figure 7-24: Pressure profile on DHMTU lower surface with road on and off h/c 0.9

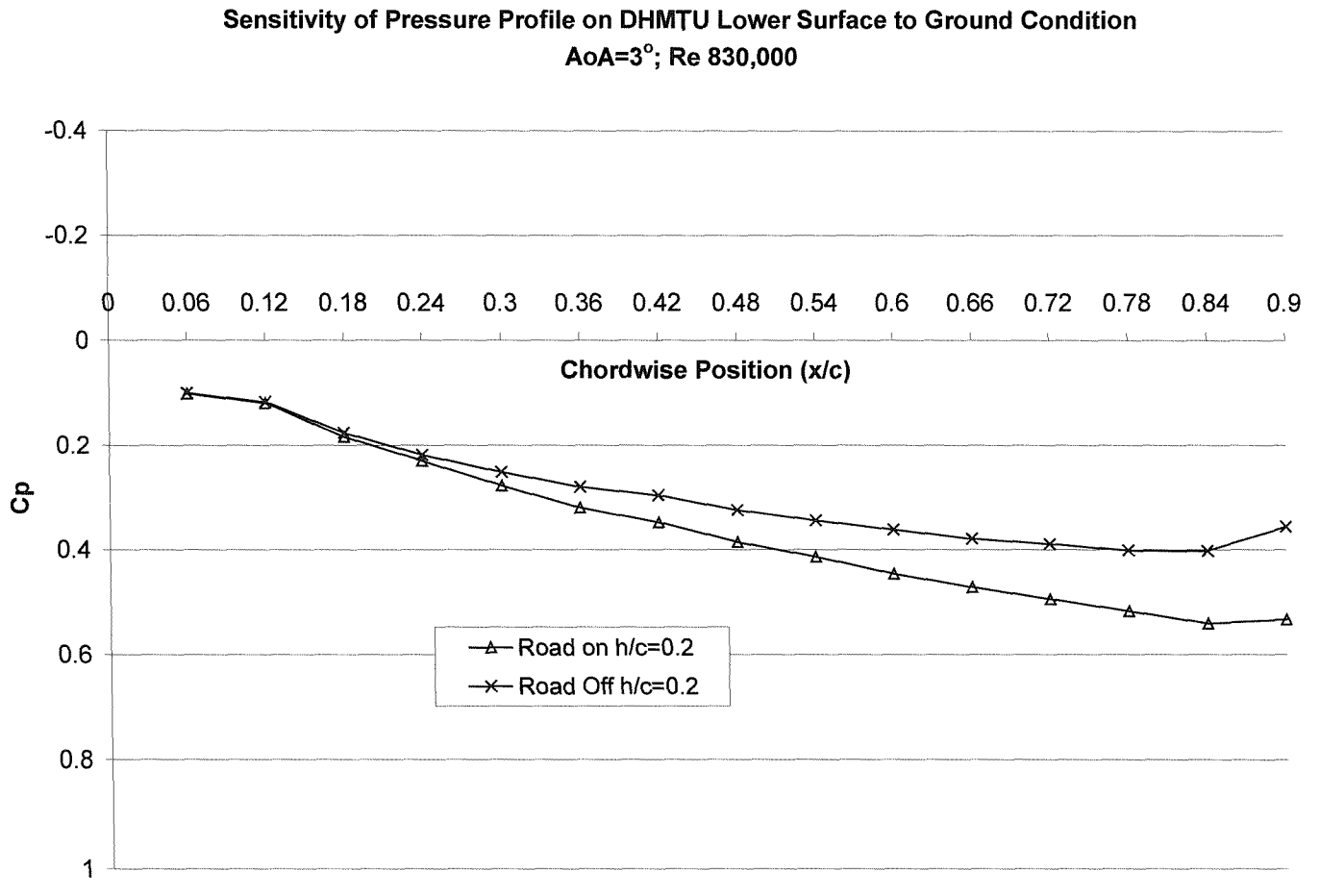

Figure 7-25: Pressure profile on DHMTU lower surface with road on and off h/c 0.2

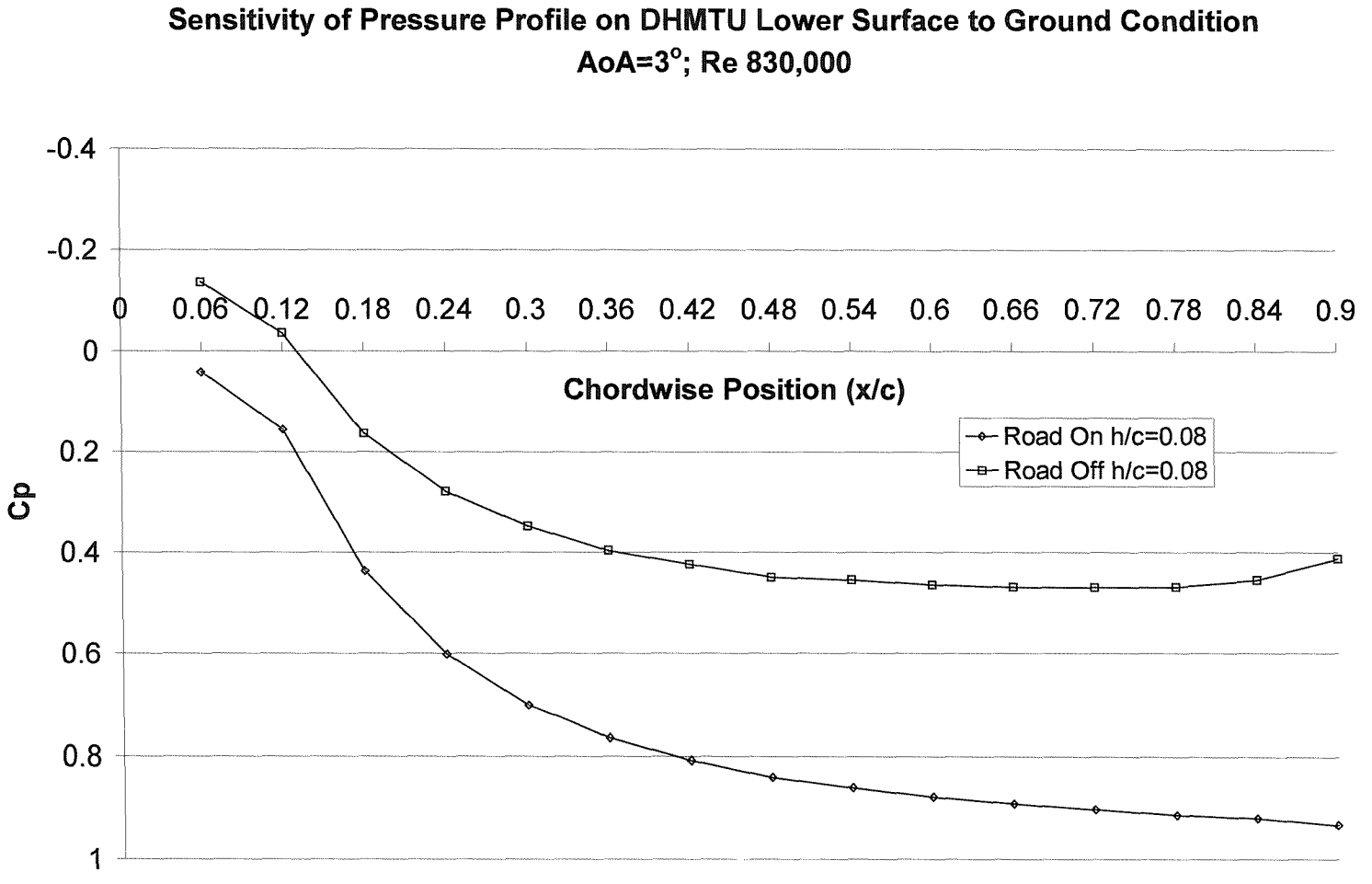

Figure 7-26: Pressure profile on DHMTU lower surface with road on and off h/c 0.08

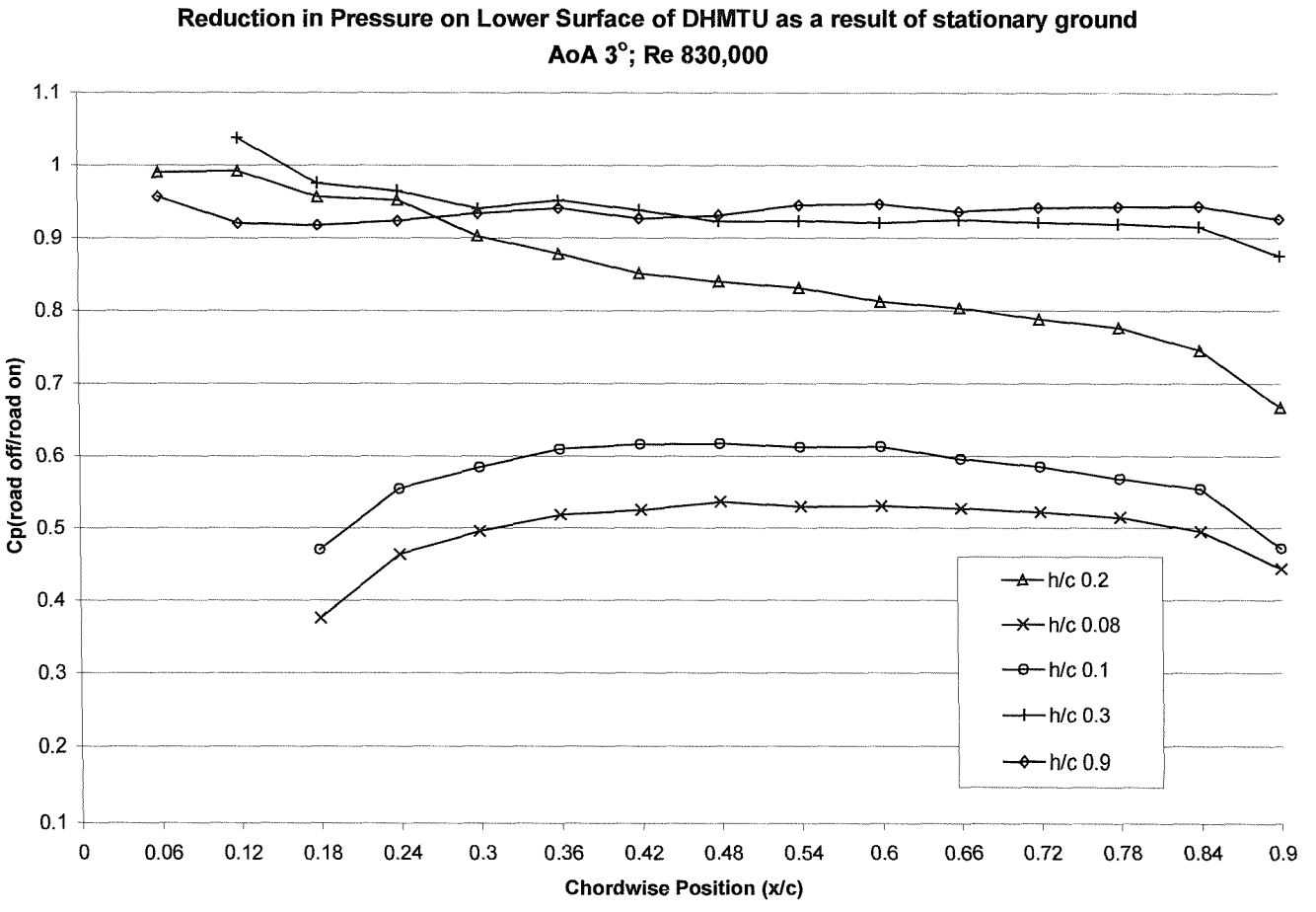

Figure 7-27: Reduction in Pressure on the under surface of the DHMTU aerofoil as a result of a stationary surface

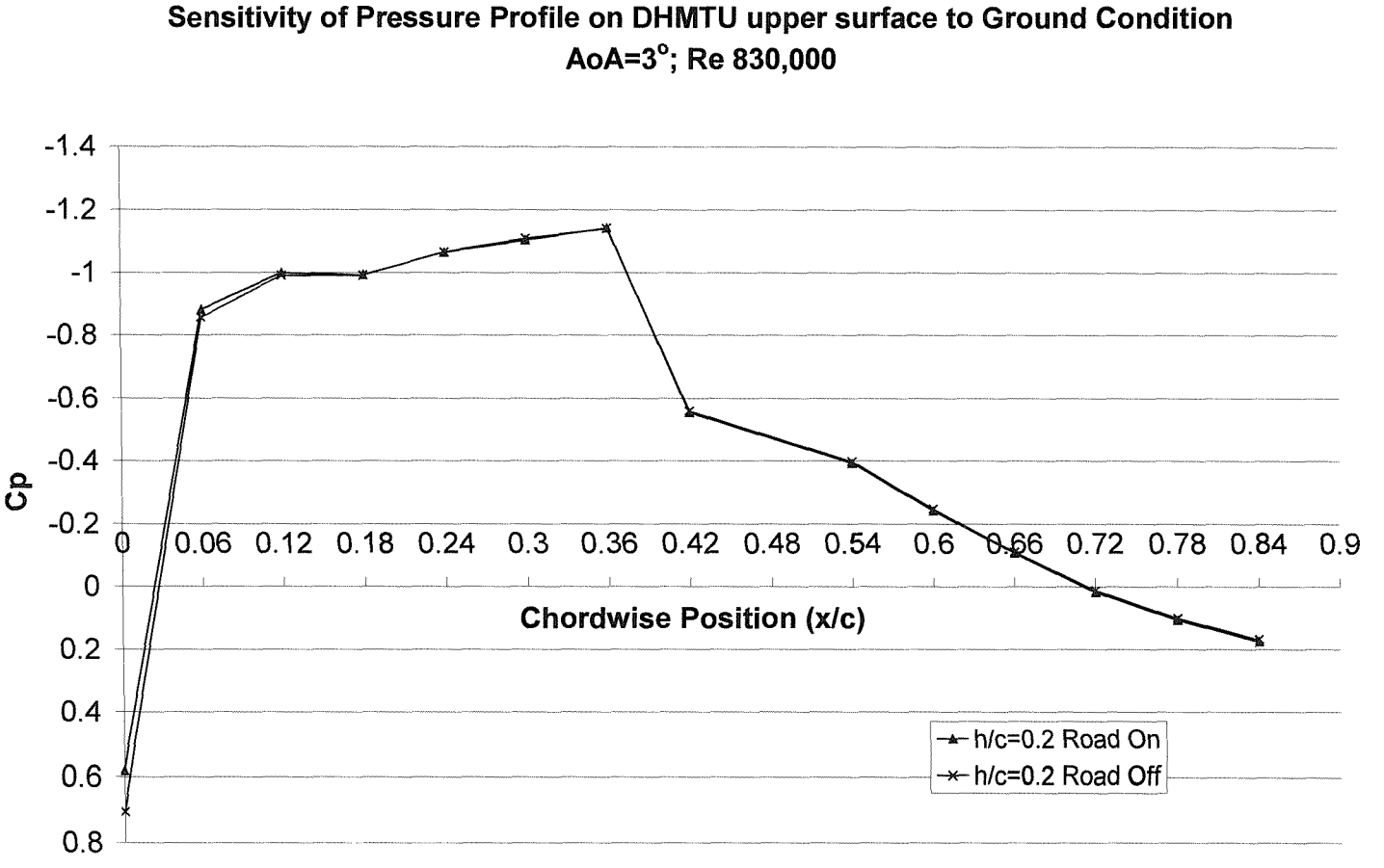

Figure 7-28: Pressure profile of upper surface of DHMTU section with road on and off h/c 0.2

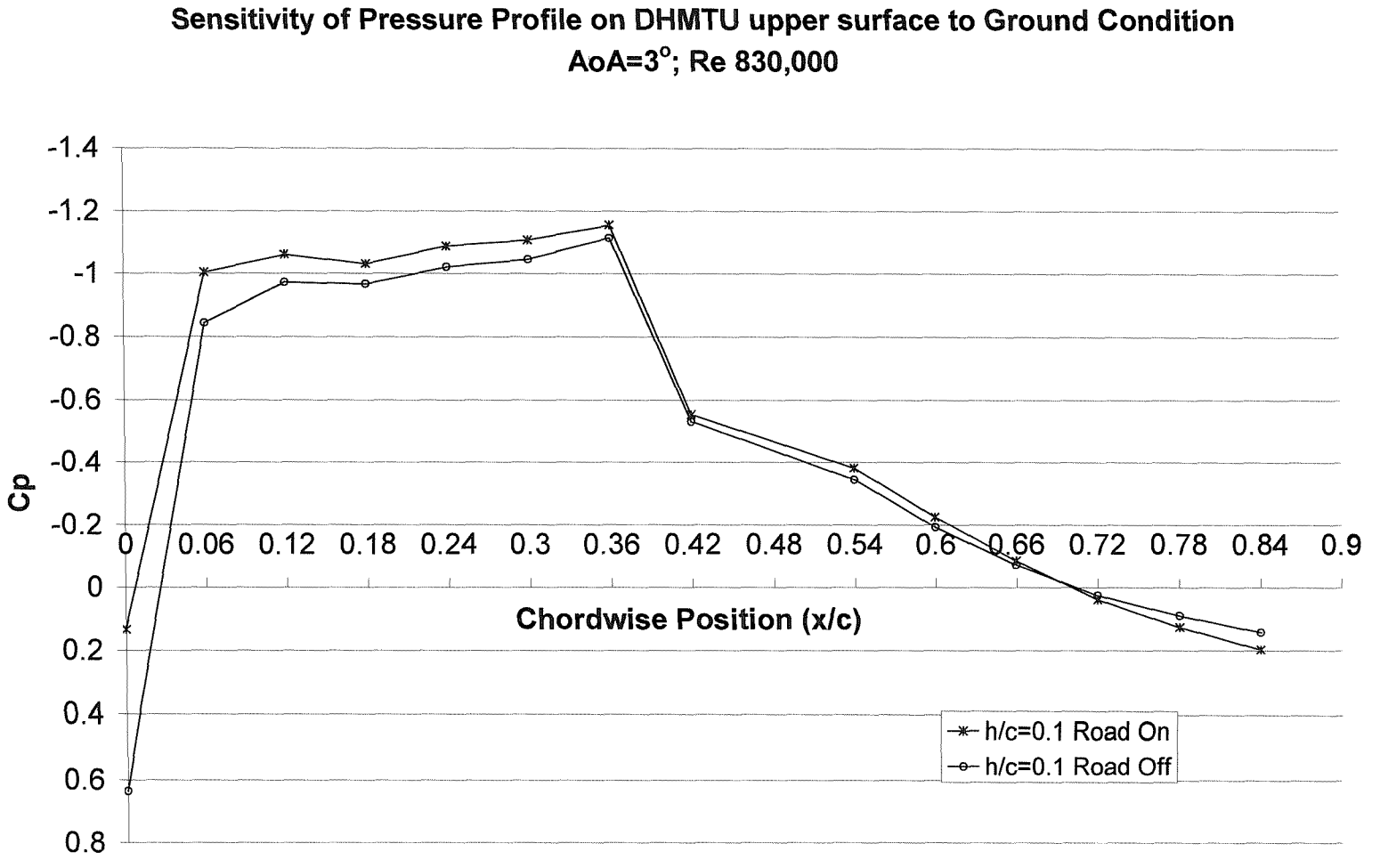

Figure 7-29: Pressure profile of upper surface of DHMTU section with road on and off h/c 0.1

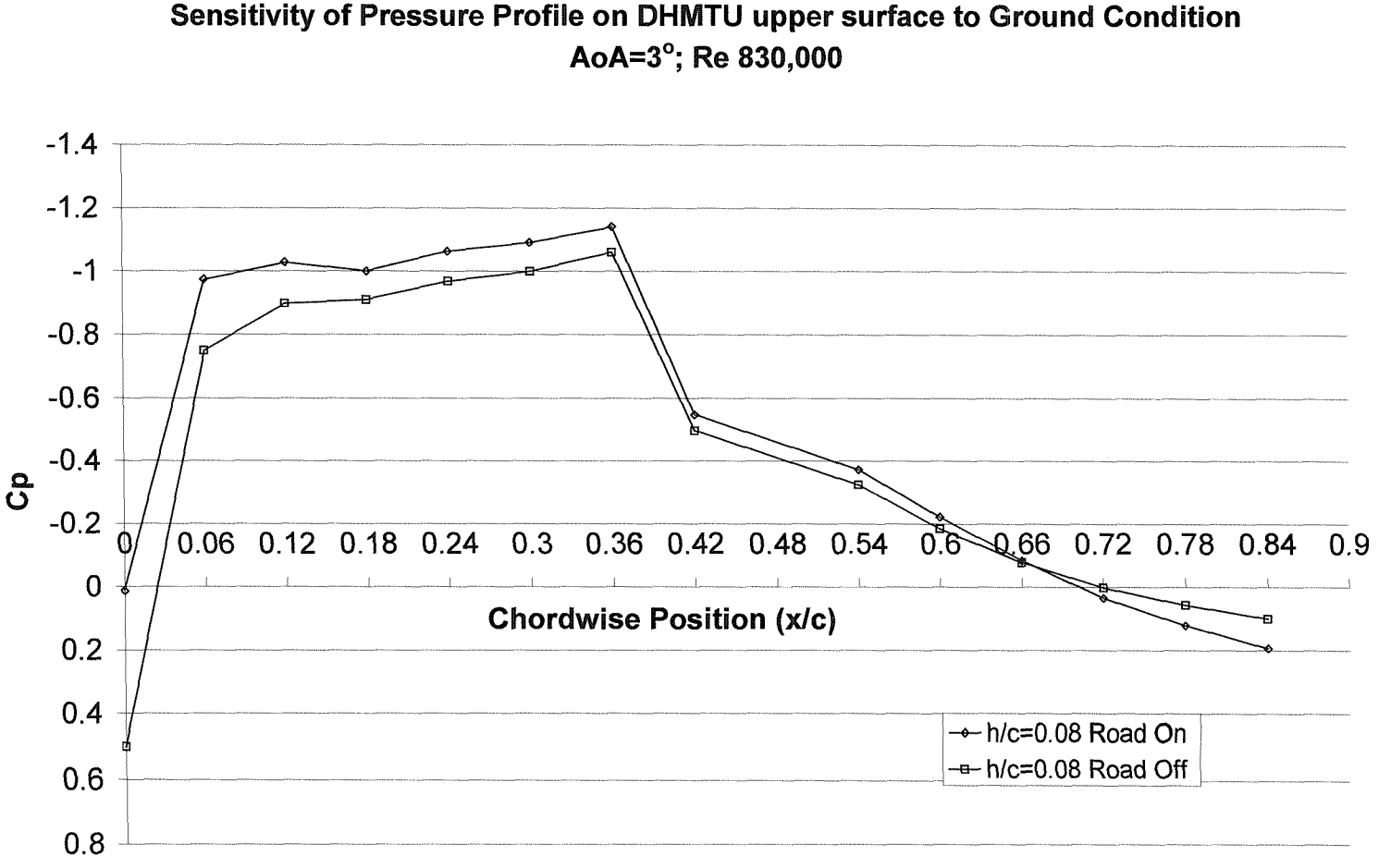

Figure 7-30: Pressure profile of upper surface of DHMTU section with road on and off h/c 0.08

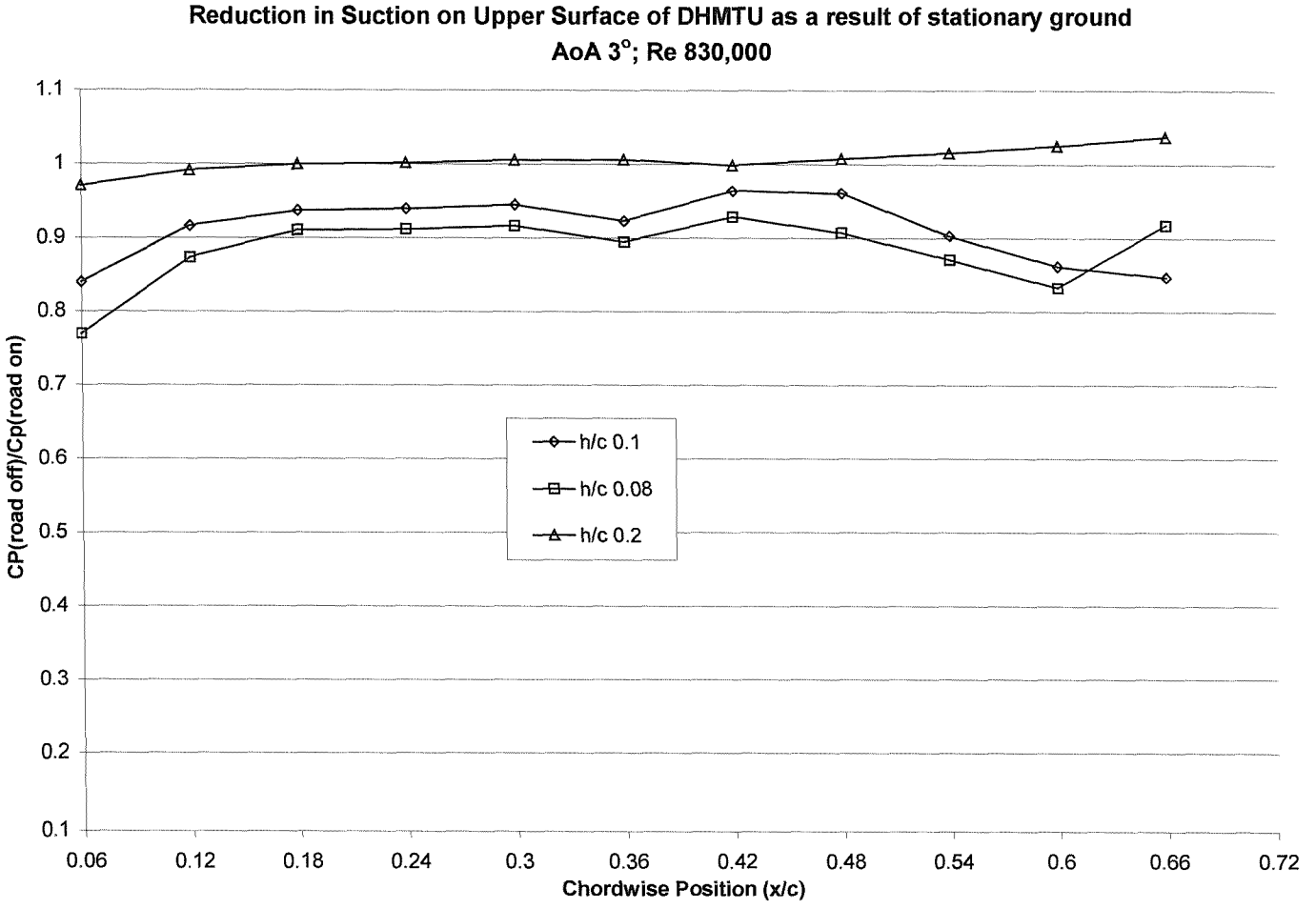

Figure 7-31: Reduction in suction over DHMTU upper surface as a result of stationary ground

8 Lift and Drag over Wavy Surfaces In Ground Effect

8.1 Overview

The previous two chapters have dealt with a wing in ground effect operating over a flat surface. In reality an operational WIG craft would be flying over the sea, which is a dynamic surface. This will result in a variation of the aerodynamic properties of the wing as it passes over a wavy surface. The fluctuation in lift, drag and pitching moment as a function of the wing's position along a wavy surface coupled with the effects of altitude result in challenging flight control characteristics. The reader should note that the measuring rig used to obtain data for this chapter could not measure pitching moment. This chapter presents an analysis of the experimental results for the DHMTU 12-35.3-10.2-80.12.2 wing operating over wavy surfaces.

The experimental facilities available at the University of Southampton and Southampton Institute are not suitable for the investigation of an aerofoil operating in a maritime environment. This is because it is not practical or feasible to attach wavy surfaces to the floor of either facility. Appendix C describes an alternative method of using the water tank to investigate DHMTU performance over a wavy surface but this was not successful. The author was fortunate in being granted access to the Circulating Water Channel (CWC) facility owned by QinetiQ, a UK research company, in order to address this shortcoming. The main strength of this facility from the point of view of this research is that it allows for the attachment of wavy surfaces onto the floor of the working section of the CWC. To the authors knowledge no one has used a CWC facility to investigate wing in ground effect over wavy surfaces.

8.2 Validity of Methodology

In employing the CWC facility to investigate the variation of lift and drag over a wavy surface several limitations in its use need to be appreciated. In reality a WIG's wing would transit over the sea resulting in motion of the wing over a slower moving wavy surface. This cannot be replicated in the CWC as the wing and the waves are stationary (Figure 8-1) with the flow moving. This arrangement is analogous to operating in a conventional wind tunnel with a stationary ground.

As discussed in the previous chapter wind tunnel data indicated that below an altitude of h/c 0.2 lift and drag data will not reflect the physical reality of flying in ground effect.

To reflect these limitations data obtained from the CWC trials was only taken down to an altitude of h/c 0.2. This minimum altitude will negate the most serious effects of the incorrect boundary layer conditions between the waves and the wing.

The flow of the water as it passes over the solid waves could result in the formation of turbulence and eddies. These have the potential to affect the flow and hence force readings obtained from the wing. During the trial runs there was no visual indication of turbulence being produced over the waves.

The solid waves fitted to the CWC floor are not compressible and will not reflect the deformation of the wavy surface that would be produced by the pressure under the wing. This is a factor that would be difficult to take into account in any scaled experimental investigation of flight over wavy surfaces.

A more serious effect is that the CWC working section is not very deep, when the wing is at its highest altitude of h/c 1 it is only at a depth of h/c 1.1 below the water surface. This means that the wing could be susceptible to the disturbance of the water surface as it flows around the mounting rig (Figure 8-2).

Due to the stationary nature of the testing method the mounting rig has to be moved for every part of the wavelength that is to be tested over. Time constraints precluded fine sampling of the wing over the wavy surfaces. This resulted in data only being taken at intervals of a quarter wavelength. This may result in the absolute maximum and minimum values of drag and lift produced along a wavy surface not being observed.

8.3 Experimental Setup

8.3.1 Equipment

The CWC consists of circulating flow with water being propelled around the circuit by an impeller. For very low speeds (<0.98 ms^{-1}) a small 1.49 kW motor propels the water, for higher speeds a larger 74.6 kW motor is employed. Figure 8-3 depicts the upper working section of the CWC. This facility has the capacity to operate at speeds of up to 5.5 ms^{-1} but during WIG wing testing the maximum run speed was restricted to 1.9 ms^{-1} due to the deformation of the water's surface and consequent risk of flooding. Figure 8-2 illustrates the state of the water's surface flowing at 1.9 ms^{-1} when the wing was at an altitude of h/c of 0.2.

In order to run these trials a dedicated WIG test rig was constructed (Figure 8-4). This consisted of two channel sections laid span wise across the CWC working section and rigidly held by G-clamps to the CWC sides. Bridging these channels were two smaller sections that were held in place by square clamping plates. Attached to these smaller channels were two orthogonal mounted force blocks allowing the simultaneous measurement of the lift and drag forces (Figure 8-5). The outputs from these force blocks were fed to a Spider 8 analogue to digital converter that inputted into a standard PC running data acquisition (TowAcq) software. At each run the data was acquired over a 60 s time period at a sample rate of 10 Hz.

Each set of force blocks was rigidly bolted to a streamlined sword section with the DHMTU wing clamped at the bottom of the swords (Figure 8-6). Wing height above the ground was adjusted by means of a series of holes spaced at intervals of 0.1 of a chord down the sword length. Three different sets of wavy surfaces (Figure 8-1) were bolted to the floor of the CWC and the wing's rotation point was set parallel to the wave crests.

8.3.2 Experimental Procedure

The set-up procedure was to drain the CWC tank and then clamp the supporting rig in place (Figure 8-4). The vertical angles of the swords were initially checked so they were perpendicular to the horizontal. The wing's angle of attack was set manually in the tank and tightened in place. The wing height above the wave crest was set to h/c 0.2 by measuring the distance from the wing's rotation point. The wing rotation point was located a distance c/3 from the aerofoil leading edge along the chord line joining the leading and trailing edges of the aerofoil. The CWC tank was flooded and the impeller was started and the power increased until the desired flow speed of 1.9 ms^{-1} was attained.

The water velocity was measured via a pitot probe that was located in the CWC working section. A graduated dial on the control console controlled water velocity, this dial had been calibrated before use and a separate manometer was also in place in order to corroborate the velocity of the water. After allowing a minute to pass in order for the flow to reach steady state readings were acquired. To check the short-term repeatability of the results a second set of readings was acquired 2 minutes later.

After the runs for an altitude were completed the power on the impeller was reduced to zero. When the water flow had stopped the vertical struts were unbolted and the wing's height was adjusted by moving the swords up an altitude step of h/c 0.1. The impeller was restarted and the whole measurement procedure detailed above was repeated. For all sets of runs the wing started at the lowest altitude of h/c 0.2 increasing to h/c 1.0. When the whole altitude range over one wave position had been tested the supporting rig was unclamped and moved to the next wave position.

8.3.3 Accuracy and Sources of Error

The inaccuracies in the measurements taken in the CWC are presented in Table 8-1. The setting up errors of the wing's angle of attack is due to the inaccuracy in levelling and locating the testing rig as well as the accuracy of the electronic

level. The accuracy to which the vertical swords could be situated was a function of how level the rig was when it was clamped into place and the change in the angle of the vertical swords when the bolts were tightened at each altitude setting. It was determined that the inaccuracy in changing the wings altitude was h/c 0.03.

The inaccuracy in the lift and drag measurement was the combination of the averaging of the data over the sampling time and the accuracy of the force blocks. Considering these uncertainties in the measurement process the lift coefficient C_L has an uncertainty of $\pm$ 36 x 10^{-2} and the drag coefficient C_D $\pm$ 1.4 x 10^{-3}. Appendix A discusses the sources of uncertainty and repeatability in greater detail.

Figure 8-7 plots the variation in free stream water velocity as a function of altitude. It can be seen that at an altitude of h/c 1 the water velocity increases by 0.05 ms^{-1} of its h/c 0.1 value. This is above the $\pm$0.01 ms^{-1} accuracy that readings from the manometer level can be read to, leading to the conclusion that the free stream velocity is increasing slightly as the surface is approached.

To obtain an indication of the span wise variation of the water velocity the pitot was placed in the centre of the tank and 265 mm from the tank side, corresponding to the wing tip position. The free stream velocity varied from 1.9 ms^{-1} in the centre to 1.6 ms^{-1} at the side.

As with the wind tunnel experiment the wing constrains the flow in the operating section of the CWC. Pope's expression (equation 4-1) allows the change in velocity due to model blockage to be calculated. The values and parameters of the blockage calculation are presented in Table 8-2. The resulting change in velocity $\frac{u_1}{V}$ is 4.1 x 10^{-4} that corresponds to a variation in velocity of 7.8 x 10^{-4} ms^{-1}. This is a negligible change in velocity due to the presence of the wing.

The CWC runs were conducted at a free stream water velocity of 1.9 ms^{-1} unless otherwise stated. This corresponds to a Reynolds Number of 5.5 x 10^5 based

upon wing chord. Due to the time constraints the section was only tested at an angle of attack of 5 degrees. This was selected on the basis of the results obtained from wind tunnel testing (see Chapter 5). The wing's altitude was measured from the wing rotation point that is located c/3 from the leading edge. This position has been selected in order to maintain consistency with the wind tunnel experiments. The wing rotation point was used as a datum for locating the wing over the wavy surface. The wing was varied in altitude from h/c 0.2 to 1 in 0.1 steps above the wave crest. The experimental variables are summarised in Table 8-3.

8.4 Wave Selection

The time available in the CWC only allowed for the testing of three different sinusoidal wavelengths. It was decided to test the DHMTU section over waves that possessed wavelengths equal to 1,2 and 3 times the chord (λ=c, λ=2c, λ=3c) of the wing (Figure 8-1). For these trials the amplitude of the waves were all kept constant at 0.25 of the DHMTU wing chord. The 'waves' were 1.2 m in width and varied in length from 1.65 m (λ= c) to 2.1 m (λ= 3c). The 'waves' were manufactured from marine plywood and protected by a waterproof coating. Unfortunately this did not completely stop the absorption of water and resulted in swelling of the 'waves'. Markings were applied on each side of the wavy surfaces to indicate the desired wavelength positions for the wing location. The waves were marked as shown in Figure 8-8 with the ¼ wavelength position being upstream of the flow.

8.5 Discussion of Results

8.5.1 Variation of Lift over Wavy Surfaces

The behaviour of the lift of the wing as it moves over the wavy surfaces is illustrated in Figure 8-10, Figure 8-12 and Figure 8-14. Each plot shows the recorded lift over the wave crest (0 and 1), 0.25λ, wave trough (0.5λ) and 0.75λ positions. The general trend over all three surfaces is similar; the lift varies between a maximum and a minimum value and the amplitude of this variation increases as the altitude decreases. It can be seen that the minimum and

maximum values of the lift do not correspond to the position of the wing rotation point over the crest and trough of the wavy surfaces.

When the wavelength of the surface is equal to the wing chord the results show that the lowest magnitude of lift is obtained when the wing rotation point is over the wave peak (0 and 1 position). It can be seen from Figure 8-11A that a large portion of the rear of the wing is over the wave trough. This results in an increase in the distance between the wing and the wavy surface over a significant proportion of the wing chord. As a result the pressure under the aft portion of the wing decreases resulting in a reduction of lift.

As the wing is moved along the wave, the magnitude of the lift increases. The highest magnitude of lift recorded is when the rotation point is over the ¼λ position (Figure 8-11D). Figure 8-11C nicely illustrates why lift is not a minimum when the wing rotation point is over the wave trough. The rear part of the wing is over the wave crest resulting in increased pressure.

As the wavelength increases to equal twice the wing's chord the positions of minimum and maximum lift alter. Here the maximum lift is obtained when the wing rotation point is over the wave trough. Figure 8-13C depicts the wing surface geometry, at this point the trailing edge of the wing and the aft section are in very close proximity to the wavy surface. At very low altitudes the gap between the wavy surface and the wing trailing edge is very small. Similarly when the wing rotation point is over the ¾λ position the high magnitude of lift force can be ascribed to the rear part of the wing's close proximity to the wave crest (Figure 8-13B).

The lowest values of lift are produced when the wing's rotation point is over the ¼λ position (Figure 8-13D) and the wave crest (Figure 8-13A). One very interesting feature of the results is that when the wing rotation point is over the wave crest very low values of lift are produced, in fact at altitudes below h/c 0.3 a downward force is generated (Figure 8-12).

As the wavelength increases to three times the wing chord the peak lift is obtained when the wing rotation point is over the ¾λ position. Figure 8-15B illustrates that the trailing edge and the rear section of the wing are in very close proximity to the wavy surface. As the wing moves to the wave trough (Figure 8-15C) and ¼λ position (Figure 8-15D) the lift is reducing. As when the wavelength was equal to 2c the smallest magnitude of lift is recorded at the wave peak. The lift also becomes negative when the altitude falls below h/c 0.3. If the images in Figure 8-13C and Figure 8-15B are compared it can be seen that the trailing edge is creating a seal between the wing and the wavy surface. This would have the effect of slowing the flow under the wing down and increasing the pressure.

Table 8-4 presents the position of minimum and maximum lift for each wavy surface as a function of altitude. When λ=2c and λ=3c the minimum lift consistently occurs at the wave crest, the exception to this is when the wavelength is equal to the wing chord and the lift is recorded between the ¾ wavelength to wave crest position. The maximum lift occurs when the wing's rotation point is over the trough when λ=2c and the ¾ wavelength position for λ=3c. When the wavelength equals the wing chord the maximum lift occurs at the ¼λ position. The results in Table 8-4 do show that for each wavelength the positions of recorded minimum and maximum lift are consistent with a variation in altitude.

The reader should note that the terms maximum and minimum lift are relative and relate to a comparison of the values obtained when the wing rotation point is at one of the four sampling positions along the wavelength. They do not reflect that maximum and minimum values that may occur along the wavelength. These results do illustrate the need to obtain more results by finer sampling of the wavelength to increase the understanding of what is occurring between the presently sampled wave positions.

As in ground effect over a flat surface a decrease in altitude results in an increase in lift. This can be seen in Figure 8-16 where the maximum lift coefficient as a function of altitude are plotted for each of the wavy surfaces. It

can be seen that down to the tested altitude of h/c 0.2 the maximum lift is increasing with decreasing altitude. Figure 8-16 also illustrates that the gradient of change of lift with altitude (dC_L/dH) decreases with shorter wavelengths. This means that a wing operating in ground effect will experience a smaller change in maximum lift with decreasing altitude as the wavelength of the surface decreases. It can be seen that when λ=c maximum lift is appreciably less than is obtained over the other two wavelengths.

The variation of minimum lift with altitude is shown in Figure 8-17. An interesting result from this is that a reduction of lift is experienced when the wavelength of the surface is equal to two and three times the wing chord. It can be seen that this effect occurs from an altitude of h/c 0.7. The rate of the reduction in lift is also the same for both wavelengths. In distinct contrast when the λ=c the minimum lift increases with altitude as occurs over a flat surface.

As the wavelength of the surfaces increase the difference between the minimum and maximum lift coefficient increases. This can be seen in Figure 8-18 where the ratio between the maximum and minimum lift coefficient ($C_L max/C_L min$) are plotted as a function of altitude for each of the wavy surfaces tested.

When the wavelength is equal to the wing chord the ratio of minimum and maximum lift is relatively constant between altitudes of h/c 0.2 to h/c 1. The maximum lift coefficient varies from 1.2 to 2.2 the value of the minimum lift. The general trend is for a slight increase in the $C_L max/C_L min$ ratio as altitude decreases. There is a significant difference in behaviour when the wavelength increases to 2c and 3c. When the wavelength is increased to twice the wings chord at h/c 1 the ratio $C_L max/C_L min$ is 1.8, increasing to 14.1 at h/c 0.4. Similarly when the wavelength equals three times the wings chord at h/c 1 the ratio is 2.4 increasing to 9.1 at h/c 0.4. This illustrates that for constant wave amplitude the shorter the wavelength of the surface that the wing is flying over the smaller the difference in extremes of lift coefficient experienced. This large difference between maximum and minimum values of lift is heavily dependent upon the low values of lift obtained when the wing rotation point is over the wave crest when the wavelength is 2c and 3c.

8.5.2 Comparison of flight over Wavy and Flat Surfaces

To quantify the effects on lift of flying over a wavy surface a comparison has been made with the experimental data obtained in the rolling road wind tunnel (see Chapter 5). The reader should note the altitude datum for the flat ground and wavy surfaces being used, this is illustrated in Figure 8-9, where the wave crest and flat surface are at the same level. The reader should also remember that the wind tunnel and CWC data were obtained at Reynolds Numbers of 830,000 and 550,000 respectively.

When the wavelength of the surface is equal to the wing's chord the mean lift produced below an altitude of h/c 0.7 is greater than that obtained over the flat surface of the wind tunnel (Figure 8-19). At an altitude of h/c 0.2 the increase in mean lift over a wavy surface compared to the flat is in the region of 26%. At the same altitude the maximum value of recorded lift obtained at the ¼ λ position is 60% greater than that produced over the flat. The minimum value of lift over the wavy surface is about the same as the wind tunnel flat surface level.

As the wavelength of the ground surface increases to 2c the mean lift over the wavy surface and wind tunnel data over flat ground are close to each other (Figure 8-20). At h/c 0.2 the mean lift over the waves is 13% greater than that over the flat surface. One feature that stands out from this plot is the decrease in lift with a reduction in altitude when the wing rotation point is over the wave peak. As the altitude reduces below h/c 0.3 negative values of lift are seen.

When the wavelength is increased to 3c the mean lift over the wavy surface is still greater than that of the wind tunnel data over the flat (Figure 8-21). Both sets of data are near identical down to an altitude of h/c 0.7. Again when the wing rotation point is over the wave crest a reduction in lift is produced below an altitude of h/c 0.7. As for when the wavelength was equal to 2c a negative value of lift is produced below h/c 0.3.

Comparing all three wavelengths (see Figure 8-22) it can be said that the mean lift force over the wavy surfaces and that obtained over the flat ground in the wind

tunnel is the same down to an altitude of h/c 0.7. Below this altitude the mean lift produced over the wavy surfaces is greater than that produced over the flat. As the wavelength increases the mean lift produced over the waves is higher than that recorded over a flat surface.

8.5.3 Variation of Drag over Wavy Surfaces

The behaviour of the drag as a function of altitude and wavelength are presented in Figure 8-23, Figure 8-24 and Figure 8-25. These graphs show that there is variation in the values of the drag along the wavelength at all the tested altitudes. As the wing is moved along the wavelength the drag varied between a maximum and minimum value. As with a wing operating in ground effect over a flat surface these drag values also varied with altitude.

The behaviour of the drag with altitude was similar for all three wavy surfaces. As the altitude reduced from h/c 1.0 the drag decreased over the wave crest for all three wavelengths. There is some fluctuation above the wave crest when λ=c above an altitude of h/c 0.5 but the difference in values is small. When λ=2c and λ=3c the drag decreases with altitude over the wave crest and ¼λ position and increasing with altitude over the trough and ¾λ. Unlike in the wind tunnel it was not possible to record data out of ground effect due to the depth of the CWC working section.

The position of the wing rotation point where minimum and maximum drag occurred is presented in Table 8-5. One particularly striking feature of this data is the fluctuation of minimum and maximum drag positions when the wavelength is equal to the wing chord (Figure 8-23). The main reason why this variation exists is that the difference between minimum and maximum drag values is only 2-10%. Such small fluctuations in the data can be disproportionately effected by experimental error. This small fluctuation can readily be seen in Figure 8-28 where the ratio of maximum to minimum drag ($C_D$max/$C_D$min) is plotted against altitude. The small value of this ratio and its minimal variation compared to the other two wavelengths is evident. When the wing was tested over the

wavelengths equal to two and three times the wing chord there was a much better degree of consistency for the position of minimum and maximum drag.

The minimum drag occurs when the wing rotation point is above the wave crest for λ=2c and λ=3c. As can be seen in Figure 8-26 below an altitude of h/c 0.7 the drag recorded at these wavelengths over the wave crest rapidly reduces, in a similar manner to the lift in Figure 8-17. The peak drag occurs at the wave trough when the λ=2c and the ¾ wave position when the λ=3c. Though greater values of drag are recorded at λ=2c and λ=3c similar behaviour is exhibited at all wavelengths, that is the peak drag increases with a reduction of altitude (Figure 8-27). The positions of maximum and minimum lift correspond with those of the drag as shown in Table 8-4.

8.5.4 Comparison of Drag over Wavy and Flat Surfaces

Figure 8-29 to Figure 8-31 presents the ratio of the drag over a wavy surface to the drag over the flat ground ($C_D$wave/$C_D$flat) as a function of altitude. The data over the flat has been obtained from the wind tunnel experiments operating at a Reynolds Number of 830,000 (see Chapter 5). When the λ=c the peak drag is increased by up to 1.5 times that of operating over a flat surface at an altitude of h/c 0.2. As the altitude is increased to h/c 1.0 the peak drag is 1.14 times that of operating over a flat surface.

As the wavelength increases to 2c the peak drag has increased to over 2 times that obtained operating over the flat (Figure 8-30). The drag over the wave crest and ¼λ has reduced below that obtained over a flat surface between h/c 0.2 to h/c 1.0. Similar results are obtained when the wavelength is 3c as shown in Figure 8-31 with a decrease in drag below that obtained over the flat when the wing is over the wave crest and ¼ λ.

The mean value of the drag produced as a function of altitude over the various wavelengths is shown in Figure 8-32. It can be seen that the mean drag produced over the wavy surfaces is up to 50% greater than that recorded over

the flat in the wind tunnel. At the higher altitude of h/c 0.9 and 1.0 the mean drag and drag over the flat are within few percent of each other. As the altitude reduces below h/c 0.8 this gap increases. The reader should note that this difference is not due to operating at different Reynolds Number. As shown in Figure 5-28 increasing the Reynolds Number from 430,000 to 830,000 only increases the drag by approximately 2 % at an angle of attack of 5 degrees.

8.5.5 Aerodynamic Efficiency over Wavy Surfaces

The mean aerodynamic efficiency of the wing over the wavy and flat surfaces is illustrated in Figure 8-33. It can be seen that operating over a wavy surface results in a loss of aerodynamic efficiency. As the wavelength of the surface increases the aerodynamic efficiency reduces. Particularly evident is the decrease in efficiency when λ=3c below an altitude of h/c 0.4. This is a result of the reduction in lift that occurs when the wing is over the wave crest (Figure 8-14).

8.5.6 Comparison with Byelinsky and Zinchuk

As discussed in Chapter 2 Byelinsky and Zinchuk [18] of the Ukrainian Institute of Hydrodynamics have performed the only other detailed experimental investigation into the effects that wavy surfaces have on a wing when operating in ground effect. They have employed a different research method, moving a TsAGI SR-16-6M aerofoil section (t/c=6%) on a towing sled over solid waves that are attached to the bottom of a towing tank. They have used a range of wavelengths varying from λ=c to λ=20c. It is instructive to compare their method and results with that of the CWC trials carried out for this research. One shortcoming is that their published work mainly describes the effect that the wavy surfaces have on the lift and does not discuss the variation of drag in any detail.

As the wing moves over the waves the Byelinsky and Zinchuk's method has the advantage of recording the forces experienced by the wing along the whole portion of the wavy surface. This allows a continuous oscillogram to be generated resulting in the identification of the magnitude and location of the peak

and trough forces. A disadvantage of the CWC method is that the whole mounting rig has to be placed over the point of interest on a wave. This results in a much coarser sampling of the lift and drag forces along a wavy surface. As stated in section 7.2 the CWC method with the four sample positions employed may not measure the extremes in forces produced as the wing translates over a wave. The advantage with the CWC approach is that it is less demanding in manpower, construction effort and time to set up. This is an important consideration, as Byelinsky and Zinchuk were part of a large research program that had access to significantly greater resources than the author.

In both the towing tank and CWC the amplitude of oscillation in the lift and drag forces was found to increase with a decrease in altitude. Both experimental methods indicate that a reduction in wavelength resulted in a decrease of mean lift.

Byelinsky and Zinchuk found that the wing did not experience the effect of the wavy surfaces when the altitude increased above h/c 0.7. This research found that an effect was present up to an altitude of h/c 1.0 in the CWC. The reason for the difference in results may be that the towing tank was of sufficient depth to eliminate the influence of the free water surface. The nearest the wing ever came to the surface in the towing tank was h/c 2.8 below the water surface. This can be compared to a depth below the surface of h/c 1.1 for the CWC trials. The large surface hump produced as a result of the flow around the test rig resulted in a non-quantifiable effect and resultant inaccuracy in the results (Figure 8-2).

8.6 Applicability of the CWC Static Measurements to the Dynamic Case

An important issue to address is how the static measurements taken in the CWC would compare to the dynamic case if the wing were moving across the wavy surfaces. As discussed above as the wing moves along the wavy surfaces lift varies as a function of wave position. The values of lift obtained when the DHMTU wing is over a wavy surface do not correspond to the results obtained over a flat surface as a result of the water flow over the waves. At each position over the wavy surface the lift corresponds to an effective angle of attack (α_{eff}). The value of α_{eff} is obtained by reading the AoA value for the recorded lift over a

wavy surface from the DHMTU lift-AoA curves over the flat (Figure 5-18). This α_{eff} can be smaller or larger than the fixed geometrical angle of attack (5^{O}) depending upon the wings position over the wave and surface wavelength. As the wing is moving along the wavy surface it is fluctuating over an effective angle of attack range.

This fluctuation in the effective angle of attack is analogous to the oscillation of an aerofoil with an incoming flow. In this case when the dynamic angle of attack exceeds the static stall angle of attack flow reversal appears on the rear of the aerofoil. This reversal of flow progresses up the surface of the aerofoil. Then the flow no longer remains attached and a strong vortical flow develops and the lift slope increases until moment stall occurs. As the angle of attack is reduced the boundary layer reattaches from the front to the rear resulting in the aerofoil returning to unstalled values. This results in a hysteresis loop for the lift-AoA curve of an aerofoil. The effects of this behaviour have been documented by Lawrence [55] who investigated the dynamic stall of a NACA 0012 aerofoil.

The fluctuation of effective angle of attack can be seen in Figure 8-34 and Figure 8-35. When the λ=1c the effective angle of attack varies from 5.4^{0} to 10^{0} as a function of wave position at an altitude of h/c 0.2. In this case the extreme α_{eff} approaches but does not exceed the stalling angle at this height. In contrast when the altitude has increased to h/c 1.0 α_{eff} varies from 4.3^{O} to 5.2^{O} resulting in only a small difference of 0.9^{O}. This would indicate that there would be little hysteresis when λ=1c as the stall angle has not been exceeded.

As the wavelength of the surface increases to λ=3c the effective angle of attack increases to values greater the 13^{O}. A specific α_{eff} cannot be put to this as it exceeds the values recorded in the wind tunnel over the flat ground. There is a high probability that the α_{eff} is operating in the stalled region.

The water was moving past the wing at a velocity of 1.9 ms^{-1}, in the dynamic case the wing would be moving over the waves at a rate of 6 Hz (λ=1c), 3 Hz (λ=2c) and 2 Hz (λ=3c). This can be compared to the static CWC method where the wing is stationary and the flow was allowed to develop and settle over the

wing. Here the wing would experience the extremes of lift, as it would not be moving at several Hz above the wavy surface. Therefore the results generated in the static CWC experiments can be considered as design extremes.

8.7 Summary

1. As a wing flies over a wavy surface the lift varies from a maximum to a minimum. The amplitude of the lift force oscillation increases with decreasing altitude. The maximum and minimum values of lift do not correspond to the position of the wing's rotation point over the physical peak and troughs of the wavy surfaces. The minimum lift occurs when the wing rotation point is over the wave peak at all altitudes. The position of maximum lift varies between ¼ to ¾ wavelength dependent upon the surface wavelength.

2. As when flying in the ground effect regime over a flat surface the peak lift obtained over a wavy surface increases with decreasing altitude. This contrasts sharply to the minimum lift that decreases with a reduction in altitude when the wavelength is equal to two and three time the wing chord. A general result is that as the wavelength of the surface increases the maximum lift experienced by the wing increases and the minimum lift decreases. The maximum lift increases at a greater rate than the minimum lift decreases.

3. When the wavelength is equal to 2c and 3c the aerofoil experiences a downward force when the wing rotation point is over the wave crest below an altitude of approximately h/c 0.3. Even at higher altitudes the lift force is much reduced compared to the peak lift forces recorded.

4. The aerodynamic performance of a wing in ground effect operating over a wavy surface is dependent upon the wavelength of the surface. As the wavelength of the surface increases the difference between the minimum and maximum lift coefficient increases. This results in a wide variation in the magnitude of lift force that the flight control system of a WIG craft has to cope with when flying over the sea's surface. One of the merits of

adopting a medium to high aspect ratio wing planform for a WIG craft is that the higher cruising altitude attainable results in a smaller variation in lift. This could considerably simplify the design of the flight control system as well as improving ride comfort for passengers.

5. The drag on the wing over a wavy surface in ground effect varies with altitude and as a function of wing position over the wavelength. Like lift it varies between a minimum and maximum value. It was found that the drag was effected over the whole altitude range tested, though allowance has to be made for the effect near the surface of the CWC.

6. When the wavelength equalled the wing chord the peak drag was 1.5 times greater than that obtained over the flat at h/c 0.2. When the wavelength equalled two and three times the wing chord minimum drag consistently occurred over the wave peak. Maximum drag occurred when the wing rotation point was over the wave trough for λ = 2c and ¾ wavelength for λ = 3c. The positions over the wavy surfaces where minimum and maximum drag was recorded are identical to the extremes of lift. As the wavelength reduced to equal the wing chord the maximum drag decreased and minimum drag increased.

7. Compared to the wind tunnel data obtained over flat ground, operating over a wavy surface results in greater values of drag. The peak drag can be over twice that obtained over flat ground at low altitude (h/c 0.2). The difference between minimum and maximum drag is much less than that of lift for all three wavy surfaces.

8. The method of Byelinsky and Zinchuk involving flying a wing above waves submerged in a towing tank provides a limited degree of corroboration of the CWC method. The trends in lift and drag produced in both experimental approaches are similar.

9. It was found that the proximity of the wing to the water's surface in the CWC effected the altitude range at which the effect of the waves was

experienced. Additional limitations in the CWC method include the discrete sampling that could miss any peaks and troughs in the data unless sufficient time is available to finely sample the wavelength. Advantages of the CWC method are the rapidity that the experimental apparatus can be set-up and run combined with the limited, typically two, number of personnel required.

10. In the case of a wing flying over waves in ground effect the wing will not experience the full range of effective angle of attack, thus this CWC static method will produce magnitudes of lift that are greater than in the dynamic case. Therefore the results generated in the CWC experiments can be considered as design extremes.

Magnitude of Uncertainty	Magnitude
C_L	$\pm$ 36 x 10^{-2}
C_D	$\pm$ 1.4 x 10^{-3}
Wing AoA	$\pm$0.1 degree
Wing Yaw	$\pm$0.1 degree
Wing Height	$\pm$0.03 h/c

Table 8-1: Magnitude of uncertainty for CWC experiments

Nomenclature	Description	Value
Volume (wing volume)	0.7 x chord x thickness x span	0.019 ft^3
h_t	Length of other side of tunnel	2.6 ft
b_t	Length of tunnel side parallel to wing span	4.7 ft

Table 8-2: Nomenclature and values for CWC blockage corrections

Parameter	Experimental Range
Angle of Attack	5 degrees
Height above wave crest	h/c 0.2 to 1.0 at 0.1 steps
Wave Positions	Wave peak, ¼ λ, wave trough and ¾ λ
Reynolds Number	5.5 x 10^5

Table 8-3: Experimental variables for CWC Runs

	λ = wing chord		λ = 2 x wing chord		λ = 3 x wing chord	
Altitude (h/c)	**$C_L$min**	**$C_L$max**	**$C_L$min**	**$C_L$max**	**$C_L$min**	**$C_L$max**
0.2	Crest	¼ λ	Crest	Trough	Crest	¾ λ
0.3	¾ λ- Crest	¼ λ	Crest	Trough	Crest	¾ λ
0.4	¾ λ- Crest	¼ λ	Crest	Trough	Crest	¾ λ
0.5	¾ λ- Crest	Trough	Crest	Trough	Crest	¾ λ
0.6	¾ λ- Crest	¼ λ	Crest	Trough	Crest	¾ λ
0.7	¾ λ- Crest	¼ λ	Crest	Trough	Crest	¾ λ
0.8	¾ λ- Crest	¼ λ	Crest	Trough	Crest	¾ λ
0.9	¾ λ- Crest	¼ λ	Crest	Trough	Crest	¾ λ
1.0	¾ λ- Crest	Peak	Crest	Trough	Crest	¾ λ

Table 8-4: Position of minimum and maximum C_L for each wavelength as a function of altitude

	λ = wing chord		λ = 2 x wing chord		λ = 3 x wing chord	
Altitude (h/c)	**$C_D$min**	**$C_D$max**	**$C_D$min**	**$C_D$max**	**$C_D$min**	**$C_D$max**
0.2	¼ λ	¾ λ	¾ λ	Trough	Crest	¾ λ
0.3	¼ λ	¾ λ	Crest	Trough	Crest	¾ λ
0.4	¼ λ	Crest	Crest	Trough	Crest	¾ λ
0.5	¾ λ	Trough	Crest	Trough	Crest	¾ λ
0.6	¾ λ	Crest	Crest	Trough	Crest	¾ λ
0.7	¾ λ	Trough	Crest	Trough	Crest	¾ λ
0.8	¾ λ	Crest	Crest	Trough	Crest	¾ λ
0.9	¼ λ	Crest	Crest	Trough	Crest	¾ λ
1.0	Trough	Crest	Crest	Trough	Crest	¾ λ

Table 8-5: Position of minimum and maximum C_D for each wavelength as a function of altitude

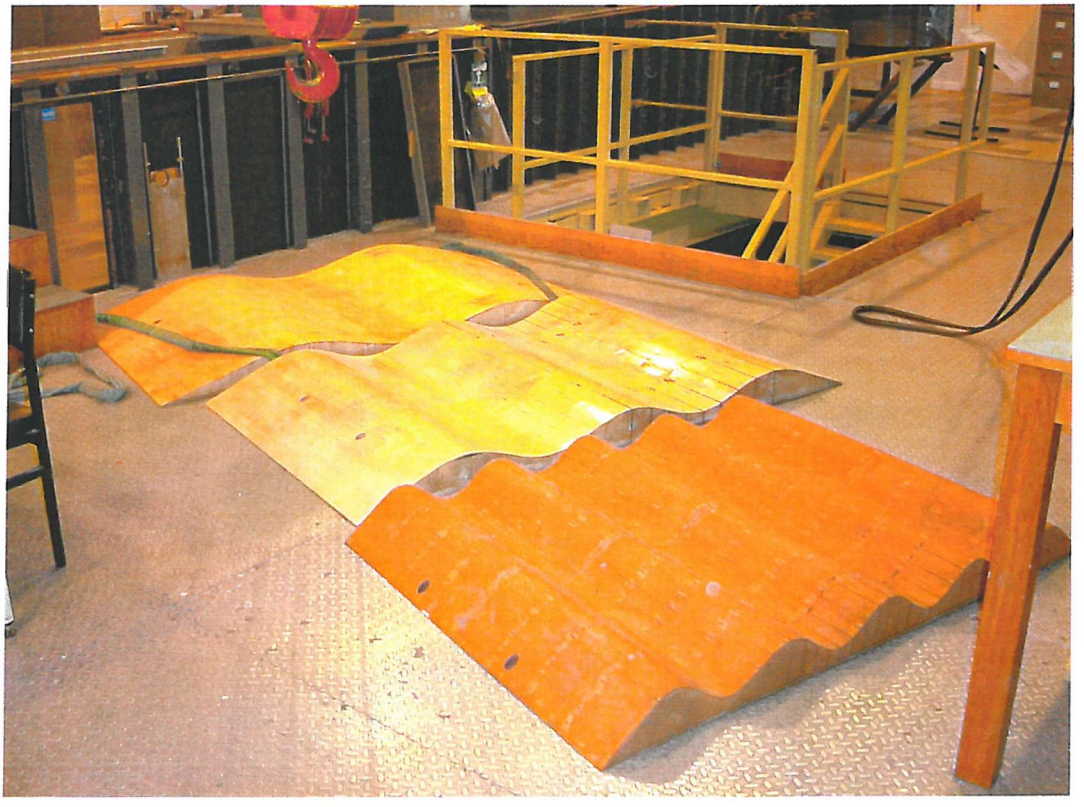

Figure 8-1: CWC Wave Selection, from back to front λ=3c, λ=2c and λ=c

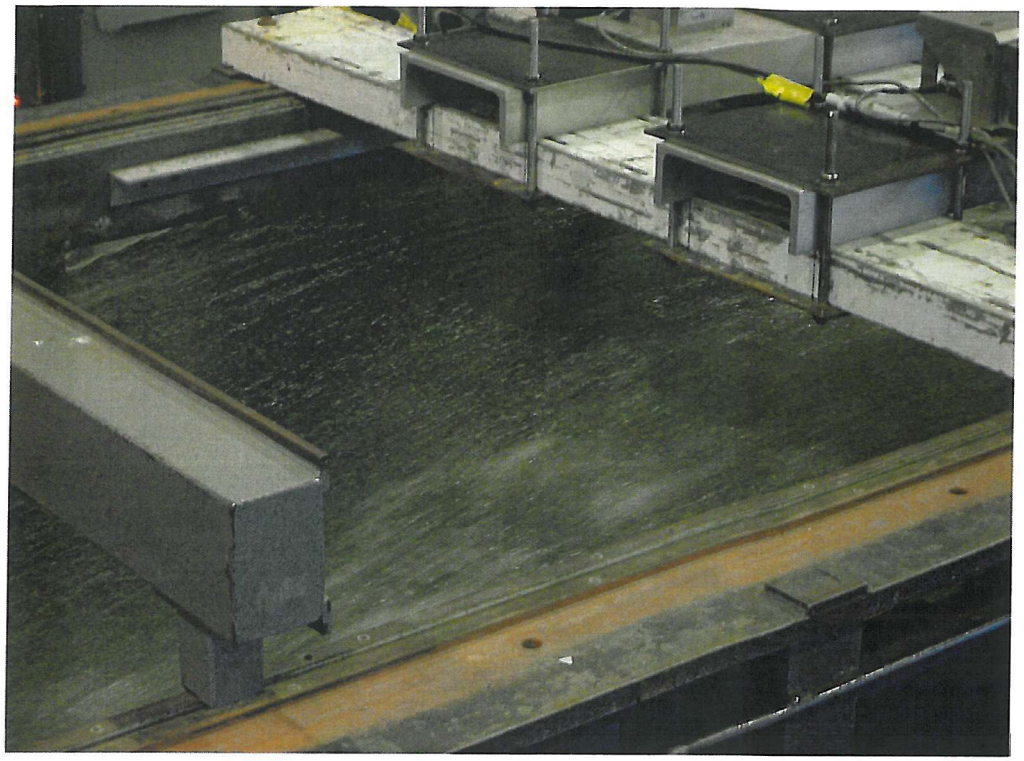

Figure 8-2: Illustration of the surface conditions of the CWC, water speed 1.9 ms^{-1} and wing altitude h/c 0.2

Figure 8-3: Upper Working Section of QinetiQ Haslar's CWC

Figure 8-4: WIG mounting rig located in the working section of the CWC

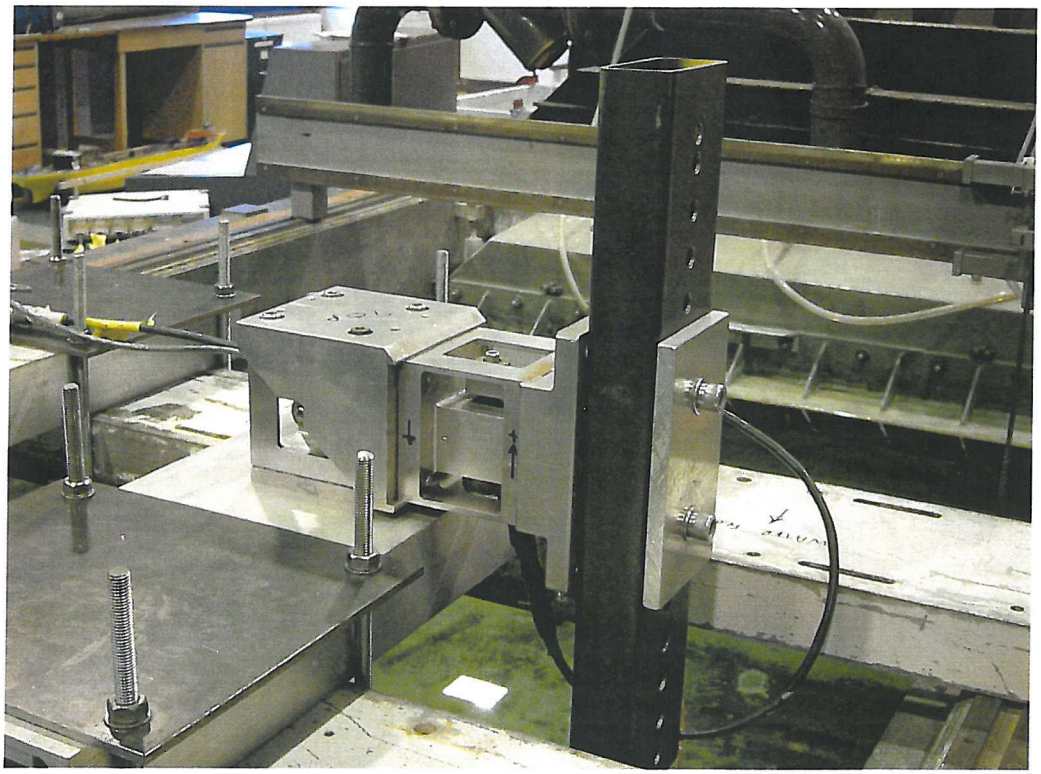

Figure 8-5: Force block mountings

Figure 8-6: DHMTU wing located over a wavy surface

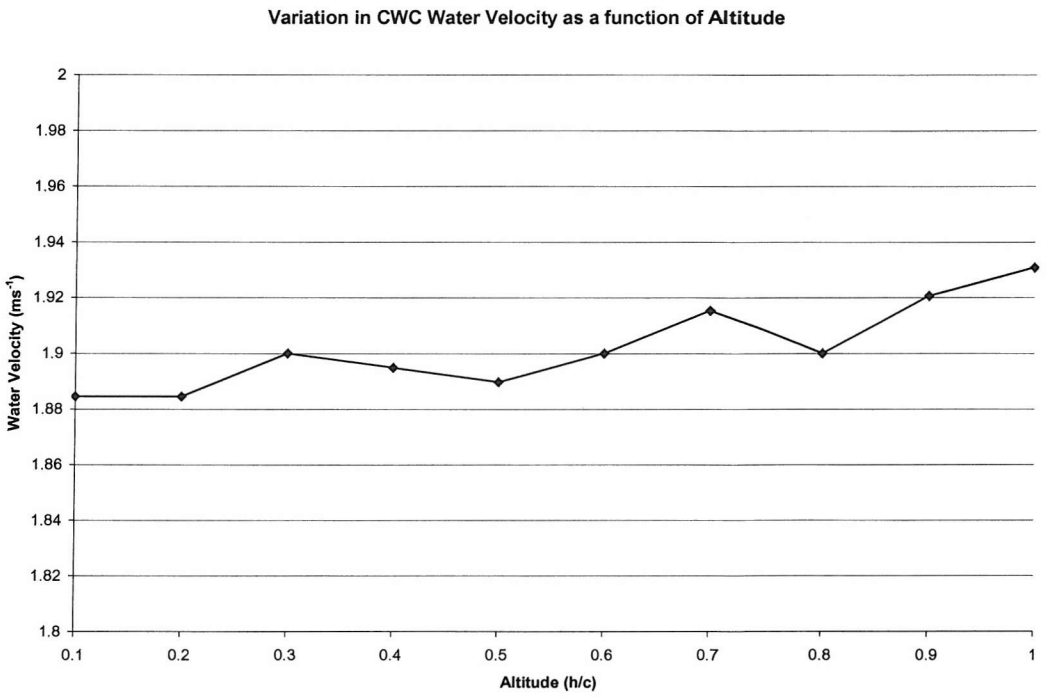

Figure 8-7: Variation in CWC Water Velocity as a function of Altitude

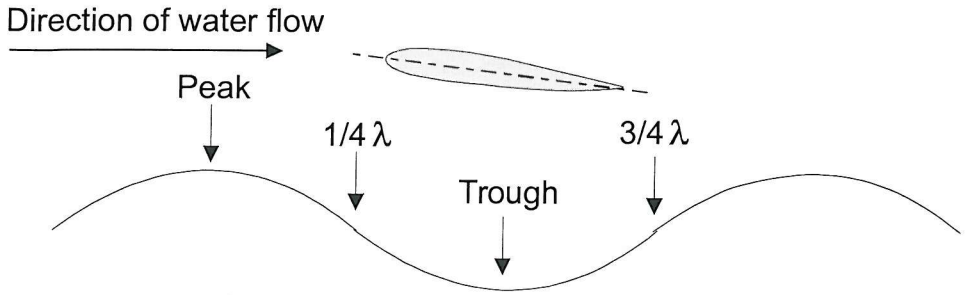

Figure 8-8: Wavelength positions used in study

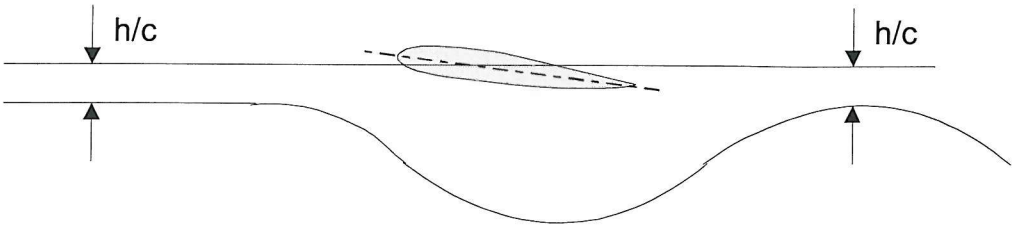

Figure 8-9: Definition of altitude reference points over wavy and flat surfaces

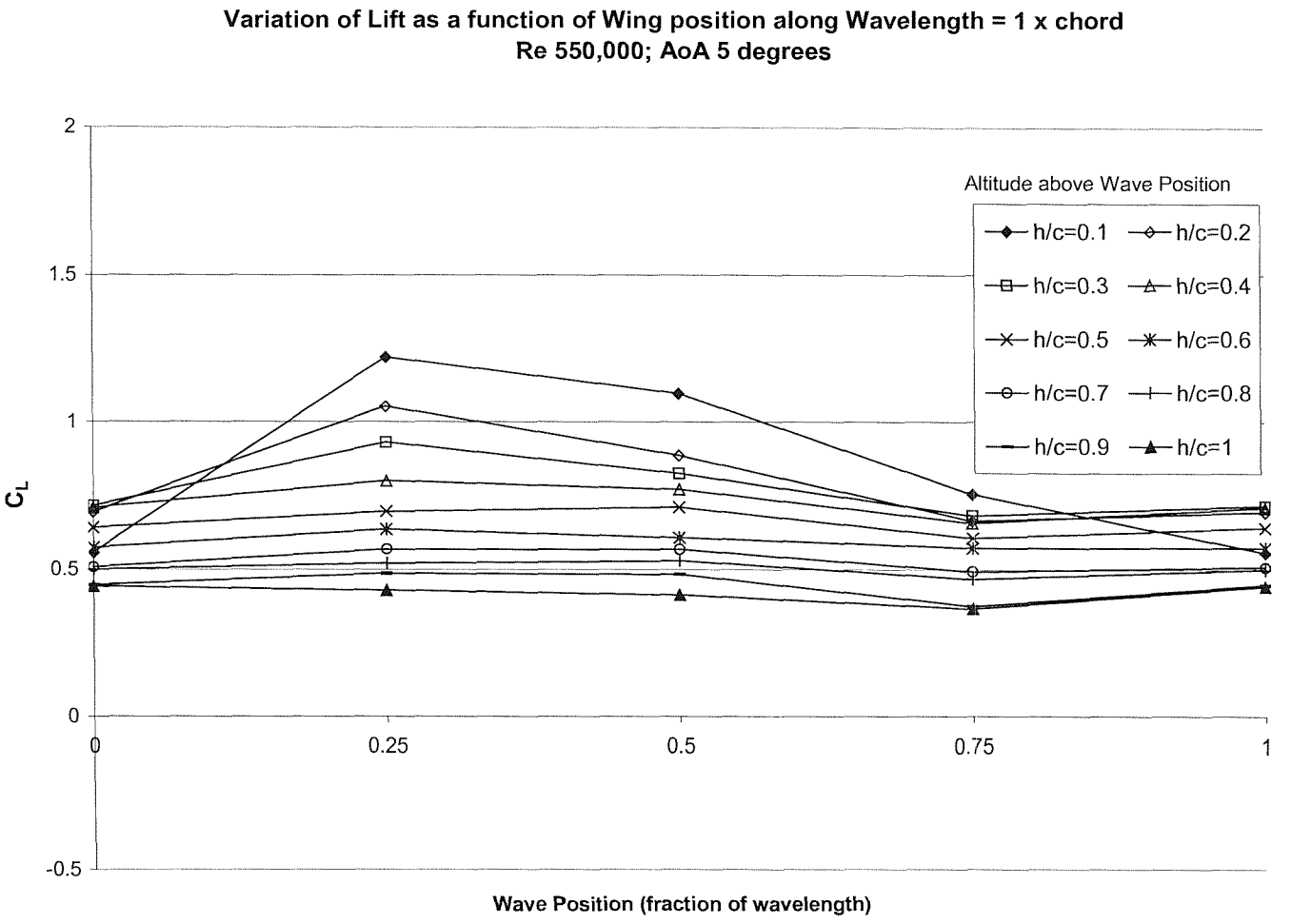

Figure 8-10: Variation of Lift along wavy surface (wavelength = wing chord)

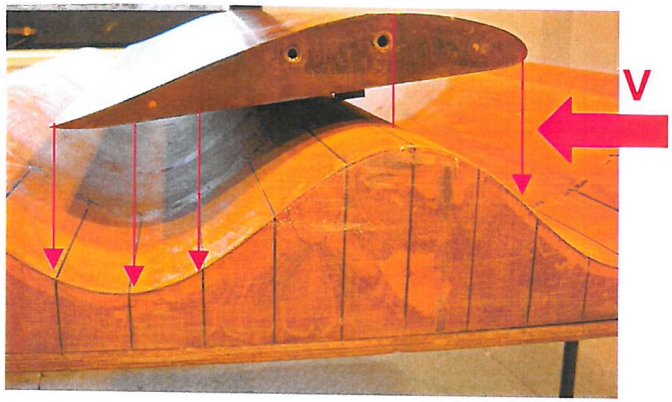

A) Rotation point over Wave Crest

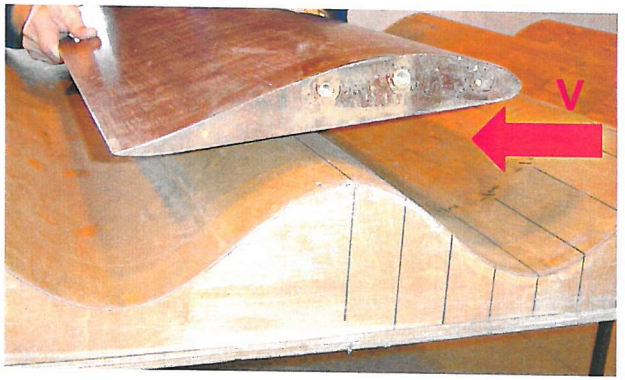

B) Rotation point over ¾ λ

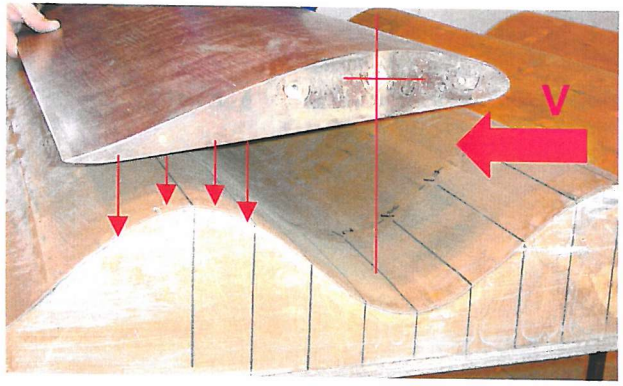

C) Rotation point over Wave Trough

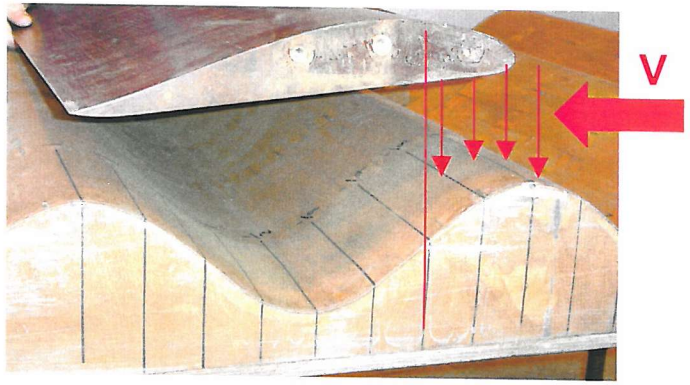

D) Rotation point over ¼ λ

Figure 8-11: Wing-wave geometry over wavelength = wing chord

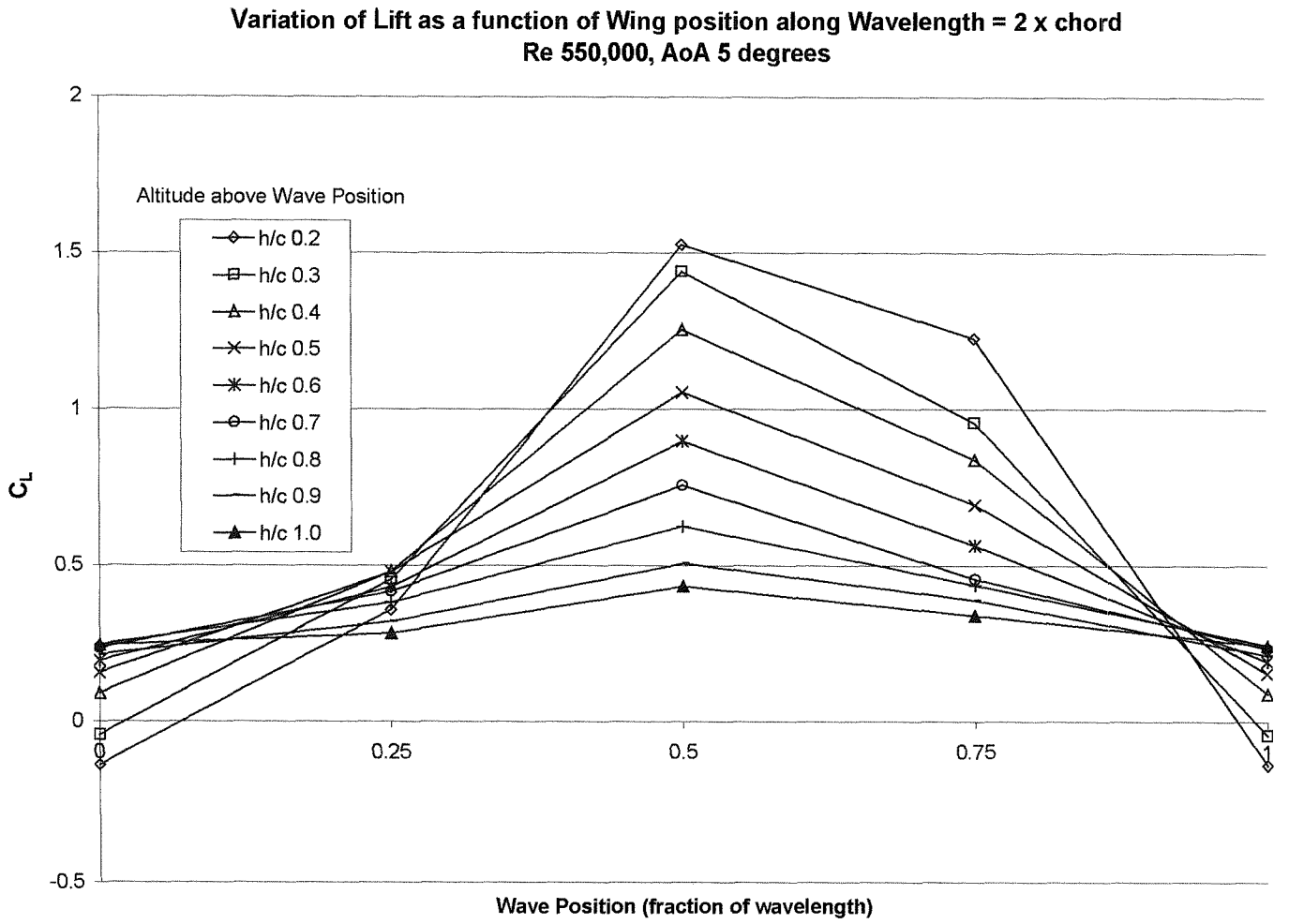

Figure 8-12: Variation of Lift along wavy surface (wavelength = 2 x wing chord)

A) Rotation point over Wave Crest

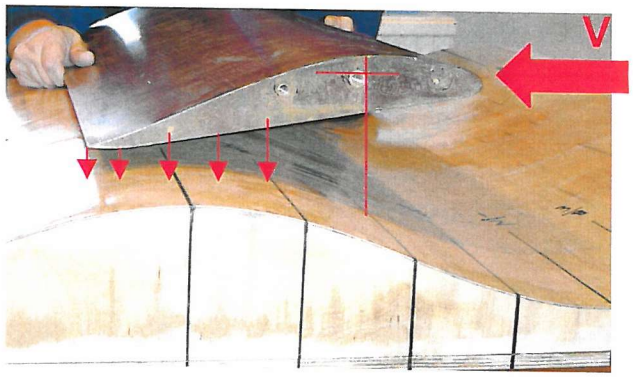

B) Rotation point over ¾ λ

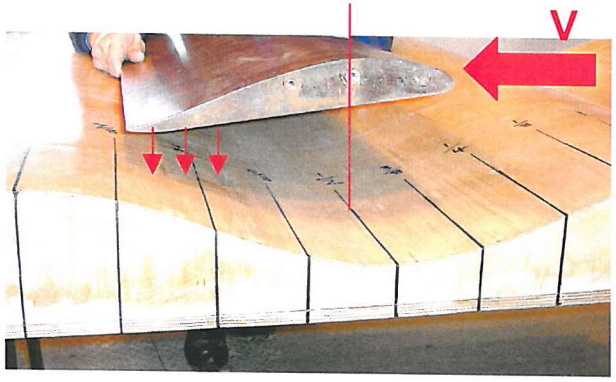

C) Rotation point over Wave Trough

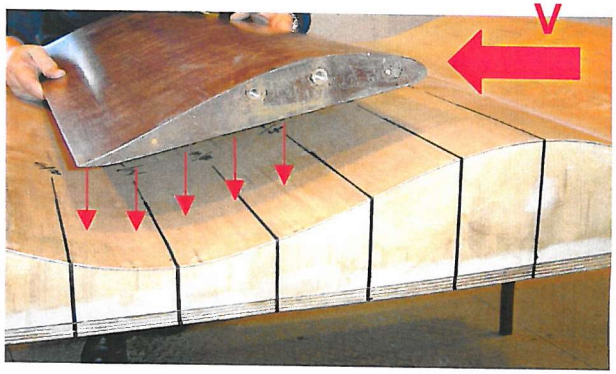

D) Rotation point over ¼ λ

Figure 8-13: Wing-wave geometry over wavelength = 2 x wing chord

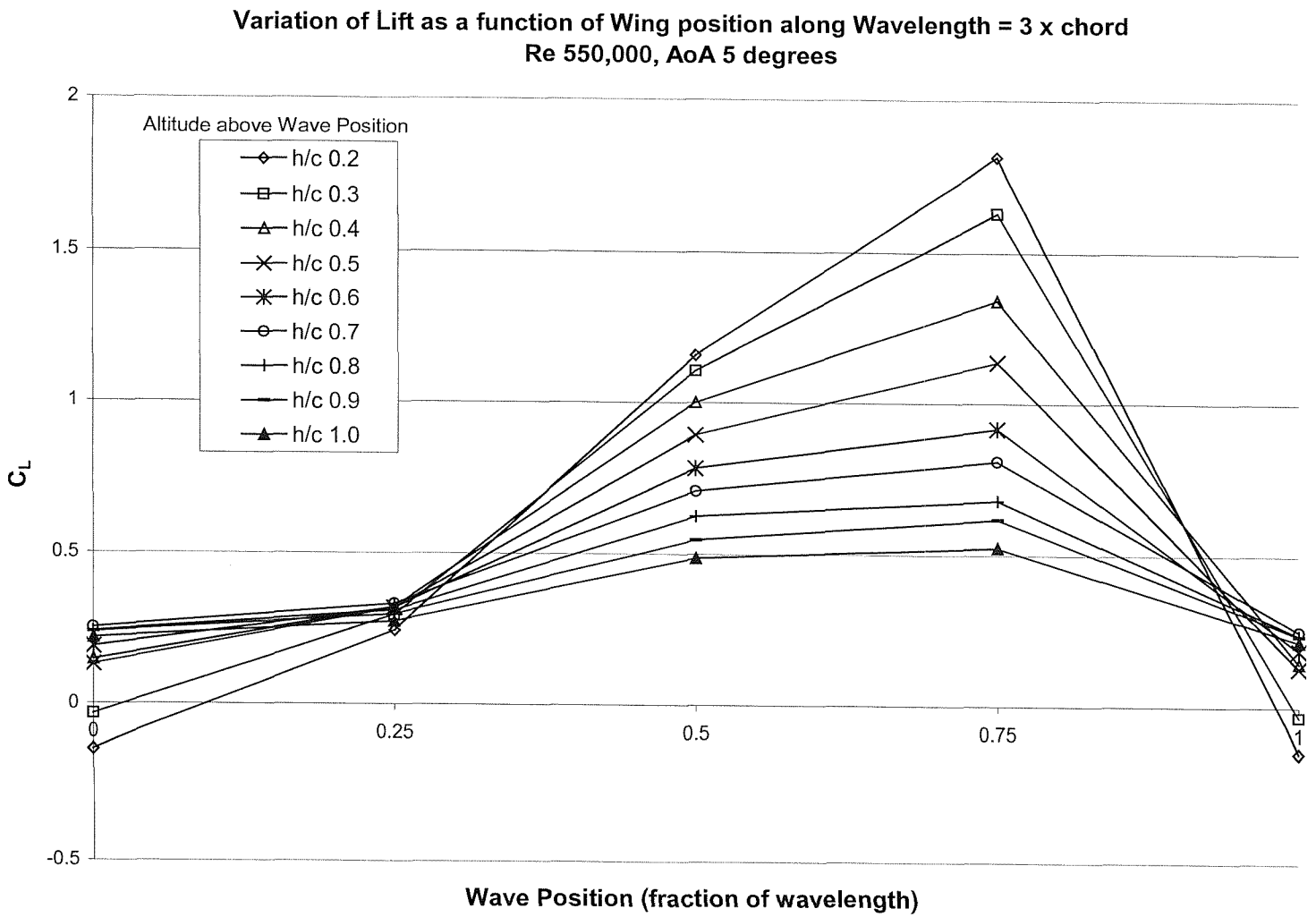

Figure 8-14: Variation of Lift along wavy surface (wavelength = 3 x wing chord)

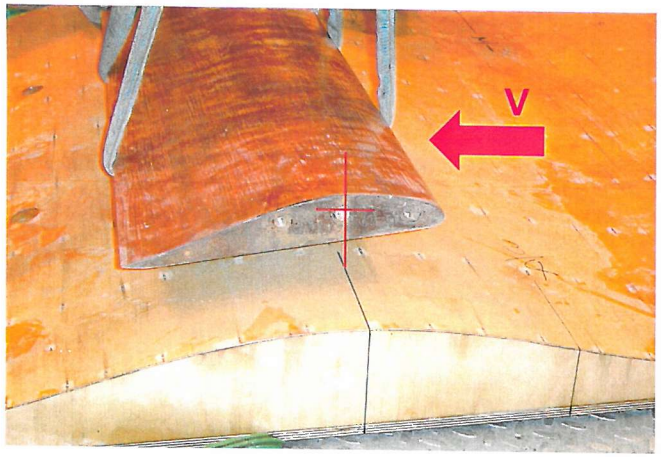

A) Rotation point over Wave Crest

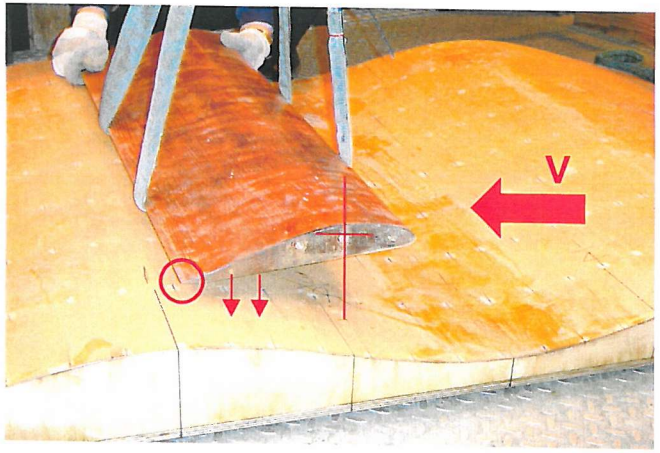

B) Rotation point over ¾ λ

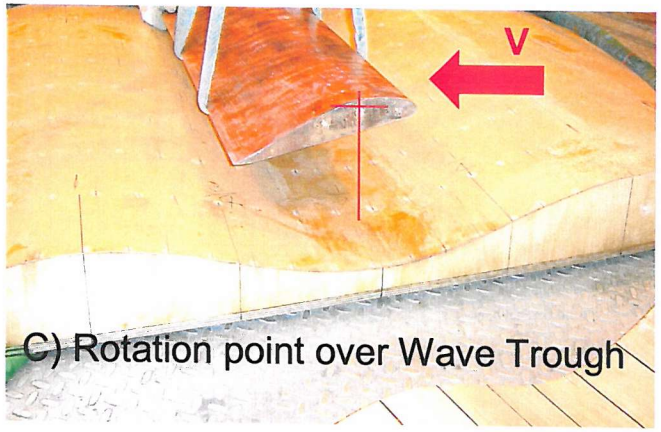

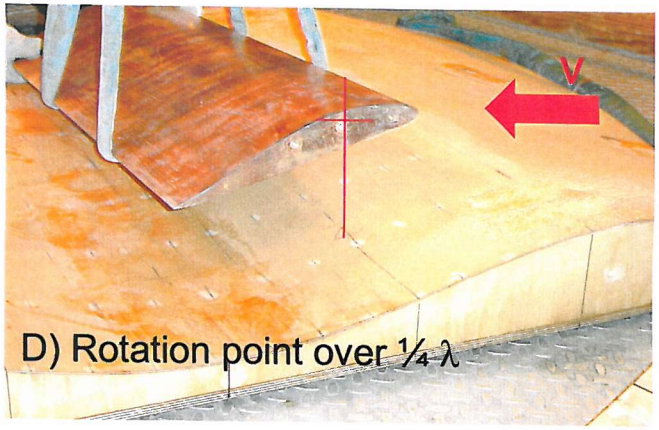

Figure 8-15: Wing-wave geometry over wavelength = 3 x wing chord

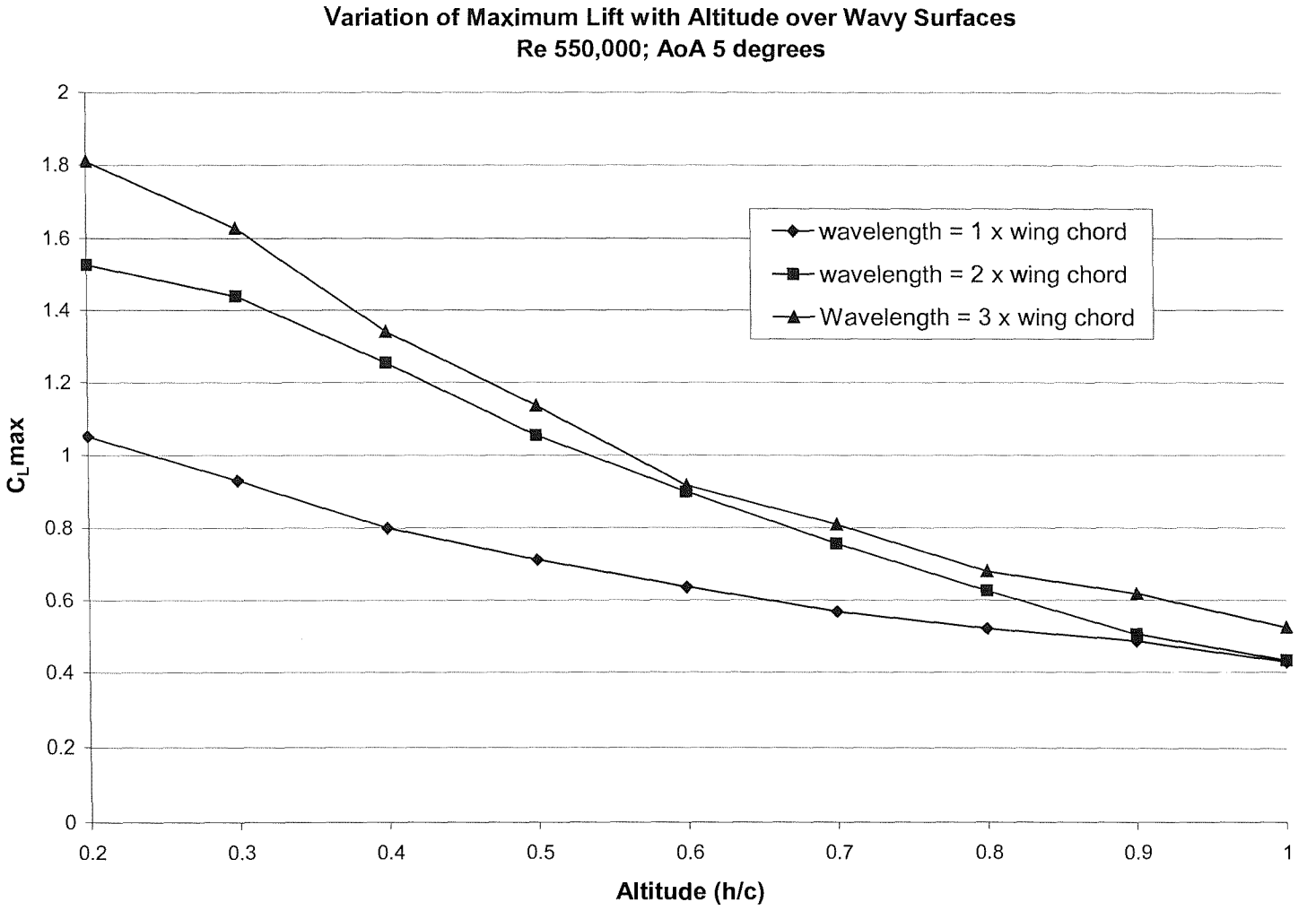

Figure 8-16: Variation of maximum lift coefficient with altitude over the wavy surfaces

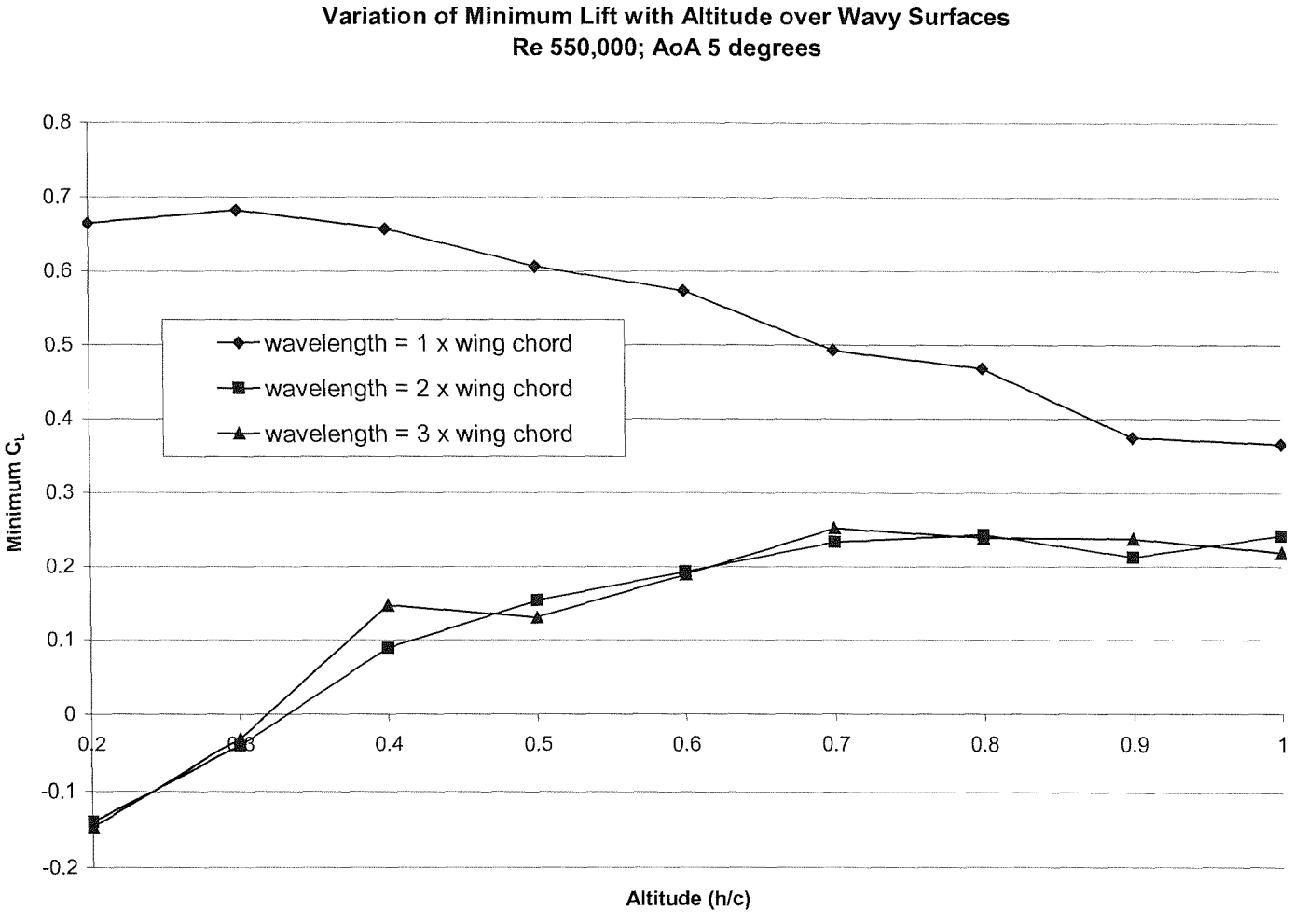

Figure 8-17: Variation of minimum lift coefficient with altitude over the wavy surfaces

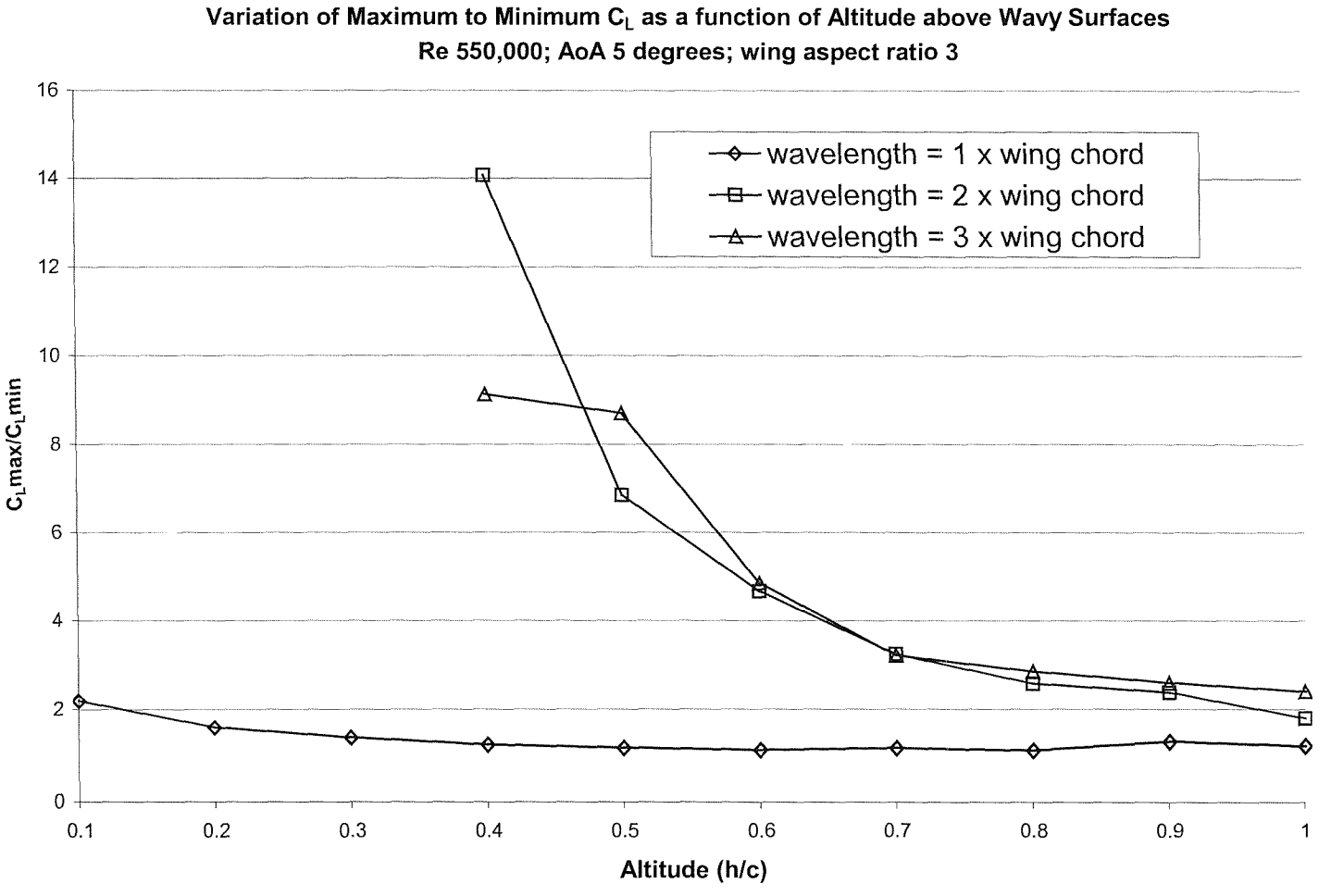

Figure 8-18: Variation of Maximum to Minimum C_L as a function of Altitude over the wavy surfaces tested

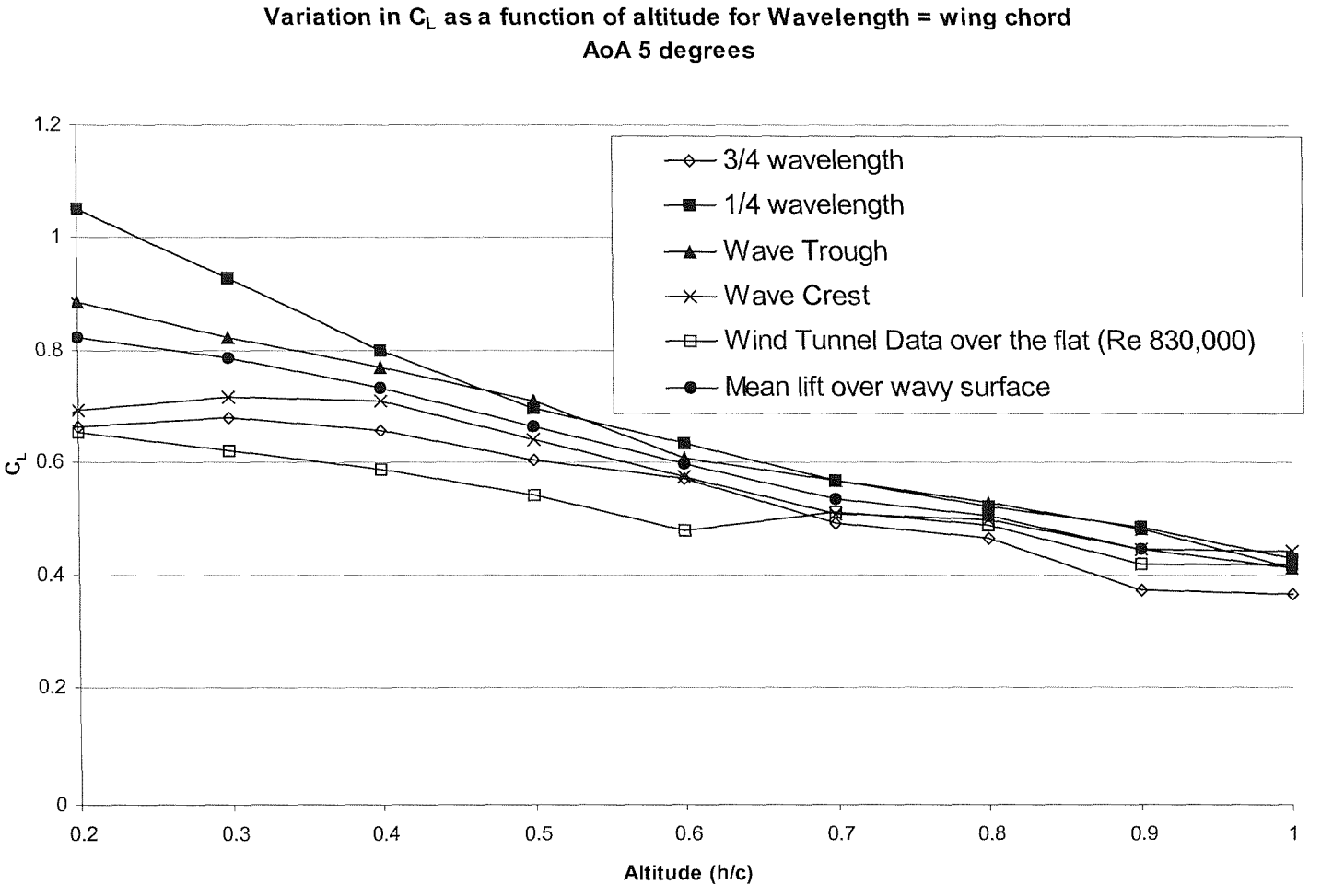

Figure 8-19: Variation in C_L as a function of altitude for surface with wavelength = wing chord

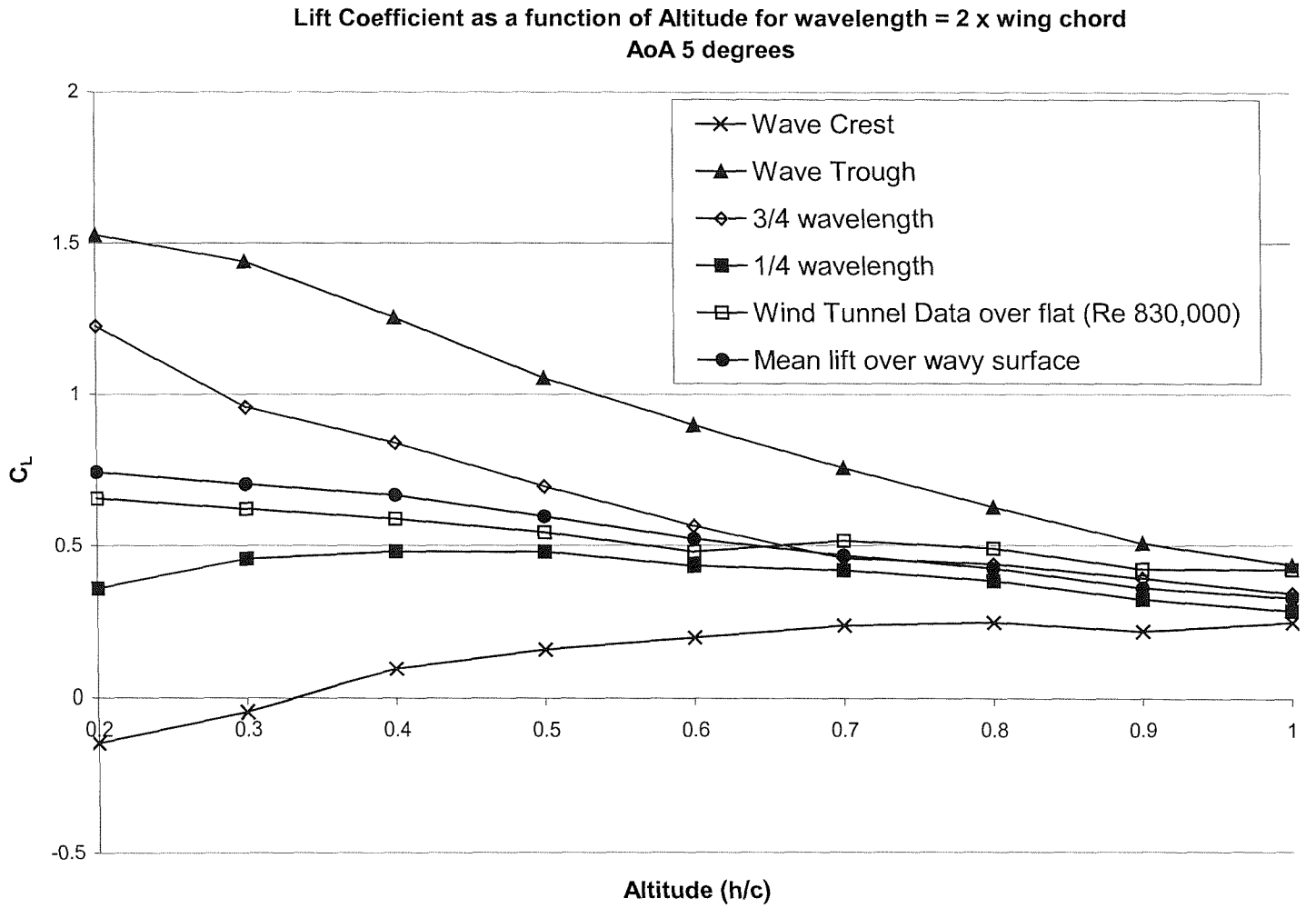

Figure 8-20: Variation in C_L as a function of altitude for surface with wavelength = 2 x wing chord

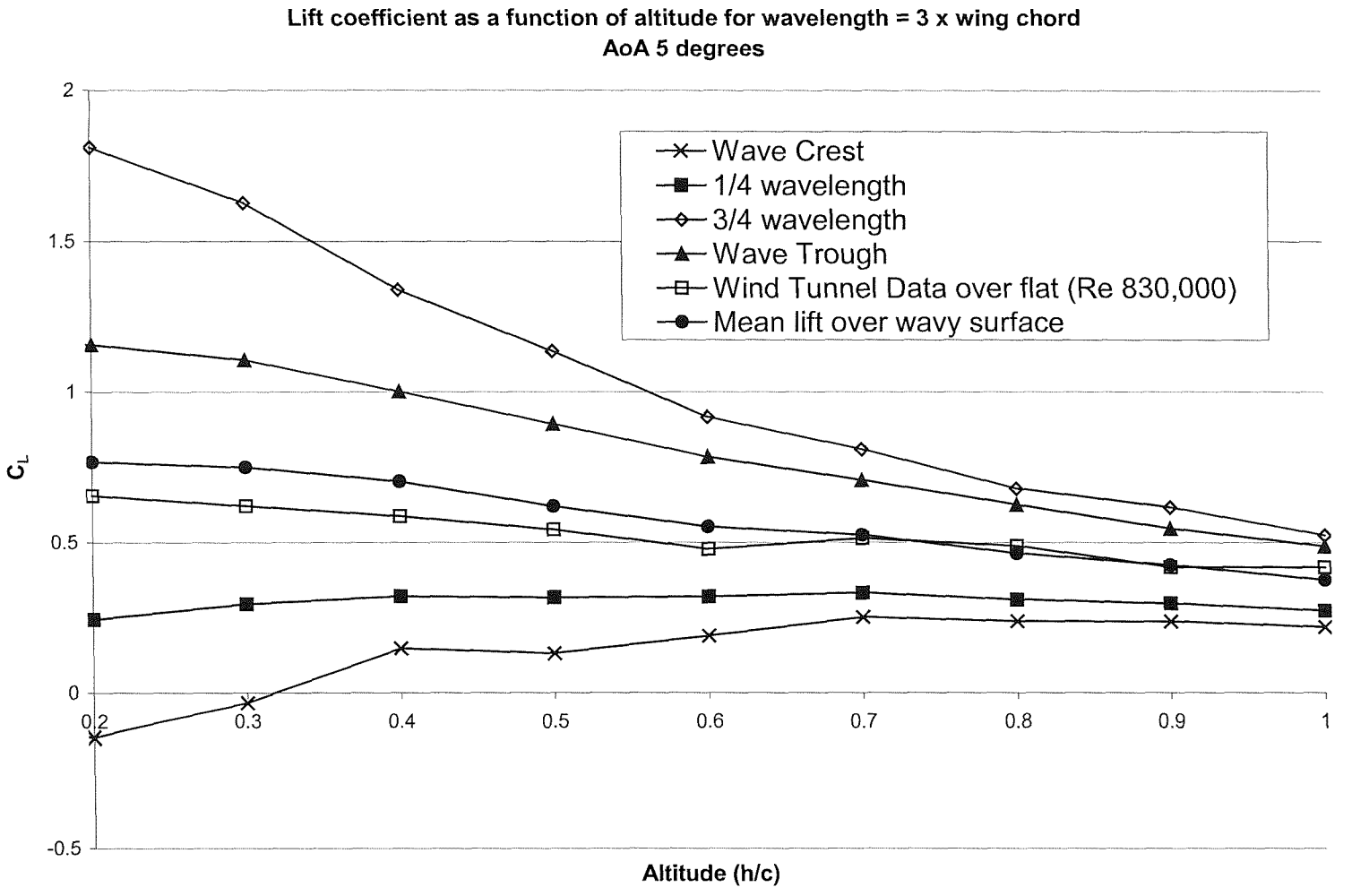

Figure 8-21: Variation in C_L as a function of altitude for surface with wavelength = 3 x wing chord

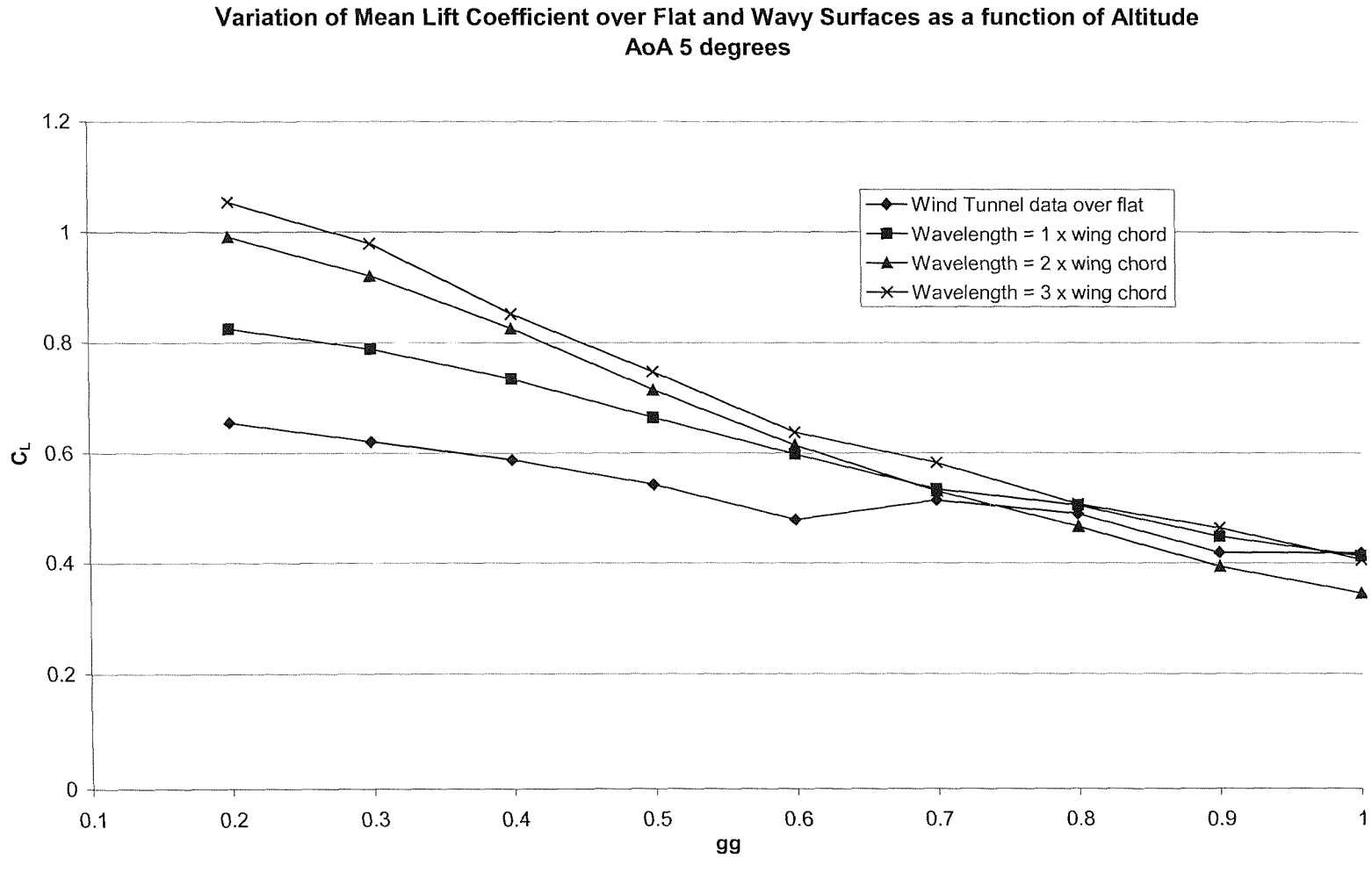

Figure 8-22: Variation of the mean lift coefficient over wavy surfaces as a function of altitude

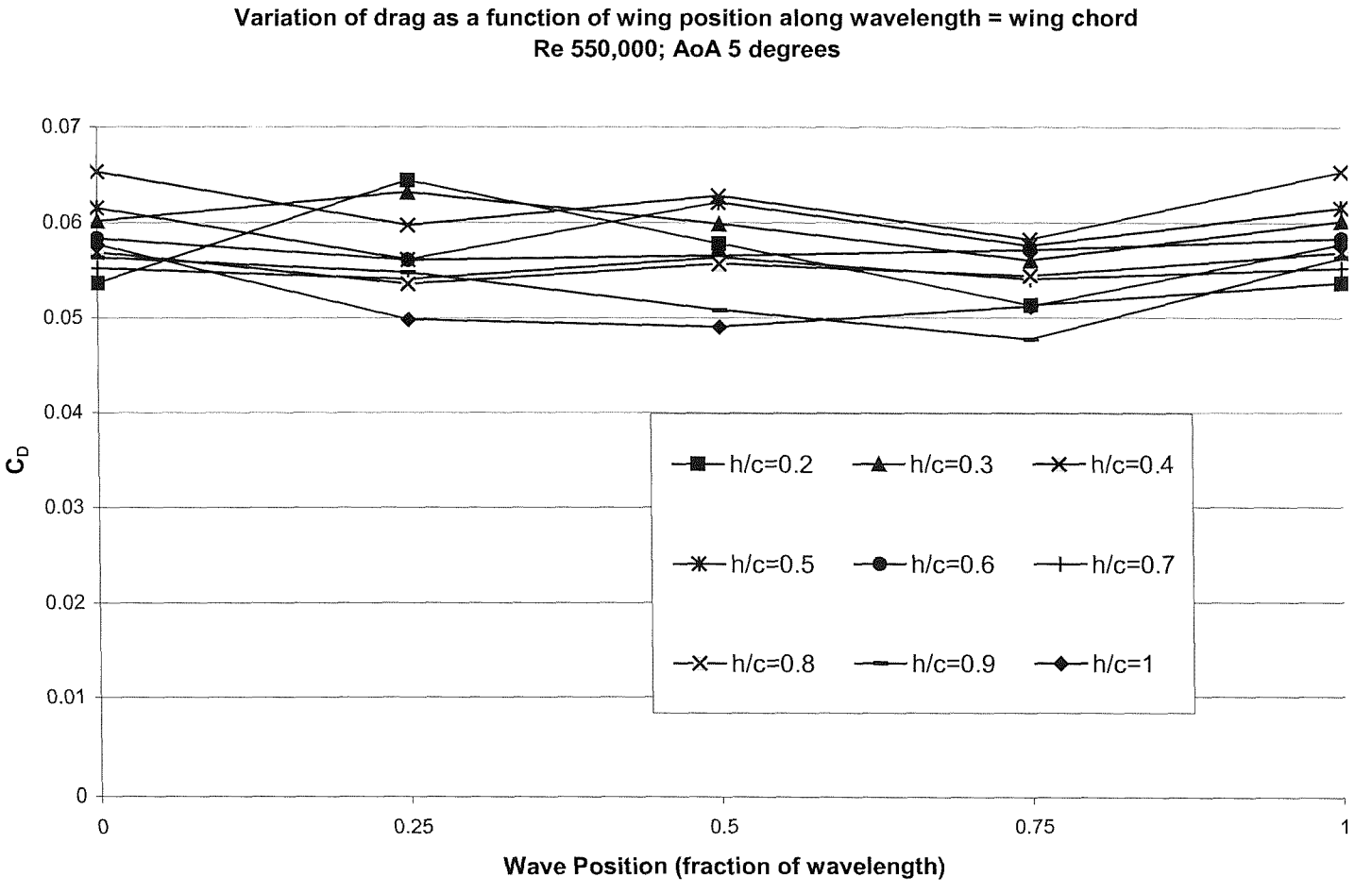

Figure 8-23: Variation in C_D as a function of altitude for surface with wavelength = wing chord

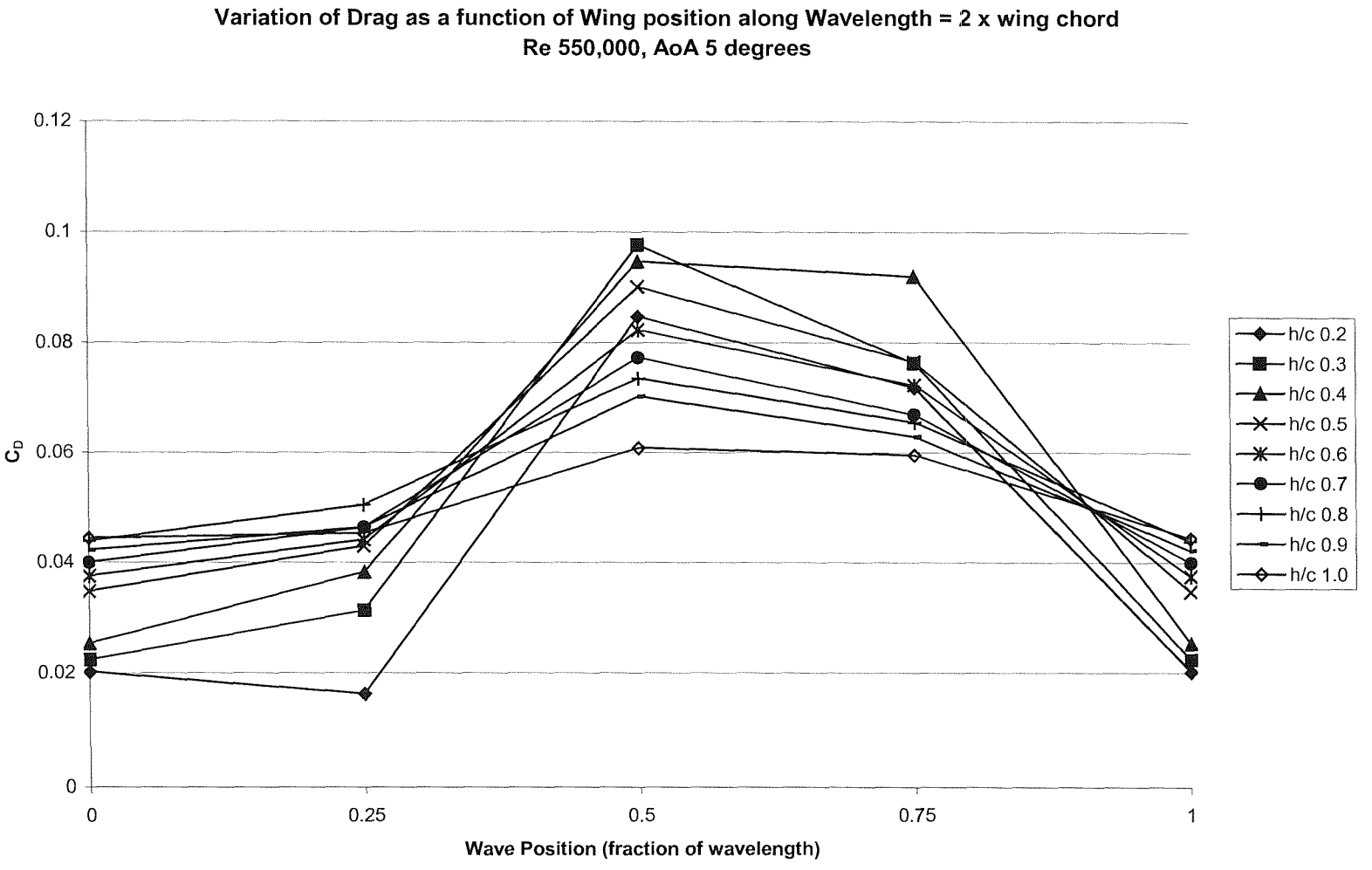

Figure 8-24: Variation in C_D as a function of altitude for surface with wavelength = 2 x wing chord

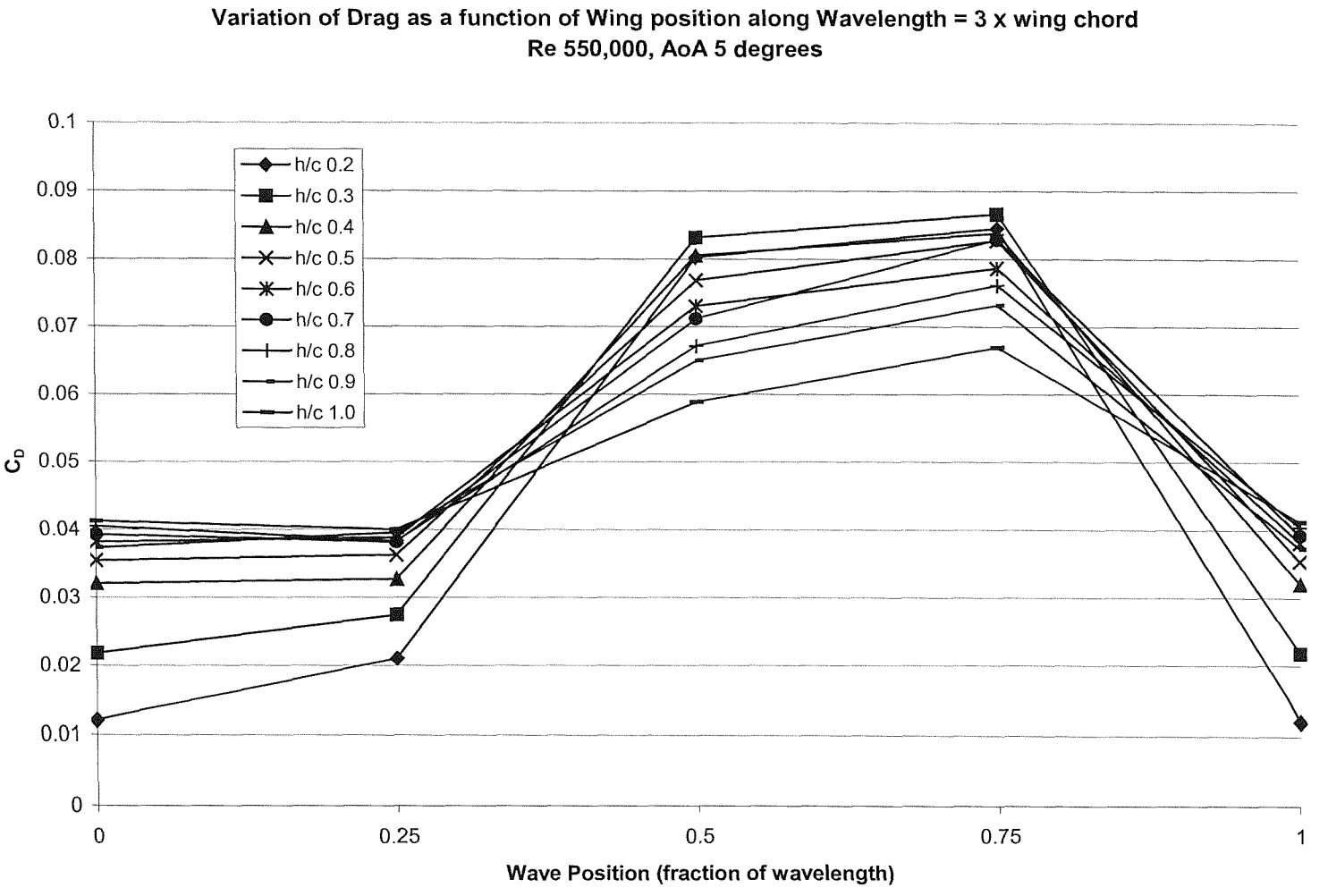

Figure 8-25: Variation in C_D as a function of altitude for surface with wavelength = 3 x wing chord

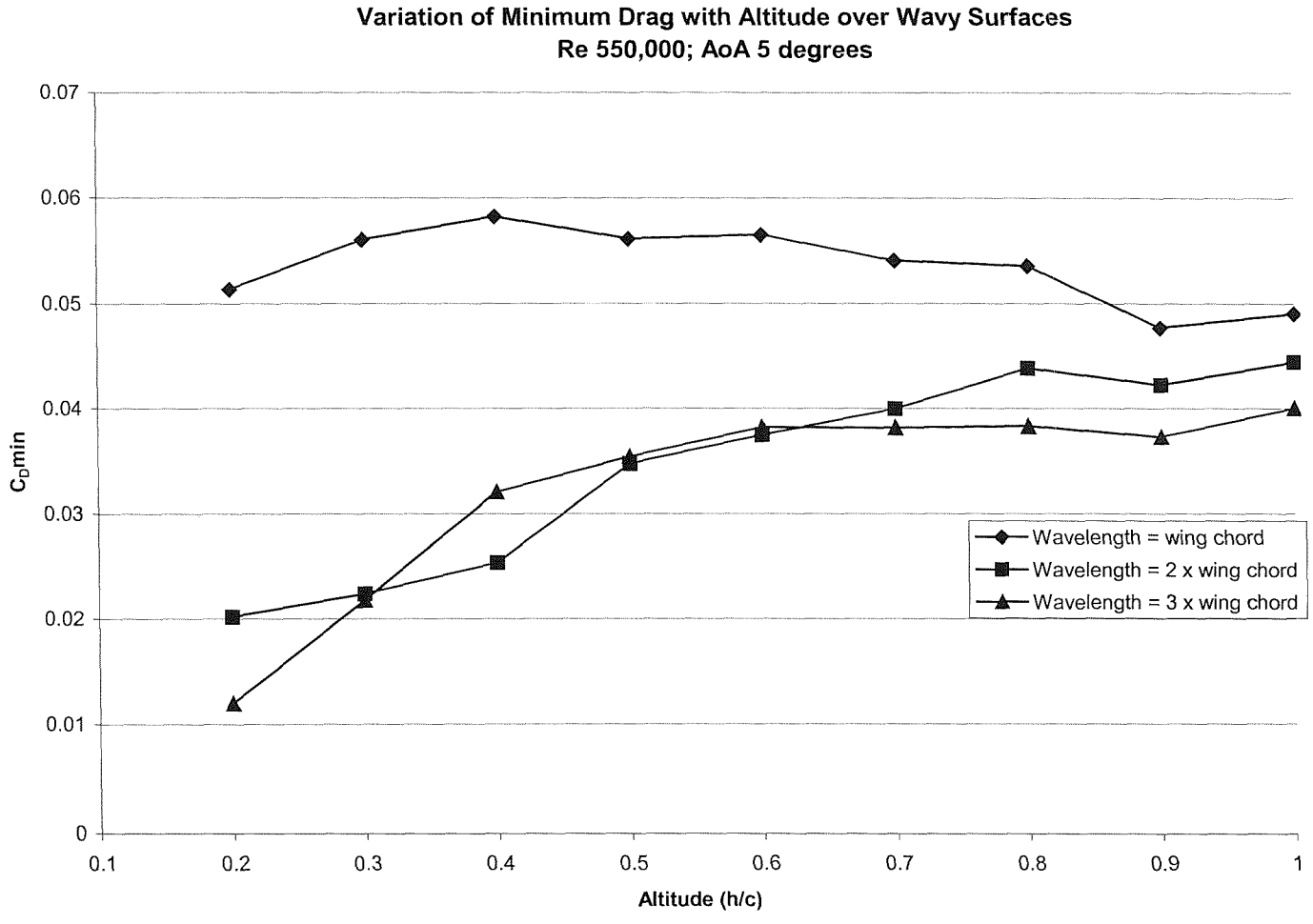

Figure 8-26: Variation of minimum drag coefficient with altitude over the wavy surface

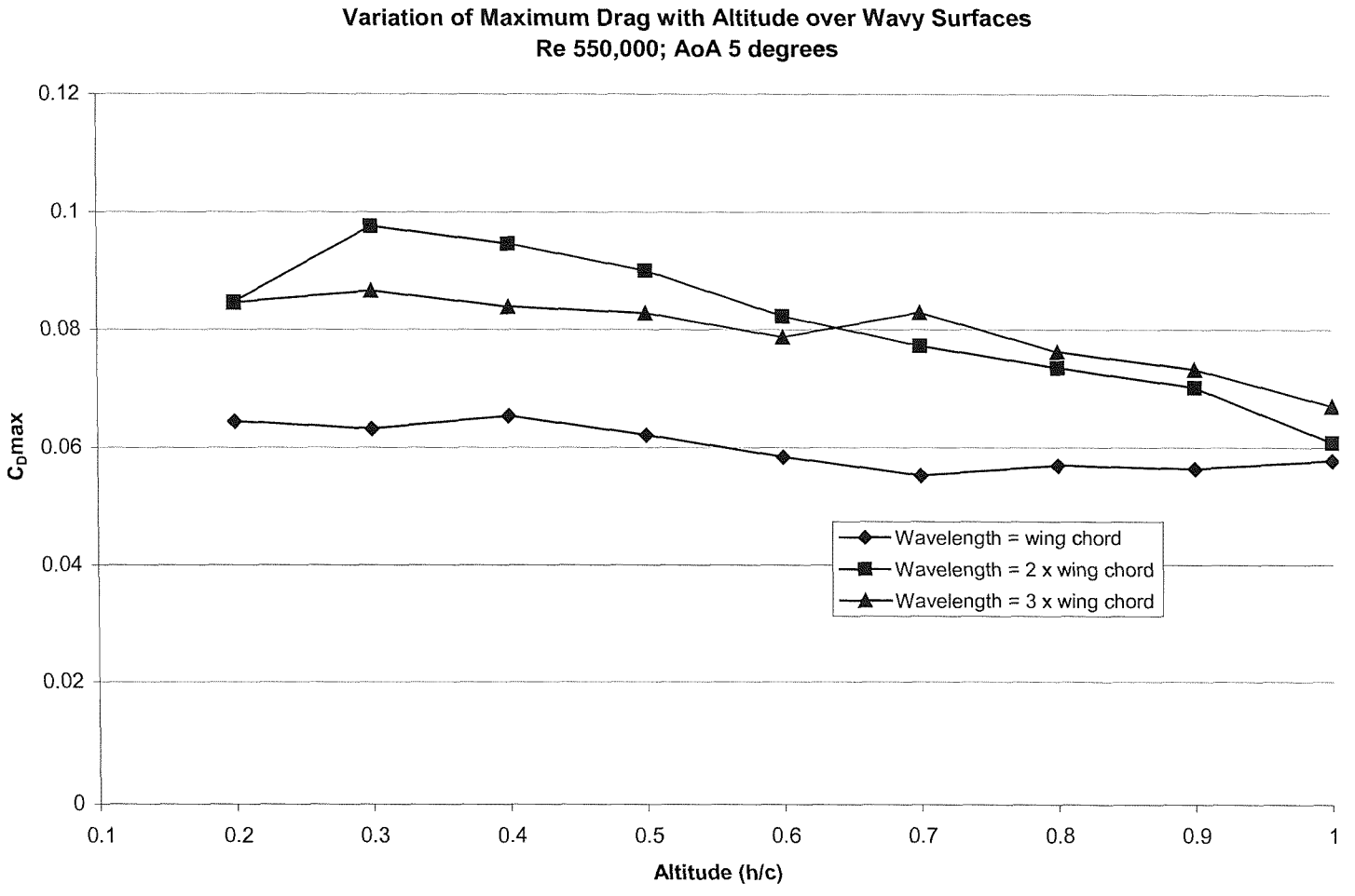

Figure 8-27: Variation of maximum drag coefficient with altitude over the wavy surfaces

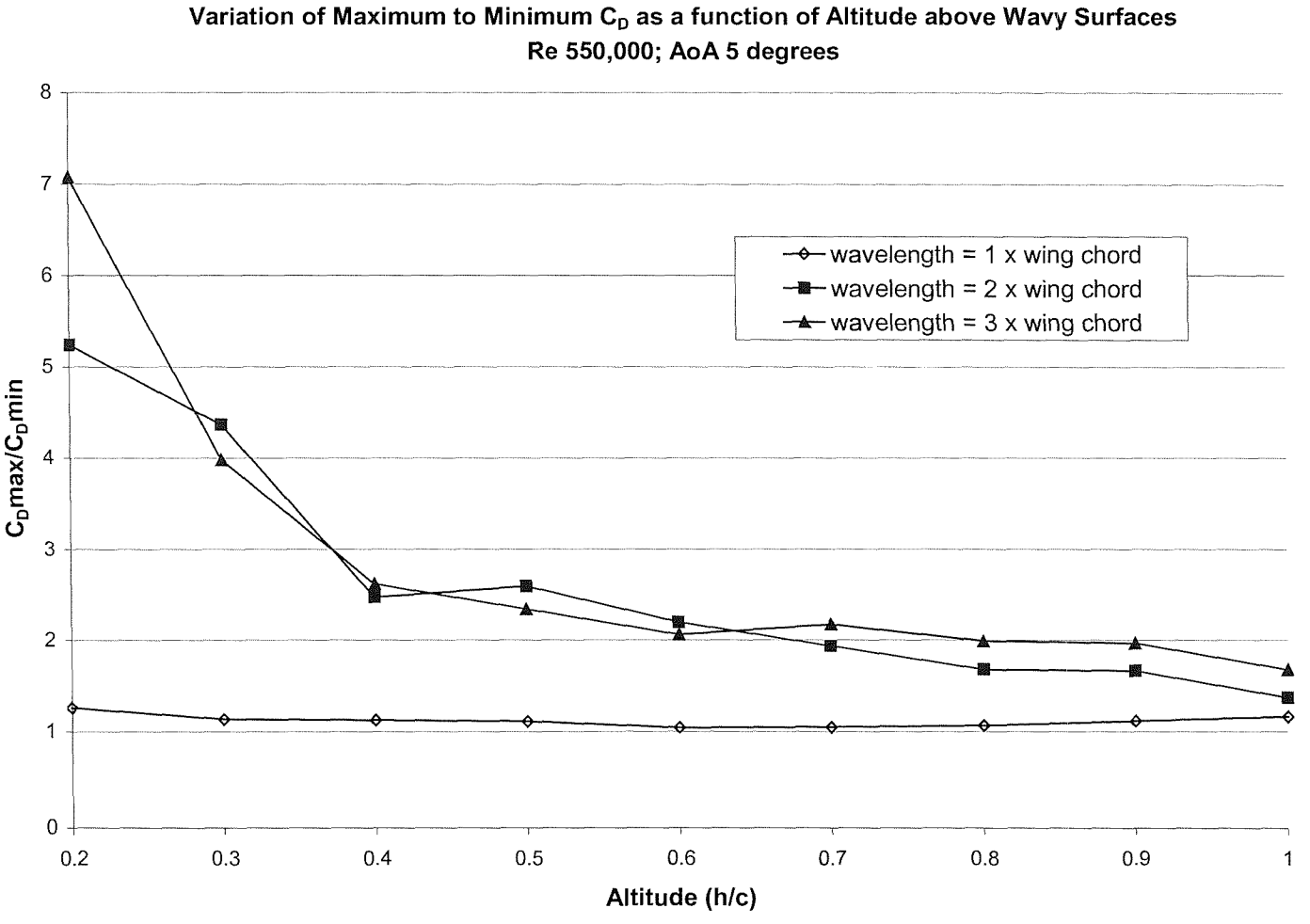

Figure 8-28: Variation of Maximum to Minimum C_D as a function of Altitude over the wavy surfaces tested

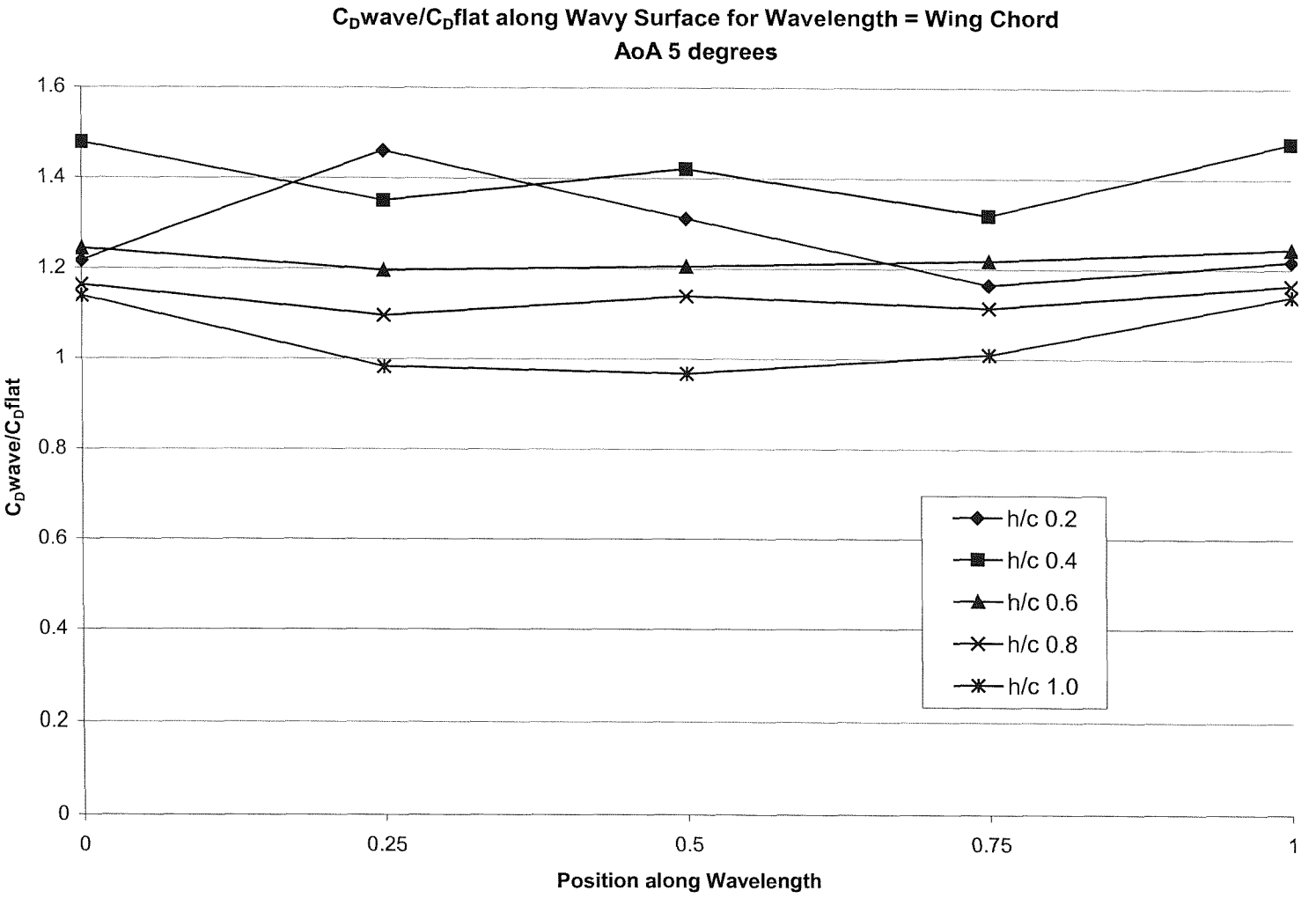

Figure 8-29: Variation in drag when operating over wavy surface compared to a flat surface (wavelength = wing chord)

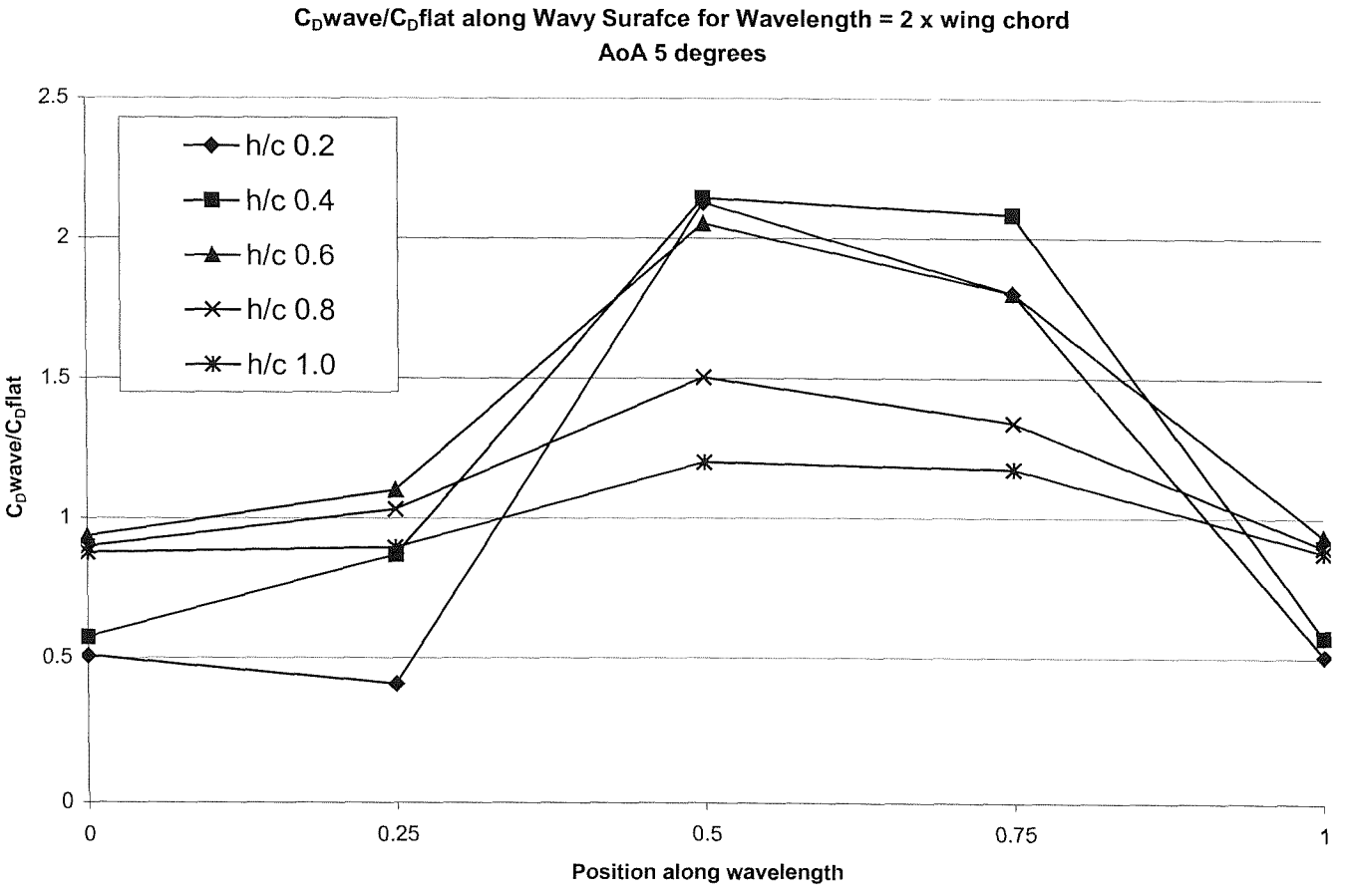

Figure 8-30: Variation in drag when operating over wavy surface compared to a flat surface (wavelength = 2 x wing chord)

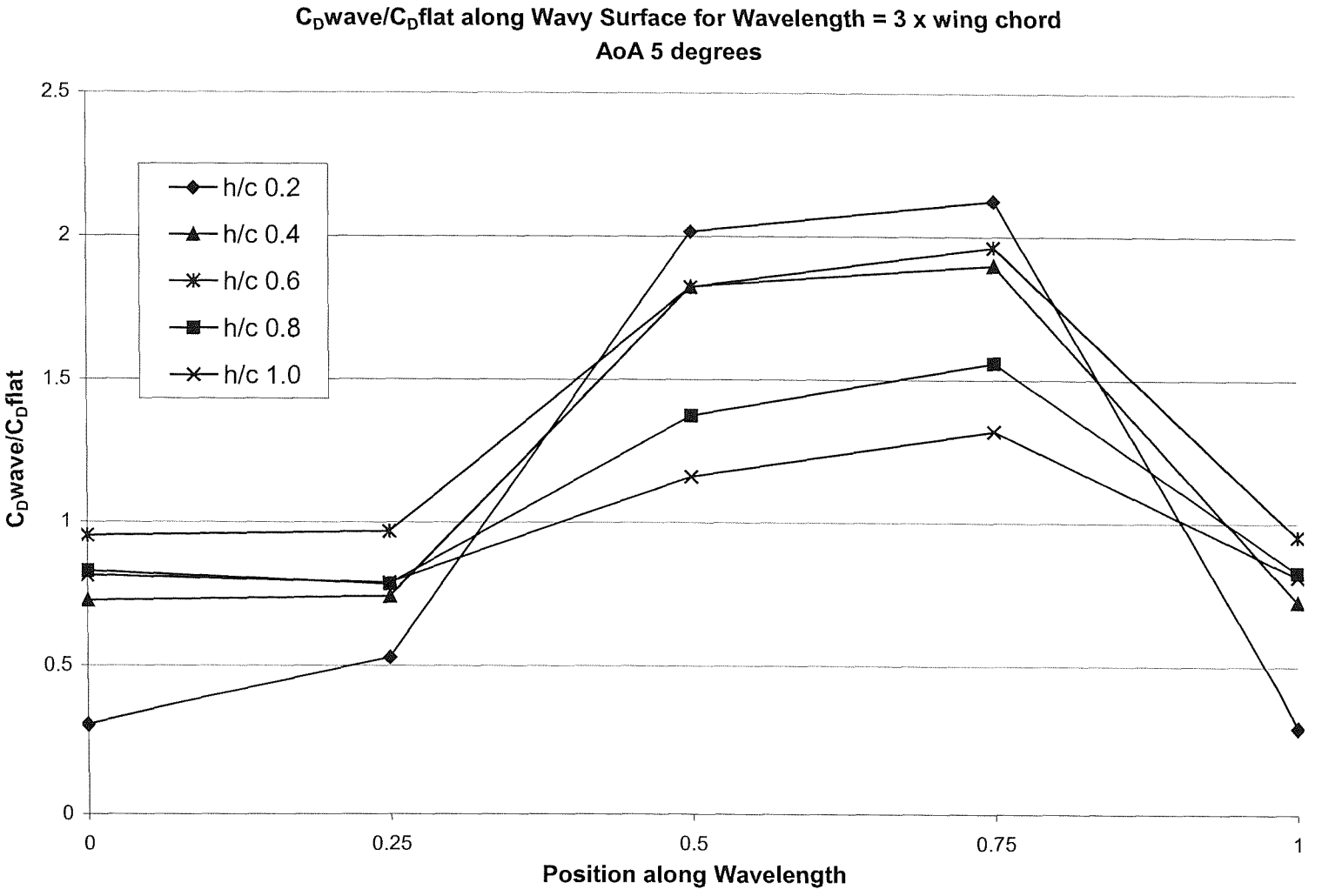

Figure 8-31: Variation in drag when operating over wavy surface compared to a flat surface (wavelength = 3 x wing chord)

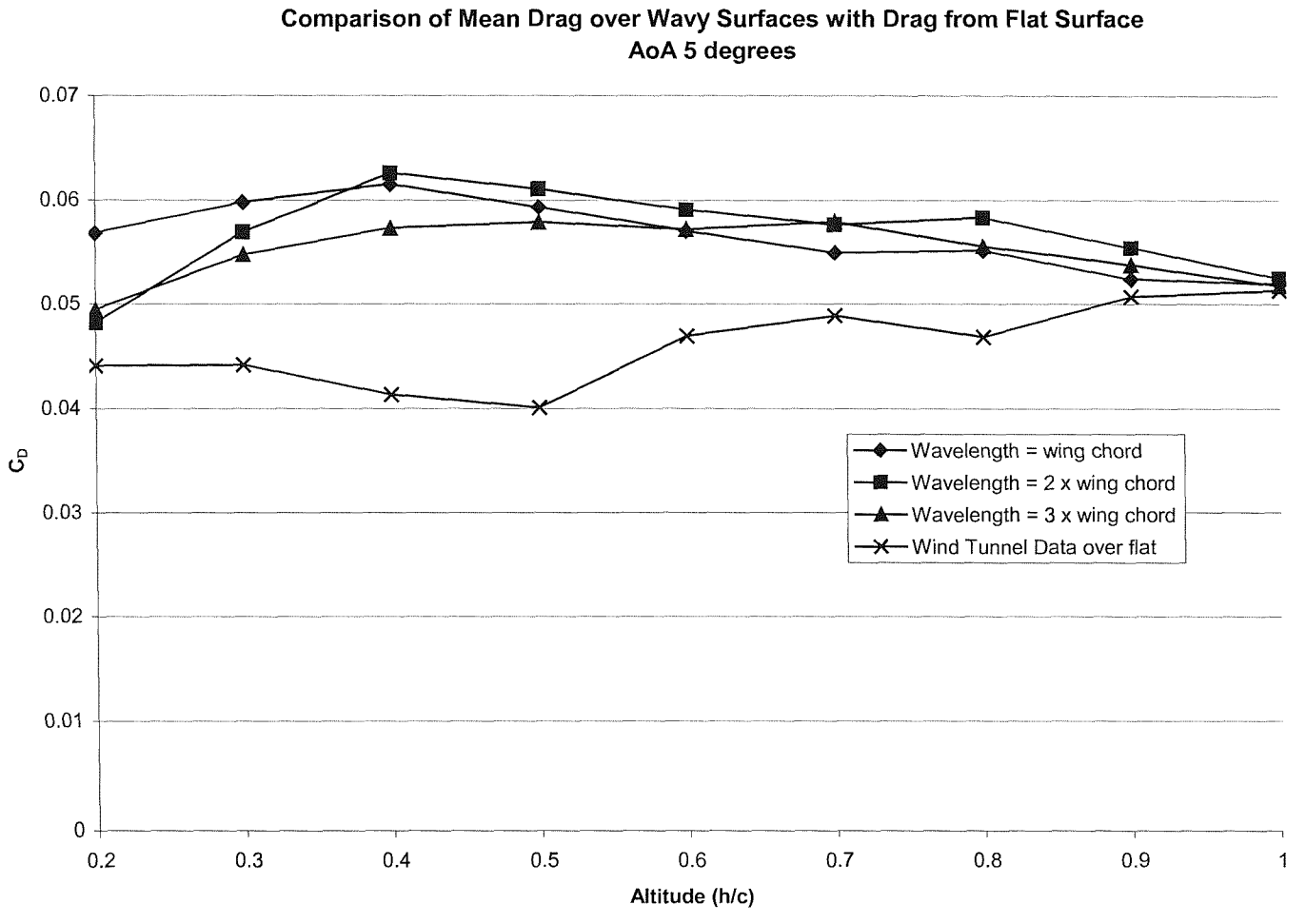

Figure 8-32: Variation of the mean drag coefficient over wavy surfaces as a function of altitude

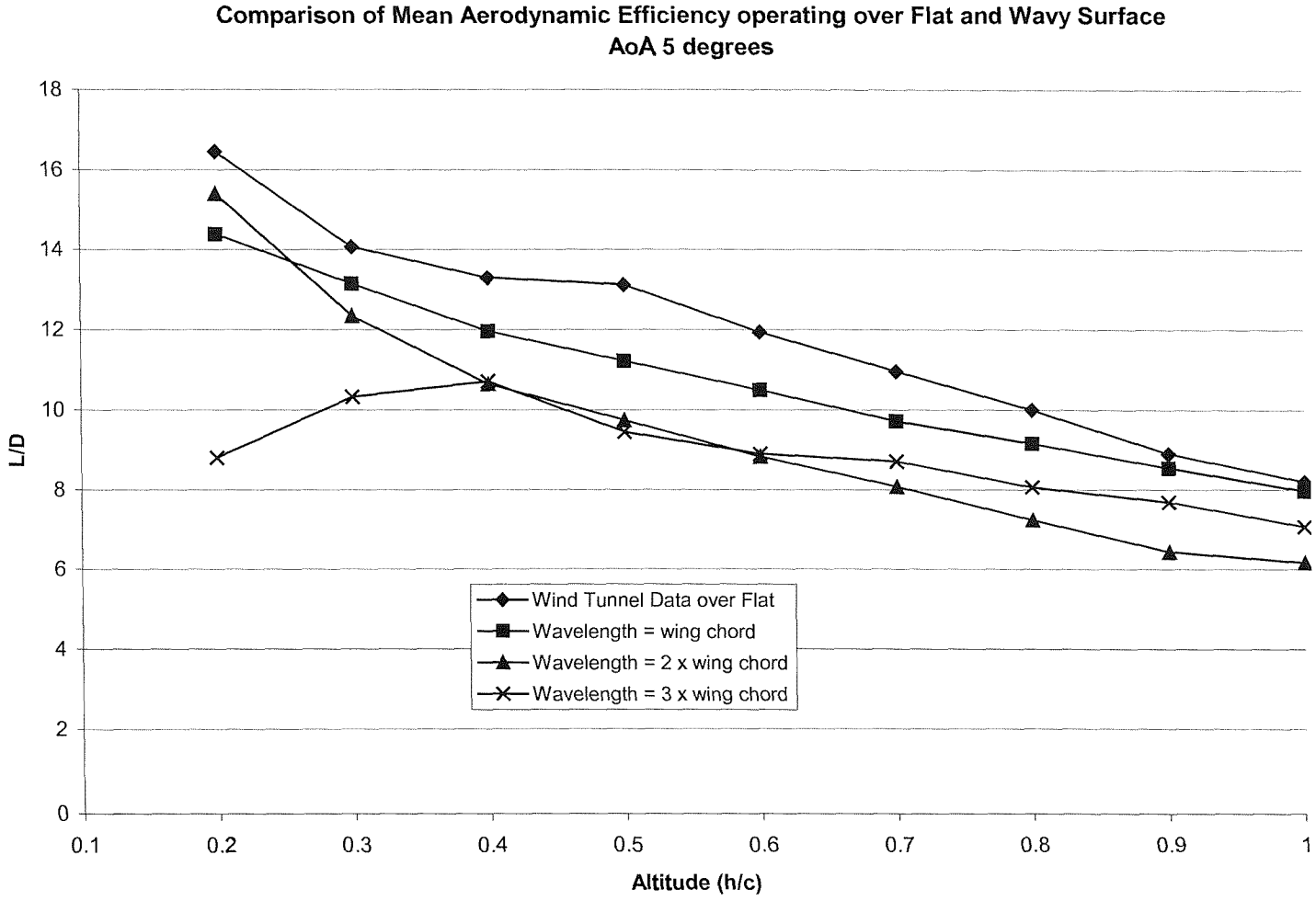

Figure 8-33: Comparison of Mean Aerodynamic Efficiency over Flat and Wavy Surfaces

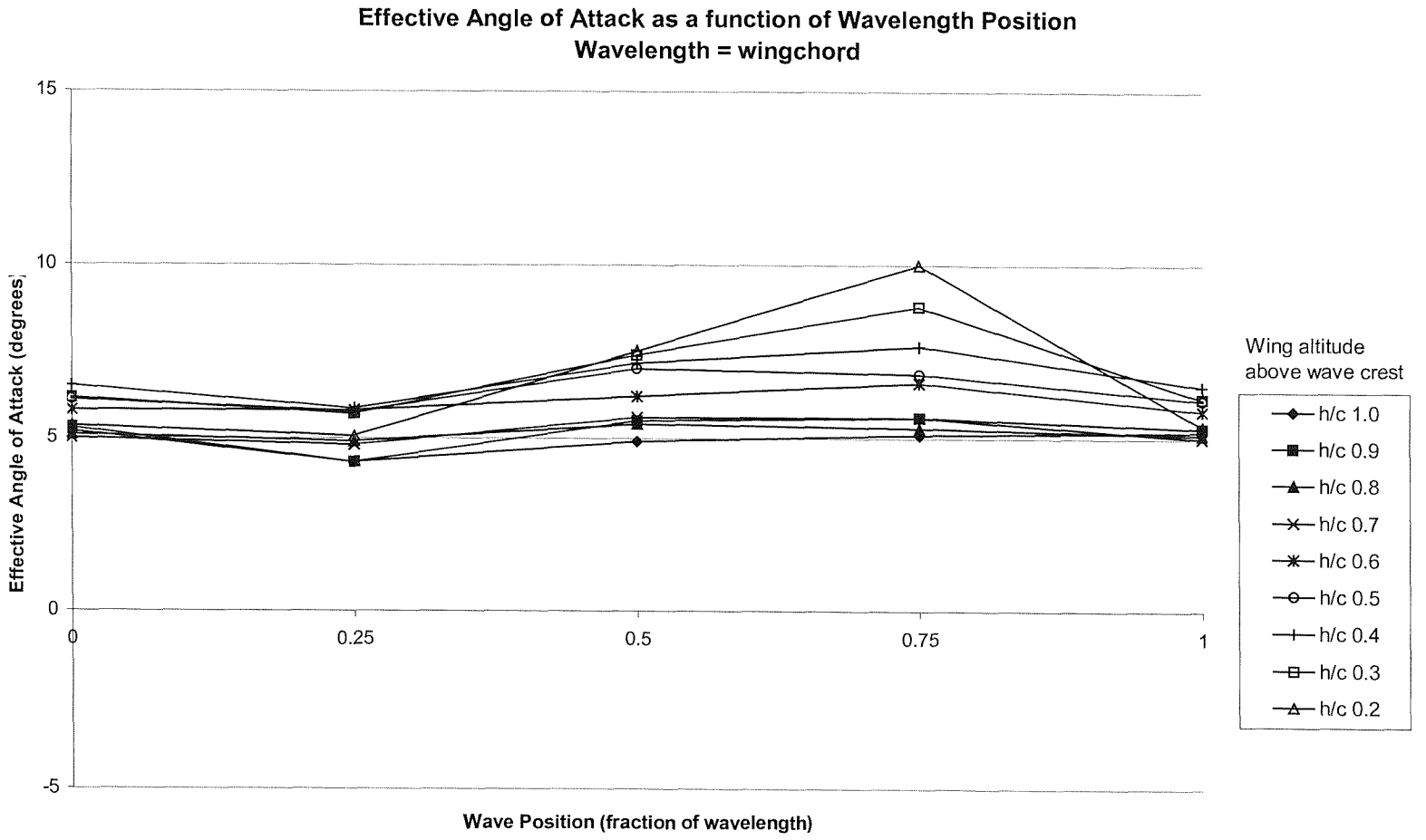

Figure 8-34: Effective Angle of Attack as a function of Wavelength Position (λ=1c)

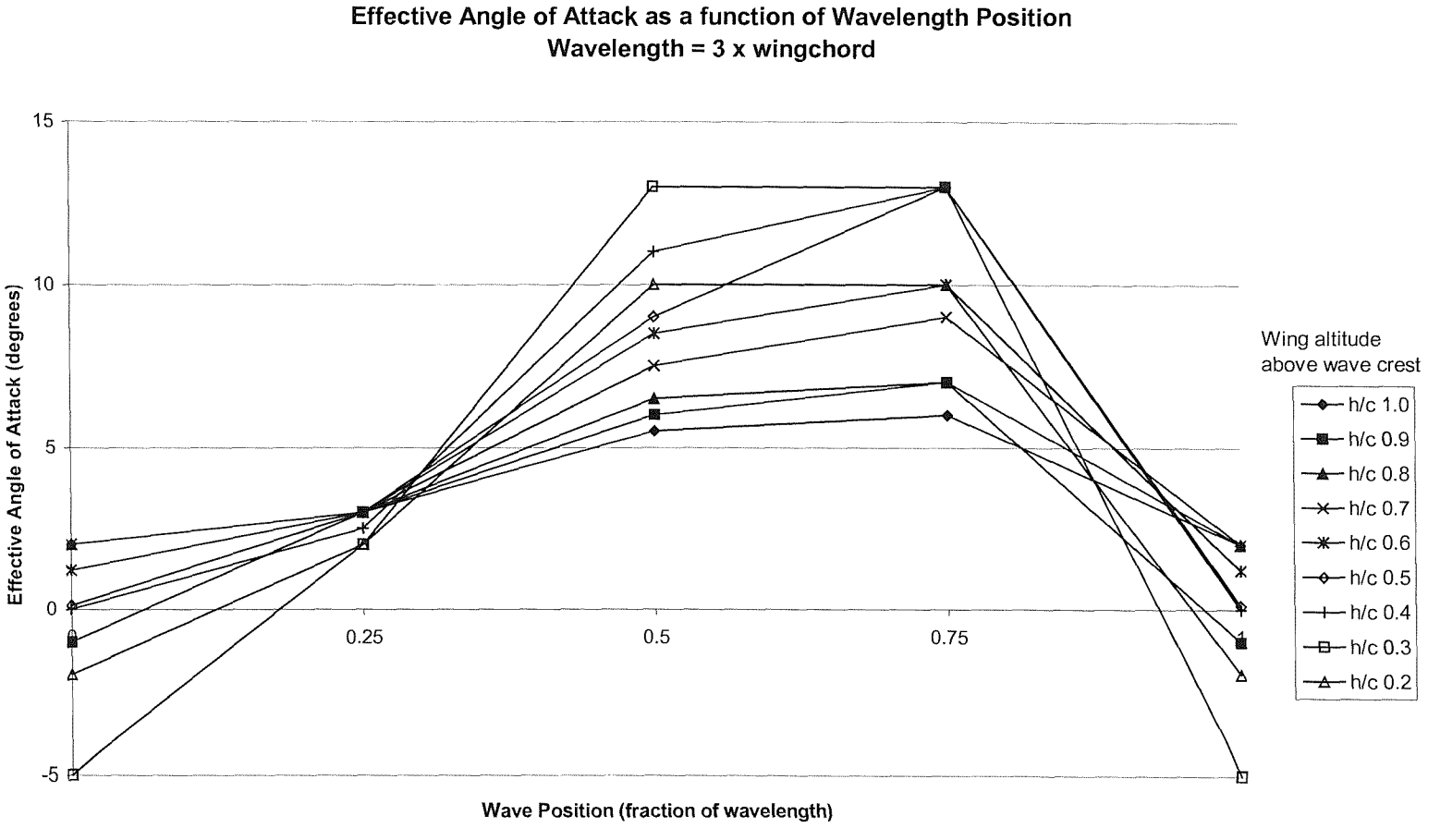

Figure 8-35: Effective Angle of Attack as a function of Wavelength Position (λ=3c)

9 Effectiveness of fitting Endplates in Ground Effect

9.1 Overview

This chapter analyses the performance issues associated with fitting endplates to aerofoils operating in ground effect at low a Reynolds Number. A series of endplates were fitted to the NACA 0012 and DHMTU 12-35.3-10.2-80.12.2 wings and the resulting lift and drag values were recorded. Of particular interest to this research is any enhancement in aerodynamic efficiency that could be obtained by employing endplates for use on the UWIGV concept.

These experiments were conducted in the same 2.1 x 1.7 m rolling road wind tunnel used in the wind tunnel trials detailed in Chapter 4. The experiments were conducted at an operating Reynolds Number of 830,000. The wings with endplates were tested at a moderate ground effect altitude of h/c 0.4. This allowed for testing the endplates throughout a range of angle of attack up to 10 degrees. Owing to the small wing-ground clearances in the extreme ground effect regime the lowest altitude that could be safely attempted was h/c 0.15.

9.2 Endplate Selection

Two distinct designs of endplate were considered:

- a rectangular set which extended above and below the aerofoil Figure 9-1(a)
- a set which only extended below the aerofoil Figure 9-1(b).

A range of sizes were tested (Table 9-1, Table 9-2, Figure 9-2 and Figure 9-3) varying in length L, depth H_d and protrusion from the section trailing (L_{TE}) and leading edges (L_{LE}) of the aerofoil. All the endplates were manufactured from aluminium and were 1 mm thick. The endplates were attached to the sides of the aerofoils by two screws and the inner faces were taped to the aerofoil in order to prevent any leakage of the airflow.

9.3 Discussion of Results

9.3.1 Effect of Endplates on Drag

Figure 9-5 and Figure 9-6 present the drag polar for the DHMTU and NACA 0012 aerofoil sections with the endplate configurations detailed above. As would be expected the larger endplates posses greater wetted area (Table 9-3) and as a result produce higher values of zero lift drag (CD_0). The values of CD_0 are presented in Table 9-5 where the small lower endplate produces the lowest zero lift drag coefficient and the large rectangular endplate the highest. If the large rectangular endplate is fitted to the DHMTU CD_0 increases by 27% of the aerofoils original value compared to 4% for the small lower endplate (Table 9-6). The same trends in CD_0 are evident when endplates are fitted to the NACA 0012. The increase in drag as a result of fitting endplates is greater for the NACA 0012 as the basic section possesses a smaller CD_0 value.

The effectiveness of the different endplate configurations in reducing the overall drag of the wing sections is shown in Figure 9-5 and Figure 9-6. It can be seen that the drag polar curves of the aerofoils fitted with endplates at some point crosses the drag polar of the aerofoil sections with no endplates. Below this crossover point the endplates result in the generation of greater drag than the basic aerofoil. After this crossover point the reduction in vortex drag and increase in lift produced by the endplates results in the same lift being developed for less drag than produced by the basic aerofoil. In this region the effectiveness of the endplates outweighs their penalty in parasitic drag. The lift coefficients and angles of attack that the endplates become effective from are given in Table 9-7 for the DHMTU and Table 9-8 for the NACA 0012.

The lift coefficients that drag reduction were achieved at varied between 0.35 to 0.60 CL_{max} of the basic DHMTU aerofoil. This value depends on the size and geometry of the endplate fitted. The large lower endplate produces a reduction in overall drag at the lowest lift coefficient (0.35 CL_{max}). As a result of the high parasitic drag of the large rectangular endplate it does not result in a reduction of drag until a much higher lift coefficient of 0.60 CL_{max}.

The optimum angle of attack to achieve maximum aerodynamic efficiency for the DHMTU aerofoil is 5 degrees (Figure 9-7) and 7 degrees for the NACA 0012 (Figure 9-8). The data indicated that the large rectangular endplate produced its highest aerodynamic efficiency 1 degree above the other endplate configurations. This trend was present on both the DHMTU and NACA 0012 wing sections (Table 9-9). Referring to Table 9-7 and Table 9-8 it can be seen that all four endplates tested will start to reduce drag below the optimum cruising angle of attack for both wings.

Table 9-10 presents the overall drag coefficients at the optimum angle of attack for maximum aerodynamic efficiency for both the DHMTU and NACA 0012 aerofoils. The rectangular endplates result in a large increase in drag when attached to both the wings. The lower endplates result in a much smaller increase in drag at the optimum angle of attack. This is attributable to their smaller wetted area (Table 9-3) as discussed earlier.

The effective aspect ratio (see Chapter 5) of the DHMTU and NACA 0012 due to the addition of endplates are presented in Table 9-11, ranked in decreasing order of effectiveness. The large rectangular endplate provides the greatest blockage (Table 9-4) of the wing tip flow and hence the highest effective aspect ratio. The small lower endplate with the least blockage area was the least effective.

9.3.2 Effect of Endplates on Lift

Fitting endplates increases the lift and the gradient of the lift curve slope of both the DHMTU (Figure 9-9) and NACA 0012 (Figure 9-10) sections. Table 9-12 details the lift coefficient and percentage increase in lift over the basic wing sections as a result of fitting endplates. The endplates with the largest blockage area produced the greatest increase in lift with the smaller endplates producing the least. The data shows that the percentage increase in lift as a result of the endplates was nearly identical for both wings. The large rectangular endplates produced a 20% increase in lift, the highest out of all the endplates tested. In contrast the small lower endplates resulted in a 6% increase in lift, the smallest increase for any of the endplate configurations. This behaviour was mirrored in the increase of the lift curve slope gradient over the basic wings. The large

rectangular endplates resulted in the largest increase in the lift curve slope and the small rectangular endplates the least. Table 9-13 presents the values of the lift curve slope gradient in descending order of increase.

As can be seen from Figure 9-9 fitting endplates increases the maximum lift coefficient and a consequent reduction in stalling speed. A drawback of this is that the stalling angle will occur at a lower angle of attack. This is shown inTable 9-14 for the DHMTU aerofoil where the larger endplates produce the highest increase in C_{Lmax} resulting in the stalling angle being reduced by 1 degree.

The aerodynamic efficiencies of the wings fitted with the various endplates are shown in Table 9-15. It can be seen that the NACA 0012 possesses higher L/D ratios than the DHMTU as a result of lower values of drag (Table9-10). The large lower endplates produce the greatest increase in aerodynamic efficiency on both wings (Figure 9-4) with the small rectangular endplates being the most inefficient.

This data indicates that endplates that only extend below the aerofoil are more effective than the rectangular endplates that block the flow over the upper and lower surfaces. This is a result of the extra drag incurred due to their greater wetted area. The greater lift resulting due to an increase in blockage area is not sufficient enough to compensate for the increase in drag that results.

Due to the small ground clearance at h/c 0.15 only the small lower endplates could be fitted in extreme ground effect. The endplates become effective at the same lift coefficient (C_L=0.4) as at the moderate ground effect altitude of h/c 0.4 (Figure 9-11). In this flight regime the endplates produced over twice the aerodynamic efficiency compared to operating at a moderate ground effect altitude of h/c 0.4 (Table 9-16). This is due to the greater increase in lift encountered due to the ram air under the section (Figure 9-12). The increase in drag as a result of fitting endplates is nearly the same as for operating at h/c 0.4.

Flow visualisation experiments provide a good illustration of the effectiveness of the endplates. When the DHMTU is fitted with the large rectangular endplates it can be seen that strut vortex is flowing straight backwards (Figure 9-13b). This

makes an interesting comparison when no endplate is fitted (Figure9-13a) where the strut vortex is deflected inwards by the wing tip vortex. This illustrates the efficiency with which the large rectangular endplate reduces the lateral airflow around the wing. Figure 9-14 shows that a reduction in the size of the endplate resulted in the strut vortex being deflected away from the wingtip.

9.4 Pressure Profiling

A series of rectangular endplates (Table 9-17 and Figure 9-15) were fitted to a DHMTU pressure tapped section to investigate the resultant pressure profiles. All the endplates posses the same heights but are different in length. All the endplates extend past the DHMTU leading and trailing edge as a result of the attachment method. This consisted of small clamping plates located at the leading and trailing edges to hold the endplates in place.

Figure 9-16 and Figure 9-17 illustrate the position of the tappings and their identifying number. The associated tubes that prevented lower endplates being attached can clearly be seen. The row of tappings is located 20 mm from the DHMTU wingtip. As a result of the pressure tubes exiting the end of the wing near the pressure tappets only rectangular endplates could be fitted for pressure profiling measurements.

To investigate the efficacy of fitting endplates it is worth comparing the pressure profiles at the midspan of the DHMTU with those near the wingtip for various altitudes with no endplates fitted. Due to the spanwise component of flow, suction is present on the lower surface at the wingtip for the majority of the DHMTU chord. This occurs when the wing is in and out of ground effect as illustrated in Figure 9-18. This is in distinct contrast to the pressure that is recorded at the midspan of the DHMTU. The magnitude of the suction on the lower surface near the wingtip is increasing as the altitude decreases from h/c 2.9 to 0.2. There is a significant increase in suction when the wingtip lower surface is at an altitude of h/c 0.2 compared to that present at moderate ground effect altitudes (h/c 0.3 to 1.0).

In extreme ground effect (h/c<0.1) the difference in pressure between the midspan and wingtip is even more significant. Figure 9-19 shows the pressure profiles when the DHMTU is OGE and in extreme ground effect. The reader should note that the data presented in Figure 9-19 is for an angle of attack of 3 degrees, as this is the highest angle that could be realised at an altitude of h/c 0.08. It is noticeable that the large increases in pressure recorded at midspan are not reflected by such large increases in suction near the wingtip with changes in altitude.

On the upper surface of the DHMTU the suction at midspan is greater over the frontal half of the DHMTU compared to that present at the wingtip (Figure9-20). The midspan pressure profile shows that there is pressure present near the trailing edge. Compare this to the wingtip where suction is present along the whole chord length and a large reduction in suction is not seen. There is a greater increase in suction at the midspan than the wingtip as altitude reduces. This mirrors the behaviour seen on the lower surface where greater changes in pressure with decreasing altitude are observed at midspan and not near the wingtip.

As the altitude decreases the difference in pressures between the centre span and wing tip increases (Figure 9-18). This means that as the altitude of the DHMTU decreases the magnitude of the wingtip loss due to lateral flow increases. This indicates that fitting endplates will provide a greater degree of benefit at low altitudes.

The pressure profile data illustrates that fitting endplates increases the pressure on the wingtip lower surface when the DHMTU is in and out of ground effect. When the DHMTU is out of ground effect (h/c 2.9) fitting endplates has resulted in an increase in pressure near the wingtip over the rear of the lower surface only (Figure 9-21). At this altitude there is little effect on the pressure on the lower surface at mid span. The increase in pressure due to endplates is more noticeable when the DHMTU is at the moderate ground effect altitude of h/c 0. 9 (Figure 9-22). At this altitude a noticeable increase in pressure on the wingtip lower surface results. Compared to OGE operation the increase in pressure near

the wingtip occurs over the whole length of the chord. As when the DHMTU was OGE there is very little increase in pressure at mid span due to the endplates at this altitude. The increase in pressure under the midspan of the DHMTU aerofoil as a result of fitting endplates is not significant until the altitude is h/c 0.4 (Figure 9-23). When the DHMTU is operating at very low altitudes (h/c 0.2) the fitting of endplates can significantly increase the pressure under the centrespan and wingtip (Figure 9-24).

The addition of endplates increases the upper surface wingtip suction even when the section is out of ground effect (Figure 9-25). The addition of endplates has a negligible effect on the mid span pressure distribution on the upper surface of the DHMTU at all altitudes. This can be seen even when the DHMTU is at an altitude of h/c 0.2 as shown in Figure 9-26.

No improvement in performance is obtained by increasing the length of the endplates from either the trailing or leading edge. This is shown in Figure 9-27 for an altitude of h/c 0.4. The extra wetted area as a result of extending endplate length just increases the parasitic drag and has no effect on blocking the wingtip lateral flow.

9.5 Summary

1. Endplates are not effective at low lift coefficients as a result of their parasitic drag. An angle of attack is reached where the vortex drag reduction as a result of fitting endplates outweighs the penalty incurred in parasitic drag. It was found that for the DHMTU aerofoil endplate effectiveness occurred from $0.35C_{Lmax}$ to $0.60C_{Lmax}$ dependent upon endplate size and geometry. The large lower endplate configuration became effective from 0.35 C_{Lmax} compared to the large rectangular endplate that did not become effective until 0.60 C_{Lmax}.

2. All the endplates tested increased the wing lift, maximum lift coefficient and the gradient of the lift curve slope. The large rectangular endplates increased

the DHMTU's lift by 20% above that of the basic wing. This can be compared to the small lower endplates that increased the lift by 6%.

3. The lower endplate configurations produced the highest increase in aerodynamic efficiency. A 7% increase in L/D is produced when the large lower endplates are fitted. The small lower endplates produce a 3% increase in L/D compared with the large rectangular endplates that produced an increase of 2%. This research has shown that it is best to employ endplates that extend only below the aerofoil lower surface.

4. There is no real benefit in fitting small rectangular endplates, as the increase in lift produced is cancelled by the resultant drag increase at the optimum angle of attack for the DHMTU. The large rectangular endplates have produced the greatest increase in lift due their large surface area, which provides the greatest blockage of lateral circulation around the wingtip. The results indicate that though the rectangular endplate configuration produces respectable increases in section lift the drag penalty associated with them is so great rendering them not very practical.

5. The addition of endplates to the DHMTU aerofoil increases the pressure on the lower and suction on the upper surface at the wingtip when operating both in and out of ground effect. At the midspan of the DHMTU the pressure on the lower surface is unaffected by fitting endplates when out of ground effect. The change in suction on the upper surface at the midspan location as a result of fitting endplates is negligible at all altitudes. As the DHMTU enters moderate ground effect ($h/c<1.0$) the effect of endplates on the wingtip lower surface pressure becomes increasingly evident. Thought the increase in pressure on the lower surface midspan is not significant until the altitude has reduced to h/c 0.4.

6. No improvement in the pressure distribution at the wingtip is achieved as a result of increasing the length of the endplates past the leading or trailing edge of the DHMTU.

Configuration	L	L_{LE}	L_{TE}	H_d
Small rectangular	1.2c (380 mm)	0.1c (32 mm)	0.1c (32 mm)	0.2c (70 mm)
Large rectangular	1.2c (380 mm)	0.1c (32 mm)	0.1c (32 mm)	0.4c (140 mm)
Large lower	1c (317 mm)	N/A	N/A	0.26c (89 mm)
Small lower	1c (317 mm)	N/A	N/A	0.17c (54 mm)

Table 9-1: NACA 0012 Endplate Dimensions

Configuration	L	L_{LE}	L_{TE}	H_d
Small rectangular	1.2c (380 mm)	0.1 c (31 mm)	0.1 c (31 mm)	0.2 c (70 mm)
Large rectangular	(1.2 c) 380 mm	0.1 c (31 mm)	0.1 c (31 mm)	0.4 c (140 mm)
Large lower	1 c (319 mm)	N/A	N/A	0.28 c (90 mm)
Small lower	1 c (319 mm)	N/A	N/A	0.17 c (55 mm)

Table 9-2: DHMTU Endplate Dimensions

	Wetted Area (mm^2)	
Configuration	DHMTU	NACA 0012
Small rectangular	44,700	45,282
Large rectangular	98,040	98,622
Large lower	41,828	45,162
Small lower	15,764	22,902

Table 9-3: Endplate Wetted Areas

	Blockage Area (mm^2)	
Configuration	DHMTU	NACA 0012
Small rectangular	16,800	17,782
Large rectangular	43,800	44,382
Large lower	15,836	17,781
Small lower	2,838	6,686

Table 9-4: Endplate blockage areas

	Zero Lift Drag Coefficient CD_0	
Endplate Configuration	**NACA 0012**	**DHMTU**
No endplate	0.0169	0.0233
Small Lower	0.0185	0.0242
Medium Lower	0.0196	0.0252
Small rectangular	0.0197	0.0261
Large rectangular	0.0229	0.0296

Table 9-5: CD_0 for endplates on NACA 0012 and DHMTU at h/c 0.4

	Increase in CD_0 over basic aerofoil	
Endplate Configuration	**NACA 0012**	**DHMTU**
Small Lower	10%	4%
Large Lower	16%	8%
Small rectangular	17%	12%
Large rectangular	36%	27%

Table 9-6: Increase in CD_0 for NACA 0012 and DHMTU at h/c 0.4 as a result of fitting endplates

	DHMTU Endplate Drag Reduction Effectiveness		
Endplate Configuration	C_L*	C_{Lmax}**	Angle of Attack* (degrees)
Large Lower	0.36	0.35	2.2
Small Lower	0.46	0.45	3.5
Small rectangular	0.59	0.58	4.2
Large rectangular	0.61	0.60	4.2

Table 9-7: Lift coefficients and angle of attack for the DHMTU aerofoil that endplates start to become effective

*At which endplates become effective
**Fraction of maximum lift coefficient at which endplates become effective

	NACA 0012 Endplate Drag Reduction Effectiveness	
Endplate Configuration	C_L*	Angle of Attack* (degrees)
Large Lower	0.40	5.0
Small Lower	0.46	5.6
Small rectangular	0.59	7.0
Large rectangular	0.54	6.0

Table 9-8: Lift coefficients and angle of attack for the NACA 0012 aerofoil that endplates start to become effective

*At which endplates become effective

	Optimum angle of attack (degrees)	
Endplate Configuration	DHMTU	NACA 0012
Large Lower	5	7
Small Lower	5	7
Small rectangular	5	7
Large rectangular	6	8
No endplates	5	7

Table 9-9: Optimum angle of attack for maximum aerodynamic efficiency with endplates fitted

	DHMTU (AoA 5°)		NACA 0012 (AoA 7°)	
	C_D	C_D Increase	C_D	C_D increase
With large rectangular endplates	0.0576	18%	0.0500	15%
With small rectangular endplates	0.0554	14%	0.0478	10%
With large lower endplates	0.0528	8%	0.0467	7%
With small lower endplates	0.0504	3%	0.0451	3%
Aerofoil alone	0.0488	N/A	0.0436	N/A

Table 9-10: Drag coefficients of wing-endplate combinations at h/c 0.4 for optimum angle of attack

	Effective Aspect Ratio (Ae)	
Endplate Configuration	**NACA 0012**	**DHMTU**
Large rectangular	5.40	6.22
Large Lower	4.94	5.61
Small rectangular	4.35	5.08
Small Lower	4.28	4.81
No endplate	3.79	4.50

Table 9-11: Effective Aspect Ratios for endplates on NACA 0012 and DHMTU at h/c 0.4

	DHMTU (AoA 5°)		**NACA 0012 (AoA 7°)**	
	C_L	C_L increase	C_L	C_L increase
With large rectangular endplates	0.709	20%	0.640	19%
With large lower endplates	0.680	15%	0.613	14%
With small rectangular endplates	0.667	13%	0.588	9%
With small lower endplates	0.625	6%	0.569	6%
Aerofoil alone	0.589	N/A	0.538	N/A

Table 9-12: Lift coefficients and increase in lift for tested aerofoils with endplates at h/c 0.4

	Lift curve slope gradient ($dC_L/d\alpha$) per radian	
Configuration	DHMTU	NACA 0012
Large rectangular endplate	5.3	5.6
Large lower endplate	5.1	5.4
Small rectangular endplate	4.9	4.9
Small lower endplate	4.7	4.8
No endplate	4.5	4.6

Table 9-13: Variation in lift curve slope gradient with endplates

Configuration	C_{Lmax}	Stall Angle of Attack (degrees)
Large rectangular endplate	1.09	10
Large lower endplate	1.06	10
Small rectangular endplate	1.04	10
Small lower endplate	1.03	11
No endplate	1.02	11

Table 9-14: Maximum lift coefficient and stalling angle for DHMTU aerofoil at h/c 0.4 with and without endplates

	Aerodynamic Efficiency(L/D)	
	DHMTU (AoA 5°)	NACA 0012 (AoA 7°)
With large lower endplates	12.88	13.12
With large rectangular endplates	12.31	12.93
With small lower endplates	12.41	12.62
With small rectangular endplates	12.04	12.29
Aerofoil alone	12.06	12.33

Table 9-15: Aerodynamic efficiency at h/c 0.4

Altitude (h/c)	Lift Improvement (%)	Drag Increase (%)	L/D Increase (%)
0.4	6	3	3
0.15	9	2	7

Table 9-16: Comparison of small lower endplate performance at h/c 0.4 and h/c 0.15

Configuration	L	L_{LE}	L_{TE}	H
Endplate A	1.1 c (350 mm)	0.02 c (5 mm)	0.08 c (26 mm)	0.22 c (70 mm)
Endplate B	1.3 c (410 mm)	0.12 c (38 mm)	0.17 c (53 mm)	0.22 c (70 mm)
Endplate C	1.4 c (445 mm)	0.12 c (38 mm)	0.28 c (88 mm)	0.22 c (70 mm)

Table 9-17: DHMTU Endplate Dimensions used in pressure tapping experiments

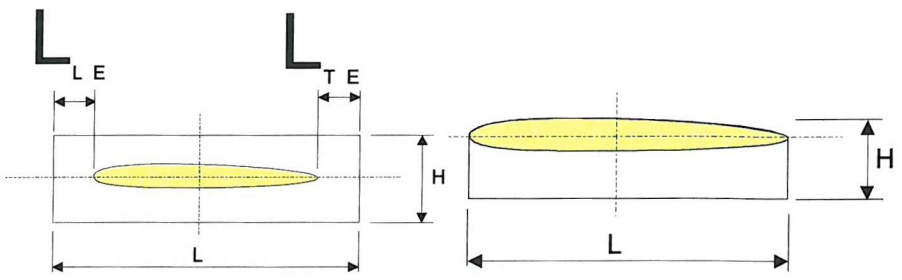

Figure 9-1: Endplate Configurations (a) rectangular set (b) lower set

Figure 9-2: NACA 0012 Endplate Selection

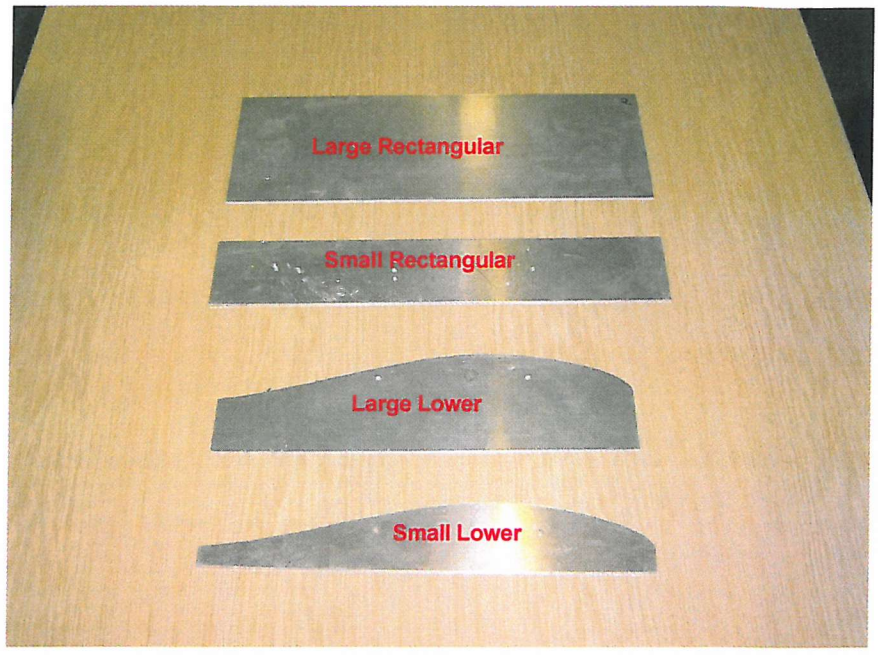

Figure 9-3: DHMTU Endplate Selection

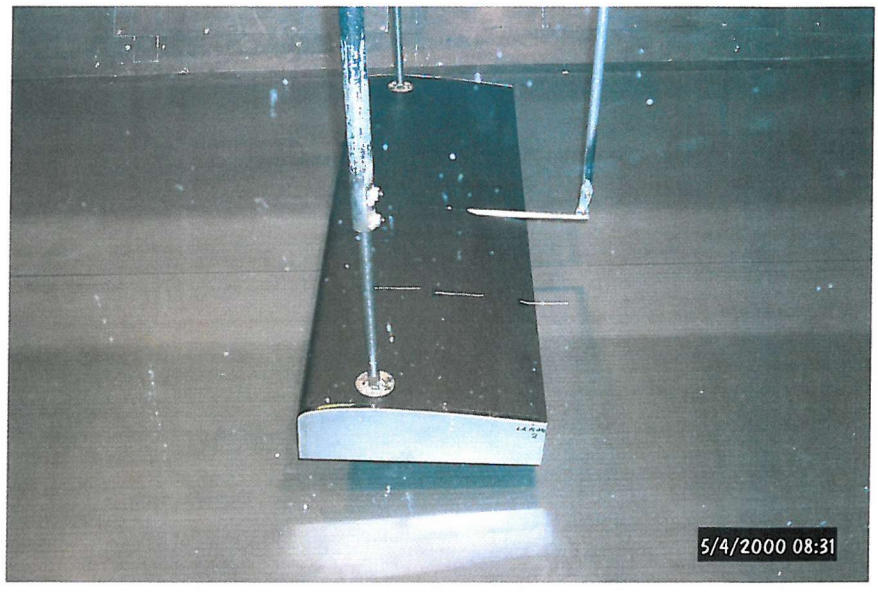

Figure 9-4: Large lower endplates fitted to the DHMTU, these produced the highest increase in L/D out of the tested endplates in moderate ground effect (h/c 0.4)

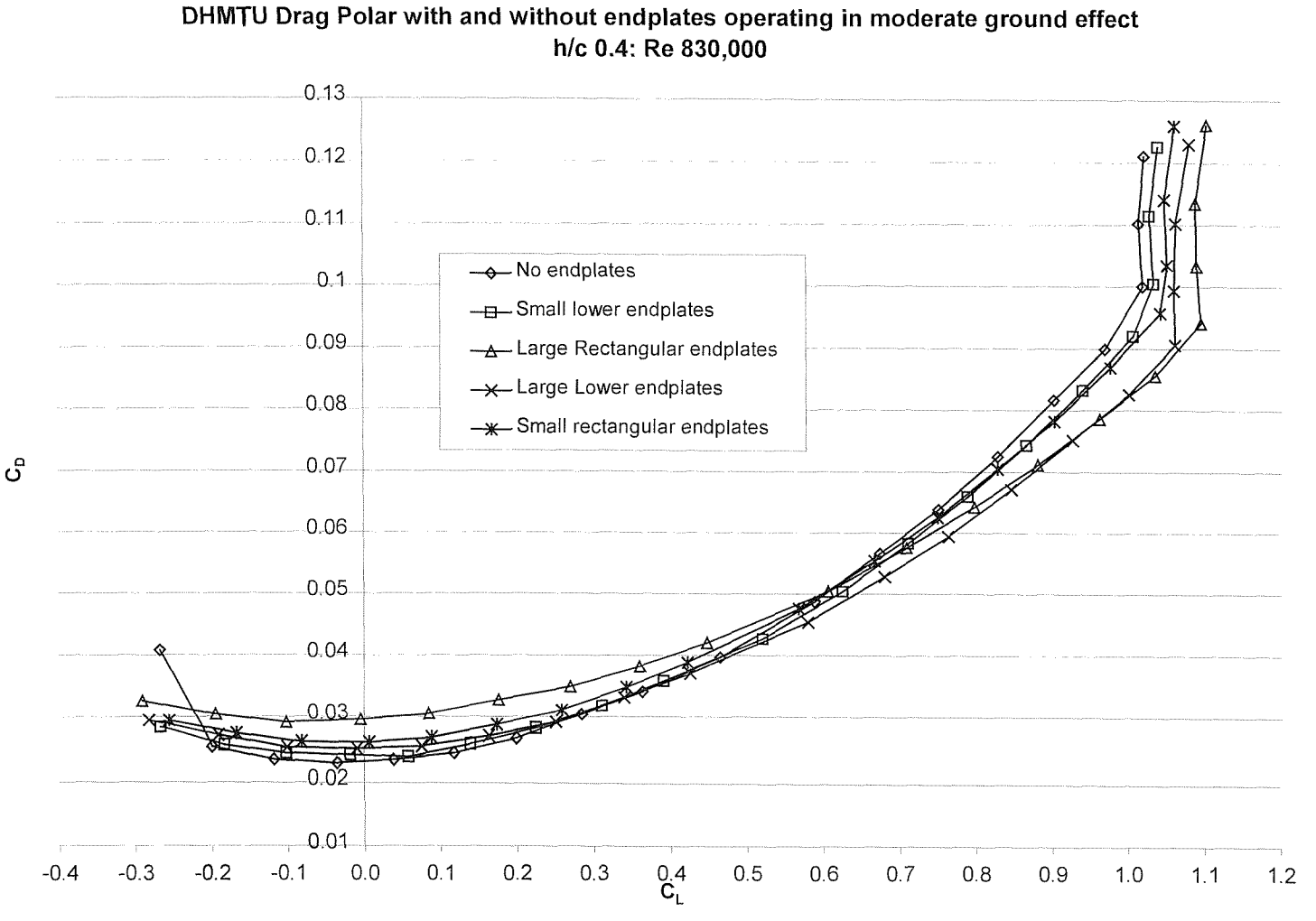

Figure 9-5: Drag polar of DHMTU aerofoil operating in moderate ground effect (h/c 0.4) with and without endplates

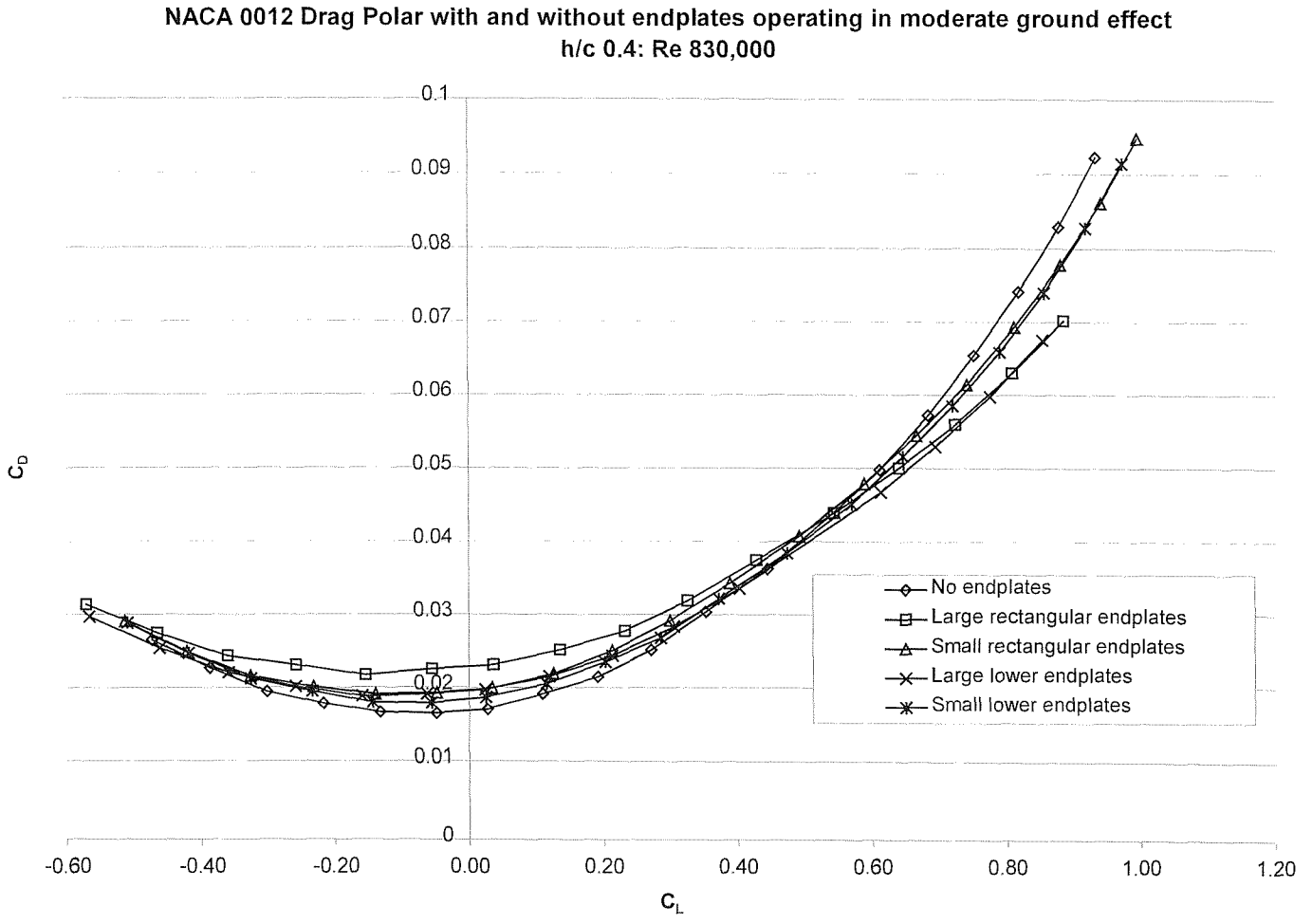

Figure 9-6: Drag polar of NACA 0012 aerofoil operating in moderate ground effect (h/c 0.4) with and without endplates

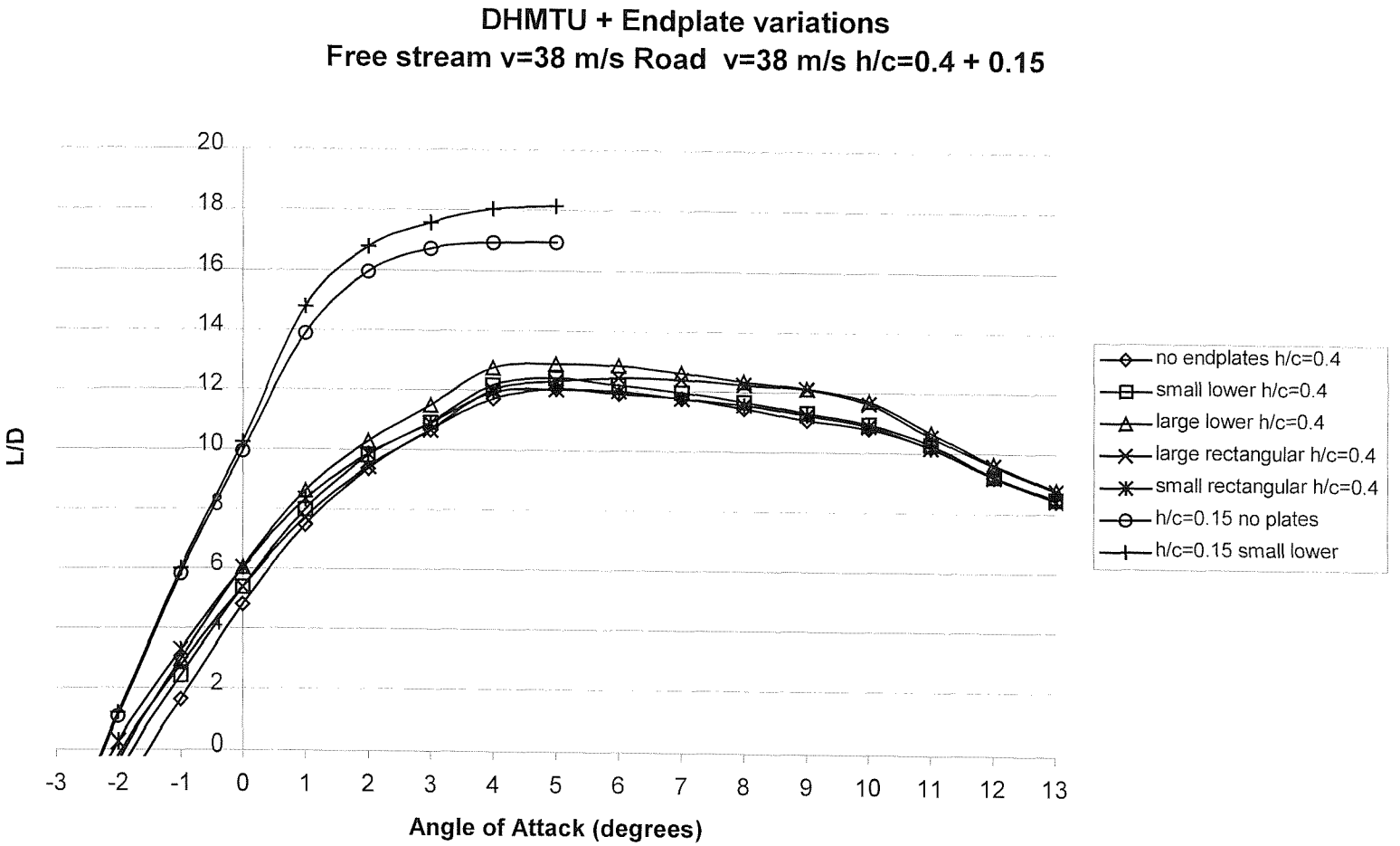

Figure 9-7: Aerodynamic efficiency of DHMTU with various endplate configurations

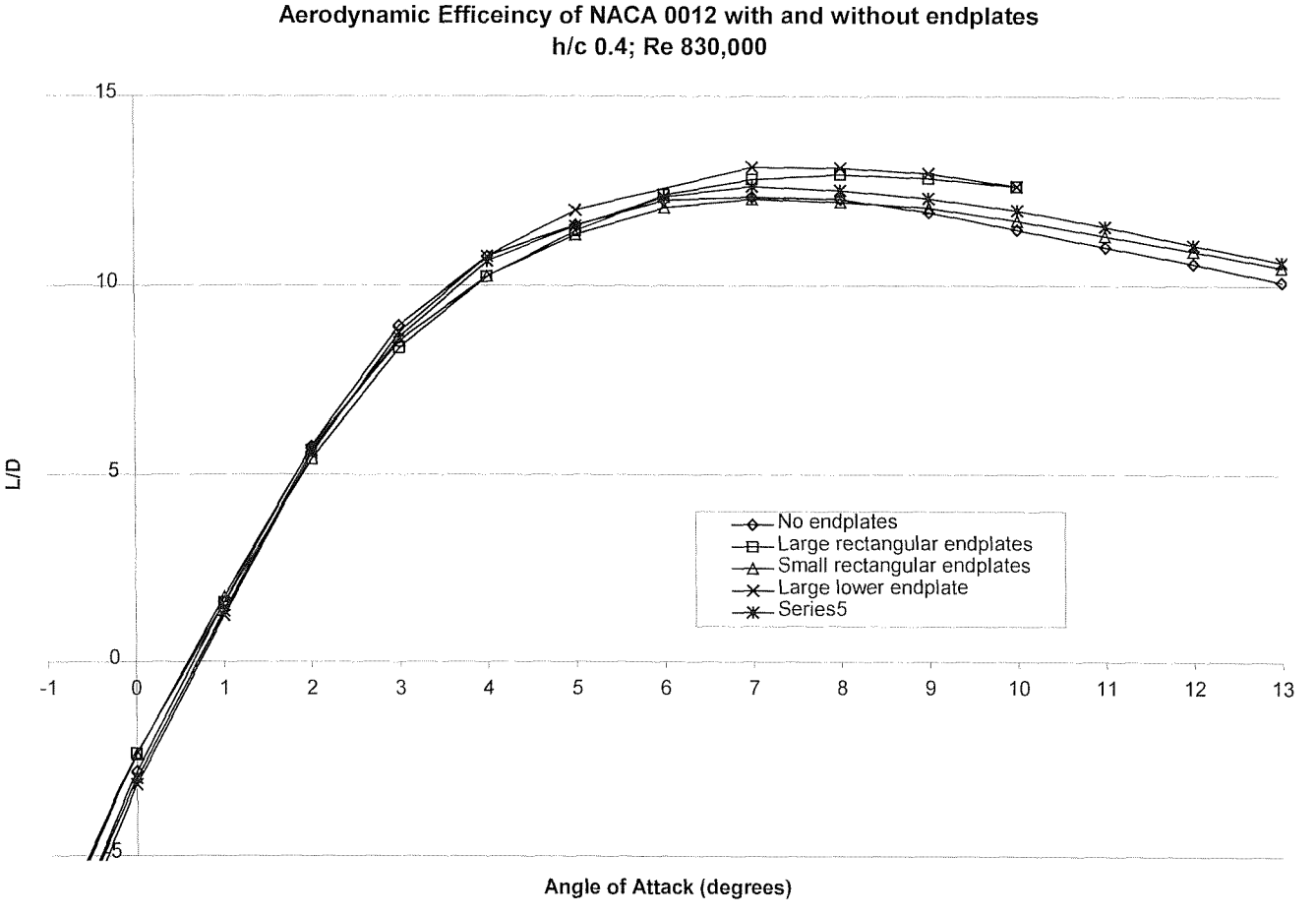

Figure 9-8: Aerodynamic efficiency of NACA 0012 with various endplate configurations h/c 0.4

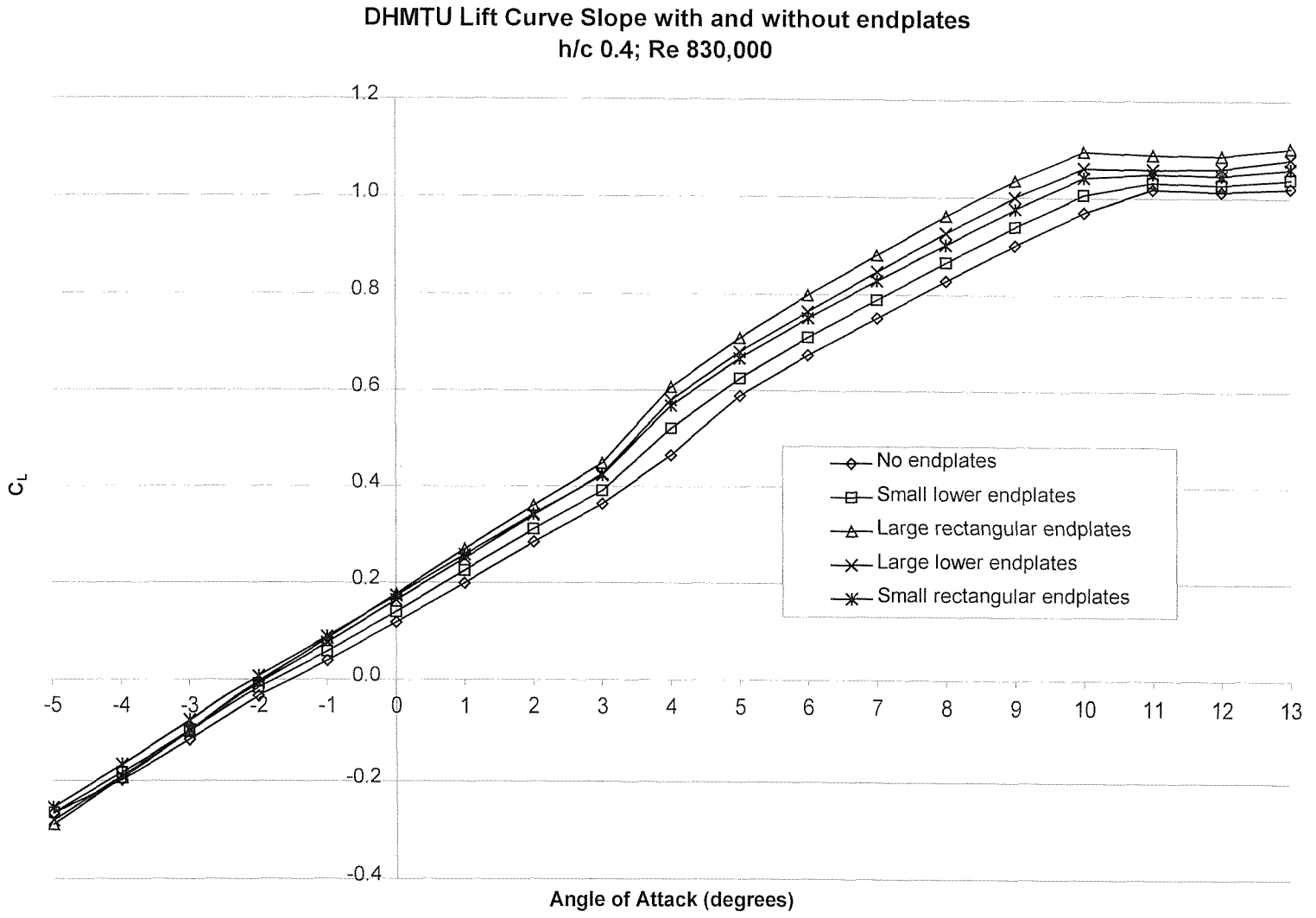

Figure 9-9: Lift curve slope of DHMTU aerofoil in moderate ground effect (h/c 0.4) with and without endplates

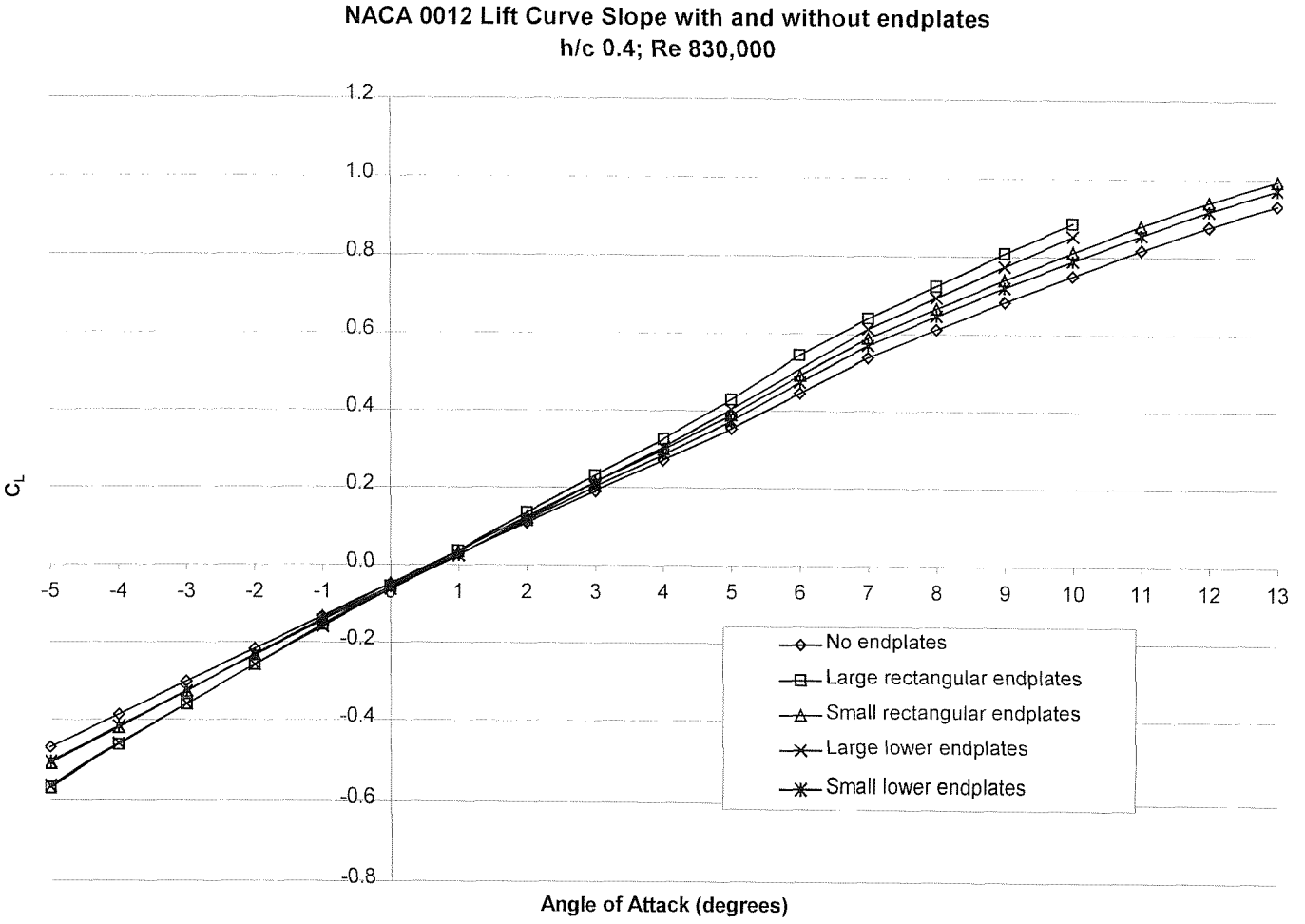

Figure 9-10: Lift curve slope of NACA 0012 aerofoil in moderate ground effect (h/c 0.4) with and without endplates

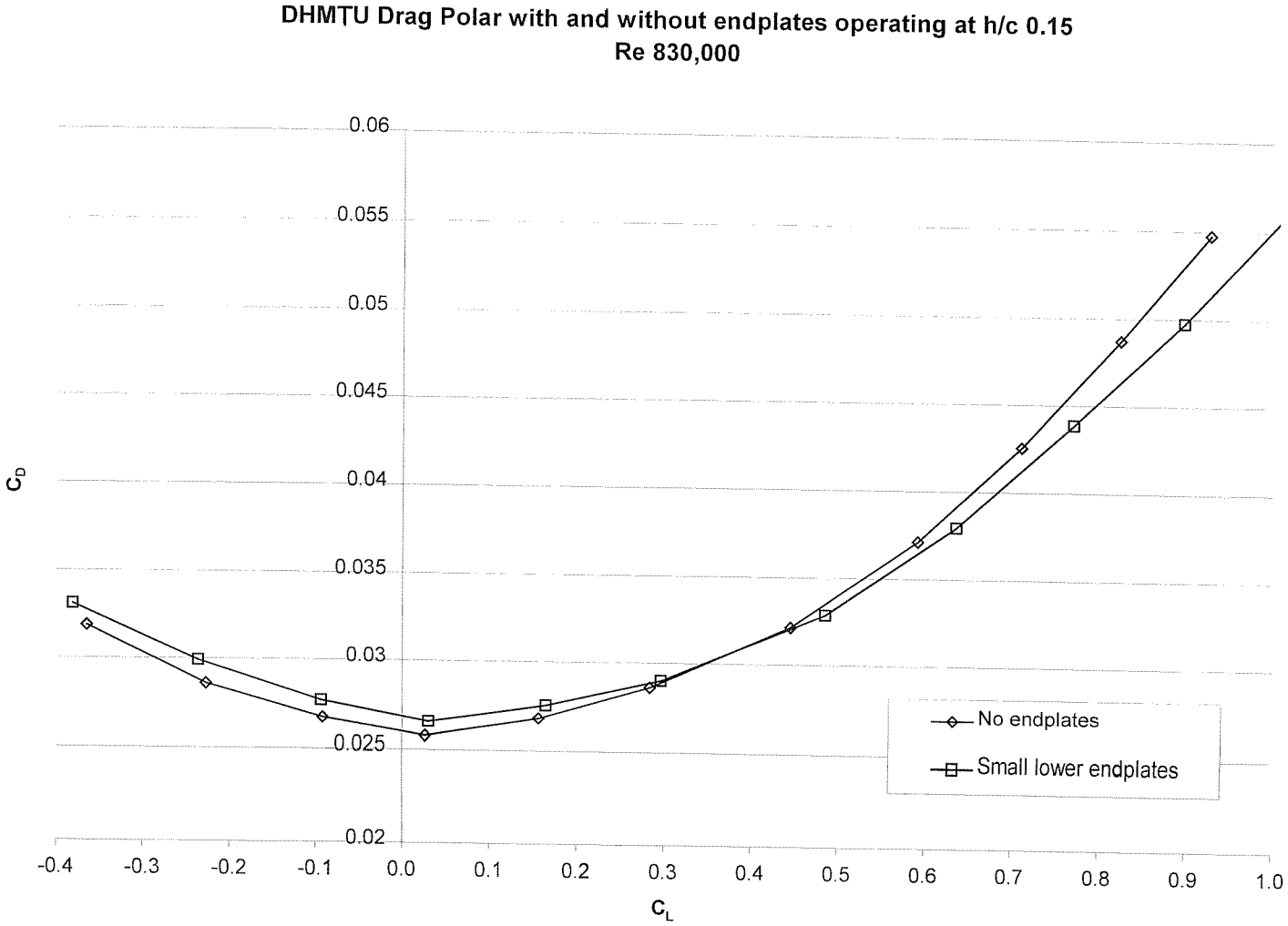

Figure 9-11: Drag polar of DHMTU aerofoil operating at h/c 0.15 with and without endplates

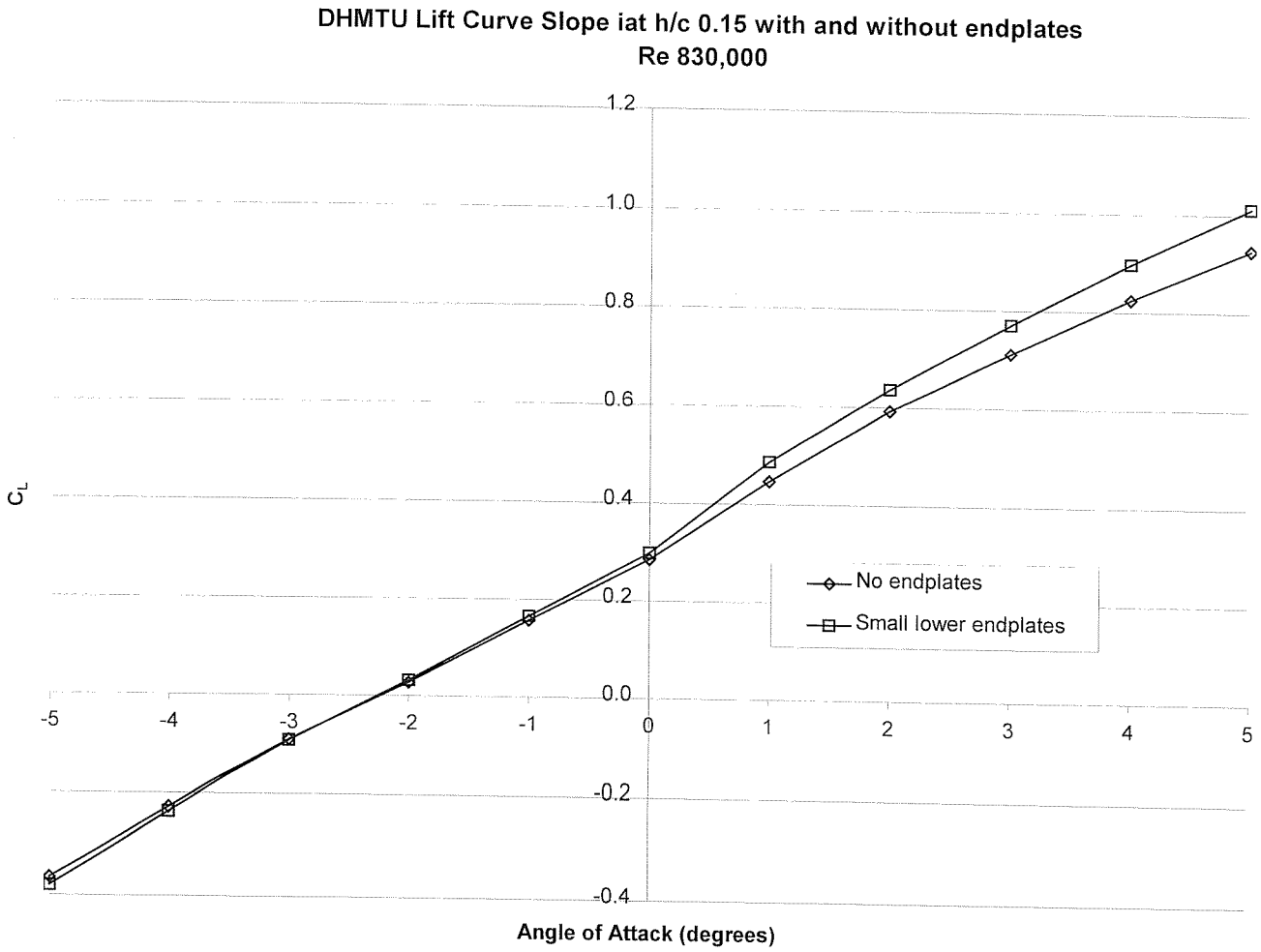

Figure 9-12: Lift curve slope of DHMTU aerofoil at h/c 0.15 with and without endplates

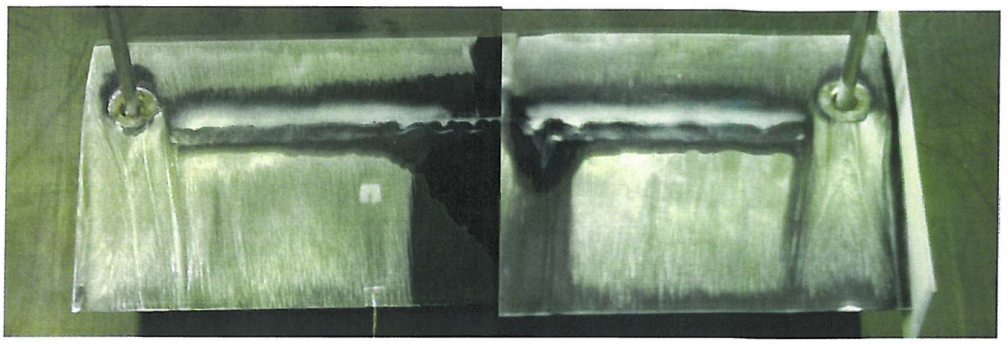

Figure 9-13: Upper surface of DHMTU, h/c 0.4, AoA=5 degree, (a) no endplate (left) and (b) large endplate (right)

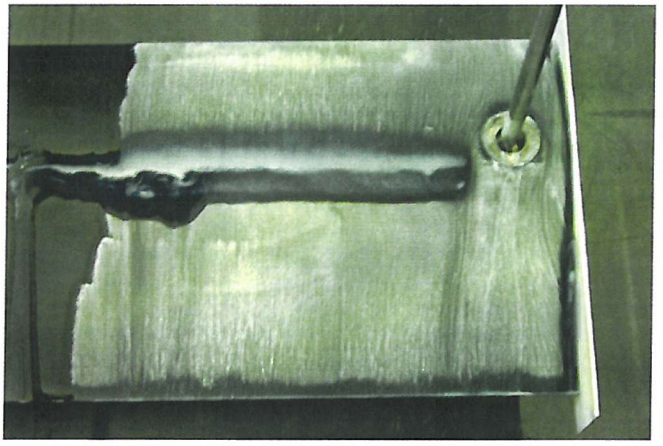

Figure 9-14: Upper surface of DHMTU, h/c 0.4, AoA=5 degree, small rectangular endplate

Figure 9-15: Endplates used in pressure tapping experiments

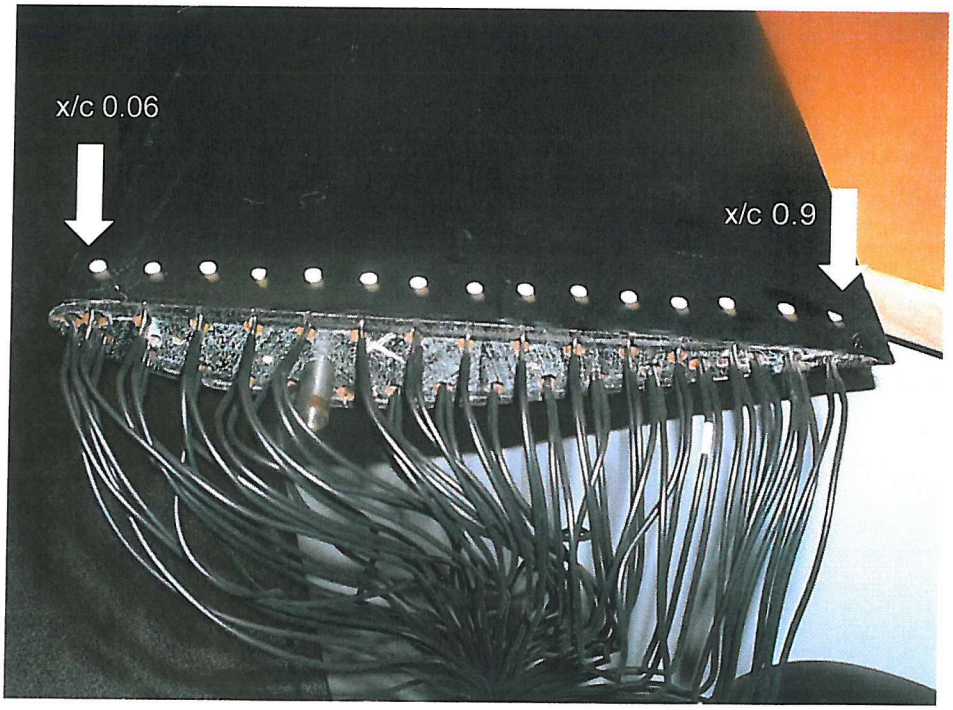

Figure 9-16: Location of wingtip pressure tappings on DHMTU lower surface

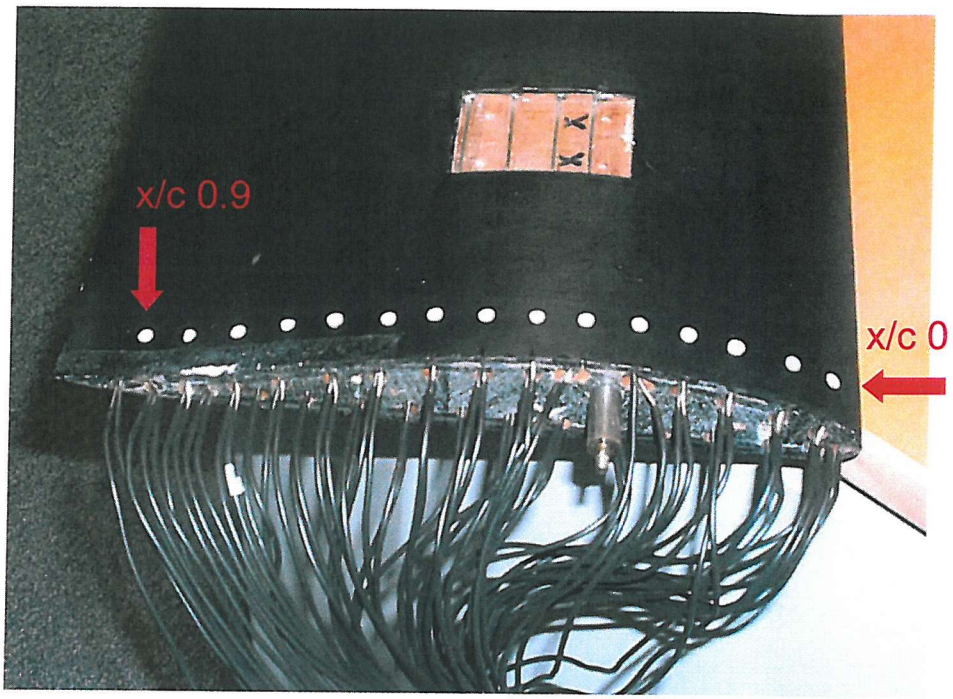

Figure 9-17: Location of wingtip pressure tappings on DHMTU upper surface

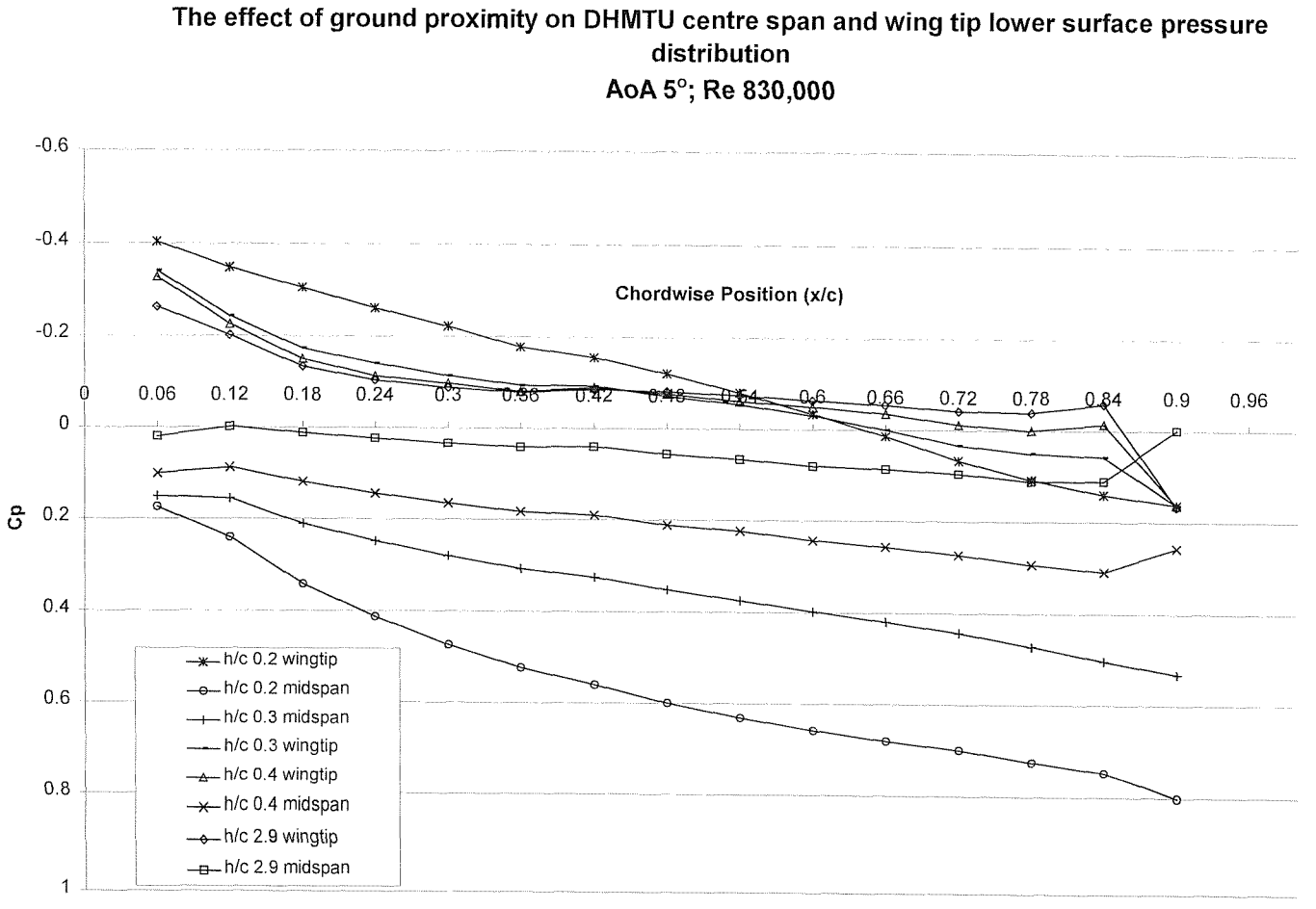

Figure 9-18: The effect of ground proximity on the DHMTU centre span and wing tip lower surface pressure distribution

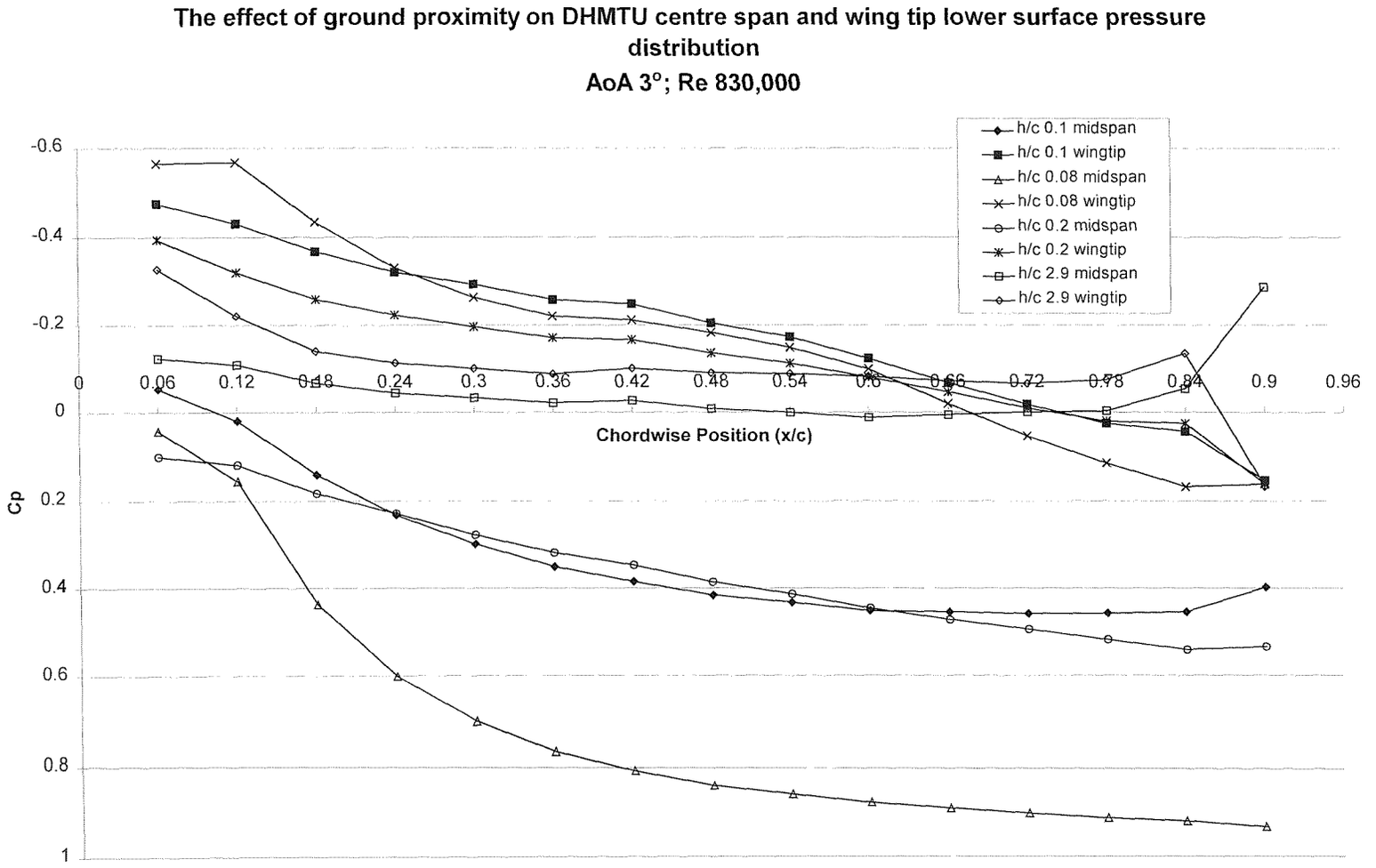

Figure 9-19: The effect of ground proximity on the DHMTU centre span and wing tip lower surface pressure distribution in extreme ground effect

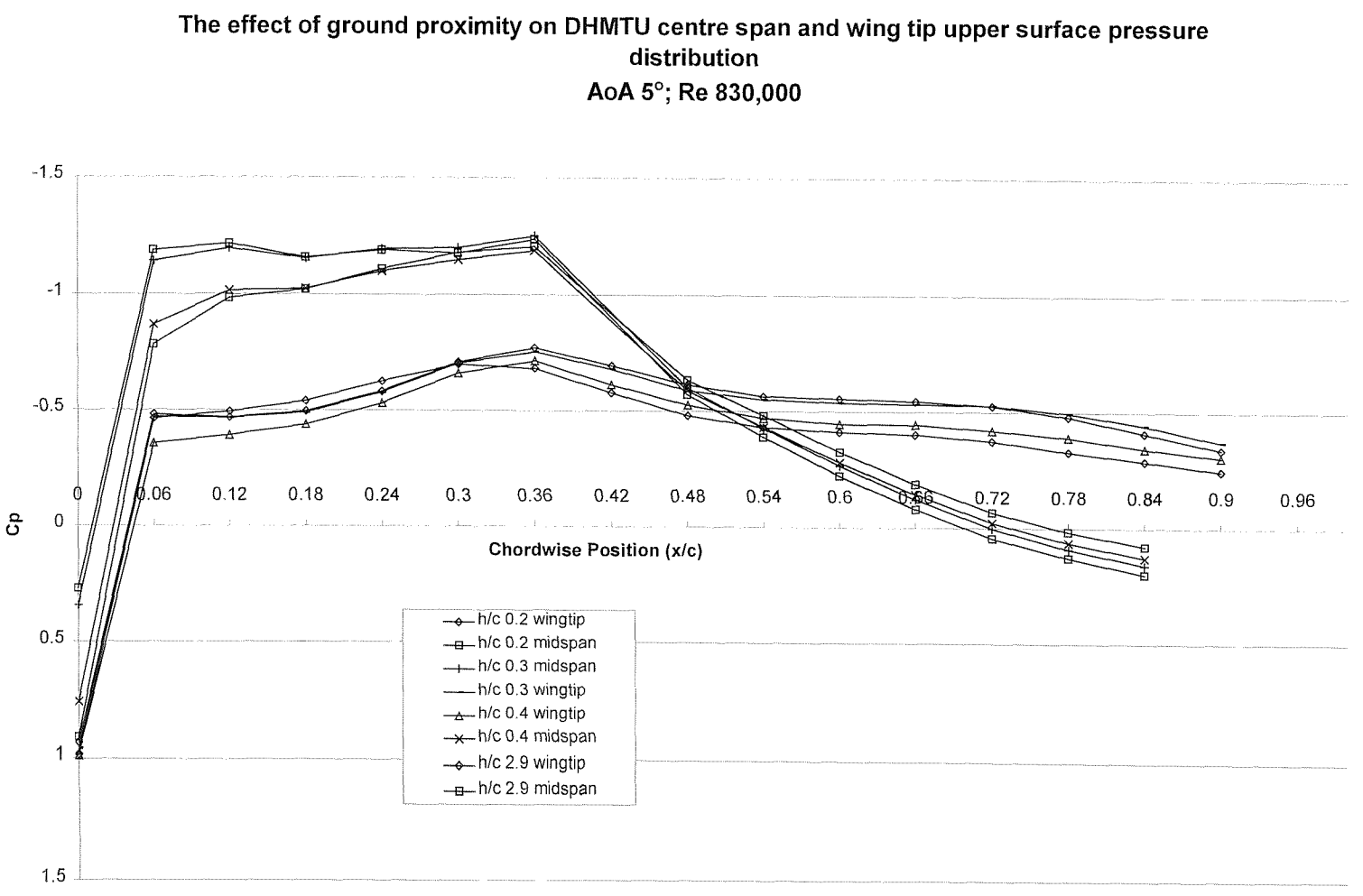

Figure 9-20: The effect of ground proximity on the DHMTU centre span and wing tip upper surface pressure distribution

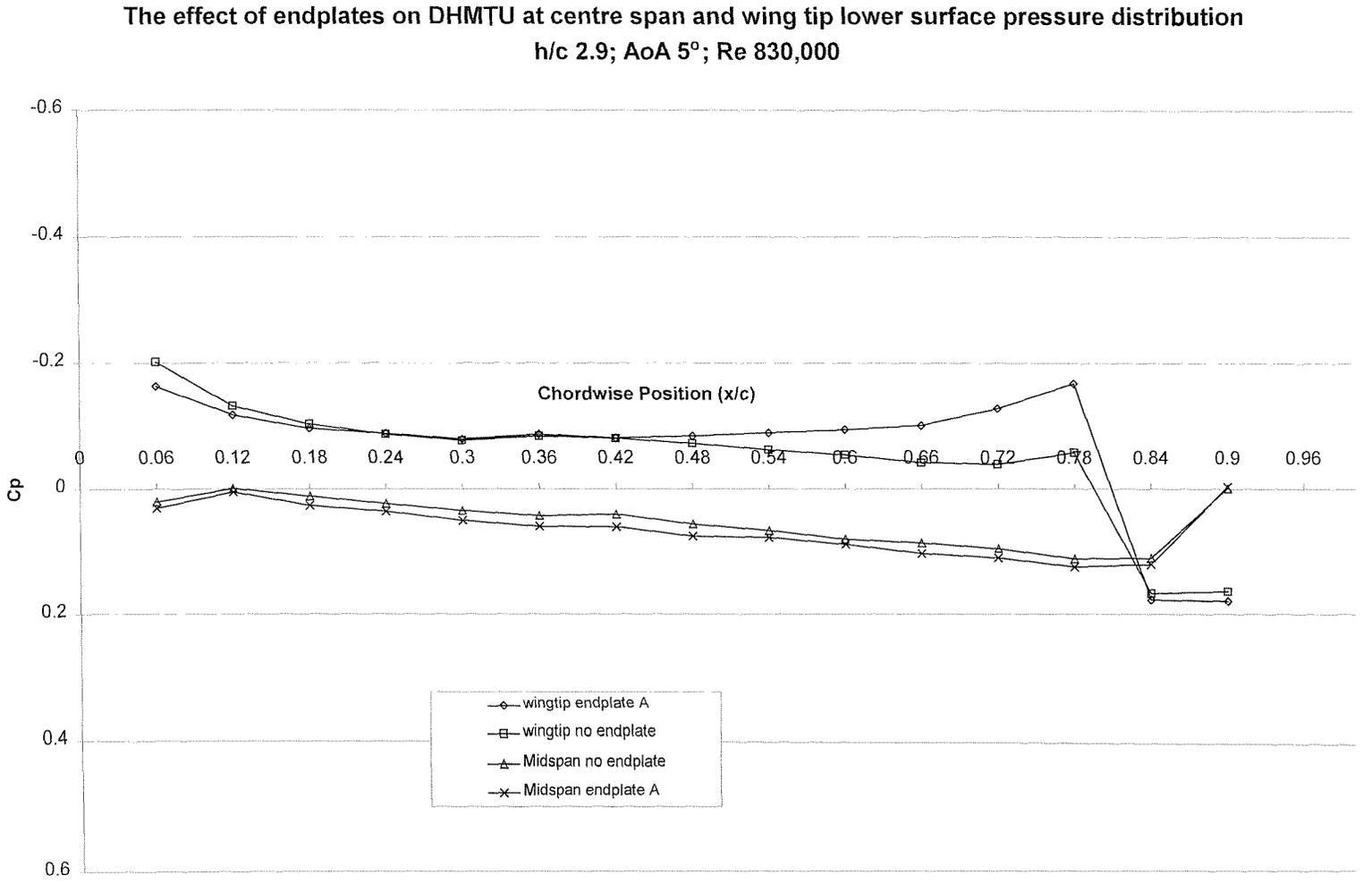

Figure 9-21: The effect of endplates on the DHMTU pressure distribution on the lower surface out of ground effect

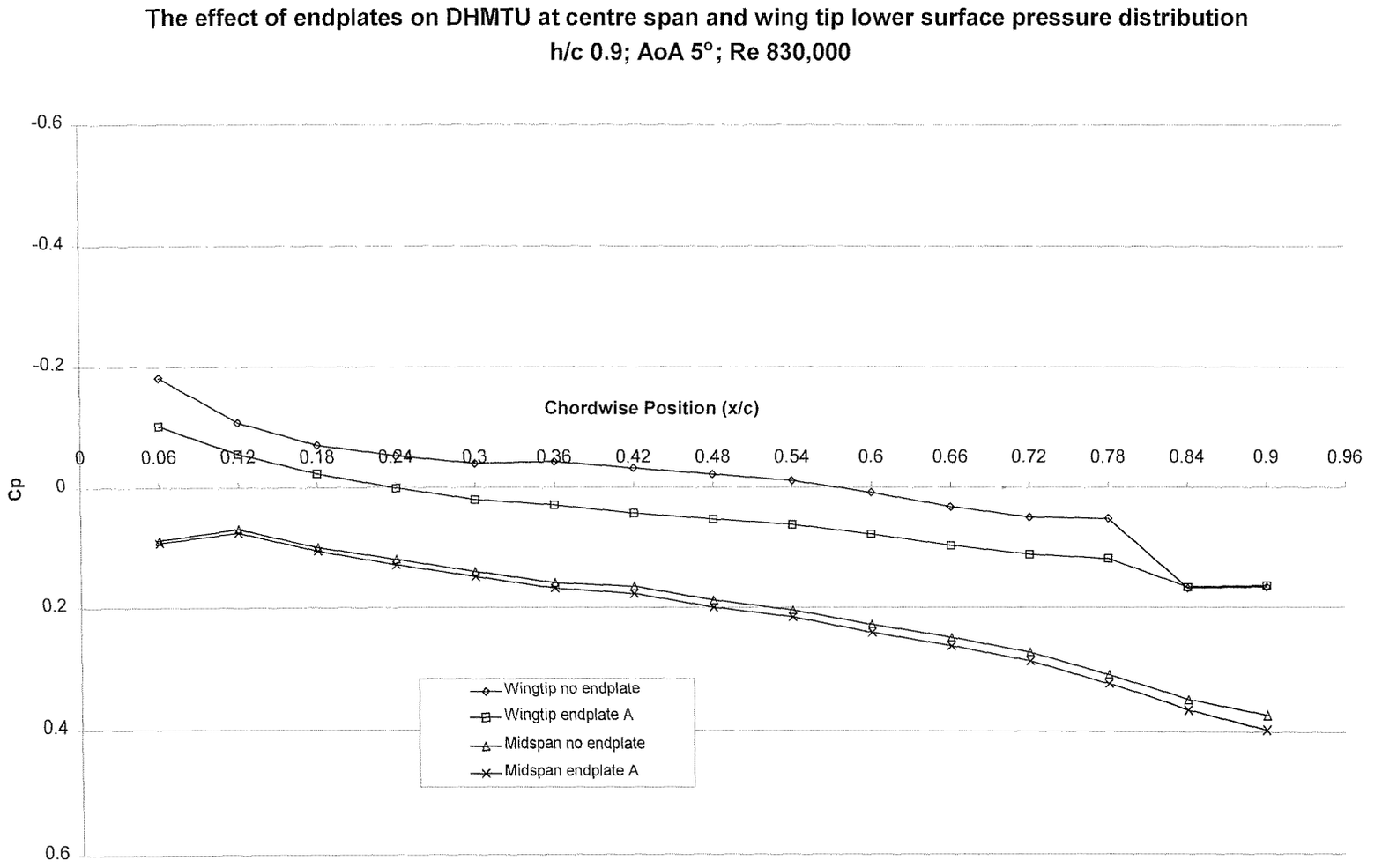

Figure 9-22: The effect of endplates on the DHMTU pressure distribution on the lower surface at h/c 0.9

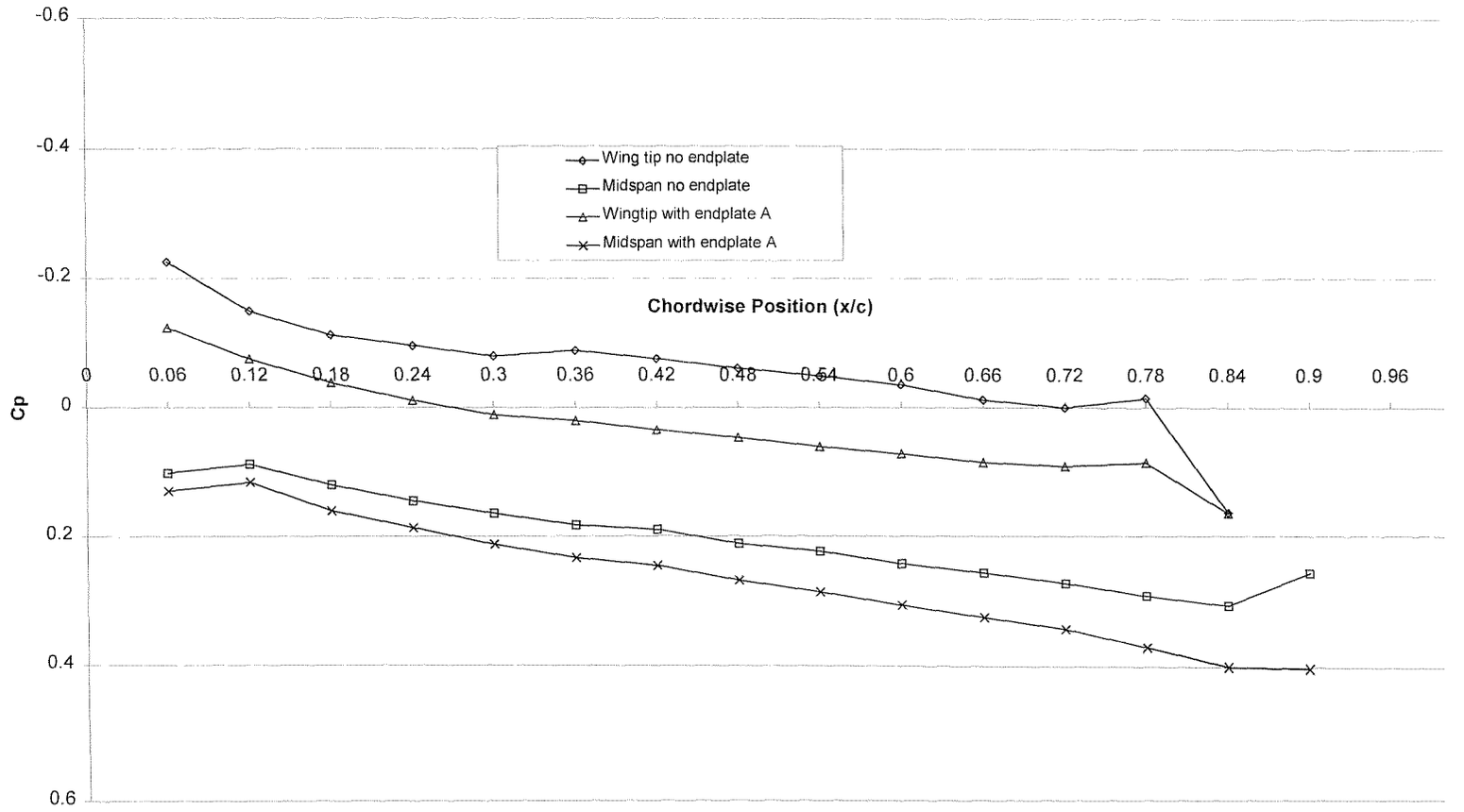

Figure 9-23: The effect of endplates on the DHMTU pressure distribution on the lower surface at h/c 0.4

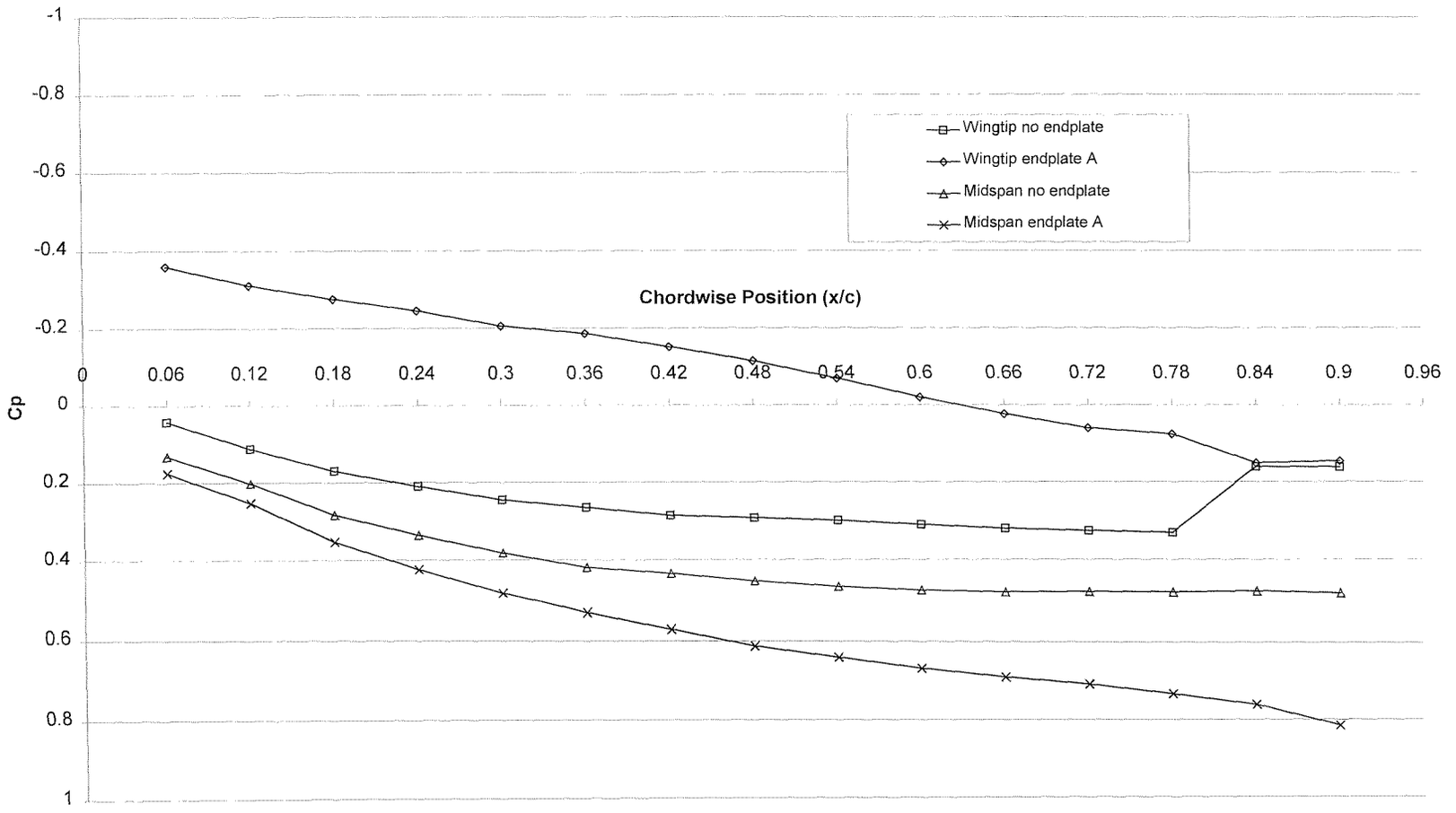

Figure 9-24: The effect of endplates on the DHMTU pressure distribution on the lower surface at h/c 0.2

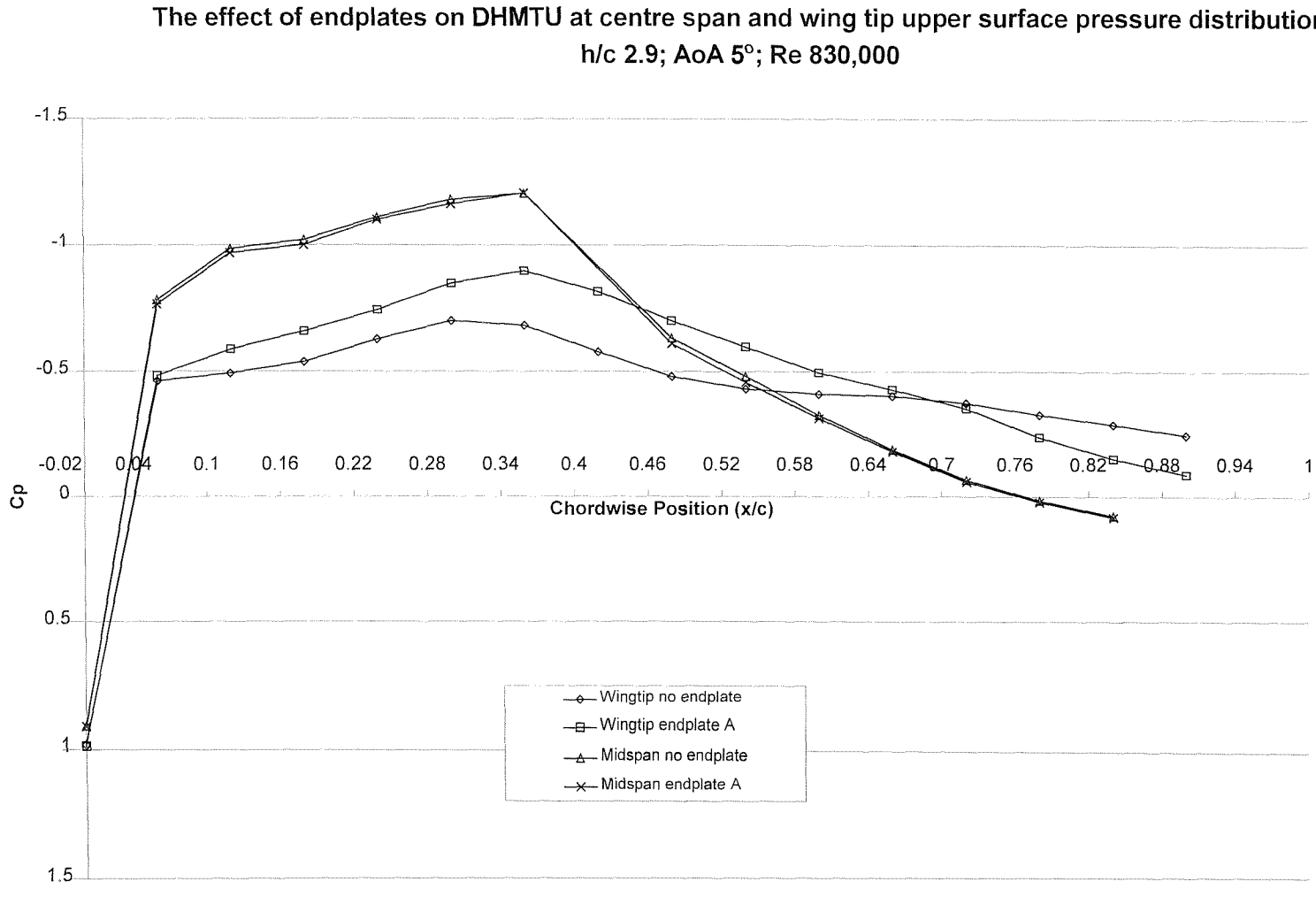

Figure 9-25: The effect of endplates on the DHMTU pressure distribution on the upper surface at h/c 2.9

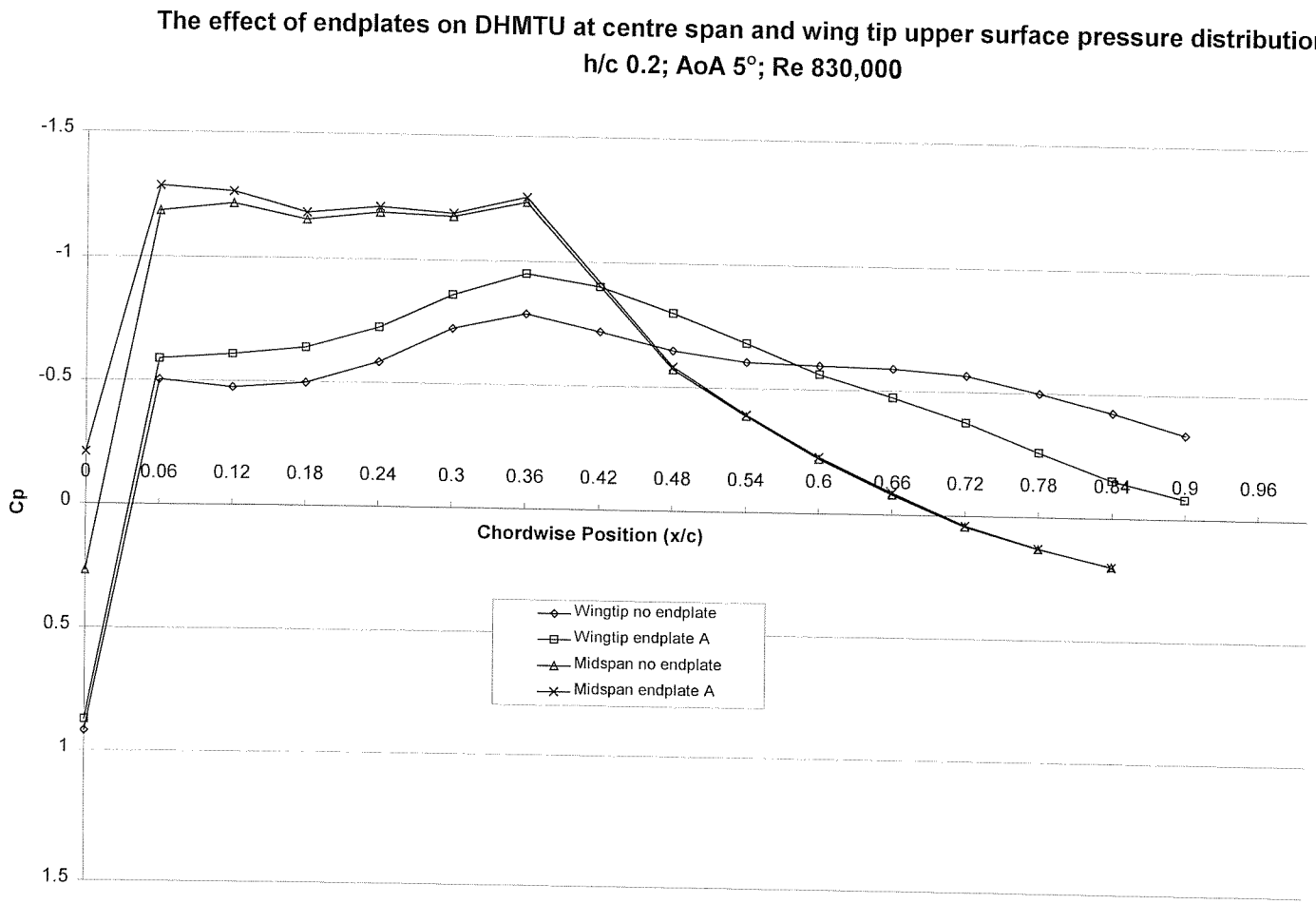

Figure 9-26: The effect of endplates on the DHMTU pressure distribution on the upper surface at h/c 0.2

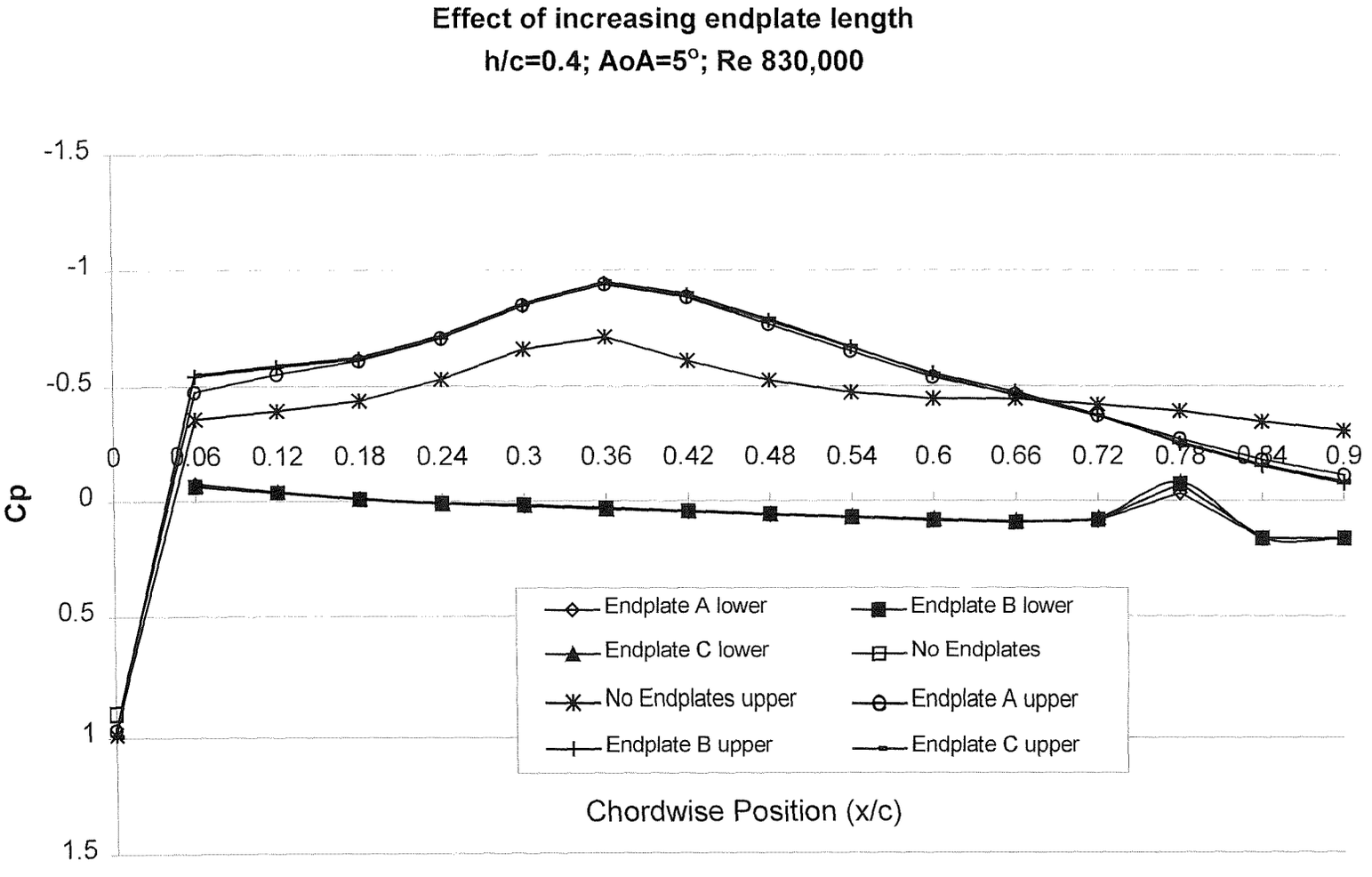

Figure 9-27: Effect of increasing endplate length over aerofoil chord

10 Conclusions and Recommendations

10.1 Overview

This experimental research has derived data from a combination of wind tunnel and circulating water channel facilities to investigate the aerodynamic characteristics of a wing operating in ground effect. The data was obtained at a Reynolds Number of 830,000, applicable to a small UWIGV concept. The influence of wavy surfaces on the lift and drag of a DHMTU aerofoil has been investigated. The following sections summarise that main findings of this research

10.2 Wing In Ground Effect over a Flat Surface

1. This research has shown that the overall drag (C_D) of both the DHMTU and NACA 0012 aerofoils is greater in ground effect than out of ground effect. This is an important result, as wing in ground effect flight does not result in the reduction of overall drag for the two sections tested. The reason for this is the increase in the zero lift component of drag (C_{D0}) with a reduction in altitude. The ground effect values of zero lift drag of the NACA 0012 and DHMTU increase by a factor of 2.2 and 1.5 respectively over there out of ground effect values. This research has shown that the CD_0 of an aerofoil section operating in the ground effect regime can be up to double its out of ground effect value.

2. A significant reduction in the vortex drag (CD_V) of both aerofoils is produced as a result of flying in ground effect. When operating in the extreme ground effect regime (h/c 0.1) the aerofoil sections tested will typically possess only 20% of the out of ground effect vortex drag. Even flying in moderate ground effect will result in considerable vortex drag reduction. Flying at an altitude of h/c 0.5 will result in a wing possessing 70% of OGE vortex drag. Unfortunately the significant reduction in vortex drag coupled with the increase in the zero lift drag is not sufficient enough to reduce the overall drag of the trial sections in ground effect.

3. These trials have shown that the vortex drag reduction factor is independent of aerofoil geometry. Comparing the experimental results with existing theoretical models based upon the horseshoe vortex, it was found that Houghton's method provides a more accurate description of the reduction in vortex drag than that presented by McCormick. Suh and Ostowari's modification of Houghton's equation does match experimental data if a priori knowledge of the span efficiency factor 'e' is available. With the knowledgeof a sections out of ground effect drag characteristic, accurate estimates of the vortex drag in ground effect can be obtained.

4. When operating in extreme ground effect (h/c 0.1) both aerofoils possess an effective aspect ratio of approximately 14 compared to their geometrical aspect ratio of 3. As the altitude of the DHMTU aerofoil reduced to h/c 0.08 the effective aspect ratio increased to 20.

5. As the altitude of both the aerofoils decreases the lift increases. There is a noticeable demarcation between the moderate ground effect regime of h/c 1.0–0.2 and operating in extreme ground effect (h/c<0.1). This is indicated by an increase in the gradient of the lift curve slope $dC_L/d\alpha$ with a reduction in altitude. The DHMTU and NACA 0012 exhibit similar values of $dC_L/d\alpha$ in moderate ground effect, with the DHMTU possessing higher $dC_L/d\alpha$ in extreme ground effect. A dramatic increase in the lift curve slope gradient is evident when the altitude reduces to h/c 0.1. At this altitude the value of $dC_L/d\alpha$ for the DHMTU has increased to 12 units/radian from 5 units/radian at h/c 0.3.

6. In the moderate ground effect region the lift of the DHMTU increases from $1.05CL_{OGE}$ (h/c 1.0) to 1.64 CL_{OGE} (h/c 0.2). When operating at extreme ground effect altitudes h/c<0.1 the lift doubles compared to that generated out of ground effect. The DHMTU aerofoil generates greater lift than the NACA 0012, upto 1.6 times the lift in extreme ground effect. A distinct advantage of the DHMTU aerofoil is that it generates lift at low angles of attack (<3 degrees) when in extreme ground effect (h/c 0.1). This is in

contrast to the NACA 0012 that generates a downward force under these conditions making it unsuitable for applications in ground effect craft.

7. The aerodynamic efficiency of both the DHMTU and NACA 0012 aerofoils increase with a reduction in altitude. When operating out of ground effect the DHMTU aerofoil produced a peak aerodynamic efficiency of 8.4. As the DHMTU enters the moderate ground regime the L/D is 12.7 at an altitude of h/c 0.5 increasing to 16.5 at h/c 0.2. As the DHMTU descends to the extreme ground effect altitude of h/c 0.1 the aerodynamic efficiency doubles compared to the out of ground effect value to 22. In extreme ground effect at low angles of attack the L/D reduces at a much higher rate than when operating in moderate ground effect. The angle of attack of the peak aerodynamic efficiency varies between 5 to 6 degrees. The advantage of the DHMTU over the NACA 0012 is that it provides useful performance at low angles of attack when operating in extreme ground effect. The NACA 0012 aerofoil is particularly unsuited to operation in extreme ground effect due to its poor lift and drag performance at low angles of attack.

8. When operating in the extreme ground effect regime ($h/c<0.1$) as has been suggested by some authors the WIG craft designer needs to be aware that small changes in altitude or angle of attack result in significant variations in lift, drag and aerodynamic efficiency.

9. An increase in Reynolds Number results in an increase in zero lift and vortex drag. The variation in Reynolds Number results in no discernible effect on the lift of the DHMTU aerofoil.

10. As the DHMU aerofoil enters the ground effect regime the pressure on the lower surface and the suction on the upper surface increases. The increase in pressure on the DHMTU lower surface due to ground effect is greater than the increase in suction over the upper surface. With a reduction in altitude the pressure profile on the lower surface of the DHMTU incrementally increases down to an altitude of h/c 0.3. Further reductions in altitude below h/c 0.3

result in significant increases in pressure. This is most evident when the DHMTU enters extreme ground effect (h/c <0.1).

11. On the upper surface of the DHMTU the effect of ground proximity is most evident over the frontal half of the aerofoil. Pressure profile data and flow visualisation show that flow separation and reattachment occurs on the aerofoil's upper surface. This is a result of the combination of low Reynolds Number (830,000) and camber of the upper section.

12. As the altitude decreases the angle of attack that flow separation on the upper surface of the DHMTU aerofoil occurs at reduces. At the higher end of the moderate ground effect regime (h/c 1.0 to h/c 0.4) this angle of attack remains relatively constant around 9-10 degrees. At h/c 0.3 and 0.2 upper surface flow separation occurs at 8 degrees. At these low angles of attack no upper surface flow separation was observed due to the ground constraint on achievable angle of attack.

13. Tripping the boundary layer reduces the suction over the upper surface and pressure on the lower surface of the DHMTU aerofoil. When the boundary layer is tripped the DHMTU wing experiences a 8% reduction in lift coefficient. The pressure profile on the upper surface over the rear part of the DHMTU now experiences suction as a result of tripping the boundary layer.

14. The lower surface of the DHMTU aerofoil is much more effected by a stationary ground than the upper surface. Pressure profiling data has indicated that the lower surface has a noticeable reduction of the pressure coefficient, typically 80% of the peak moving ground value, when operating in the moderate ground effect regime (h/c 1.0-0.3). In contrast the upper surface of the DHMTU is not influenced by the ground speed until an altitude of h/c 0.2. In extreme ground effect the pressure coefficient on the lower surface is reduced to 50-60% of the moving ground value at h/c 0.1. This compares with the pressure coefficient on the upper surface is 85-96% the moving ground value.

15. Overall this indicates that when the DHMTU is operating at altitudes below h/c 0.2 a stationary ground surface reduces the pressure coefficient on the upper and lower surfaces and as a result the lift of the aerofoil is lower. This indicates that data obtained in the CWC trials below an altitude of h/c 0.2 should be treated with extreme caution.

16. When the NACA 0012 enters ground effect there is an increase in the magnitude of the pitching moment at all angles of attack compared to out of ground effect operation. On entering moderate ground effect the pitching moment is approximately its OGE value. As the altitude decreases the magnitude of the pitching moment steadily increases until at an altitude of h/c 0.3 it is 1.4 times its OGE value. As the extreme ground effect region is entered a rapid rise in the magnitude of the pitching moment occurs so that at an altitude of h/c 0.1 it is nearly 4 times its OGE value. The experimental data reveals that there is a distinct difference between the pitching moment behaviour when in moderate (h/c 1.0 to h/c 0.3) and when operating in or near extreme ground effect (h/c<0.2). In the moderate ground effect regime the NACA 0012 is stable over a wide range of positive angles of attack. As the section nears extreme ground effect (h/c 0.2) the pitching moment curve becomes non-linear at angles of attack above 3 degrees. This reduces to 1 degree when operating in extreme ground effect (h/c 0.1).

17. The gradient of the pitching moment angle of attack curve ($dCm/d\alpha$) is constant down to an altitude of h/c 0.3. When the NACA 0012 is at h/c 0.1 the pitching moment angle of attack curve is non-linear. A general observation is that over positive ranges of angles of attack the stability of the NACA 0012 decreases with a reduction in altitude.

18. The DHMTU produces similar trends with an increase in the magnitude of the pitching moment and a reduction in longitudinal stability occurring with a decrease in altitude. As with the NACA 0012 a distinction can be seen in the experimental data between moderate and extreme ground effect. A feature not present with the NACA 0012 is a reduction in stability as a result of flow separation occurring at low angles of attack.

19. The NACA 0012 and DHMTU both possess similar trends in pitching moment behaviour when operating in ground effect. The DHMTU possesses significant longitudinal stability advantages when operating in extreme ground effect. The NACA 0012 generates a much greater magnitude of pitching moment than the DHMTU. In moderate ground effect this is between 2 to 7 times the DHMTUs value. The increase in pitching moment when operating in extreme ground effect is much more significant for the NACA 0012 than the DHMTU. The DHMTU possesses a higher $dCm/d\alpha$ than the NACA 0012 resulting in a greater rate of restoring moment. The DHMTU possesses a more gradual variation in Cm with decreasing altitude than the NACA 0012. Compared to operating OGE the pitching moment increases by 1.6 for the DHMTU and 3.8 for the NACA 0012.

20. As altitude reduces the trim angle of both sections reduces. The DHMTU possesses the advantage of a positive trim angle over the whole ground effect range resulting in the production of lift. The NACA 0012 in contrast produces a negative trim angle below an altitude of h/c 0.6 resulting in a downward force being produced. This is further evidence that the NACA 0012 is unsuited to operation in ground effect.

10.3 Wing In Ground Effect over Wavy Surfaces

1. As a wing flies over a wavy surface the lift varies from a maximum to a minimum. The amplitude of the lift force oscillation increases with decreasing altitude. The maximum and minimum values of lift do not correspond to the position of the wing's rotation point over the physical peak and troughs of the wavy surfaces. The minimum lift occurs when the wing rotation point is over the wave peak at all altitudes. The position of maximum lift varies between ¼ to ¾ wavelength dependent upon the surface wavelength.

2. As when flying in the ground effect regime over a flat surface the peak lift obtained over a wavy surface increases with decreasing altitude. This contrasts sharply to the minimum lift that decreases with a reduction in

altitude when the wavelength is equal to two and three time the wing chord. A general result is that as the wavelength of the surface increases the maximum lift experienced by the wing increases and the minimum lift decreases. The maximum lift increases at a greater rate than the minimum lift decreases.

3. When the wavelength is equal to 2c and 3c the aerofoil experiences a downward force when the wing rotation point is over the wave crest below an altitude of approximately h/c 0.3. Even at higher altitudes the lift force is much reduced compared to the peak lift forces recorded.

4. The aerodynamic performance of a wing in ground effect operating over a wavy surface is dependent upon the wavelength of the surface. As the wavelength of the surface increases the difference between the minimum and maximum lift coefficient increases. This results in a wide variation in the magnitude of lift force that the flight control system of a WIG craft has to cope with when flying over the sea's surface. One of the merits of adopting a medium to high aspect ratio wing planform for a WIG craft is that the higher cruising altitude attainable results in a smaller variation in lift. This could considerably simplify the design of the flight control system as well as improving ride comfort for passengers.

5. The drag on the wing over a wavy surface in ground effect varies with altitude and as a function of wing position over the wavelength. Like lift it varies between a minimum and maximum value. It was found that the drag was effected over the whole altitude range, though allowance has to be made for the effect near the surface of the CWC.

6. When the wavelength equalled the wing chord the peak drag was 1.5 times greater than that obtained over the flat at h/c 0.2. When the wavelength equalled two and three times the wing chord minimum drag consistently occurred over the wave peak. Maximum drag occurred when the wing rotation point was over the wave trough for λ = 2c and ¾ wavelength for λ = 3c. The positions over the wavy surfaces where minimum and maximum drag

was recorded are identical to the extremes of lift. As the wavelength reduced to equal the wing chord the maximum drag decreased and minimum drag increased.

7. Compared to the wind tunnel data obtained over flat ground, operating over a wavy surface results in greater values of drag. The peak drag can be over twice that obtained over flat ground at low altitude (h/c 0.2). The difference between minimum and maximum drag is much less than that of lift for all three wavy surfaces.

8. The method of Byelinsky and Zinchuk involving flying a wing above waves submerged in a towing tank provides a degree of corroboration of the CWC method. The trends in lift and drag produced in both experimental approaches are similar.

9. It was found that the proximity of the wing to the water's surface in the CWC effected the altitude range at which the effect of the waves was experienced. Additional limitations in the CWC method include the discrete sampling that could miss any peaks and troughs in the data unless sufficient time is available to finely sample the wavelength. Advantages of the CWC method are the rapidity that the experimental apparatus can be set-up and run combined with the limited, typically two, number of personnel required.

10. In the case of a wing flying over waves in ground effect the wing will not experience the full range of effective angle of attack, thus this CWC static method will produce magnitudes of lift that are greater than in the dynamic case. Therefore the results generated in the CWC experiments can be considered as design extremes.

10.4 Endplates in Ground Effect

1. Endplates are not effective at low lift coefficients as a result of their parasitic drag. An angle of attack is reached where the vortex drag reduction as a result of fitting endplates outweighs the penalty incurred in parasitic drag. It

was found that for the DHMTU aerofoil endplate effectiveness occurred from $0.35C_{Lmax}$ to $0.60C_{Lmax}$ dependent upon endplate size and geometry. The large lower endplate configuration became effective from 0.35 C_{Lmax} compared to the large rectangular endplate that did not become effective until 0.60 C_{Lmax}.

2. All the endplates tested increased the wing lift, maximum lift coefficient and the gradient of the lift curve slope. The large rectangular endplates increased the DHMTU's lift by 20% above that of the basic wing. This can be compared to the small lower endplates that increased the lift by 6%.

3. The lower endplate configurations produced the highest increase in aerodynamic efficiency. A 7% increase in L/D is produced when the large lower endplates are fitted. The small lower endplates produce a 3% increase in L/D compared with the large rectangular endplates that produced an increase of 2%. This research has shown that it is best to employ endplates that extend only below the aerofoil lower surface.

4. There is no real benefit in fitting small rectangular endplates, as the increase in lift produced is cancelled by the resultant drag increase at the optimum angle of attack for the DHMTU. The large rectangular endplates have produced the greatest increase in lift due their large surface area, which provides the greatest blockage of lateral circulation around the wingtip. The results indicate that though the rectangular endplate configuration produces respectable increases in section lift the drag penalty associated with them is so great rendering them not very practical.

5. The addition of endplates to the DHMTU aerofoil increases the pressure on the lower and suction on the upper surface at the wingtip when operating both in and out of ground effect. At the midspan of the DHMTU the pressure on the lower surface is unaffected by fitting endplates when out of ground effect. The change in suction on the upper surface at the midspan location as a result of fitting endplates is negligible at all altitudes. As the DHMTU enters moderate ground effect (h/c<1.0) the effect of endplates on the wingtip lower

surface pressure becomes increasingly evident. Thought the increase in pressure on the lower surface midspan is not significant until the altitude has reduced to h/c 0.4.

6. No improvement in the pressure distribution at the wingtip is achieved as a result of increasing the length of the endplates past the leading or trailing edge of the DHMTU.

10.5 Recommendations for Future Work

This research has illustrated the need for more investigation into the effect of a wing in ground effect operating over wavy surfaces. One very important area of investigation is why such low values of lift are being produced when the wing rotation point is over the wave crest. The results obtained during this research have highlighted the need for finer sampling of the wavy surfaces in order to determine the magnitude and location of the extremes of lift and drag as well as to quantify the aerodynamic performance of a wing over the whole of the wavy surface.

11 References

1. Husa B, "WIG Configuration Development from Component Matrix", Orion Technologies, available online at www.oriontechnologies.net/, accessed on 05/08/00
2. Hooker S, "Wingships: A Prospect for High Speed Ocean Transport", Jane's the Worlds Surface Skimmers 1982, Jane's Information Group
3. Raymond A E, "Ground Influence on Aerofoils", NACA Technical Note No.67, December 1921
4. Ollila R G, "Historical Review of WIG Vehicles", Journal of Hydronautics, Vol 14 No.3, July 1980, pp.65-76
5. "Airlift 2025 The first with the most", available on-line at http://www.au.af.mil/au/2025/, accessed in January 2001
6. "The Pelican – A big bird for the long haul", available on-line at http://www.boeing.com/news/frontiers/i_pw.html, accessed in July 2002
7. Hayashi M, Endo E, "Measurement of Flow Fields Around an Aerofoil Section with Separation", Transactions Japanese Society of Aerospace Sciences, Vol.21, No.52, 1978, pp.69-75
8. Hsiun C, Chen C, "Aerodynamic Characteristics of a Two-Dimensional Aerofoil with Ground Effect", Journal of Aircraft, Vol.33, No.2, March-April 1996, pp.386-392
9. Steinbach D, "Comment on 'Aerodynamic Characteristics of a Two Dimensional Aerofoil with Ground Effect", Journal of Aircraft, Vol.34, No.3, May-June 1997
10. Chun H H, Chang R H, "Turbulence Flow Simulation for Wings in Ground Effect with Two Ground Conditions – Fixed and Moving Ground", Submitted to the Transaction of RINA, 6th August 2001
11. Halloran M, O'Meara S, "Wing in Ground Effect Craft Review", DSTO-GD-0201, available on-line at http://www.dsto.defence.gov.au/corporate/reports/DSTO-GD-0201.pdf, accessed on August 2002
12. Handler E H, "Practical Considerations Regarding Wing In Ground Effect Aircraft", Journal of Hydronautics, Vol.11, No.2, April 1977
13. Lange R, Moore J, "Large Wing-in-Ground Effect Transport Aircraft", Journal of Aircraft, Vol.17, No.4, April 1980

14. Maskalik A, "Ekranoplans – The Features and Theory of Designing", Sudostroenie, St Petersburg Russia, 2000, ISBN ISBN 5-7355-0509-2
15. Rozhdestvensky K V, "Nonlinear Aerodynamics of Ekranoplan in Strong Ground Effect", Proceedings of FAST95, Germany Sept 25-27 1995, Vol1, pp.621-630
16. Kirillovikh V N, "Russian Ekranoplans", Proceedings of a Workshop on Twenty First Century Flying Ships, Australia, Nov 7-8 1995, pp.71-117
17. Grebeshev, E P, "Aerodynamical Characteristics of Wing Profile Near Flat and Wavy Screen" TsAGI Proceedings, Moscow, 1976, Issue 1725, pp.31-58
18. Byelinskyy V G, Zinchuk P I, "Hydrodynamical Characteristics of an Ekranoplane Wing Flying Near the Wavy Sea Surface, Fluid Dynamics Problems of Vehicles Operating Near or in the Air-Sea Interface, RTO/NATO, February 1999, ISBN 92-837-0004-X
19. Maskalik A I, Rozhdestvensky K V, Sinitsyn D N, "A View of the Present State of Research in Aero and Hydrodynamics of Ekranoplans", Fluid Dynamics Problems of Vehicles Operating Near or in the Air-Sea Interface, RTO/NATO, February 1999, ISBN 92-837-0004-X
20. Comprehensive website on WIG craft and physics located at http://www.se-technology.com/wig , accessed on November 2000
21. http://www.foster-marine.com/WIGCRAFT/web.pusan.ackr%20(DHMTU)/minggu.dir/~minggu/main.html, accessed on November 2000
22. Chun H H, Park I R, Chung K H, "Computational and Experimental Studies on Wings in Ground Effect and a WIG Effect Craft", Workshop Proceedings of Ekranoplans & Very Fast Craft, University of New South Wales, Sydney, Australia, 5-6 December,pp.38-59
23. Im Y H, Chang K S, "Unsteady Aerodynamics of a Wing-in-Ground-Effect Airfoil Flying over a Wavy Wall", Journal of Aircraft, Vol.37, No.4, July-August 2000
24. Katz J, "New Directions in Race Car Aerodynamics – Designing for Speed", Bentley Publishers, 1995, ISBN 0-8376-0142-8
25. Barnard R H, "Road Vehicle Aerodynamic Design", Longman, 1996, ISBN 0-582-24522-2
26. Soso M, "An Investigation into the Aerodynamics of a Wing In Ground Effect in Generic Racing Car Wake Flows", Transfer Thesis, University of Southampton, September 2003

27. Zerihan J D C, "An Investigation into the Aerodynamics of Wings in Ground Effect", Ph.D Thesis, University of Southampton, April 2001
28. Reid E G, "The Effect of Shielding the Tips of Aerofoils", NACA Technical Report No,201, 1925
29. Riley D R, "Wind-Tunnel Investigation and Analysis of the Effects of End Plates on the Aerodynamic Characteristics of an Unswept Wing", NACA Technical Note 2440, 1951
30. Chawla M D , "Wind-Tunnel Investigation of Wing-in-Ground Effects", Collection of Technical Papers AIAA 6th Applied. Aerodynamics. Conference ,pp. 147-153. April 1990
31. Standingford DWF, Tuck E O, "Optimal Rectangular End Plates", Journal of Aircraft, Vol 33, No.3, May-June 1996
32. Standingford DWF, Tuck E O, "Lifting Surfaces in Ground Effect", Workshop Proceedings of Ekranoplans and Very Fast Craft, University of New South Wales, 1996, ISBN 0 959641122
33. Kühmstedt T, "Aerodynamic Design Procedure and Results of the Commercial WIG Craft", Workshop Proceedings of Ekranoplans and Very Fast Craft", University of New South Wales, 1996, ISBN 0 9596411 2 2
34. Hoener S, "Fluid Dynamic Drag", Hoerner Fluid Dynamics, 1965
35. Hoener S, Borst H, "Fluid-Dynamic Lift", 1975
36. Beek van C M, Oskam B, Fantacci G, "Progress Report on Aerodynamic Analysis of a Surface Piercing Hydrofoil Controlled Wing In Ground Effect Seabus Configuration", Fluid Dynamics Problems of Vehicles Operating Near or in the Air-Sea Interface, RTO/NATO, February 1999, ISBN 92-837-0004-X
37. Akimoto H, Kubo S, Fukushima K, Fukushima N, "Development of a New Wing In Service Effect Craft for 8 passengers", FAST 2001 Papers Vol III, The Royal Institute of Naval Architects, ISBN 0 903055 70 8
38. Gross M G, Gross E, "Oceanography – 7th Edition", Prentice-Hall, 1996, ISBN 0-13-231788-5
39. Hogba N, Dacuna N M C, Olliver G F "Global Wave Statistics", British Maritime Technology, 1986, ISBN 0 946653 38 0
40. Pope A, "Wind Tunnel Testing", John Wiley & Sons, 1947
41. Tothill G M, "Flow Problems of WIGs/Ekranoplanes", University of Southampton, Ship Science, 2001

42. XFOIL available for download on the Internet at http://raphael.mit.edu/xfoil/, accessed, accessed on November 2000
43. Houghton E L, Carpenter P W, "Aerodynamics for Engineering Students – 5th Edition", Butterworth-Heinmann, 2003, ISBN 0-7506-5111-3
44. McCormick B W, "Aerodynamics, Aeronautics and Flight Mechanics – 2nd Edition", John Wiley & Sons, 1995, ISBN 0-471-11087-6
45. Jacobs E N, Kenneth E W, Pinkerton R M, "The Characteristics of 78 related Airfoil Sections from Tests in the Variable Density Wind Tunnel", NACA report 460, 1931
46. Suh Y B, Ostowari C, "Drag Reduction Factor due to Ground Effect", Journal of Aircraft, November 1988, Vol.25, No.11, pp1071-1072
47. Ganin S M, "Analysis of the Configuration Design Solutions of Ekranoplans Based on Experience of the Russian Ekranoplan Building", Proceedings of the International Conference on Ground Effect Machines, Saint-Petersburg Russia, 21-23 June, 2000, ISBN 5-88303-199-4
48. "Jane's High Speed Craft 1999-2000", Jane's Information Group, 1999
49. BAI website located at http://www.baiaerosystems.com/payload.html, accessed in March 2002
50. GPS error data located on the internet at http://www.wsrcc.com/wolfgang/gps/accuracy.html, accessed in March 2002
51. Roke Manor Research located on the internet at http://www.roke.co.uk/aviation/miniature_radar_altimeter.asp, accessed in March 2002
52. http://www.diyelectronics.com/Accessories/URF.html, accessed in March 2002
53. Trial results located on the Internet at http://www.arl.army.mil/sedd/acoustics//slides-tien-leng.htm, accessed in March 2002
54. Weiss A, "Take-off", Nexus Special Interests, 1998, ISBN 1-85486-166-2
55. Anderson J D, "Introduction to Flight – 4th Edition", McGraw Hill, 2000, ISBN 0-07-116034-5
56. Lawrence W C, "Progress in Analysis and Prediction of Dynamic Stall", Journal of Aircraft", Volume 25, January 1988, pp.6-17

Appendix A

Uncertainty and Repeatability of Experimental Results

A1. Uncertainty in Wind Tunnel Force Measurements

The uncertainty in the wind tunnel force measurements can be broken down into setting up errors in the wing position on the wind tunnel balance, inaccuracy in measuring the aerodynamic forces and environmental factors. The setting up errors consists of inaccuracy in placement of the wing in altitude and angle. The data acquisition errors include:

- Averaging of the force data in the window sampling time
- Accuracy of the force balance

The sections below quantify the inaccuracies that were present during the experimental data obtained for this thesis.

A1.1 inaccuracy due to Setting up

When the wing was attached to the vertical struts of the wind tunnel balance it was levelled in its spanwise direction by adjusting the length of the vertical struts. This was done in conjunction with a horizontal angular reading from a digital inclinometer placed on the wings upper surface. Similarly the pitch incidence of the wing was set using the digital inclinometer. This instrument displayed an angle to 2 decimal places. It is assessed that the accuracy that the wing was set up in pitch and roll was ±0.1 degree. Each time the altitude of the wing was varied this levelling procedure had to be carried out.

The altitude of the wing above the ground was set by adjusting the height of the vertical struts. The altitude was measured by a ruler set perpendicular from the ground to the reference point, located a distance one third of the chord from the leading edge. It was possible to measure and adjust the altitude of the wing to ±2 mm. This translates into an uncertainty in altitude of ±h/c0.006 for the wings tested. Table A-1 summarises the inaccuracies in setting up the wing sections in the wind tunnel.

A1.2 Averaging of Force Data in Window Sampling Time

The force measurements obtained from the wind tunnel force balance are sampled by a computer program that records the mean value based upon 75 data samples with a sampling rate of 5 Hz. In order to investigate the uncertainty in this sample the program was set to output all 75 recorded values. Statistical analysis of this data at a height of h/c = 0.2 resulted in a mean C_L of 0.6572976 with a standard deviation of 0.0008. The 95% confidence level for the uncertainty using 2 standard deviations gives an uncertainty level based on the sample of $C_L \pm 0.0016$. Similarly for the drag data at a height of h/c 0.2 the uncertainty level over the sampling period was $C_D \pm 0.007$.

A1.3 Accuracy of Wind Tunnel Force Balance

The wind tunnel force balance system acquires data in terms of steps where 59.903 steps equals 1 N. The accuracy of the wind tunnel balance is 4 steps this corresponds to ±0.0668 N.

A2. Repeatability of Wind Tunnel Force Measurements

The repeatability of the experimental data acquired can be divided into the short, and medium term. The short-term repeatability indicates any variations in the data as a result of fluctuations in the airflow over the test wing. To assess the short-term repeatability two sequential sets of data was acquired with the wind tunnel left on between measurements. The medium term repeatability was assessed by comparing measurements made initially at the start of a run with data recorded at the same angle of attack at the end of all the runs. In this case the wind tunnel was turned off and then run up to speed again.

The standard deviation of this data was calculated and a confidence level of twice the standard deviation (95%) is applied. This results in a quantitative assessment in the repeatability of the force data for lift and drag as a function of varying times (Table A-2 and Table A-3).

A3. Uncertainty in Surface Pressure Measurements

The errors in setting the wing up are the same as for the force measurements discussed above (section A1.1). The main difference is in the accuracy of the ZOC (Zero Operate Calibrate) pressure transducer. Zeros were taken with the wind off and the wing at the required incidence. The tunnel was run up to speed and a number of runs recorded. The quoted accuracy of the pressure transducer was ±0.8 mm of water that corresponds to a Cp of 8.8×10^{-3} for all tappings. The equipment outputs values to 3 decimal places corresponding to an uncertainty of Cp±0.009.

A4. Repeatability of Wind Tunnel Pressure Measurements

To determine the repeatability of the wind tunnel pressure measurements the same methodology described in section A2 for the repeatability of force measurements was employed. The standard deviation of this data was calculated and a confidence level of twice the standard deviation (95%) is applied. The results are shown in Table A-4.

A5. Uncertainty in Circulating Water Channel Data

The lift and drag force measurements obtained from the force blocks on the CWC rig are sampled by a computer program that records the mean value based upon 597 samples with a sampling rate of 10 Hz. In order to investigate the uncertainty in this sample the program was set to output all 597 recorded values. Statistical analysis of this data at a height of h/c = 0.2 resulted in a mean C_L of 1.527 with a standard deviation of 0.018. The 95% confidence level for the uncertainty using 2 standard deviations gives an uncertainty level based on the sample of C_L±0.036.

The mean C_D at h/c = 0.2 was 0.169 with a standard deviation of 0.0006. The 95% confidence level for the uncertainty using 2 standard deviations gives an uncertainty level based on the sample of C_D±0.0012.

The accuracy of the force blocks was ± 0.1 N this translates to C_L and C_D± 1.8×10^{-4}. This results in an overall uncertainty of C_L±0.036 and C_D±0.0014.

A6. Repeatability of Circulating Water Channel Data

To assess the short-term repeatability two sequential sets of data was acquired with the water flowing through the CWC working section between measurements. The medium term repeatability was assessed by comparing measurements made initially at the start of a run with data recorded at the same angle of attack at the end of all the runs. The standard deviation of this data was calculated and a confidence level of twice the standard deviation (95%) is applied. The results of this analysis for the lift and drag are presented in Table A-5 to Table A-8.

Wing Setting up Inaccuracy	**Magnitude**
Wing Bank Angle	±0.1 degree
Wing Angle of Attack	±0.1 degree
Wing Height	±0.006 h/c

Table A-1: Summary of wing setting up inaccuracy

	Standard Deviation (sd)	**Repeatability (2sd)**
Short Term	2.86×10^{-4}	5.72×10^{-4}
Medium Term	5.25×10^{-3}	10.5×10^{-3}

Table A-2: Standard deviation and confidence level in C_L for the repeatability of lift force measurement results

	Standard Deviation (sd)	**Repeatability (2sd)**
Short Term	1.05×10^{-3}	2.1×10^{-3}
Medium Term	3.15×10^{-3}	6.3×10^{-3}

Table A-3: Standard deviation and confidence level in C_D for the repeatability of drag force measurement results

	Standard Deviation (sd)	**Repeatability (2sd)**
Short Term	Cp±0.049	Cp±0.098
Medium Term	Cp±0.072	Cp±0.103

Table A-4: Standard deviation and confidence level in Cp for the repeatability of pressure measurement results

	Standard Deviation (sd)	Repeatability (2sd)
Short Term	0.05446 N	0.10892 N
Medium Term	0.39336 N	0.78672 N

Table A-5: Standard deviation and confidence level in the repeatability of CWC lift force results

	Repeatability (2sd)
Short Term	$C_L \pm 2.0 \times 10^{-4}$
Medium Term	$C_L \pm 1.4 \times 10^{-3}$

Table A-6: Confidence level in the repeatability of CWC C_L results

	Standard Deviation (sd)	Repeatability (2sd)
Short Term	0.12222 N	0.24431 N
Medium Term	0.48935 N	0.97870 N

Table A-7: Standard deviation and confidence level in the repeatability of CWC drag force results

	Repeatability (2sd)
Short Term	$C_D \pm 4 \times 10^{-4}$
Medium Term	$C_D \pm 1.7 \times 10^{-3}$

Table A-8: Confidence level in the repeatability of CWC C_D results

Appendix B

Theoretical Ground Effect Drag Reduction Factors

B1. McCormick's Drag Reduction Factor

McCormick adopts the approach of comparing the ratio of the downwash at the wings centre span to the wings wingtip vortices into that of the effect of the wingtip vortices of the image wing.

The first step is to determine the effect that the wingtip vortices of the real wing have on the centre of the span. Figure B-1 depicts a rear view of a wing operating out of ground effect. An elliptic load distribution across the span of the wing has been assumed, this results in the wingtip vortices being $\pi b/4$ apart, where b is the geometric wingspan.

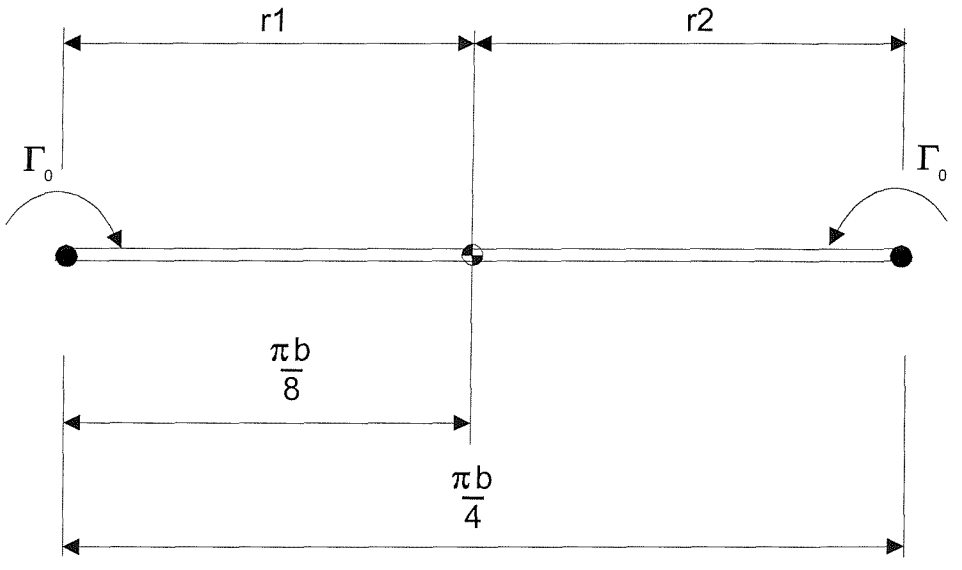

Figure B-1: Rear view of wing out of ground effect

The Biot-Savart law states that the change in downwash Δw from a linear vortex at distance r_1 and r_2 can be expressed as

$$\Delta w = \frac{\Gamma_0}{4\pi r_1}\mathrm{Cos}\,\theta_1 + \frac{\Gamma_0}{4\pi r_2}\mathrm{Cos}\,\theta_2 \qquad \text{Equation B-1}$$

where Γ_0 is the vorticity or circulation at wingtip vortices, $\theta 1$ and $\theta 2$ are the angles between the horizontal and the point of action.

As we are considering a point at centrespan

$r_1 = r_2 = r = \frac{\pi b}{8}$

$\theta_1 = \theta_1 = \theta = 0$

Equation B-1 now becomes

$$\Delta w_{OGE} = \frac{\Gamma_0}{4\pi r_1} + \frac{\Gamma_0}{4\pi r_2} = \frac{\Gamma_0}{4\pi r}\left[\frac{1}{r} + \frac{1}{r}\right] = \frac{\Gamma_0}{4\pi r}\left[\frac{2}{r}\right]$$

Substituting in $r = \frac{\pi b}{8}$

$$\Delta w_{OGE} = \frac{\Gamma_0}{4\pi r}\left[\frac{16}{\pi b}\right] \qquad \text{Equation B-2}$$

To determine the effect of the wing when in ground effect at an altitude h, an image wing is placed at an altitude h below the ground. The image wing is inverted and possesses vortices acting in an opposite direction to the real wing (Figure B-2).

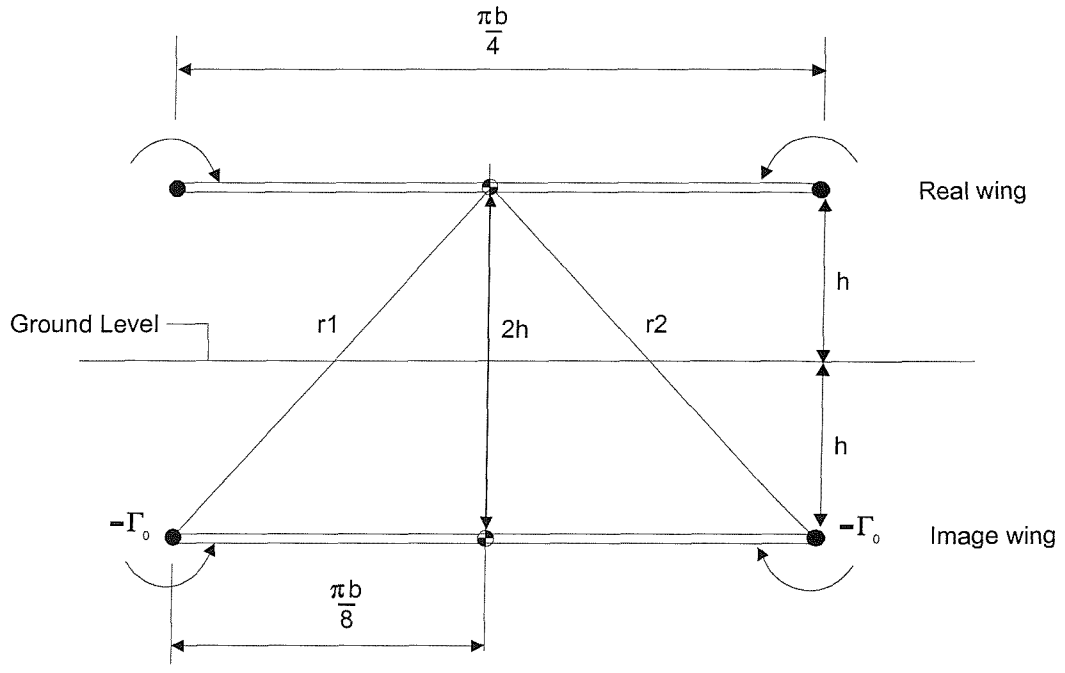

Figure B-2: Rear view of wing in ground effect

Applying the Biot-Savart law (Equation B-1) to calculate the effect of the vortices of the image wing on the centrespan of the real wing. As we are considering a point at centrespan

$\theta_1 = \theta_1 = \theta$ and $r_1 = r_2$

From the geometry shown in Figure B-2

$$r^2 = (2h)^2 + \left(\frac{\pi b}{8}\right)^2 = 4h^2 + \frac{\pi^2 b^2}{64}$$ Equation B-3

$$\Delta w_{IGE} = \frac{-\Gamma_0}{4\pi r_1}\left[\text{Cos}\,\theta_1 + \text{Cos}\,\theta_2\right] = \frac{-\Gamma_0}{4\pi r_1}\left[\frac{\pi b}{8r} + \frac{\pi b}{8r}\right] = \frac{-\Gamma_0}{4\pi r_1}\left[\frac{\pi b}{4r^2}\right]$$ Equation B-4

The minus sign in front of the circulation is to take into account the opposite circulation of the image wingtip vortices.

Substituting equation B-3 into equation B-4

$$\Delta w_{IGE} = \frac{-\Gamma_0}{4\pi r_1}\left[\frac{\pi b}{4\left(4h^2 + \frac{\pi^2 b^2}{64}\right)}\right] = \frac{-\Gamma_0}{4\pi r_1}\left[\frac{\pi b}{16h^2 + \frac{\pi^2 b^2}{16}}\right] \qquad \text{Equation B-5}$$

To obtain the ratio of the downwash in ground effect to the downwash out of ground effect, equation B-5 is divided into equation B-2.

$$\frac{\Delta w_{IGE}}{\Delta w_{OGE}} = -\left[\frac{\pi b}{16h^2 + \frac{\pi^2 b^2}{16}}\right]\left[\frac{\pi b}{16}\right] = -\left[\frac{\pi^2 b^2}{256h^2 + \pi^2 b^2}\right]$$

Dividing through by $\pi^2 b^2$

$$\frac{\Delta w_{IGE}}{\Delta w_{OGE}} = -\left[\frac{1}{\frac{256h^2}{\pi^2 b^2} + 1}\right] = \left[\frac{1}{1 + \left(\frac{16h}{\pi b}\right)^2}\right]$$

The above equation gives $-\Phi$, we require Φ that is obtained by

$$\Phi = 1 - \Phi$$

This results in

$$\Phi = 1 - \left[\frac{1}{1 + \left(\frac{16h}{\pi b}\right)^2}\right]$$

Which can be tidied up to

$$\Phi = \left[\frac{\left(\frac{16h}{\pi b}\right)^2}{1+\left(\frac{16h}{\pi b}\right)^2} \right]$$

Equation B-6

Equation B-6 gives the reduction in vortex drag of a wing when in ground effect. Where h is the height of the wing above the ground and b is the geometric wingspan.

B2. Houghton's Drag Reduction Factor

This method actually calculates the change in vortex drag of a wing in ground effect over its whole span. This is in contrast to McCormick (above) who only considers the change in downwash at the centre of the wingspan. The geometry for the analysis is shown in Figure B-3 below.

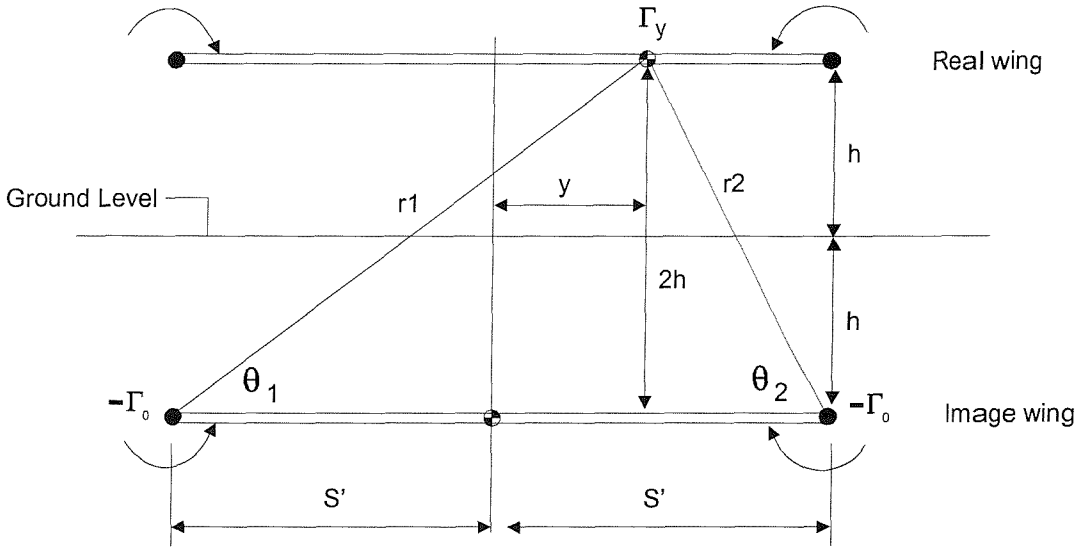

Figure B-3: Rear view of wing in ground effect with its image

The change in downwash Δw at point y along the real wingspan due to the wingtip vortices of the image wing is given by the Biot-Savart Law.

$$\Delta w = \frac{\Gamma_0}{4\pi r_1} \mathrm{Cos}\,\theta_1 + \frac{\Gamma_0}{4\pi r_2} \mathrm{Cos}\,\theta_2$$ Equation B-7

Cos θ_1 and Cos θ_2 can be expressed in terms of the geometry of Figure B-3.

$$\mathrm{Cos}\,\theta_1 = \frac{S'+y}{r_1} \text{ and } \mathrm{Cos}\,\theta_2 = \frac{S'-y}{r_2}$$

Where S' is the semi-span of the elliptic load distribution, y is the distance from the centrespan of the wing to the point under consideration and r_1 and r_2 are the distance to this point from the image wing tip trailing vortices.

Substituting the above geometric expressions into Equation B-7

$$\Delta w = \frac{\Gamma_0}{4\pi r_1}\frac{S'+y}{r_1} + \frac{\Gamma_0}{4\pi r_2}\frac{S'-y}{r_2}$$

$$\Delta w = \frac{-\Gamma_0}{4\pi}\left[\frac{S'+y}{r_1^2} + \frac{S'-y}{r_2^2}\right]$$ Equation B-8

The lift L along the span is given by

$$L = \rho V \Gamma dy$$ Equation B-9

Where ρ is the density of the medium the wing is operating in, V is the wing's velocity, Γ is the vorticity and dy is an element width of the wingspan.

The change in vortex drag ΔD_v is

$$\Delta D_v = \frac{L\,\Delta w}{V}$$ Equation B-10

Substituting Equation B-9 into B-10 yields

$$\Delta D_v = \rho \Gamma_0 \Delta w \, dy$$ Equation B-11

Substitute Equation B-8 into B-11

$$\Delta D_v = \frac{-\rho \Gamma_0^{\,2}}{4\pi}\left[\frac{S'+y}{r_1^{\,2}} + \frac{S'-y}{r_2^{\,2}}\right] dy$$ Equation B-12

Inspection of the geometry shown in Figure B-3 yields the following expressions for r_1^2 and r_2^2

$$r_1^{\,2} = (2h)^2 + (S'+y)^2 = 4h^2 + (S'+y)^2$$

$$r_2^{\,2} = (2h)^2 + (S'-y)^2 = 4h^2 + (S'-y)^2$$

Substituting the expressions for r_1^2 and r_2^2 into Equation B-12 and then integrating over the whole span of the wing

$$\Delta D_v = \frac{-\rho \Gamma_0^{\,2}}{4\pi} 2 \int_0^{S'}\left[\frac{S'+y}{4h^2 + (S'+y)^2} + \frac{S'-y}{4h^2 + (S'-y)^2}\right] dy$$

Solving the integral and considering the first expression

$$\int \frac{S'+y}{(S'+y)^2 + 4h^2} dy$$

As the term (S'+y) is a linear function of y

$$\int S'+y \frac{dy}{dz} = 1$$

$$\int \frac{Z}{Z^2 + 4h^2} dy = \int \frac{Z}{Z^2 + 4h^2} \frac{dy}{dz} dz = \int \frac{Z}{Z^2 + 4h^2} dz$$

The above integral is of the form $\int \frac{f'(y)}{f(y)} dy = \ln\{f(x)\}$

$$\int \frac{Z}{Z^2 + 4h^2} dz = \frac{1}{2} \int \frac{2Z}{Z^2 + 4h^2} dz = \frac{1}{2} \ln 4h^2 + (S'+y)^2$$

Therefore $\int \frac{S'+y}{(S'+y)^2+4h^2}dy = \frac{1}{2}\ln 4h^2+(S'+y)^2$

Similarly for the second expression

$$\int \frac{S'-y}{(S'-y)^2+4h^2}dy$$

$$\int S'-y\frac{dy}{dz} = -1$$

$$\int \frac{Z}{Z^2+4h^2}dz = \frac{1}{2}\int \frac{2Z}{Z^2+4h^2}dz = -\frac{1}{2}\ln 4h^2+(S'-y)^2$$

Resulting in $\int \frac{S'-y}{(S'-y)^2+4h^2}dy = -\frac{1}{2}\ln 4h^2+(S'-y)^2$

$$\Delta D_v = \frac{-\rho\Gamma_0^{\,2}}{4\pi}2\int_0^{S'}\left[\frac{1}{2}\ln 4h^2+(S'+y)^2 - \frac{1}{2}\ln 4h^2+(S'-y)^2\right]dy$$

Taking the ½ out of the bracket that cancels the 2.

$$\Delta D_v = \frac{-\rho\Gamma_0^{\,2}}{4\pi}\left[\ln 4h^2+(S'+y)^2 - \ln 4h^2+(S'-y)^2\right]_0^{S'}$$

$$\Delta D_v = \frac{-\rho\Gamma_0^{\,2}}{4\pi r_1}\left[\ln\frac{4h^2+(S'+y)^2}{4h^2+(S'-y)^2}\right]_0^{S'}$$

Evaluating the expression within the limits S' and 0.

$$\ln\left[\frac{4h^2+(S'+S')^2}{4h^2+(S'-S')^2}\right] - \ln\left[\frac{4h^2+(S'+0)^2}{4h^2+(S'-0)^2}\right]$$

$$\ln\left[\frac{4h^2+(2S')^2}{4h^2}\right] - \ln\left[\frac{4h^2+S')^2}{4h^2+S'^2}\right]$$

$$\ln\left[\frac{4h^2+4S'^2}{4h^2}\right] = \ln\left[\frac{h^2+S'^2}{h^2}\right] = \ln\left[1+\left(\frac{S}{h}\right)^2\right]$$

$$\Delta D_v = \frac{-\rho \Gamma_0^{\,2}}{4\pi} \ln\left[1 + \left(\frac{S'}{h}\right)^2\right]$$ Equation B-13

Put Equation B-13 into coefficient form

$$D_v = \frac{1}{2}\rho V^2 S C_{DV}$$ Equation B-14

Where S is the surface area of the wing and C_{DV} is the coefficient of vortex drag

$$\Gamma_0 = \frac{C_L V S}{\pi S'}$$ Equation B-15

Substituting Equation B-14 and B-15 into Equation B-10 yields

$$\frac{1}{2}\rho V^2 S C_{DV} = \frac{-\rho}{4\pi}\left(\frac{C_L^{\,2} V^2 S^2 4}{\pi^2 b^2}\right)\ln\left[1 + \left(\frac{S'}{h}\right)^2\right]$$ Equation B-16

Rearranging equation B-16 gives

$$C_{DV} = \frac{-C_L^{\,2}}{\pi}\left(\frac{2S}{\pi^2 b^2}\right)\ln\left[1 + \left(\frac{S'}{h}\right)^2\right]$$

A wing's Aspect Ratio (AR) is $\frac{b^2}{S}$ therefore $\frac{S}{b^2} = \frac{1}{A}$, substituting this in the above

$$C_{DV} = \frac{-C_L^{\,2}}{\pi A}\left\{\frac{2}{\pi^2}\ln\left[1 + \left(\frac{S'}{h}\right)^2\right]\right\}$$ Equation B-17

The definition of vortex drag is

$$C_{DV} = k C_L^{\,2} \text{ where } k = \frac{1}{\pi A}$$

Therefore the drag reduction factor Φ is

$$C_{DV} = \Phi k C_L^{\ 2}$$

$$C_{DV} = -k C_L^{\ 2} \left\{ \frac{2}{\pi^2} \ln \left[1 + \left(\frac{S'}{h} \right)^2 \right] \right\}$$

At the present we have obtained an expression for $-C_{DV}$, to convert this to a positive value apply the following

$$kC_L^{\ 2}\Phi = kC_L^{\ 2} - \Phi kC_L^{\ 2}$$

$$kC_L^{\ 2}\Phi = kC_L^{\ 2}\left[1 - \Phi\right]$$

This results in

$$C_{DV} = \frac{C_L^{\ 2}}{\pi A}\left[1 - \frac{2}{\pi^2} \ln \left[1 + \left(\frac{S'}{h} \right)^2 \right] \right]$$

$$\Phi = \left[1 - \frac{2}{\pi^2} \ln \left[1 + \left(\frac{S'}{h} \right)^2 \right] \right]$$

For an elliptic spanwise load distribution $S' = \frac{\pi b}{8}$ the ground effect drag reduction factor becomes

$$\Phi = \left[1 - \frac{2}{\pi^2} \ln \left[1 + \left(\frac{\pi b}{8h} \right)^2 \right] \right] \qquad \text{Equation B-18}$$

Where b is the geometric wingspan and h is the height of the wing above the ground.

B3. Suh and Ostowari's Modification to Houghton

The process for deriving Suh and Ostowari's modification to Houghton is identical upto equation B-17

$$C_{DV} = \frac{-C_L^{\,2}}{\pi A}\left\{\frac{2}{\pi^2}\ln\left[1+\left(\frac{S'}{h}\right)^2\right]\right\}$$

The only difference is that the authors have defined the constant of proportionality 'k' in the drag equation ($C_D=C_{D0}+ kC_L^2$) to be

$$k = \frac{1}{\pi A e}$$

Where Houghton has assumed a perfect elliptical distribution (e=1) and therefore defined k as

$$k = \frac{1}{\pi A}$$

$$C_{DV} = \Phi k C_L^{\,2} = \frac{1}{\pi A e}$$ Equation B-19

Equating equation B-17 with B-19

$$\Phi\frac{C_L^{\,2}}{\pi A e} = \frac{-C_L^{\,2}}{\pi A}\left\{\frac{2}{\pi^2}\ln\left[1+\left(\frac{S'}{h}\right)^2\right]\right\}$$

Resulting in

$$\Phi = -\left\{\frac{2e}{\pi^2}\ln\left[1+\left(\frac{S'}{h}\right)^2\right]\right\}$$

Knowing that $\Phi = 1 - \Phi$

Suh and Ostowari's modification of Houghton's drag reduction factor

$$\Phi = 1 - \frac{2e}{\pi^2} \ln\left[1 + \left(\frac{S'}{h}\right)^2\right]$$ Equation B-20

Appendix C

Towing Tank Trials

C1 Overview

In an attempt to obtain performance characteristics in a more realistic environment the DHMTU section was run in the towing tank at Southampton Institute. Table C-1 presents the characteristics of this facility.

The maximum carriage speed of 4.6 ms^{-1} would result in lift and drag forces of only several Newtons if the wing model used in the rolling road wind tunnel experiments is propelled above the towing tank surface (see Chapter 4). The small magnitude of these aerodynamic forces could be lost in the noise produced by forces as a result of perturbations in the movement of the carriage. To increase the magnitude of the forces the wing could be submerged and towed under the water. Running the wind tunnel DHMTU model under the water would result in the measured forces increasing to thousands of Newtons.

There are two potential experimental methods that could be employed when operating the wing in a submerged environment. The bottom of the towing tank could be used as the ground or the wing could be inverted using the water-air interface to simulate the ground. The disadvantages of using the towing tank floor are:

- Restricted to a flat surface, as it would not be practical or economically feasible to put a wavy surface in Southampton Institute's tank. Therefore in this scenario it would not provide any difference to running the wing in the wind tunnel
- The vertical struts of the existing mounting rig do not extend to the required depth, extending the length of the struts could potentially result in significant torque on the carriage mounting rig.

This is not to discount this method but the depth of the tank and accessibility of the floor mitigates against this method. Trials conducted in QinetiQ Haslar's Circulating Water Channel (CWC) employ this method but the constraints are not the same (Chapter 7).

The advantages of running the wing inverted near the water's surface meant that that the wave making capability of the towing tank could be employed. An additional benefit is that an existing mounting rig was available that with minimum modification could be employed for this purpose. Unfortunately this rig could not sustain the magnitude of forces generated by the wind tunnel DHMTU wing. To rectify this a smaller 1/3.5 scale section was constructed that provided a practical and economical solution to this problem (Table C-2).

C2 Experimental Method

The wing support rig was clamped to the edge of the towing tank carriage. The wing was held by two vertical struts, which were rigidly attached to a horizontal channel (Figure C-1). On top of the horizontal channel a force block was mounted. A force block is a steel cube that is designed to be flexible in only one plane. In this plane a transducer measures the applied mechanical force that is converted into an analogue electrical signal. This signal is then converted into digital format and recorded on a PC. To measure drag and lift forces the force block was positioned in perpendicular orientations to each other. To compensate for the difference in height when the block is measuring lift a spacer has been fitted.

The experimental ranges of variables are presented in Table C-3. The range of wing altitudes was the same as in the wind tunnel experiments. An angle of attack of 5 degrees has been selected as wind tunnel results indicate this provides the highest aerodynamic efficiency (Chapter 5).

C3 Discussion of Results and Conclusions

This method was not successful, as the results were not repeatable when the mounting rig was removed and reattached between experimental runs. This was a consequence of the uneven nature of the towing sled platform surface it was difficult to level the mounting rig with any degree of confidence.

Tank Length	60 m
Tank Width	3.7 m
Tank Depth	1.85 m
Maximum Carriage Speed	4.6 ms^{-1}

Table C-1: Characteristics of Southampton Institute's Towing Tank

Chord	90 mm
Span	270 mm
Area	0.024 m^2
Reynolds Number	270,000

Table C-2: 1/3.5 scale DHMTU Parameters

Experimental Variable	**Range of Values**
Angle of Attack	+5 degrees
Sled towing speed	2 and 4 ms^{-1} 1,2,3,4 ms^{-1} at h/c=0.7 for sensitivity
Reynolds Number	2.7 x 10^5
Wing altitude	2 h/c to 0.15 h/c (0.1 h/c steps)

Table C-3: Experimental Variables for Towing Tank Runs

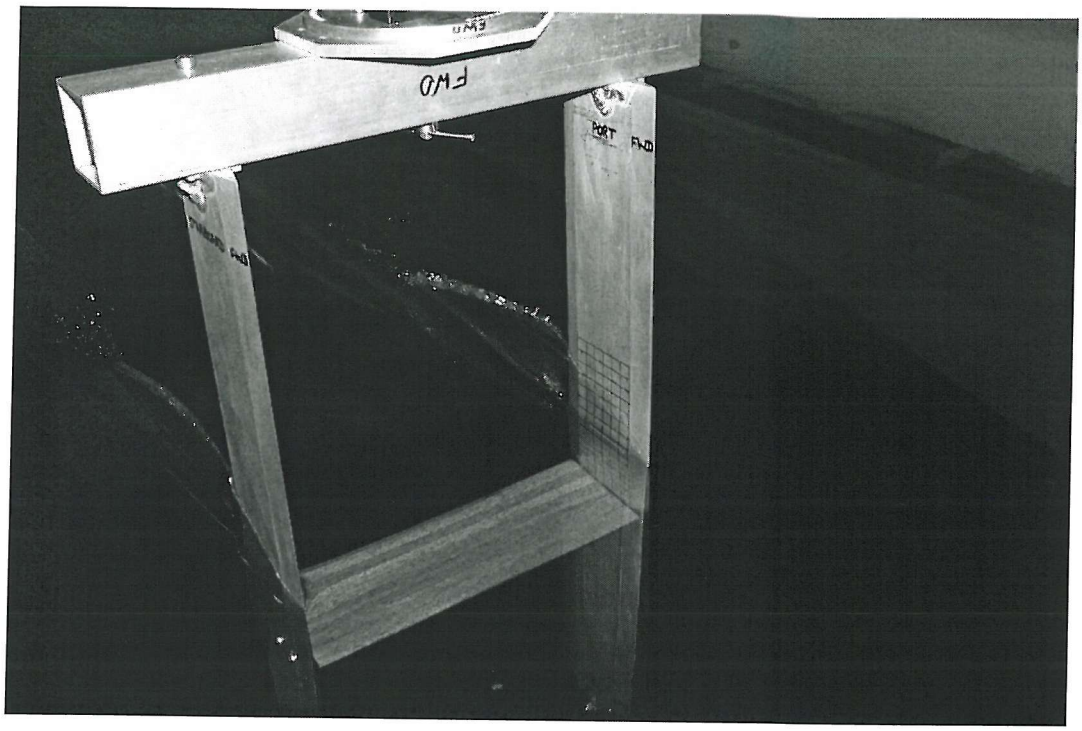

Figure C-1: Wing support arrangement with the wing moving at h/c=0.8 v=4 ms^{-1}

Appendix D

WIG Configuration and Size Constraints

The research being conducted into ground effect aerofoil sections is being constrained to WIG craft of main wing and tail configuration. This appendix provides an overview of WIG craft configurations. WIG craft can be classified into a number of generic classes:

- tandem wing
- canard
- catamaran
- main wing and tail

The tandem configuration (Figure D-1a) has been proposed by Russian designers but has not been realised due to problems with high take-off and landing speeds. A more severe problem is that both of the wings are within ground effect and when operating over dynamic surfaces are under different conditions. The Lippisch configuration (Figure D-1b) is very popular for small displacement WIGs. The reason for this popularity is the self-stabilisation of the delta wing when IGE. Aerodynamic efficiencies up to 14 have been produced with the Lippisch configuration. The maximum theoretical mass of these craft is 300 tons [47].

The Catamaran type WIG (Figure D-2) is restricted to overall maximum L/D of 10 or less, reducing considerably when OGE. This is due to the small aerodynamic fineness of the wing; thus it is very inefficient to build large craft of this class. Catamaran WIGs posses limited seaworthiness because of their small overall physical size and hence small chord resulting in low operating altitude.

The largest WIGs employ the traditional main wing and tail arrangement of conventional aircraft. The Russian ORLYANOK WIG depicted in Figure D-3 illustrates this layout. This configuration has been used by the Russians to construct the largest WIGs yet flown. The rest of the world has also employed

this configuration for concept designs such as the Lockheed PAR-WIG and Boeing PELICAN for proposed ocean going WIG craft.

Tails on aircraft configuration WIGs are larger in tail volume and posses higher aspect ratio than on conventional aircraft. It can also be seen from Figure D-3 that the tailplane is highly swept, increasing the lever arm between the WIGs centre of gravity and tailplane's aerodynamic centre. This is to cope with the large shift in the aerodynamic centre on take-off and when changing height. The ORLYANOK has a turboprop mounted on the top of the tail fin providing propulsion in cruising flight. The location of the turboprop also increases the local dynamic pressure over the tailplane via the slipstream from the two counter-rotating propellers, resulting in tailplane effectiveness being enhanced.

This type of craft possesses low aspect ratio wings typically between 3 to 4.5. Ideally wings should be of high aspect ratio to reduce vortex drag, but due to banking requirements when in close proximity to the ground this cannot be realised as discussed in Appendix E. On the ORLYANOK the trailing edge of the wing is fitted with a five section flap-ailerons and a starting flap along the leading edge. These flaps are used to contain the pressurised air cushion under the wing [47].

The advantages of this configuration are good seaworthiness and the ability to perform dynamic jumps over obstacles or operate OGE. For commercial and military applications the aircraft configuration WIG is the only type being seriously considered.

Ganin [47] states that when the mass of this configuration exceeds 500 tonnes the configuration changes to compound or flying wing. At this point the interior of the wing can be used to house cargo or passengers. This is not borne out by the Boeing PELICAN that is an aircraft configuration WIG with a mass of over 1,000 tonnes [6].

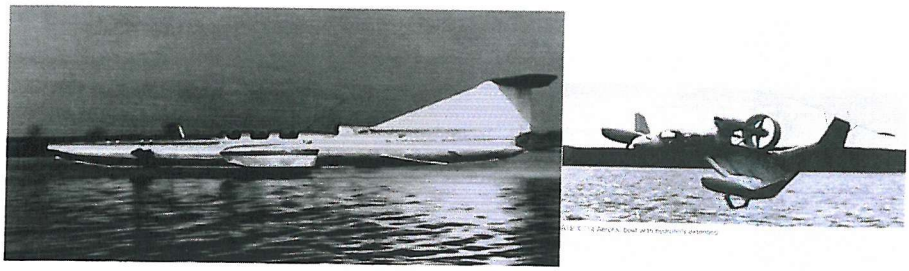

Figure D-1: (a) tandem configuration WIG [20] (b) Lippisch WIG [48]

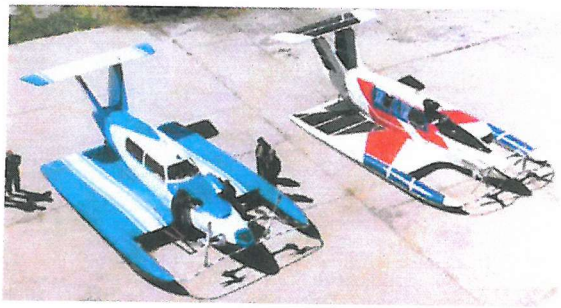

Figure D-2: Catamaran WIG [20]

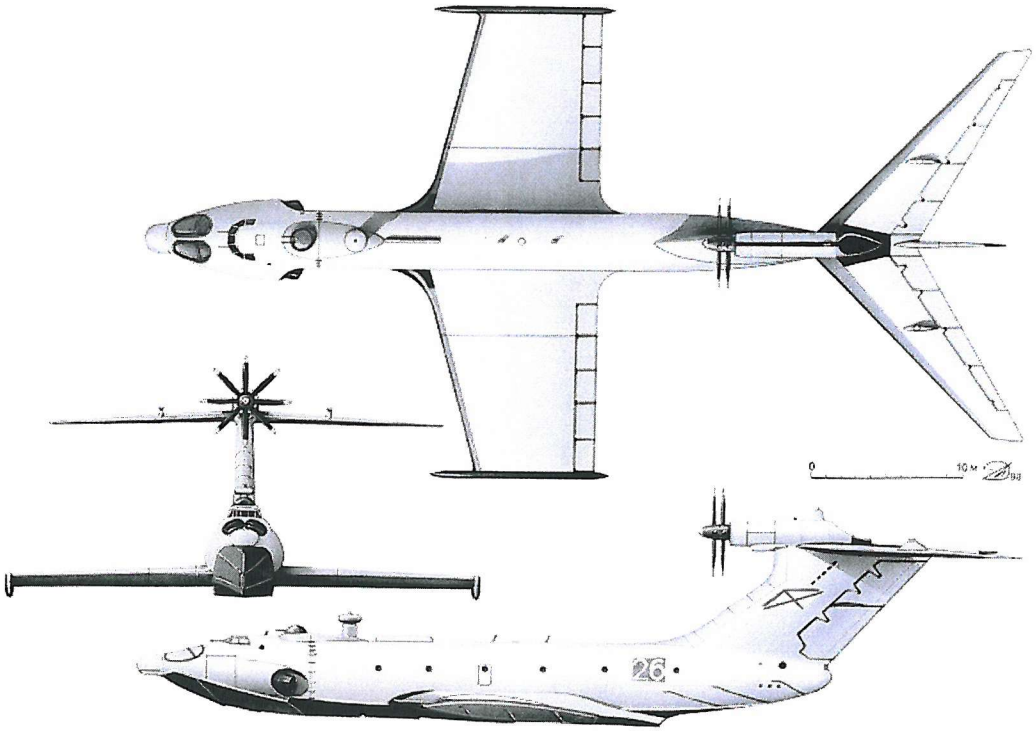

Figure D-3: The Russian first generation ORLYANOK WIG, illustrating the aircraft type configuration [20]

Appendix E

WIG Wing Aspect Ratio

One of the most noticeable features of WIG craft is their low aspect ratio wing. The aspect ratio for a WIG is restricted to less than 5 as a result of the WIG having to bank to manoeuvre at low altitudes near the ocean's surface. It is worth examining the effect that the wing aspect ratio has on WIG turning radii as a function of operational altitude. Figure E-1 illustrates a WIG in level cruising flight with the lift force equal in magnitude but opposite in direction to the craft's weight. If the WIG needs to turn it can either bank at the cruising altitude or increase altitude and bank.

If we consider the first option of the WIG banking at its cruising altitude, the maximum bank angle is constrained by wingtip contact with the water. The angle at which water contact ensues can be calculated by inspection of the geometry depicted in Figure E-2. The WIG craft has banked at an angle ϕ at its cruising height 'h', the wingtip outside the turn now is at a height 2h. The triangle formed by the wing of span 'b' and the sea surface allows the maximum banking angle ϕ to be expressed as

$$\varphi_{max} < \mathrm{Sin}^{-1}\left[\frac{2h}{b}\right] \qquad \text{Equation E-1}$$

$$\text{As Aspect Ratio } A = \frac{b}{c} \rightarrow b = A\,c$$

Where b is the wingspan and c is the wing's chord

$$\varphi_{max} < \mathrm{Sin}^{-1}\left[\frac{2h/c}{AR}\right] \qquad \text{Equation E-2}$$

Where h is the original cruising height of the WIG in terms of h/c and AR is the aspect ratio of the main wing. The achievable maximum banking angle must be less than ϕ to avoid contact with the water.

Figure E-3 presents the maximum WIG banking angle as a function of main wing aspect ratio. The rapid reduction in banking angle with an increase in wing aspect ratio is evident. It can be seen that as the wing aspect ratio increases the allowable banking angle becomes extremely small. Table E-1 compares the maximum banking angle for a wing of aspect ratio 3 and 12. The advantage of employing low aspect ratio wings to maximise the banking angle is clearly evident. For optimum aerodynamic efficiency a WIG would be cruising at an altitude of h/c 0.1 to 0.3. At these heights the banking angle of a WIG is quite small, as a comparison an airliner routinely banks at 30 degrees to manoeuvre.

The next step is to assess the effect that these small banking angles have on the WIG's turning performance. The forces acting on a WIG whilst banking are depicted in Figure E4. As the WIG banks the lift vector produced by the main wing is tilted by the banking angle ϕ. This results in the production of a horizontal centripetal force component $L\text{Sin}\phi$ and a vertical force component $L\text{Cos}\phi$. When an aircraft or WIG banks the total lift force produced must exceed the craft's weight to maintain height. The ratio of the lift force produced to the vehicle weight is known as the 'load factor' denoted by 'n'. The value of the load factor is obtained by equating the vertical forces experienced during the bank.

$$W = L\,\text{Cos}\,\phi \quad \rightarrow \frac{L}{W} = \frac{1}{\text{Cos}\,\phi} \qquad \text{Equation E-3}$$

$$n = \frac{1}{\text{Cos}\,\varphi} = \text{Sec}\,\phi \qquad \text{Equation E-4}$$

Typically transport aircraft and airliners have maximum load factors between 2.5g to 3g. It is assumed that WIGs will posses similar maximum load factors. The load factors for a range of ground effect altitudes as a function of aspect ratio are presented in Figure E-5. Table E-2 present's maximum achievable load factors as a result of ground proximity for a WIG with a main wing of aspect ratio 3. As a comparison a 30 degree banking turn which is atypical of an airliner manoeuvre corresponds to a load factor of 1.15. For a WIG with a wing of aspect ratio 3 to

achieve this it must be at an altitude greater than h/c 0.75. To achieve the maximum load factor of 2.5 to 3 the WIG would have to achieve an altitude greater than h/c 1.4.

The turn radius of a WIG can be obtained by considering the horizontal and vertical force components shown in Figure E4.

Equating the horizontal force components F_H

$F_H = L \text{ Sin } \phi$ and $F_H = mV^2/R_T$

$$L\,\text{Sin}\,\phi = m\frac{V^2}{R_T} \rightarrow \text{Sin}\,\phi = \frac{m}{L}\frac{V^2}{R_T} \qquad \text{Equation E-5}$$

Equating the vertical force components F_V

$F_V = L \text{ Cos } \phi$ and $F_V = mg$

$$L\,\text{Cos}\,\phi = m\,g \rightarrow \text{Cos}\,\phi = \frac{m}{L}g \qquad \text{Equation E-6}$$

Combing equations E-5 and E-6

$$\text{Tan}\,\phi = \frac{\text{Sin}\,\phi}{\text{Cos}\,\phi} = \frac{V^2}{gR_T} \qquad \text{Equation E-7}$$

Combining the expression for load factor $n = \text{Sec}\,\phi$ (Equation E-4) and the trigonometric identity $\text{Sec}^2\phi = 1 + \text{Tan}^2\phi$

$$\text{Tan}\,\phi = \sqrt{n^2 - 1} \qquad \text{Equation E-8}$$

Substituting Equation E-7 into Equation E-8 results in an expression for the turning radius 'R_T' of an aircraft

$$R_T = \frac{V^2}{g\sqrt{n^2 - 1}}$$ Equation E-9

Where V is the velocity of the aircraft, g is the gravitational acceleration 9.81 ms^{-2} and n is the load factor.

Figure E-6 shows the turning radii of a WIG at 100 ms^{-1} as the main wing aspect ratio increases. This speed has been selected as typical of cruising values for larger WIGs. It can be seen that as the aspect ratio increases above 4 the minimum turning radius increases above a 1 km for an altitude of h/c 0.2.

Figure E-7 shows the minimum turning capability for a generic WIG of main wing aspect ratio 3. It should always be borne in mind when looking at these results that these turn radii are when the dipped wingtip is touching the water. In reality these turning radii will be larger dependent upon the wingtip clearance decided upon. This graph illustrates that initiating a turn at h/c 0.1 would result in very large turn radii.

The reader should be aware that not all large WIGs use low aspect ratio wings. In contrast to Russian practice, Lockheed and Boeing have preferred to use moderate to high aspect ratio wings in their design concepts. This would be in order to maintain good aerodynamic performance when operating out of ground effect at conventional aircraft cruising altitudes.

The Lockheed LOW BOY concept of the 1960s employed a low slung wing of aspect ratio 12. With a wingspan of 52 m and a chord of 4.3 m the craft was stated as cruising at an altitude of 5 m which results in an operating h/c of 1.16. At first glance this seems to be overtly high as the wing is not operating in extreme ground effect and is just above the moderate ground effect regime.

But a closer investigation reveals that LOW BOY's high aspect ratio wing did confer the advantage of low vortex drag, resulting in a high effective aspect ratio (Ae) at low altitude. Applying Houghton's vortex drag reduction approximation (see Appendix B2 and section 5.3.3) results in a drag reduction factor of 0.42 for the high aspect ratio LOW BOY at h/c 1.16. For the ORLYANOK (Aspect Ratio 3) to match this vortex drag reduction it has to cruise at h/c 0.3 (Figure E-8). Figure E-9 compares the effect that ground proximity has on effective aspect ratio for LOW BOY against ORLYONOK . It can be seen that at LOW BOY's operational altitude of h/c 1.16 it has an Ae of 29. The ORLYANOK with its much lower aspect ratio wing of 3 could only achieve an Ae of 10 at h/c of 0.2. So a high aspect ratio wing confers the aerodynamic efficiency of conventional aircraft when operating out of ground effect as well as a greater reduction in vortex drag at higher altitudes than low aspect ratio planform WIGs. Though the reader should be aware of the increase in zero lift drag with a decrease in altitude as discussed in Chapter 5.

The disadvantage of employing a high aspect ratio wing on a WIG craft is that it would not benefit from extreme ground effect and the significant increase in lift at its higher cruising altitude. As mentioned above LOW BOY would cruise at h/c 1.16, where as WIGs generally cruise at an altitude between h/c 0.1 to 0.3. If a WIG with an aspect ratio of 12 were to operate at these altitudes it would be significantly constrained in its banking and hence turning ability (see Table E-1). The designer should consider using a high aspect ratio wing if the WIG craft was required to have an operational capability over land operating OGE.

	Maximum banking Angle (degrees)	
Altitude (h/c)	**Aspect Ratio 3**	**Aspect Ratio 12**
0.1	<3.8	<1
0.2	<7.7	<1.9
0.3	<11.5	<2.9
0.5	<19.5	<4.8
1.0	<42	<9.6

Table E-1: Maximum Banking Angle for WIG with Main Wing Aspect Ratio of 3 and 12

Altitude (h/c)	Maximum Load Factor (g)
0.1	<1.002
0.2	<1.009
0.3	<1.021
0.5	<1.061
1.0	<1.342
>1.4	2.5-3

Table E-2: Maximum Load Factors as a function of banking altitude

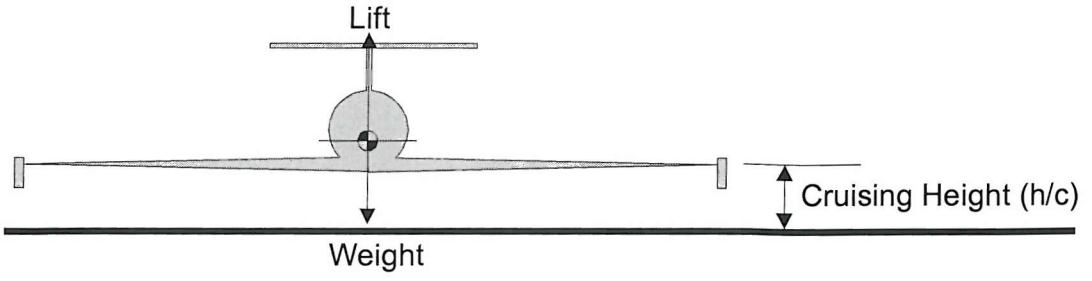

WIG in level cruising flight

Figure E-1: Forces acting on WIG in level cruising flight

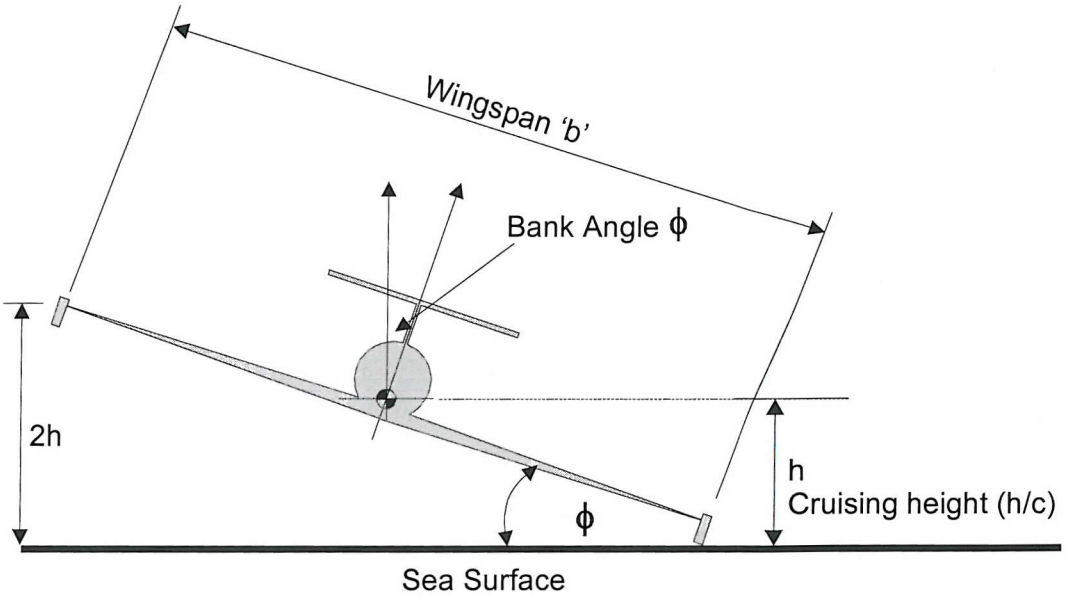

Figure E-2: Determination of Maximum Banking Angle

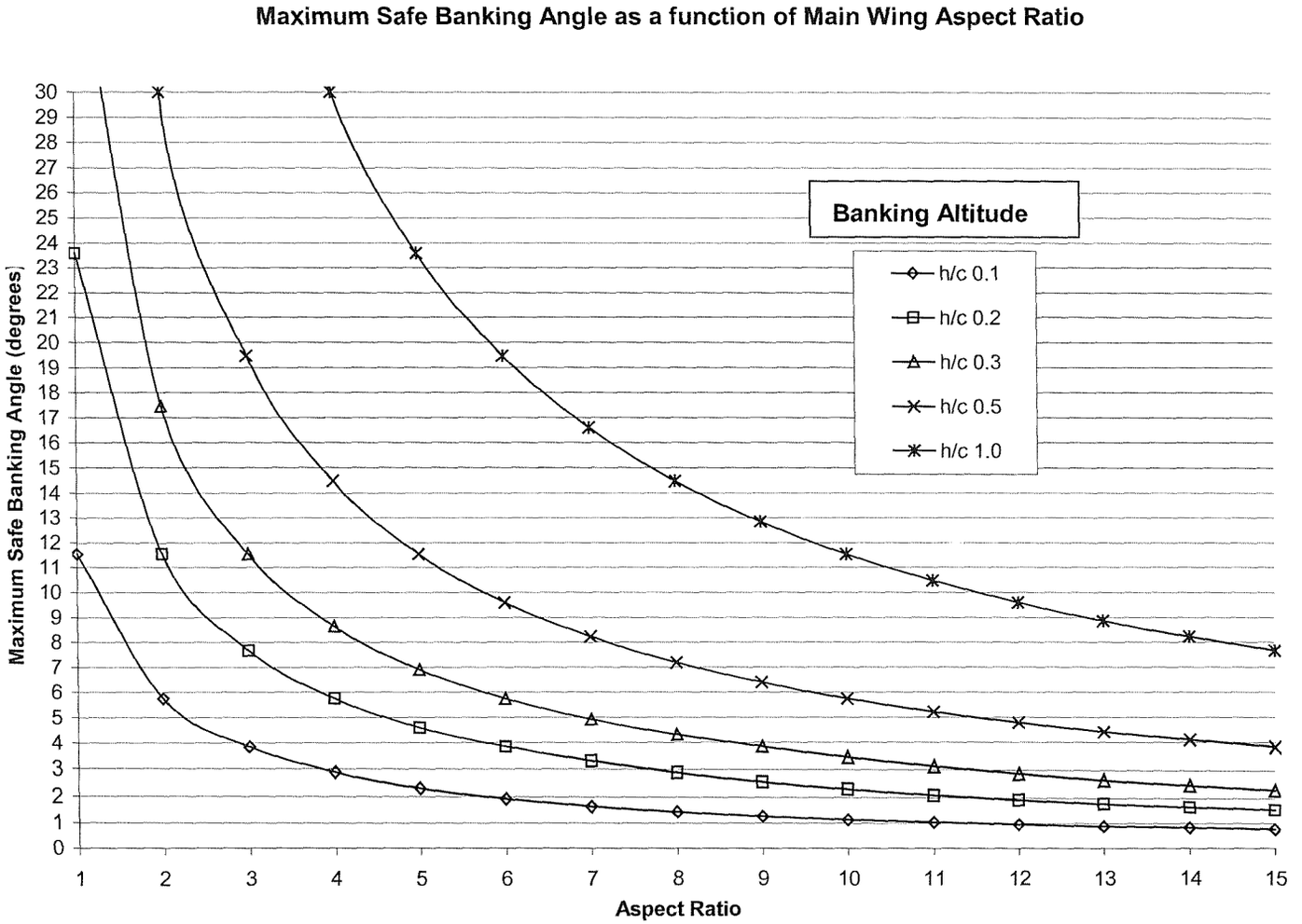

Figure E-3: Maximum WIG banking angle as a function of main wing aspect ratio

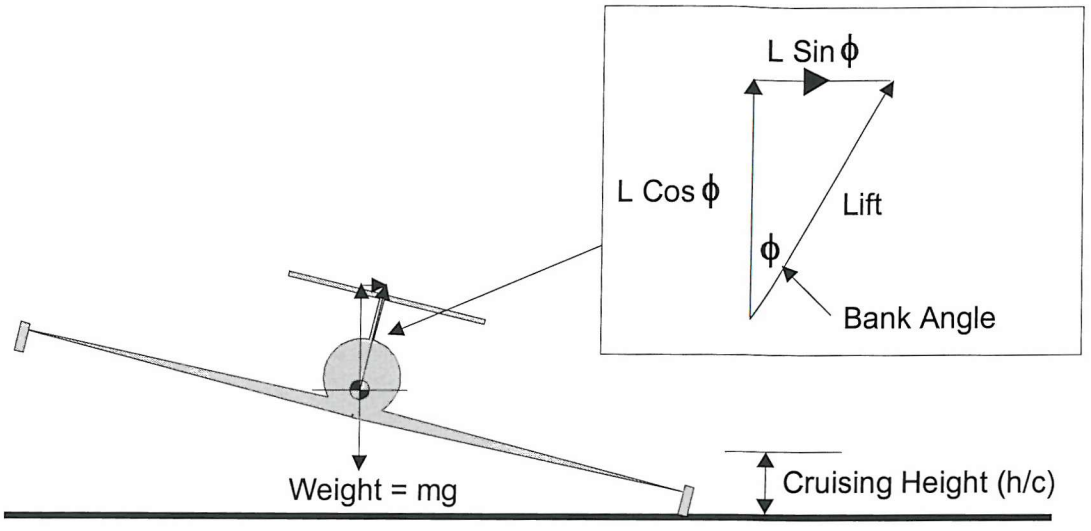

Figure E4: Forces acting on a WIG whilst banking

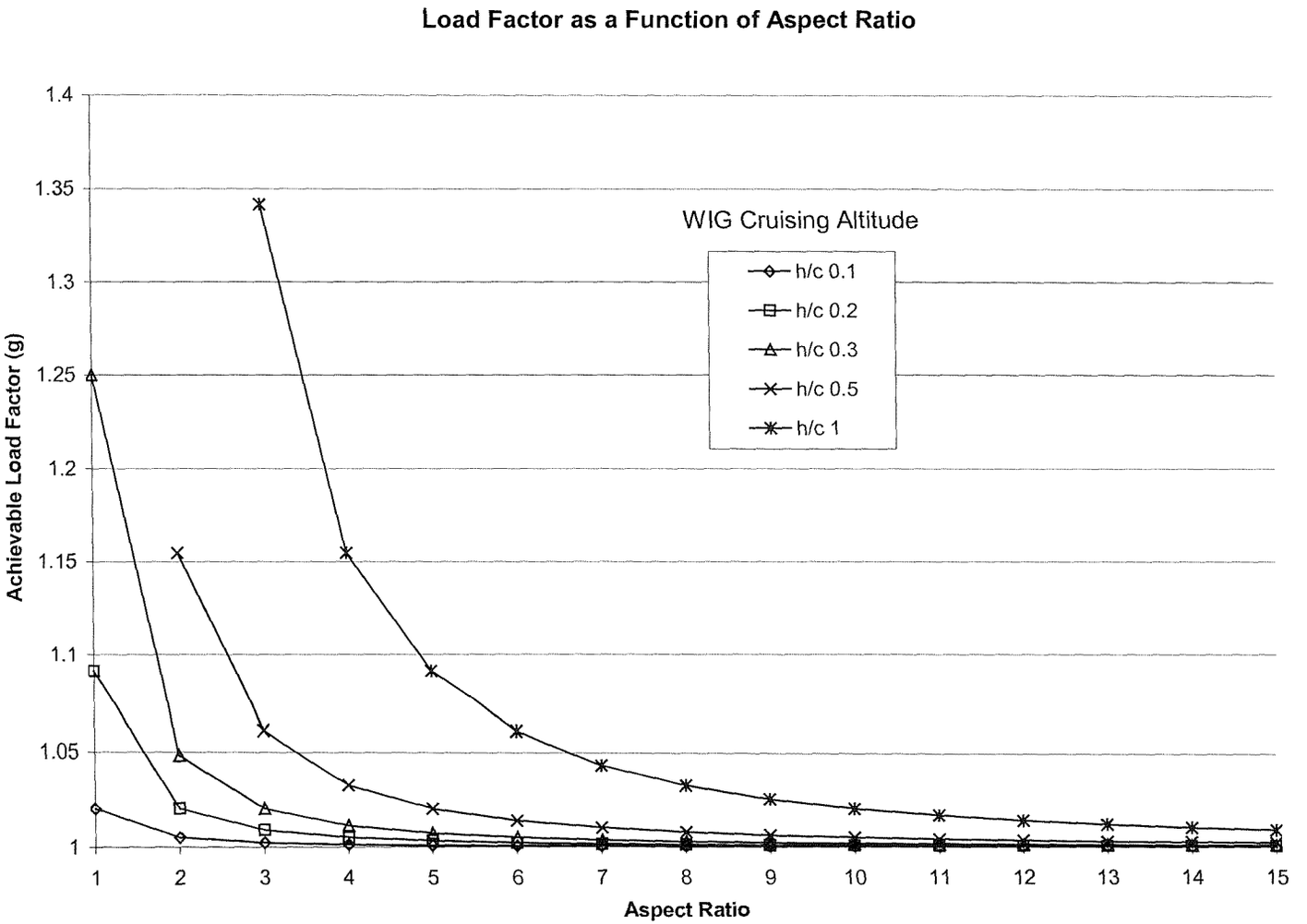

Figure E-5: Achievable Load factors as a function of aspect ratio

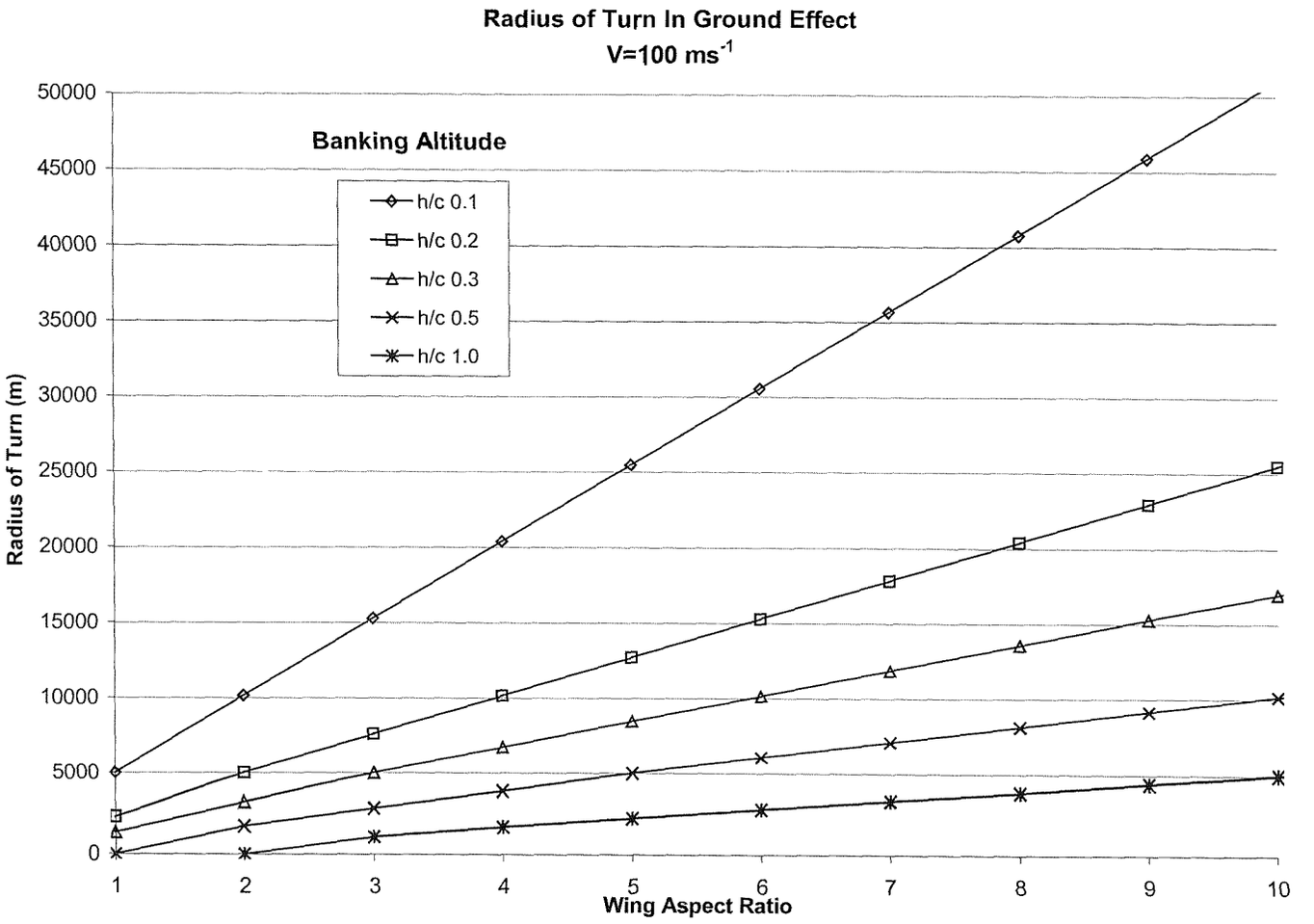

Figure E-6: Turn Radius at 100 ms^{-1} as a function of main wing aspect ratio

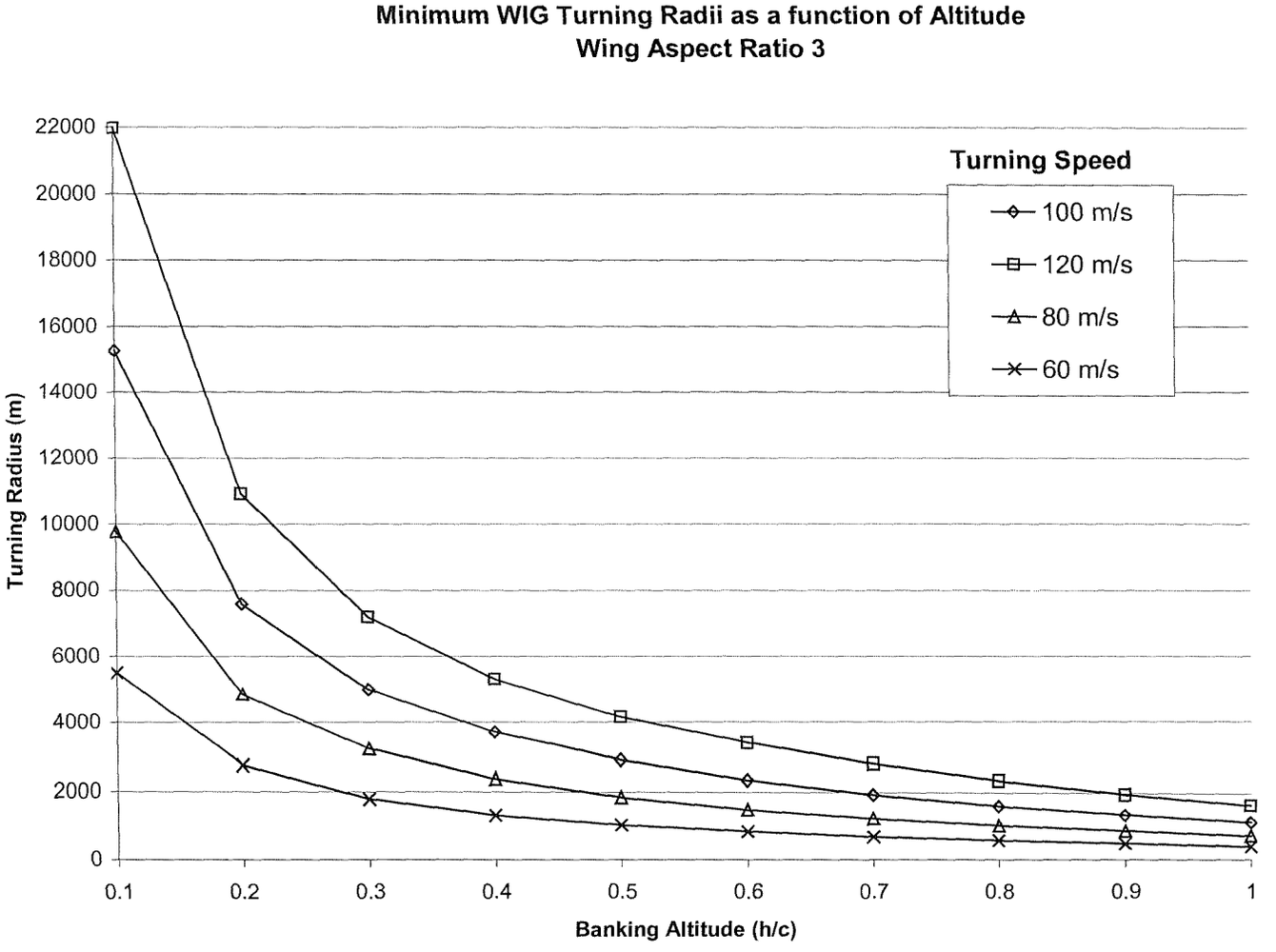

Figure E-7: Minimum Turning Radii as a function of altitude and speed for a WIG with wing of aspect ratio 3

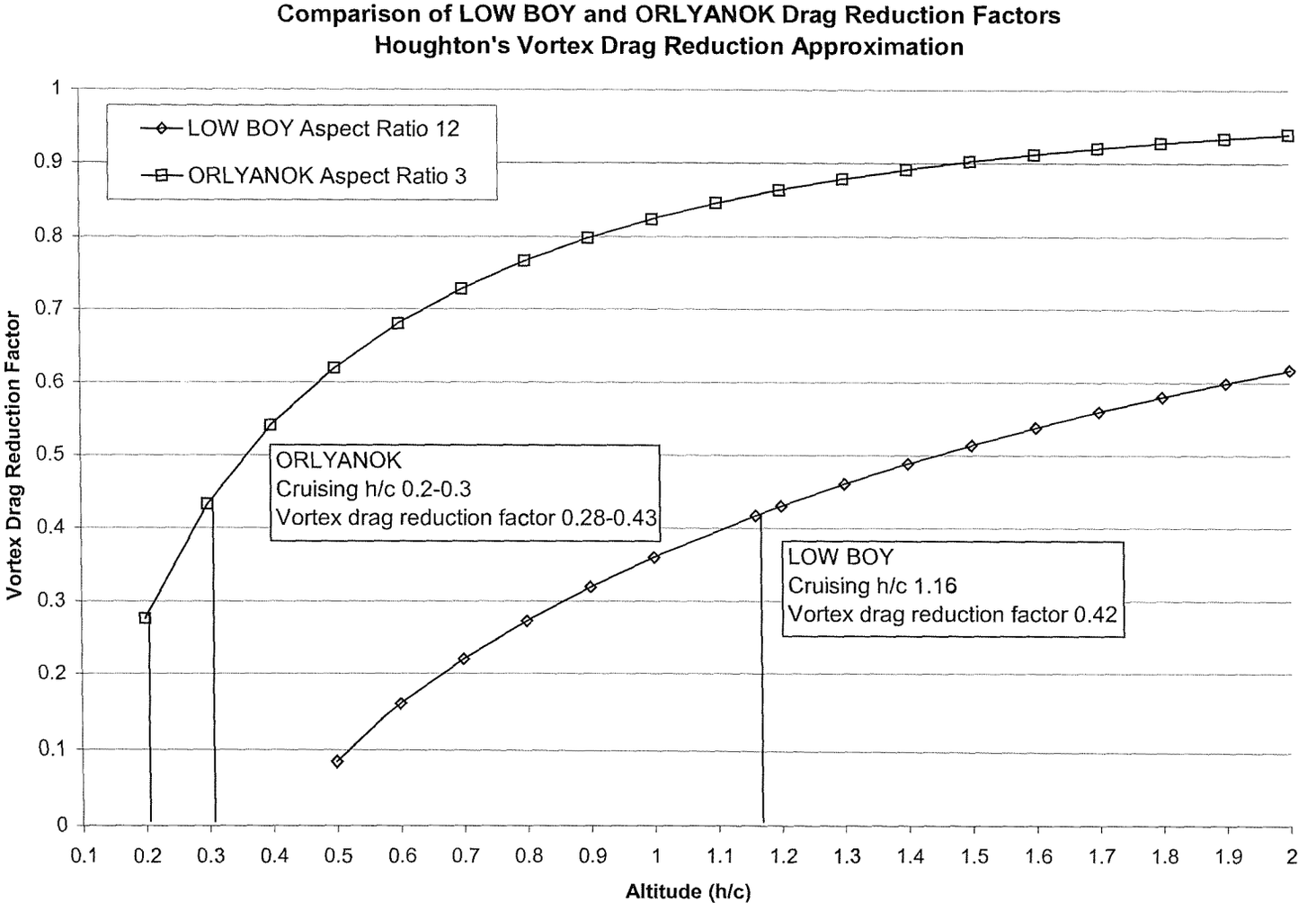

Figure E-8: Comparison of Vortex Drag Reduction for a high and low aspect ratio WIG craft

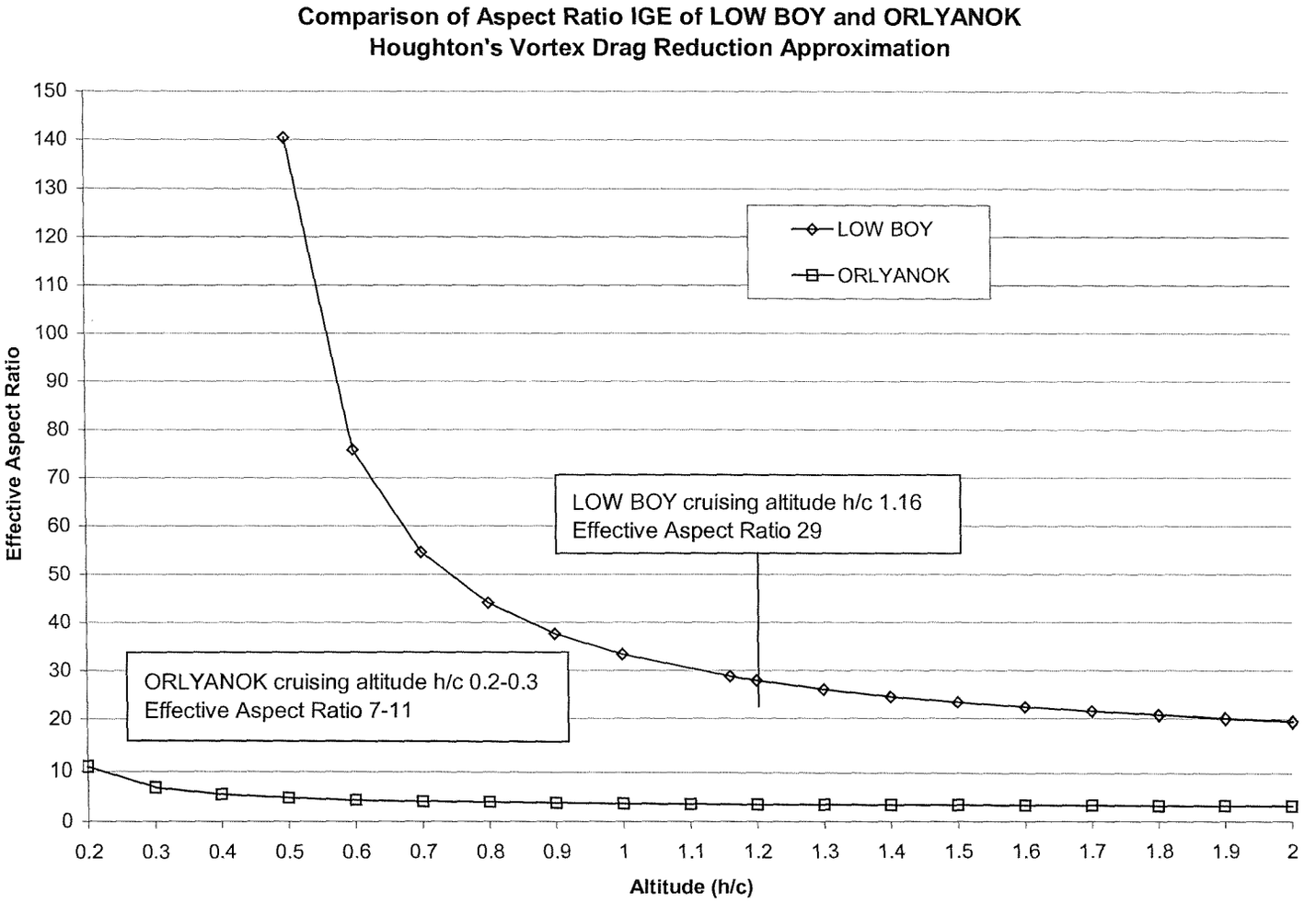

Figure E-9: Comparison of Effective Aspect Ratios for different WIG designs using Houghton's drag reduction approximation

Appendix F

Significant Wave Heights of Selected WIG Operating Areas

The tables below detail the probability of significant wave heights occurring for various operational areas as a function of season. This is the basis of the data used in the WIG seaworthiness analysis presented in Chapter 3. This data has been obtained from reference [39].

	Probability of Significant Wave Height Occurring (%)			
Significant Wave Height	**March-May**	**June-August**	**September-November**	**December-February**
0-1	29.7	31.5	19	17.5
1-2	33.6	37.2	30.9	28.3
2-3	19.4	19.6	23.3	22.5
3-4	9.3	7.7	13.3	14.3
4-5	4.3	2.6	6.8	8.2
5-6	2	2.6	3.4	4.4
6-7	1	0.3	1.7	2.3
7-8	0.7	N/A	0.6	1.2

Figure F-1: Probability of Significant Wave Height occurrence for the English Channel as a function of season

	Probability of Significant Wave Height Occurring (%)			
Significant Wave Height	**March-May**	**June-August**	**September-November**	**December-February**
0-1	53.8	63	60	46.7
1-2	30.2	27.4	29.8	34
2-3	11.1	7.5	8.1	13.7
3-4	3.6	1.8	1.8	4
4-5	1.1	0.3	0.3	1
5-6	0.2	N/A	N/A	0.6

Figure F-2: Probability of Significant Wave Height occurrence for the Persian Gulf as a function of season

	Probability of Significant Wave Height Occurring (%)			
Significant Wave Height	**December-March**	**April-May**	**June-August**	**September-November**
0-1	19.7	52.6	46.9	25.2
1-2	39.8	34.2	38.2	43.2
2-3	25.6	9.8	11.4	21.9
3-4	10.4	2.5	2.9	7.5
4-5	3.3	0.7	0.6	1.9
5-6	0.9	0.2	N/A	0.3
6-7	0.3	N/A	N/A	N/A

Figure F-3: Probability of Significant Wave Height occurrence for the Baltic as a function of season

	Probability of Significant Wave Height Occurring (%)			
Significant Wave Height	**March-May**	**June-August**	**September-November**	**December-February**
0-1	4.5	10.8	3.2	2.3
1-2	23.3	35.3	18.3	13.4
2-3	27.3	30.3	26.9	21.1
3-4	19.9	15	22.8	20.7
4-5	11.8	5.7	14.4	16
5-6	6.4	1.9	7.6	10.8
6-7	3.3	0.7	3.7	6.6
7-8	1.7	0.3	1.7	3.9
8-9	0.9	N/A	0.8	2.3
9-10	0.9	N/A	0.4	1.3
10-11	N/A	N/A	0.6	0.8
11-12	N/A	N/A	N/A	0.8

Figure F-4: Probability of Significant Wave Height occurrence for the North Atlantic as a function of season

	Probability of Significant Wave Height Occurring (%)			
Significant Wave Height	**March-May**	**June-August**	**September-November**	**December-February**
0-1	7.6	21	7.5	2.1
1-2	27.1	42.8	29.8	15.6
2-3	27.3	23.1	28.5	24.7
3-4	17.9	8.6	17.3	22.2
4-5	9.8	2.8	8.8	15.2
5-6	5	1	4.2	9.1
6-7	2.5	0.4	1.9	5.1
7-8	1.3	0.1	0.9	2.7
8-9	0.7	0.1	0.4	1.5
9-10	0.4	N/A	0.2	0.8
10-11	0.2	N/A	0.1	0.4
11-12	N/A	N/A	0.1	0.2

Figure F-5: Probability of Significant Wave Height occurrence for the Mid Atlantic as a function of season

	Probability of Significant Wave Height Occurring (%)			
Significant Wave Height	**March-May**	**June-August**	**September-November**	**December-February**
0-1	2.1	2.3	2.3	5.1
1-2	22	16.6	19.1	28
2-3	30.5	25.5	28.8	31.9
3-4	22.7	22.3	23	20.2
4-5	12.3	14.9	13.7	9.4
5-6	5.6	8.6	7	3.6
6-7	2.3	4.6	3.3	1.2
7-8	0.8	2.4	1.5	0.4
8-9	0.3	1.3	0.7	0.1
9-10	0.1	0.6	0.3	N/A
10-11	N/A	0.3	0.2	N/A
11-12	N/A	0.2	0.1	N/A

Figure F-6: Probability of Significant Wave Height occurrence for the South Atlantic as a function of season

	Probability of Significant Wave Height Occurring (%)			
Significant Wave Height	**March-May**	**June-August**	**September-November**	**December-February**
0-1	2.6	1.5	2.3	4.2
1-2	19.8	13.1	17.2	24.7
2-3	28.3	23.4	27.4	30
3-4	22.2	22.7	23.5	20.8
4-5	13.3	16.3	14.7	11.1
5-6	7	10	7.7	5.2
6-7	3.4	5.7	3.8	2.2
7-8	1.7	3.1	1.8	0.9
8-9	0.8	1.7	0.8	0.4
9-10	0.4	1	0.4	0.2
10-11	0.2	0.6	0.2	0.1
11-12	0.1	0.3	0.1	0.1

Figure F-7: Probability of Significant Wave Height occurrence for the Southern Indian Ocean as a function of season

	Probability of Significant Wave Height Occurring (%)			
Significant Wave Height	**April-May**	**June-September**	**October-November**	**December-March**
0-1	45.8	9.8	42.9	33.3
1-2	37.5	22.8	39.2	44.3
2-3	12.2	23.6	13.9	17.1
3-4	3.2	18.6	3.4	4.2
4-5	0.9	12.1	0.7	0.8
5-6	0.3	6.8	0.1	0.2
6-7	0.1	3.4	N/A	N/A
7-8	0.1	1.6	N/A	N/A
8-9	N/A	0.7	N/A	N/A
9-10	N/A	0.3	N/A	N/A
10-11	N/A	0.2	N/A	N/A
11-12	N/A	0.1	N/A	N/A

Figure F-8: Probability of Significant Wave Height occurrence for the Northern Indian Ocean as a function of season

Appendix G

Unmanned WIG Vehicle Concept

G1 Overview

This chapter details the concept of a small Unmanned WIG Vehicle (UWIGV). In this context small is defined as a take-off mass less than 50 kg. The UWIGV concept is a multi-mission vehicle for operation in a maritime environment fulfilling a variety of specialised roles including reconnaissance and electronic warfare.

G2 UWIGV Roles

The small UWIGV concept is envisioned as operating in coastal inlets and rivers providing covert surveillance coverage. Typical law enforcement missions include anti-smuggling surveillance and monitoring for illegal immigration. The whole system should be cheap to manufacture and simple to operate. The UWIGV must posses a low aural signature and small physical size in order to reduce the probability of detection. Flying in ground effect will increase the operating radii and endurance conferring a high degree of covertness.

The UWIGV will carry a dedicated flight camera and surveillance sensor. At present there are very lightweight electro-optic (EO) sensors commercially available on the open market for UAV use. To allow for reversionary manual control a lightweight miniature pan tilt zoom camera such as one marketed by BAI Aerosystems could be mounted in the fuselage nose [49]. The main surveillance sensor could be a mini pan tilt EO sensor, these can employ interchangeable daylight TV or IR sensor [49] depending upon the operational requirement. Very light models exist such, as the BAI Aerosystems that possesses a mass of only 1.3 kg are commercially available. Unlike conventional UAVs that have the sensor optics mounted in the ventral position a UWIGV would require it to be mounted dorsally. This would need to be discussed with the manufacturers to verify the applicability of this.

To take advantage of ground effect the UWIGV will cruise at altitudes between h/c 0.3 to 1.0. It should also possess the capability to fly out of ground effect though this would not be its main flight regime as the low aspect ratio wing planform is optimised for ground effect flight. Flying a UWIGV out of ground effect would result in a significant reduction in aerodynamic efficiency. The UWIGV is to operate down rivers or estuaries and not in the open sea. As a result it is designed for IGE operations in calm water conditions defined as a sea state of 1 or less (see Chapter 3; Table 3-1). If rougher surface conditions are encountered the cruising altitude is set correspondingly higher, resulting in a consequent reduction in aerodynamic efficiency (L/D) that would reduce the crafts range.

There are some unique technological and operational issues associated with the UWIGV concept that need to be addressed. These are summarised in Table G-1 along with an assessed level of risk for the technology. The most basic requirement for the UWIGV is that it must maintain its cruising altitude at the very low heights required for ground effect flight. This requires accurate measurement of altitude and the ability to maintain it. The Global Positioning System (GPS) that the UWIGV would rely upon for navigation does not provide sufficient accuracy in the altitude axis. The quoted accuracy of Differential GPS (DGPS) in altitude is 1.6 m for 50% confidence, reducing to 14.4 m for a 99.45% confidence level [50].

The most accurate method of measuring altitude is by using some form of active ranging device. Aircraft and UAVs have commonly used a FMCW (Frequency Modulated Continuous Wave) radar altimeter. This technology is routinely employed on vehicles, such as sea skimming missiles that are designed to operate close to the surface. The UWIGV concept requires measurement of very low altitudes, for the concept discussed down to 0.1 m. Roke Manor Research offer a miniature radar altimeter that measures altitudes down to 0.2 m above ground level [51]. This has an accuracy of ±0.02 m that corresponds to ±h/c 0.07. An alternative is to employ an ultrasonic rangefinder; these have minimum ranges down to 0.03 m, this corresponds to an altitude of h/c 0.1 on the DHMTU wing used in this research program [52]. Accurately measuring the altitude is assessed as presenting a low level of technological risk.

The altitude information is used by the autopilot to maintain height and adjust altitude according to the prevalent sea conditions. The design or modifications that need to be

made are not known at present. This would require a separate study to assess this issue and as such the technological level of risk has not been quantified.

An important operational issue for a UWIGV is the ability to detect surface objects and initiate avoiding action to prevent a collision. To enable the detection of objects requires a sensor of some form. If the UWIGV is being flown under manual command the operator could detect the object visually through a nose mounted TV sensor and initiate an avoidance manoeuvre. Though it may be useful to have some form of sensor to alert the operator to a possible collision hazard. If the UWIGV is under autonomous operation an active proximity-warning sensor is a must.

For a UWIGV to successfully avoid an object in its path it must initiate a manoeuvre at a minimum distance from the object. The range at which this is initiated depends upon the aerodynamic capability of the UWIGV and the cross range extent of the object. The proximity sensor could determine the spatial extent of the object. This information is then used by the autopilot to initiate a manoeuvre based upon some internal logic. Alternatively the autopilot could posses some a priori knowledge of an objects length pre-set by the user. On detection of an object the UWIGV initiates a standard evasive manoeuvre.

G3 Susceptibility Issues

The survivability of a UWIGV against any defence system relies upon the successful detection, tracking and engagement of the craft. Detection methods that could be employed include optical, either by human eyes or by magnifying optics, acoustic, thermal or radar. In a low threat scenario involving smuggling interdiction, illegal immigration or counter-insurgency the acoustic and visual signature will be the primary detection feature. In a high-level threat environment consideration has to be given to the thermal and radar signatures of the UWIGV. As this UWIGV concept is being considered for the more benign threat scenario reducing the acoustic and visual signatures are more of a priority.

The primary method of reducing detection against optical, thermal and radar sensors is the very low flight altitude (0.1 to 0.3 m) that minimises the line of sight. The optical and

radar signature will also be reduced by the small physical size of the UWIGV. The optical signature would be further minimised by finishing the craft in a suitable paint scheme to blend in with the background. As the craft is constructed of composite materials the RCS will be further reduced. No exotic radar attenuating materials are anticipated in the construction in order to keep costs down.

The acoustic signature from an aircraft is non-line of sight and is generated from the engine and propeller. Acoustic detection methods range from the human ear to hi-tech acoustic sensors. Trials conducted in the US with acoustic sensors have detected a small electrically powered POINTER UAV flying at low altitude out to ranges of 2.5 km [53].

There are some palliative measures that can be applied to reduce the acoustic signature of an aircraft. Piston engines are normally fitted with silencers to keep noise levels down. To produce further reductions in the engine's signature a second silencer can be fitted in series [54]. Fitting anti-vibration mounts and covering the engine with a cowling can result in additional engine quietening. The use of sound absorbing materials on the craft structure will reduce the airframe tendency to act as a microphone. The effectiveness of these measures needs to be balanced with the resulting increase in weight and cost on the UWIGV.

The acoustic signature of the propeller is a result of the blade tip speed operating at near sonic velocities, sweeping the propeller tips can reduce this signature component. Increasing the number of propeller blades and their diameter results in lower blade loading can also reduce the acoustic emissions from the propeller.

G4 Configuration

The most noticeable feature of a UWIGV is the low aspect ratio rectangular wing. This is driven by the need to bank in the ground effect as discussed in Appendix E. Another unusual feature is the large horizontal stabilising tail needed as a result of the increased pitch control requirements of the WIG flight regime.

Take-off could be either conventional employing electrically retractable tricycle undercarriage or launch by a pneumatic rail. The landing could be either conventional or if space is at a premium into a net. The landing gear must be retractable to provide the required ground clearance at WIG flight altitude. This results in two major advantages, firstly from an aerodynamic viewpoint the fuselage is not penalised by a hydrodynamic hull. Also if a hull were fitted it would lie below the lower surface of the wing reducing the ground clearance in cruise and hence craft safety. Not employing a waterborne take-off also lowers the thrust requirement of the UWIGV

A pusher propeller configuration is one option allowing the use of a nose mounted TV for manual command flying. The pusher configuration also provides for a non-obstructed forward view for the dorsally mounted slewable electro-optic sensor. The tail layout is a twin boom to allow for the pusher propeller layout. An all-moving horizontal tailplane maximises the surface area for stability and control requirements for ground effect flight. Figure G-1 illustrates one possible configuration for a UWIGV.

Issue	Implications	Technology Requirements	Technological Level of Risk
Fly into the sea	Asses sea state	Doppler returns from FMCW altimeter	Low – proven technology
	Accurate altitude measurement	FMCW altimeter or SONAR altimeter	
	Accurate altitude keeping	Autopilot design/modifications	Not Quantified
Collision	Detection of surface objects	Nose mounted camera (manual command mode) Proximity sensor (autonomous/command mode)	Low – proven technology
	Assess spatial extent of object	Operator assessment through nose mounted camera (manual command mode) Measurement by proximity sensor	Not Quantified
	Avoidance of surface objects	Autopilot executes pre-programmed avoidance manoeuvre	Medium – being considered for UCAV operation
Wind shear	Identify disturbance	INS measurement	Low – proven technology
	Blown into sea	Autopilot and control response	Not Quantified

Table G-1: Technological issues, requirements and level of risk for UWIGV Concept

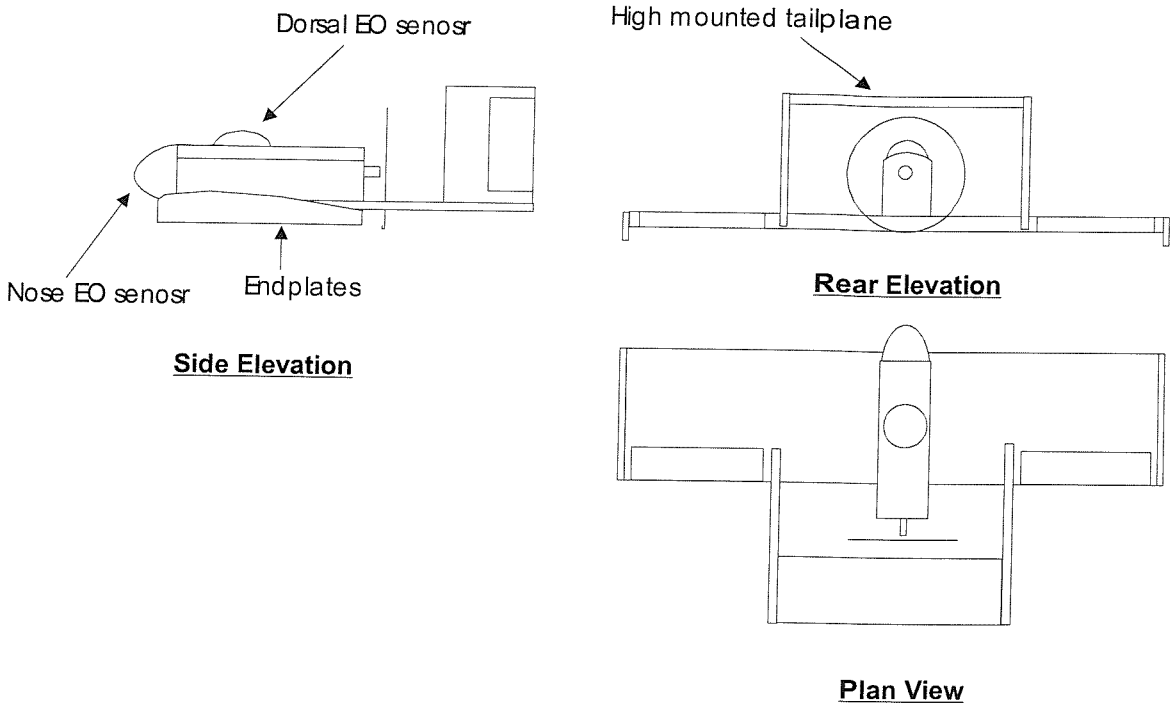

Figure G-1: Sketch of UWIGV Concept

Appendix H

DHMTU 12-35.3-10.2-80.12.2 Co-ordinates

The table below details the 'coarse' co-ordinates for the DHMTU 12-35.3-10.2-80.12.2 aerofoil (Figure H-1) obtained from the DHMTU section generator located on the se-technology website [20].

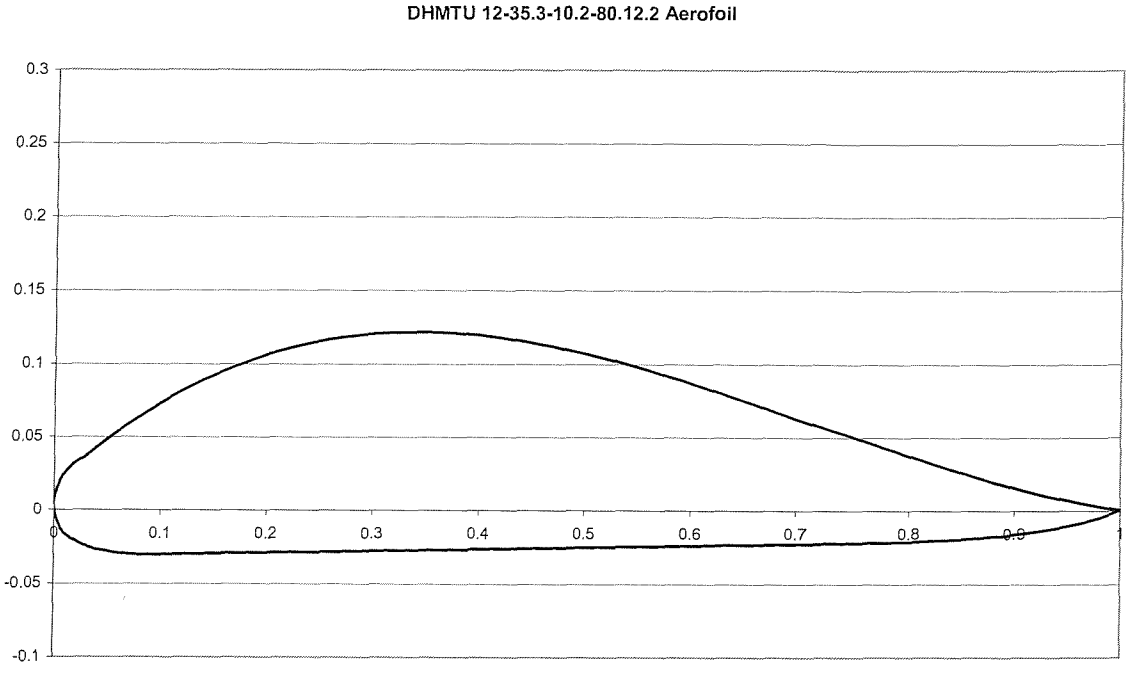

Figure H-1: DHMTU 12-35.3-10.2-80.12.2 Aerofoil

x-coordinate (x/c)	y-coordinate (y/c)
1	0.0006
0.99	-0.002325347
0.98	-0.004845738
0.97	-0.007021238
0.96	-0.008903925
0.95	-0.010538651
0.94	-0.011963768
0.93	-0.013211811
0.92	-0.014310151
0.91	-0.015281608
0.9	-0.016145029
0.89	-0.016915829
0.88	-0.017606496
0.87	-0.018227059
0.86	-0.018785519
0.85	-0.019288246
0.84	-0.019740337
0.83	-0.020145936
0.82	-0.020508526
0.81	-0.020831171
0.8	-0.021116736
0.79	-0.021368058
0.78	-0.021588089
0.77	-0.021780001
0.76	-0.021947248
0.75	-0.022093604
0.74	-0.02222315
0.73	-0.022340238
0.72	-0.022449408
0.71	-0.022555276
0.7	-0.022662381
0.69	-0.022774996
0.68	-0.022896906
0.67	-0.023031146
0.66	-0.023179703
0.65	-0.023343183
0.64	-0.023372
0.63	-0.023499
0.62	-0.023626
0.61	-0.023753
0.6	-0.02388
0.59	-0.024007
0.58	-0.024134

Continued on next page

x-coordinate	y-coordinate
0.57	-0.024261
0.56	-0.024388
0.55	-0.024515
0.54	-0.024642
0.53	-0.024769
0.52	-0.024896
0.51	-0.025023
0.5	-0.02515
0.49	-0.025277
0.48	-0.025404
0.47	-0.025531
0.46	-0.025658
0.45	-0.025785
0.44	-0.025912
0.43	-0.026039
0.42	-0.026166
0.41	-0.026293
0.4	-0.02642
0.39	-0.026547
0.38	-0.026674
0.37	-0.026801
0.36	-0.026928
0.35	-0.027055
0.34	-0.027182
0.33	-0.027309
0.32	-0.027436
0.31	-0.027563
0.3	-0.02769
0.29	-0.027817
0.28	-0.027944
0.27	-0.028071
0.26	-0.028198
0.25	-0.028325
0.24	-0.028452
0.23	-0.028579
0.22	-0.028706
0.21	-0.028833
0.2	-0.02896
0.19	-0.029087
0.18	-0.029214
0.17	-0.029341
0.16	-0.029468
0.15	-0.029595
0.14	-0.029722
0.13	-0.029849

Continued on next page

x-coordinate	y-coordinate
0.12	-0.029976
0.11	-0.030103
0.1	-0.03023
0.09	-0.030357
0.08	-0.030484
0.07	-0.030111
0.06	-0.02911971
0.05	-0.028044938
0.04	-0.026863814
0.030995677	-0.024627832
0.018820509	-0.020381438
0.006760776	-0.01336204
0	0
0.001210316	0.010182474
0.005704819	0.020364949
0.008715363	0.024165099
0.012200539	0.027400907
0.016704176	0.030572829
0.022445049	0.033681322
0.029651014	0.036726842
0.039651014	0.042428922
0.049651014	0.048094994
0.059651014	0.053518177
0.069651014	0.058702123
0.079651014	0.063650482
0.089651014	0.068366906
0.099651014	0.072855048
0.109651014	0.077118558
0.119651014	0.081161088
0.129651014	0.08498629
0.139651014	0.088597815
0.149651014	0.091999315
0.159651014	0.095194442
0.169651014	0.098186847
0.179651014	0.100980182
0.189651014	0.103578098
0.199651014	0.105984247
0.209651014	0.108202281
0.219651014	0.11023585
0.229651014	0.112088608
0.239651014	0.113764205
0.249651014	0.115266293
0.259651014	0.116598523
0.269651014	0.117764548
0.279651014	0.118768018

Continued on next page

x-coordinate	y-coordinate
0.289651014	0.119612586
0.299651014	0.120301903
0.309651014	0.12083962
0.319651014	0.121229389
0.329651014	0.121474863
0.339651014	0.121579691
0.349651014	0.121547527
0.359651014	0.121382021
0.369651014	0.121086825
0.379651014	0.120665591
0.389651014	0.12012197
0.399651014	0.119459615
0.409651014	0.118682176
0.419651014	0.117793305
0.429651014	0.116796654
0.439651014	0.115695874
0.449651014	0.114494617
0.459651014	0.113196535
0.469651014	0.111805279
0.479651014	0.1103245
0.489651014	0.108757851
0.499651014	0.107108983
0.509651014	0.105381548
0.519651014	0.103579196
0.529651014	0.101705581
0.539651014	0.099764353
0.549651014	0.097759164
0.559651014	0.095693665
0.569651014	0.093571509
0.579651014	0.091396346
0.589651014	0.089171828
0.599651014	0.086901608
0.609651014	0.084589336
0.619651014	0.082238665
0.629651014	0.079853245
0.639651014	0.077436728
0.649651014	0.074992767
0.659651014	0.072525012
0.669651014	0.070037115
0.679651014	0.067532728
0.689651014	0.065015502
0.699651014	0.062489089
0.709651014	0.059957141
0.719651014	0.057423309
0.729651014	0.054891245

Continued on next page

x-coordinate	y-coordinate
0.729651014	0.054891245
0.739651014	0.0523646
0.749651014	0.049847026
0.759651014	0.047342175
0.769651014	0.044853698
0.779651014	0.042385246
0.789651014	0.039940472
0.799651014	0.037523027
0.809651014	0.035136563
0.819651014	0.03278473
0.829651014	0.030471182
0.839651014	0.028199569
0.849651014	0.025973542
0.859651014	0.023796755
0.869651014	0.021672857
0.879651014	0.019605501
0.889651014	0.017598339
0.899651014	0.015655021
0.909651014	0.013779201
0.919651014	0.011974528
0.929651014	0.010244655
0.939651014	0.008593233
0.949651014	0.007023915
0.959651014	0.005540351
0.969651014	0.004146193
0.979651014	0.002845093
0.989651014	0.001640702
0.999651014	0.000536672

Appendix I

XFOIL Summary

I1 Overview

As part of this research project a third year student (Tothill) assisted the author in the first set of experiments in the rolling road wind tunnel during December 2000 to April 2001. As part of this student's work he conducted an Internet search, found a DHMTU aerofoil generator [20]. Additionally information on DHMTU aerofoils that South Koreans were using in their WIG research was also found [41]. This lead to the selection of a DHMTU 12-35.3-10.2-80.12.2 based upon a South Korean DHMTU aerofoil [41].

I2 XFOIL

Tothill employed the XFOIL software to aid in the visualisation of the pressure distributions over the DHMTU aerofoils in relation to a NACA 0012. He did not attempt to asses the accuracy of XFOIL or comment on the resulting XFOIL data. This appendix will present a comparison of Tothill's XFOIL results and experimental data obtained for this research.

XFOIL is a software program that is freely available on the Internet and allows the pressure profile, lift, drag and pitching moment characteristics of an infinite span aerofoil to be investigated under viscous and inviscid conditions. The inviscid analysis employs a linear-vorticity stream function panel method. The reader who requires more detail on the theory of panel methods is directed towards Houghton and Carpenter who provide a very good explanation of this technique [43]. The co-ordinates of the DHMTU aerofoil were input into XFOIL and were obtained from a DHMTU aerofoil generator located on the Internet [20].

XFOIL can only provide predictions of the aerodynamic performance of two dimensional (infinite span) aerofoil sections out of ground effect. This means that the downwash created by a finite aerofoil and the resulting vortex drag and

reduction in lift is not taken into account. Equations I-1 and I-3 allow the values of lift and drag for a finite wing of aspect ratio AR to be calculated.

$$a = \frac{a_\infty}{1 - \left[\frac{a_\infty}{\pi e AR}\right]}$$ Equation I-1

$$a_\infty = \frac{a}{1 - \left[\frac{a}{\pi e AR}\right]}$$ Equation I-2

Where a_∞ is the lift curve slope for a wing of infinite aspect ratio, e is the span efficiency factor, a is the lift curve slope of a wing of aspect ratio AR.

$$C_D = C_{D0} + C_{DV}$$ Equation I-3

Where C_D is the overall drag, C_{D0} is the zero-lift drag and C_{DV} is the vortex drag given by

$$C_{DV} = \frac{C_L^{\,2}}{\pi e AR}$$ Equation I-4

Where C_L is the lift coefficient

I3 Comparison between XFOIL and Experimental Data

Tothill initially ran an NACA 0012 section in XFOIL at an angle of attack of 4 degrees and Reynolds Number 4 x 10^5 (Figure I-1). This resulted in a C_L of 0.4391 for a wing of infinite aspect ratio i.e. two-dimensional flow. Tothill did not run XFOIL over a range of angles of attack in order to determine the predicted lift curve slope (a_∞). This meant that equation I-1 could not be used to estimate the lift coefficient for the finite span NACA 0012 that was tested in the wind tunnel.

Instead it is possible to employ equation I-2 to determine the C_L of a NACA 0012 of infinite span using the experimental data presented in Chapter 5.

It has been determined experimentally for this research that the lift curve slope of a NACA 0012 OGE is 3.5 per radian for a wing of aspect ratio 3 at Re 8.3 x 10^5 (Table 5-4). Equation I-2 shows that if the aspect ratio were infinite the lift curve slope would be 5.57 per radian. At an angle of attack of 4 degrees this corresponds to a C_L of 0.39. This is only 9% different from the predicted C_L obtained from XFOIL. This illustrates that the predicted XFOIL lift coefficient for the NACA 0012 is very close to that obtained experimentally.

XFOIL predicted a C_{D0} of 0.01445 for the NACA 0012 with an infinite aspect ratio at a Reynolds Number of 4 x 10^5. This is less than the experimentally recorded overall drag (C_D) of 0.01661 for the NACA 0012 wing of aspect ratio 3 when Re is 8.3 x 10^5. The greater experimental value of C_D is to be expected, as XFOIL cannot calculate vortex drag, it only models two-dimensional flow calculating C_{D0}. If we use equation I-2 to estimate the C_{D0} of the experimental NACA 0012 this results in C_{D0} 0.01164, this is the C_{D0} that XFOIL predicts if we remove the vortex drag from the experimental data. The experimental value of C_{D0} is 20% less than the XFOIL prediction. This difference can be accounted for by the difference in Reynolds Number as illustrated for the DHMTU 12-35.3-10.2-80.12.2 in Figure 5-17. Here the measured C_D at Re 4.3 x 10^5 is 16% greater than the C_D at 8.3 x 10^5 is 16%.

Tothill ran the case of a DHMTU 12-35.3-10.2-80.12.1 (Figure I-2) that he found on a South Korean website [41]. For reasons not stated in his report the nose radius parameter was increased from 1 to 2. Apart from this parameter the DHMTU section used for this research was nearly the same as the South Korean section.

XFOIL predicted a C_L of 0.6536 for the DHMTU 12-35.3-10.2-80.12.2 wing of infinite aspect ratio (Figure I-3). The results from the experimental research resulted in a C_L of 0.34 for the DHMTU 12-35.3-10.2-80.12.2 at an angle of attack of 4 degrees, operating OGE and for an aspect ratio of 3. Employing

equation I-2 and using the experimental data for the DHMTU 12-35.3-10.2-80.12.2 lift curve slope (a=3.9 per radian, Table 5-4), a DHMTU 12-35.3-10.2-80.12.2 of infinite aspect ratio operating OGE would produce a lift curve slope of 6.65 per radian. This results in an experimental based value for C_L of 0.4645 for a wing of infinite aspect ratio, compared to XFOIL C_L of 0.6536. This shows that XFOIL overestimates the experimental OGE lift coefficient for the DHMTU 12-35.3-10.2-80.12.2 by 29%.

XFOIL predicts a C_{D0} of 0.01392 for DHMTU 12-35.3-10.2-80.12.2. If Equation I-2 is populated with the experimental data (C_L=0.34, AR=3 and C_D 0.030385) this results in a C_{D0} of 0.01810 at a Re of 8.3 x 10^5. This experimental value of C_{D0} obtained at a Re of 8.3 x 10^5 is 23% greater than the C_{D0} XFOIL predicted at Re 4.0 x 10^5. As discussed above the C_D of the DHMTU 12-35.3-10.2-80.12.2 at an AoA of 4 degrees increases by 16% when the Reynolds Number reduces from 8.3 x 10^5 to 4.3 x 10^5.

I4 Summary

In summary XFOIL was used by Tothill to aid in qualitative understanding of the DHMTU aerofoil family at a high level. XFOIL can only provide aerodynamic parameters when the aerofoil is operating out of ground effect. His report was not a rigorous analysis of the DHMTU aerofoil family and he made no attempt to asses the accuracy of XFOIL. Table I-1 presents the experimentally and XFOIL derived lift and drag values for the NACA 0012 and DHMTU 12-35.3-10.2-80.12.2 aerofoils. XFOIL overestimated C_L for both sections and overestimated C_{D0} for the NACA 0012 and underestimated C_{D0} for the DHMTU 12-35.3-10.2-80.12.2.

Section	Data	Reynolds Number	C_L	C_{D0}
NACA 0012	Experimental	8.3×10^5	0.3900	0.01164
	XFOIL	4.0×10^5	0.4391	0.01445
DHMTU 12-35.3-10.2-80.12.2	Experimental	8.3×10^5	0.4645	0.01810
	XFOIL	4.0×10^5	0.6536	0.01392

Table I-1: Comparison of NACA 0012 and DHMTU 12-35.3-10.2-80.12.2 experimentally based and XFOIL data*

*AoA 4 degrees, two-dimensional flow, out of ground effect

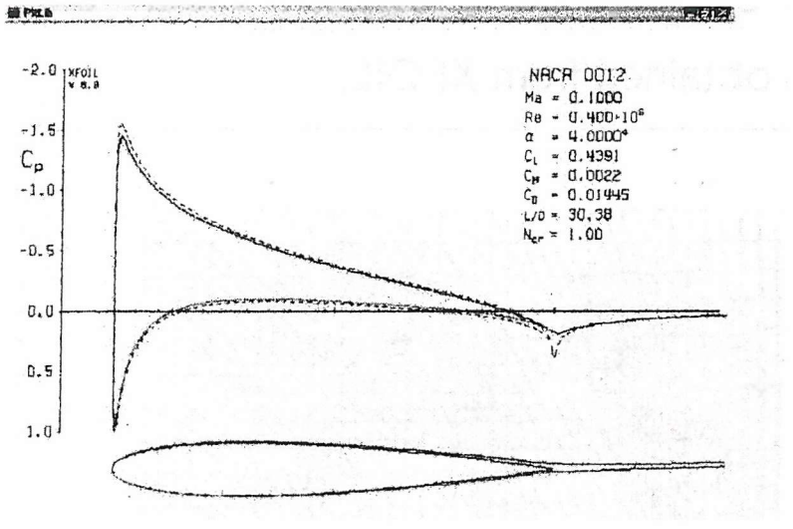

Figure I-1: NACA 0012 XFOIL Screen Capture [41]

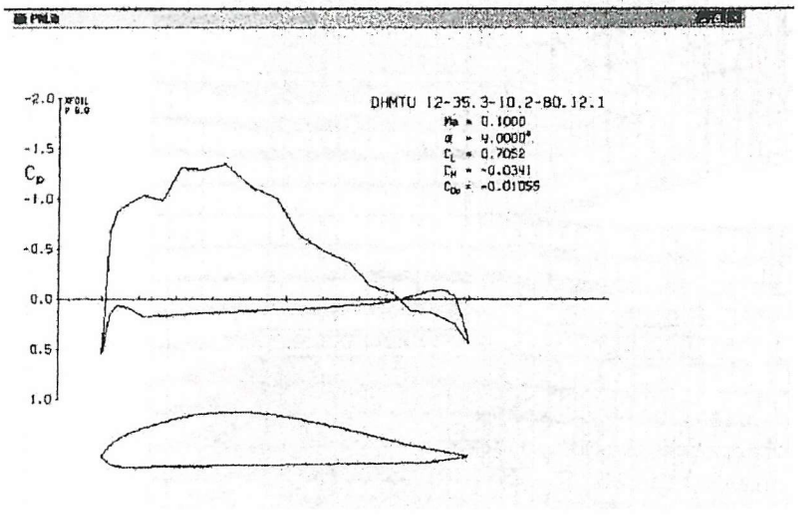

Figure I-2: South Korean DHMTU 12-35.3-10.2-80.12.1 XFOIL Screen Capture [41]

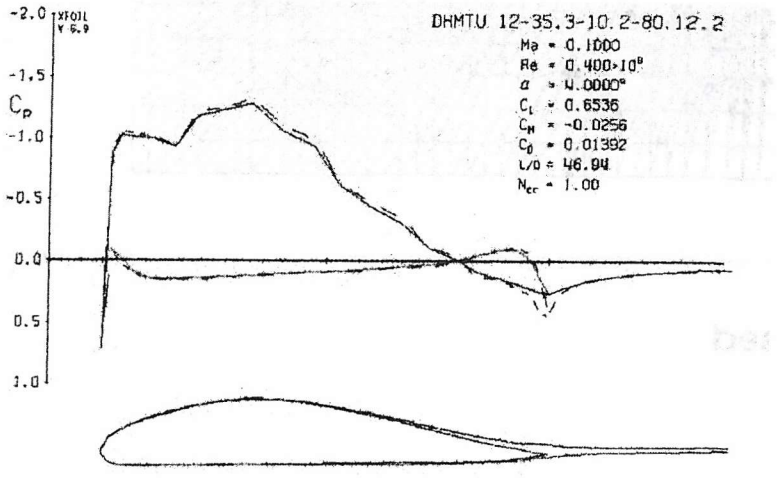

Figure I-3: DHMTU 12-35.3-10.2-80.12.2 XFOIL Screen Capture [41]